

CHARACTERIZATION OF A SONIFIED PEAK FLOW MONITOR

by

M.O. VERMEULEN

Thesis presented in partial fulfilment of the requirements for the degree of Master of
Medical Sciences (Physiology) at the University of Stellenbosch.



Supervisor: Mr. J.A. Wessels

Co-supervisor: Prof. T.W. von Backström

Department of Medical Physiology and Biochemistry

University of Stellenbosch

March 2000

DECLARATION

I the undersigned hereby declare that the work contained in this thesis is my own work and has not previously in its entirety or in part been submitted at any university for a degree.

Signature:  _____

Date: 11/02/2000

M.O. VERMEULEN

ABSTRACT

The Whistle Watch™, an innovative and commercialised peak flow monitor, inspired this study, with its abnormal and complex measuring behaviour. The Whistle Watch™ latter is an audible peak flow monitor with a threshold-activated whistle as the essential component. The whistle is calibrated for a certain flow, and then encased in a body with a variable exhaust valve to atmosphere. Using the Whistle Watch™, with the exhaust valve pre-set, executing a forced expiratory effort, the audible notification of the whistle would indicate a stable asthmatic condition at that setting. No audible notification would result in the use of medication as a preventative measure. Due to the absence of existing theories and literature on the mechanics of whistles, the Whistle Watch™ was empirically developed.

This study therefore, focuses on the characterisation and consequent improved understanding of the mechanics of a whistle, with the objective to monitor pulmonary function in a novel way.

During this study, a novel technique was developed to determine the reed activation point, or onset of oscillation, in terms of pressure. This technique was then implemented throughout the study.

The initial observation and experimentation underlined the whistle's activation sensitivity towards any irregularities of the reed surface. A statistical spread of reed activation pressures defined the reed's inherent non-linear properties. A high dependence of reed activation towards upstream geometry was noted, and a clarification hypothesis was formulated. The effect of reed dimensions on activation

pressure was exposed as a complex unexplored field. Existing mathematical reed theories only accommodate steady state oscillations, whereas the completed study indicated a high sensitivity of the reed activation pressure towards different input envelopes. This sensitivity was encapsulated in a mathematical model, with initial support and proof provided by a previous independent study.

All the observed effects and phenomena had far reaching practical application towards the production and quality control of the Whistle Watch™.

ABSTRAK

Die Whistle Watch™, 'n inoverende, kommersieel piekvloeimonitor, was die inspirasie vir die studie, deur sy abnormale en ingewikkelde meet-gedragsskenmerke. Laasgenoemde is 'n piekvloeimonitor met 'n fluit wat geaktiveer word by 'n vooraf vasgestelde drempel. Die fluit word gekalibreer vir 'n bepaalde vloei, waarna dit geënkapsuleer word in 'n hoofdeel met 'n veranderlike uitlaat na die atmosfeer. By die gebruik van die Whistle Watch™, met die uitlaatklep gestel op 'n voorafbepaalde vloeiempo, word 'n bepaalde ekspirasievlak verkry. Hierdie vlak het 'n hoorbare kennisgewing tot gevolg, wat 'n stabiele asematiese toestand aandui. In die afwesigheid van 'n hoorbare respons, word medikasie as voorkomende maatregel vereis. Die Whistle Watch™ is empiries ontwikkel in die afwesigheid van bestaande teorieë en literatuur ten opsigte van die werking van fluite.

Die fokus van hierdie studie word dus geplaas op die karakterisering van die werking van fluite, wat 'n beter begrip tot gevolg het. 'n Nuwe benadering tot die monitering van die pulmonêre funksie is dus haalbaar.

Tydens die studie is 'n unieke tegniek ontwikkel om die aktiveringspunt van die riet, of die aanvang van ossilasie in terme van druk, te bepaal. Hierdie tegniek is toe dwarsdeur die studie geïmplementeer.

Die fluit se aktiveringssensitiwiteit, in terme van die oppervlak-onreëlmatighede, van die riet was duidelik waarneembaar. Die inherente nie-liniêre eienskappe van die riet is duidelik waarneembaar in rietaktiveringsdrukke. 'n Verklarende hipotese is as gevolg van 'n afhanklikheid van die rietaktiveringsdrukke relatief tot stroom-op

geometrie, gestel. Die effek wat rietafmetings op aktiveringsdrukke het, was blootgelê as 'n komplekse onontwikkelde gebied. Bestaande wiskundige rietteorieë maak slegs voorsiening vir nie-fluktuerende ossillasies. Na voltooiing van hierdie studie is dit duidelik dat daar wel 'n hoë sensitiwiteit van die rietaktiveringsdrukke bestaan, met verwysing na verskillende ekspiratoriese profiele. Hierdie sensitiwiteit word vervat in 'n wiskundige model met toepaslike ondersteuning en bewyse uit 'n vorige, onafhanklike studie.

Alle waarneembare phenomena het resulterende praktiese impakte ten opsigte van die produksie en gehalteversekering van die Whistle Watch™.

DEDICATION

“ I can do all things through Christ who strengthens me.” Philippians 4:13

ACKNOWLEDGEMENTS

I am indebted to my supervisor, Mr. Jabus Wessels, for his guidance, patience and encouragement. His diverse field of interests and practicality created an intellectually stimulating environment for execution of this study. One can ask for no better supervisor.

In addition I am indebted to Dr. Pieter Fourie, who defined the light at the end of the tunnel. His achievements and personality are truly the portrayal of "leading by example".

I would like to extend my thanks to Prof. T.W. von Backström, who with his years of experience was always willing to listen and help.

I am indebted to Cobie Coetzee for her understanding and encouragement throughout this project.

I am grateful to the staff of the Department of Medical Physiology and Biochemistry for providing me with the facilities which made this development possible.

I would like to thank the staff of the Department of Mechanical Engineering for always having their doors open for help.

A special word of thanks to Mr. Cornelius Wijtenberg, who with his skills, illustrated that there is no substitute for experience.

Prof. P. Hoekje, at Baldwin Wallace College, is thanked for his helpful input and effort to supply the required literature.

In conclusion I thank my parents for their continuing support.

TABLE OF CONTENTS

	Page
CHAPTER 1 INTRODUCTION	1
1.1) Organisation of the Thesis	1
CHAPTER 2 PHYSIOLOGY OF THE RESPIRATORY SYSTEM	3
2.1) The bronchial tree	3
2.2) Respiratory Mechanics	5
2.2.1) Inspiration	7
2.2.2) Static Pressure-Volume Relationship	8
2.2.3) Expiration	12
2.3) Peak expiratory flow (PEF)	13
2.3.1) PEF: Is it prevalent?	14
2.3.2) Physiological factors which effect Peak Expiratory Flow	15
2.3.3) Pathological factors which limit Peak Expiratory Flow	19
2.3.4) Models describing the determinants of maximal flow	22
CHAPTER 3 PEAK FLOW MEASUREMENT	28
3.1) Historical background in the development of Peak Flow Meters	28
3.2) Present technology available in Peak Flow Meters	32
CHAPTER 4 THE WHISTLE WATCH[®] PEAK FLOW MONITOR	34
4.1) Principle of operation	34

4.2) Basic Construction of the Whistle Watch®	35
4.2.1) Sub-components of Whistle Watch body	35
4.2.2) The threshold activated reed whistle	37

CHAPTER 5 LITERATURE REVIEW: MUSICAL

INSTRUMENTS 39

5.1) Onset of oscillation	40
5.2) The interaction of a reed-valve and the air column: Linear models	41
5.3) The reed as a non-linear flow control valve	42
5.4) The interaction of a reed-valve and the air column: Non-linear models	44
5.5) The air column	46
5.6) Models of woodwind instruments	46
5.6.1) Backus's Model	46
5.6.2) Worman's Model	49
5.6.3) Hoekje's Model	51
5.6.4) Fletcher's Model	52
5.6.5) Keefe's Model	54
5.7) This study's contribution	56

CHAPTER 6 THE THRESHOLD ACTIVATED REED

WHISTLE 59

6.1) Descriptive Theory	59
6.2) Analytical Theory	61

CHAPTER 7	EXPERIMENTAL METHODS	64
7.)	Introduction	64
7.1)	The experimental apparatus	65
7.2)	The influence of nozzle geometry on reed activation pressure	68
7.3)	Defining reed activation pressure	71
7.4)	Determining the P_{RA}	71
7.5)	Validation of the reed activation pressure	83
7.6)	General characteristics of the reed activation pressure	86
7.7)	“Sidedness” of the reed	87
7.8)	The influence of reed dimensions on the P_{RA}	88
7.8.1)	The influence of reed width on P_{RA}	88
7.8.2)	The influence of reed length on P_{RA}	89
7.8.3)	The influence of reed thickness on P_{RA}	92
7.9)	Functional testing of the Whistle Watch®	93
7.9.1)	The Requirements of the American Thoracic Society (ATS)	93
7.9.2)	Customised Impulse waveforms	96
7.9.3)	Time domain changes to the customised Impulse waveforms	99
7.9.4)	Validation of P_{RA} at higher sampling rates	101
7.9.5)	Test Procedure	104
CHAPTER 8	RESULTS	107
8.1)	The influence of nozzle geometry on reed activation pressure	107
8.2)	General characteristics of the reed activation pressure	113
8.3)	“Sidedness” of the reed	116
8.4)	The influence of reed dimensions on the activation pressure	117

8.4.1) The influence of reed width on P_{RA}	117
8.4.2) The influence of reed length on P_{RA}	119
8.4.3) The influence of reed thickness on P_{RA}	121
8.5) Functional testing of the Whistle Watch®	124
8.5.1) Energy absorbing characteristics of the reed	129
8.6) General characteristics of the whistle	135
8.6.1) Hysteresis	135
8.6.2) Critical blowing pressure	135
8.6.3) Free versus Restricted reed Stability	139
8.6.4) Oscillatory effects	139
CHAPTER 9 CONCLUSION	146
9.1) Summary of findings and conclusion	146
9.2) Future Studies	147
REFERENCES	148
APPENDIX A	
APPENDIX B	
APPENDIX C	
APPENDIX D	
APPENDIX E	
APPENDIX F	
APPENDIX G	
APPENDIX H	

LIST OF ABBREVIATIONS

1. P_{pul} = Intrapulmonary pressure
2. P_{pl} = Intrapleural pressure
3. P_w = Trans-thoracic pressure
4. P_L = Transpulmonary pressure
5. PEF = Peak Expiratory Flow rate
6. Q_T = Activating flow rate of whistle
7. Q_i = Inlet flow rate to Whistle Watch
8. Q_v = Excess flow rate expelled
9. Q_w = Flow rate channeled to whistle
10. P_{atm} = Atmospheric pressure
11. LVDT = Linear Variable Differential Transformer
12. V = Volume
13. Q = Flow rate
14. PSD = Power Spectral Density

LIST OF VARIABLES

1. γ	=	Specific heat ratio	
2. T	=	Local static temperature	[K]
3. R	=	Gas constant of air	[m ² /(s ² K)]
4. a	=	Local speed of sound	[m/s ²]
5. V	=	Velocity	[m/s ²]
6. M	=	Mach number	
7. ρ	=	Density	[kg/m ³]
8. Q	=	Flow rate	[m ³ /s]
9. m	=	Mass flow rate	[kg/s]
10. μ	=	Viscosity	[N.s/m ²]
11. D	=	Diameter	[m]
12. π	=	circle circumference to diameter ratio	
13. L	=	Length	[m]

LIST OF FIGURES

		Page
1.	Figure 2.1.1 Bronchial Tree	4
2.	Figure 2.1.2 Lung Development	5
3.	Figure 2.2.1 Spirogram	6
4.	Figure 2.2.2 Inspiratory Thorax Movement	8
5.	Figure 2.2.3 Static Pressure-Volume Curves Of The Lung	10
6.	Figure 2.2.4 Pneumothorax	11
7.	Figure 2.3.1 A typical Flow-volume curve	13
8.	Figure 2.3.2 Iso-volumetric Pressure Flow Curve	14
9.	Figure 2.3.3 Posture Influencing FRC	19
10.	Figure 2.3.4 Lung Compliance	22
11.	Figure 2.3.5 Idealized Lung	23
12.	Figure 3.1.1 The Wright's Peak Flow Meter	30
13.	Figure 3.1.2 The mini Wright PFM	31
14.	Figure 3.2.1 The effect of Asthma on PEF	32
15.	Figure 4.1.1 Schematic illustration describing the basic functioning of the of the Whistle Watch®	34
16.	Figure 4.2.1 The Whistle Watch® body and whistle	35
17.	Figure 4.2.2 Sub-components of the Whistle Watch® body	35
18.	Figure 4.2.3 The basic components of the Whistle	37
19.	Figure 4.2.4 Fully Assembled Whistle	38
20.	Figure 5.1 Benade's Experimental Setup	42
21.	Figure 5.2 Aperture-flow versus reed driving pressure	42
22.	Figure 5.3 Backus Mathematical model of a Clarinet	47
23.	Figure 5.4 Backus's Experimental Setup	49

24. Figure 6.1.1	Audible Spectrum	60
25. Figure 6.2.1	Whistle layout	61
26. Figure 7.1.1	Schematic representation of the mechanical pump	65
27. Figure 7.1.2	Nozzle Design	66
28. Figure 7.2.1	Constricted Nozzle Geometry	69
29. Figure 7.2.2	Expansion Nozzle Geometry	70
30. Figure 7.4.1	Pressure-Time for a free reed	73
31. Figure 7.4.2	Transition zone indication	74
32. Figure 7.4.3	Transition zone	75
33. Figure 7.4.4	Typical Standard Deviation Graph	76
34. Figure 7.4.5	Different Standard Deviation Sampling Sizes	78
35. Figure 7.4.6	Different Standard Deviation Sampling Sizes	79
36. Figure 7.4.7	Pressure Activation Indication	80
37. Figure 7.4.8	Pressure Activation Indication in Transition Zone	81
38. Figure 7.4.9	Algorithm for calculate the reed activation pressure	82
39. Figure 7.5.1	Extracted Pressure Signal	85
40. Figure 7.5.2	Power Density Spectrum Window Indication	86
41. Figure 7.7.1	Sidedness of the reed	88
42. Figure 7.8.1	Cantilever	89
43. Figure 7.9.1	ATS 24 Waveform	94
44. Figure 7.9.2	ATS 24 Waveform Zoomed	95
45. Figure 7.9.3	ATS24 Flow-volume curve	96
46. Figure 7.9.4	Waveform comparisons	99
47. Figure 7.9.5	Time domain variations of Impulse 1	100
48. Figure 7.9.6	Time domain variations of Impulse 2	101

49. Figure 7.9.7	Varying Sampling Frequencies	102
50. Figure 7.9.8	Varying Sampling Frequencies Zoomed	103
51. Figure 7.9.9	Activation technique applied to Impulse 1	104
52. Figure 7.9.10	Pre-set WW [®] with the inserted syringe needle	105
53. Figure 7.9.11	Modified Sectioned Whistle Watch [®] , which illustrates where the pressure was measured.	105
54. Figure 8.1.1	Constricted Step length effect on a restricted reed	108
55. Figure 8.1.2	Expanding Step length effect on a restricted reed	109
56. Figure 8.1.3	Contracting section of Geometry Nozzle	110
57. Figure 8.2.1	Restricted Reed	115
58. Figure 8.2.2	Free Reed	116
59. Figure 8.4.1	Activation pressure correlation	119
60. Figure 8.4.2	Activation pressure for 175 μ m free reed	122
61. Figure 8.5.1	Time domain dependence	125
62. Figure 8.5.2	Time domain dependence	126
63. Figure 8.5.3	Time domain dependence	127
64. Figure 8.5.4	Time domain dependence	128
65. Figure 8.5.5	Integral comparisons for free reed	130
66. Figure 8.5.6	Integral comparisons for restricted reed	131
67. Figure 8.5.7	Idogowa's Artificial Clarinet Blower	133
68. Figure 8.5.8	Idogowa's Detailed Blowing Chamber	133
69. Figure 8.6.1	Time domain dependence for Impulse I	136
70. Figure 8.6.2	Time domain dependence for Impulse II	137
71. Figure 8.6.3	Critical blowing pressure	138
72. Figure 8.6.4	Transition zone comparison	142

73. Figure 8.6.5	Normalised Transition Zone comparison	143
74. Figure 8.6.6	Oscillatory effects	144
75. Figure 8.6.7	Oscillatory effects zoomed	145

LIST OF TABLES

		Page	
1.	Table 7.9.1	Rise and Dwell Times	100
2.	Table 7.9.2	Whistle insertion into pre-set WW [®] sequence	104
3.	Table 8.3.1	t-Test comparison for Sidedness	117
4.	Table 8.4.1	Activation pressure vs Reed width	117
5.	Table 8.4.2	Influence of reed thickness on P_{RA}	122
6.	Table 8.4.3	Summary of reed geometry results	124

In Chapter 5, a parallel is drawn between the Whistle Watch and woodwind instruments, with a literature review of the research and development work which is relevant to the study / thesis.

In Chapter 6, theoretical and analytical models are developed to describe the operation of the whistle.

In Chapter 7, the methods developed to address certain aspects of the whistle and the Whistle Watch are described in detail.

In Chapter 8, experimental results and observations pertaining to the methods employed in Chapter 7 is reviewed and discussed, with subsequent conclusions.

In Chapter 9, the relevance of the results obtained in this thesis is discussed, as well as recommendations for future research.

CHAPTER 2

PHYSIOLOGY OF THE RESPIRATORY SYSTEM

The American Thoracic Society (ATS) defines Peak Expiratory Flow (PEF) as “the maximum flow achieved during an expiration delivered with maximal force starting from the level of maximal lung inflation.” The European Respiratory Society (ERS) agrees with this definition, but adds, “The value obtained may differ depending upon the physical properties of the instrument used to measure it” [44]. To fully understand the measurement and factors influencing PEF, it is necessary to review some basic respiratory physiology. This chapter will first describe the physiology of PEF and then pointing out various factors influencing it, where these factors will be categorised into physiological and patho-physiological.

2.1 The bronchial tree

The main components of the respiratory system are the nose, pharynx, larynx, trachea, bronchi and lungs. Below the sternum, the trachea divides into two bronchi, which form the secondary airways. Each airway bifurcates in a dichotomous manner into two smaller branches (Figure 2.1.1) [19].

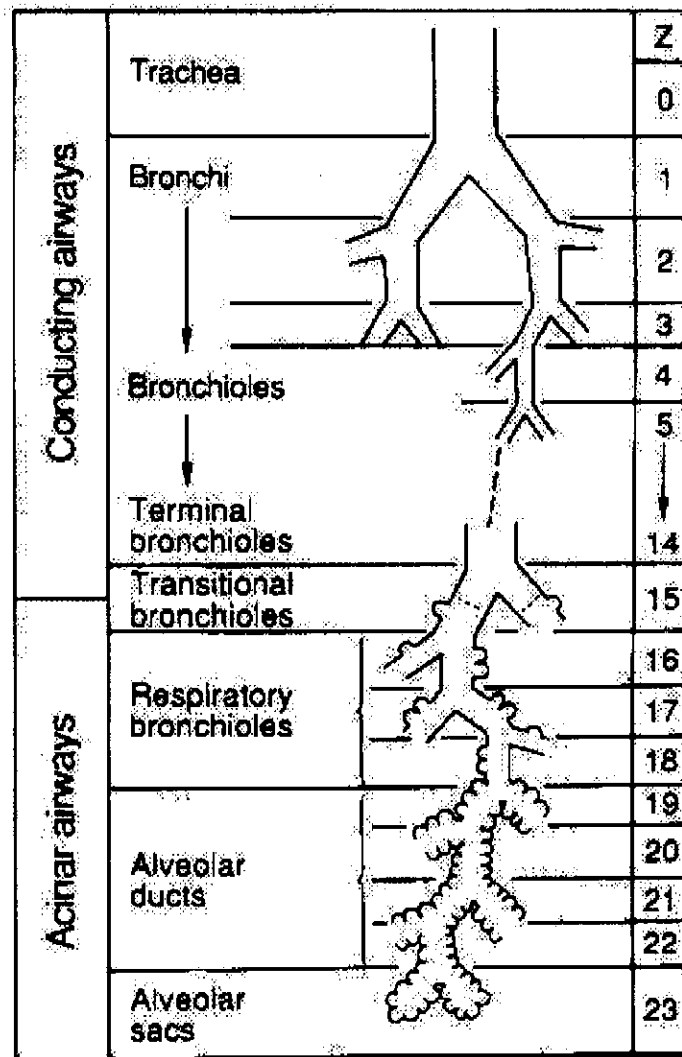


FIGURE 2.1.1
The Bronchial Tree of the Respiratory System [19]

There are differences in the diameter and length of the two daughter branches (the right and left bronchi), but each daughter branch, as a rule, is smaller than the parent. This results in the airways to become progressively narrower as it moves toward the gas-exchanging areas of the lung. While each daughter branch has a narrower diameter than the parent airway, the total cross-sectional diameter of the daughter airways exceeds that of the parent. Thus, as the airway extends, the total cross-sectional area increases markedly (Figure 2.1.2) [19].

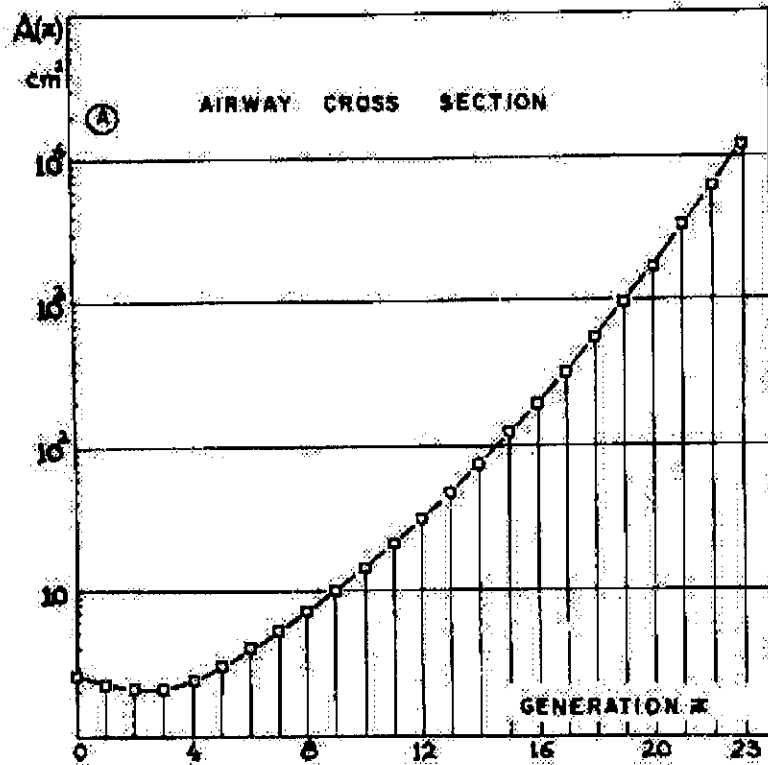


FIGURE 2.1.2
Lung Development [19]

Alveoli are microscopic bag-like structures, approximately 0.3 mm in diameter, which form the endings of the branches of the bronchial tree. They are densely supplied with capillary arteries and veins and are the section of the lung where atmospheric and blood gas exchange occurs through diffusion. The overall exchange of gases between the atmosphere and blood is called respiration.

2.2 Respiratory Mechanics

Pulmonary ventilation is the process by which gases are exchanged between the atmosphere and lung alveoli, and is subdivided into inspiration and expiration. To facilitate in the understanding of these two processes, certain descriptive terms need to be defined. Figure 2.2.1 shows a slow spirogram (a device which measures

expiratory volume with respect to time) and the subdivisions of lung gas volumes [10].

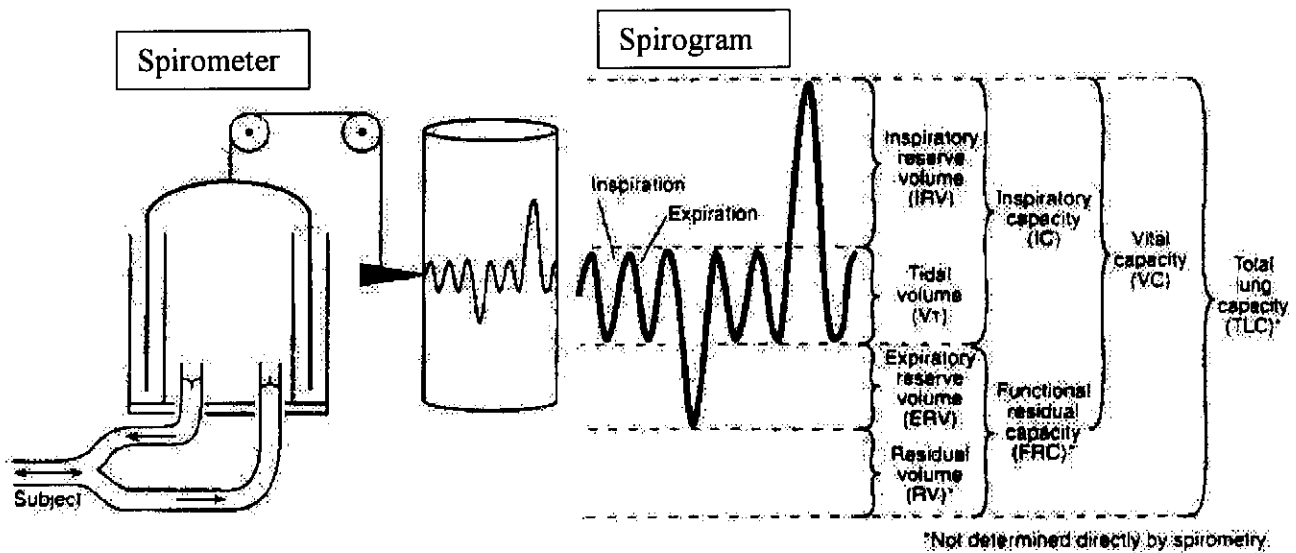


FIGURE 2.2.1
Spirogram [10]

Tidal volume (V_T) is the volume of any given breath: It may vary from a few hundred cubic millimetres at rest, to almost vital capacity during vigorous exercise. Vital capacity (VC) is the maximum volume of gas which can be expired after full (maximal) inspiration, representing the absolute upper limit of tidal volume. Inspiratory reserve volume (IRV) is the maximum volume of air which can be inspired from the end-tidal inspiratory level, whereas expiratory reserve volume (ERV) is the maximum volume of air which can be expired from the end-tidal expiratory level. Residual volume (RV) is the gas volume remaining in the lungs and airways after maximum expiration. Total lung capacity (TLC) is the total volume of gas in the lungs and airways following a maximum inspiration (cannot be determined with a Spirometer). Functional residual capacity (FRC) is the gas volume in the lungs

and airways at the end of a normal, relaxed tidal breath; it is the sum of ERV and RV. Inspiratory capacity (IC) is the gas volume which can be maximally inspired from the tidal end-expiratory level; it is the sum of IRV and V_T .

Lung volumes are directly related to body size, varying with the cube of height. Once an individual is full-grown, there is an independent variation with age, residual volume increases, the vital capacity decreases, and the total lung capacity remains virtually constant with increasing age.

2.2.1 Inspiration

For inspiration, the lungs must be expanded, which increases lung volume and thus decreases the intrapulmonic pressure (P_{pul}), as dictated by Boyle's Law of ideal gases. The first step is to increase the volume of the thorax, because the lungs follow the movement of the thorax. An increase in thorax volume involves contraction of the principal inspiratory muscles, i.e. the diaphragm and external intercostals. The diaphragm, the most important muscle for inspiration, is a dome-shaped skeletal muscle that forms the floor of the thoracic cavity. Contraction of the diaphragm causes it to flatten, lowering its' dome, which increases the vertical dimension of the thoracic cavity. This movement accounts for about 75 percent of the air entering the lungs during inspiration [4]. The anterior-posterior diameter of the thoracic cavity is increased by contraction of the external intercostal muscles, thus pulling the ribs upward and pushing the thorax forward (Figure 2.2.2)[4].

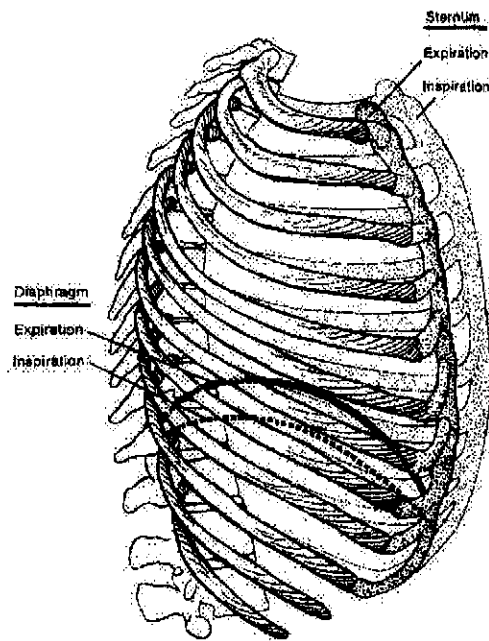


FIGURE 2.2.2
Inspiratory Thorax Movement [4]

The thoracic chamber is lined with a thin layer called the parietal pleura, whilst the lungs are encapsulated in a similar layer, the visceral pleura. The parietal and visceral pleurae are strongly attached to each other owing to surface tension created by their moist adjoining surfaces. As the thoracic cavity expands during inspiration the parietal pleura (lining the cavity) is pulled in all directions, and the visceral pleura and lungs are pulled along with it. As the volume of the lungs increases, the intrapulmonary pressure (P_{pul}) drops. A pressure gradient is thus established between the atmosphere and the alveoli. Air rushes from the atmosphere into the lungs and will continue to move into the lungs as long as the pressure difference is maintained. This constitutes the inspiratory phase of the breathing cycle.

2.2.2 Static Pressure-Volume Relationship (Gauge Pressure)

Expiration is a passive process, which harnesses the potential energy stored in the elastic structure of the lungs and chest wall to move the air from the alveoli to the

atmosphere. Understanding the interaction of the lung and chest wall is thus a prerequisite for a thorough understanding of the expiration mechanism.

During relaxed breathing, the pressure between the two pleural layers (intrapleural pressure (P_{pl})) is always sub-atmospheric. When the respiratory muscles are relaxed and the airways are open, the volume of gas within the lungs is determined by the equilibrium between the inwardly directed elastic recoil of the lung and the outwardly directed elastic recoil of the chest wall. In such a relaxed static state, alveolar pressure and pressure at the chest wall surface (equal ambient atmospheric pressure) are both zero. The pleural pressure is about $-5 \text{ cmH}_2\text{O}$, and is the result of opposing forces between the lung and the chest wall.

Inflating or deflating the respiratory system from equilibrium volume (FRC), and plotting the resulting volume against the simultaneous alveolar pressure during relaxation with a closed airway describes the pressure-volume curve of the total respiratory system (Figure 2.2.3)[2].

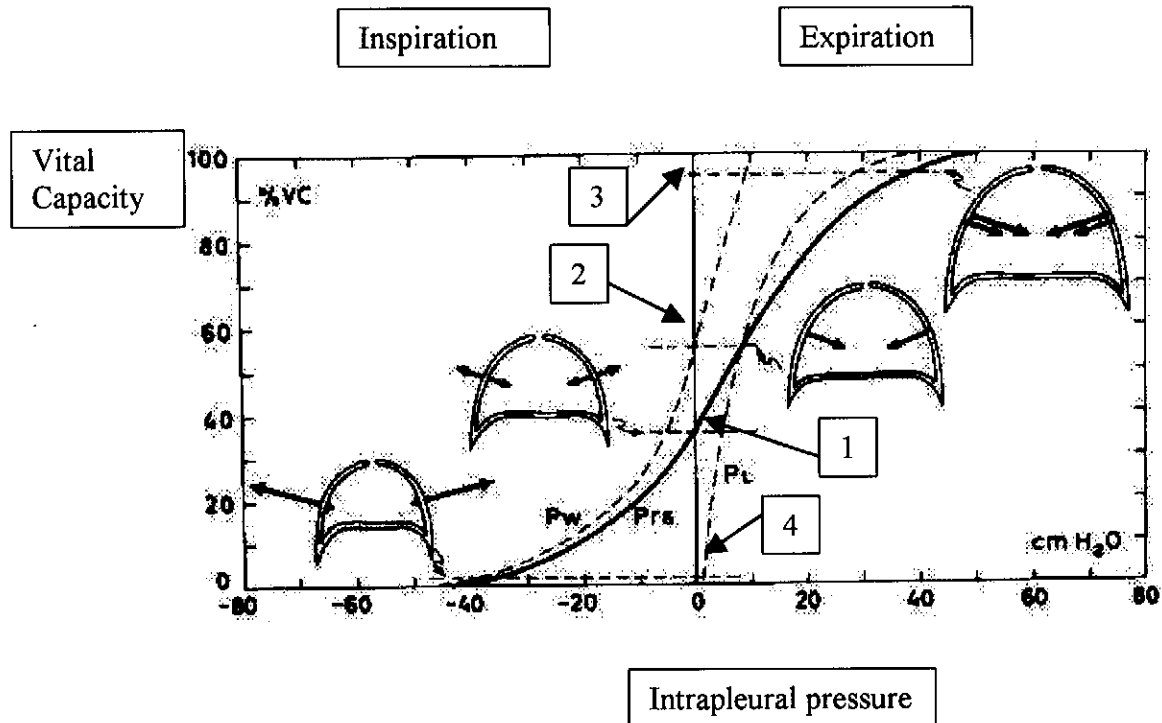


FIGURE 2.2.3

Static pressure-volume curves of lung (P_L), chest wall (P_w), and total respiratory system (P_{RS}) during relaxation, sitting. Large arrows indicate static forces of lung and chest wall. Vital Capacity (VC) is the volume of air which can be forcefully expired. Indicators 1-4 are discussed in text. [2]

The static pressure-volume curve is sigmoidal, crossing the zero pressure axes at FRC (approximately 35% of VC). The total respiratory system pressure-volume curve comprises of the sum of two pressure-volume curves, namely those of the chest wall and of the lung. These curves are obtained by plotting lung volume against the difference between pleural pressure and chest wall surface pressure (trans-thoracic pressure (P_w)), and the difference between pleural and alveolar pressures (transpulmonary pressure (P_L)). Interpreting these curves is fundamental in understanding the mechanics of the respiratory system.

The following refers to the annotations of Figure 2.2.3

1. This point indicates FRC, where the inward lung recoil (P_L) is exactly balanced by the outward chest wall recoil (P_w); both are diagrammed as vectors.
2. The chest wall curve crosses the y-axis, at this volume the chest wall is at its unstressed neutral volume and the sub-atmospheric pleural pressure is completely due to lung recoil.
3. Both lung and chest wall are being distended, at maximum volume, and their recoil forces become additive. Over this part of the curve the respiratory system is becomes stiffer, owing mostly to the increasing stiffness of the lungs.
4. At this point the inward lung recoil is minimal, while the outwardly directed chest wall recoil is a maximum. Over this volume range the system is also becoming very stiff, but in this case due to increasing stiffness of the chest wall, and less so from the lung wall.

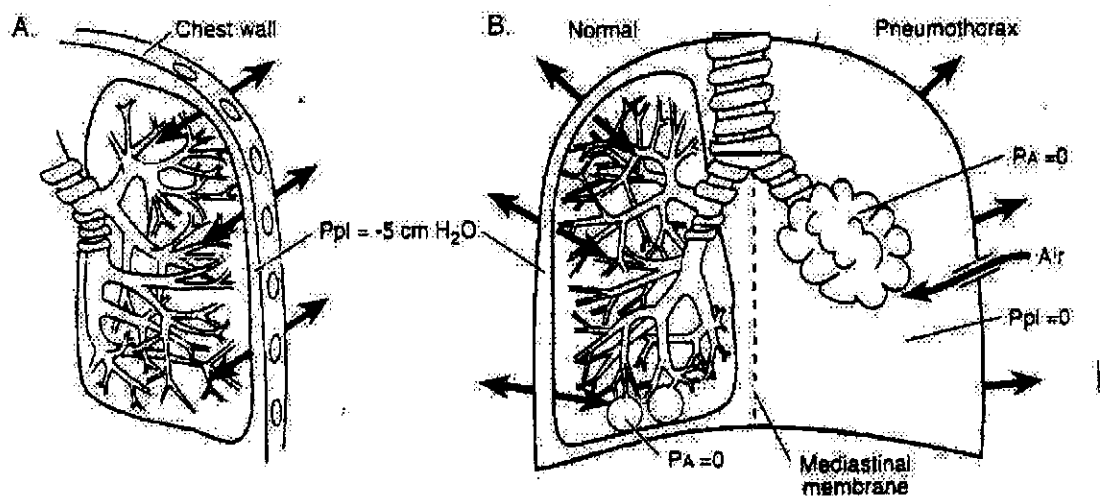


FIGURE 2.2.4
Pneumothorax [4]

If the intrapleural pressure should become zero, for example through a puncture of the parietal or visceral pleura, thereby connecting the intrapleural space with the atmosphere, a patho-physiological condition, called pneumothorax, is created. Ventilation is no longer possible, due to the loss of traction between the pleurae. As a result of the inward elastic recoil the lungs will collapse (Figure 2.2.4) [4].

2.2.3 Expiration (Absolute Pressure)

During expiration the pressure gradient is reversed (in comparison with inspiration) so that intrapulmonary pressure (P_{pul}) is greater than atmospheric pressure (P_{atm}). At rest, expiration is a passive process, since no muscular contractions are involved, it is dependent on the elastic recoil of the lungs and the chest wall (Figure 2.2.3) [2]. Expiration starts when the inspiratory muscles relax; the ribs move downward, and the diaphragm dome moves elastically upward. The result is a decrease in the vertical and anterior-posterior dimensions of the thoracic cavity, and a return to the equilibrium size. At the same time elastic basement membranes of the alveoli and elastic fibres in bronchioles and alveolar ducts recoil, causing a decrease in the lung volume. Intrapulmonary pressure (P_{pul}) increases and air moves from the area of higher pressure in the alveoli, to the area of lower pressure in the atmosphere.

During exercise or voluntary hyperventilation expiration becomes an active process, whereby the abdominal and internal intercostals, contract. Contraction of the abdominal muscles move the inferior ribs downward and compresses the abdominal viscera, thus forcing the diaphragm upward. Contraction of the internal intercostals, which run downward and backward between adjacent ribs, moves the ribs downward.

2.3 Peak expiratory flow (PEF)

Measurement of PEF requires the subject to be either in the standing or sitting position. The subject then takes a maximal inspiration (i.e. to the total lung capacity (TLC)) and then exhales as hard and fast as possible. An example of a flow-time waveform is illustrated in Figure 2.3.1.

Typical Flow-Time Waveform

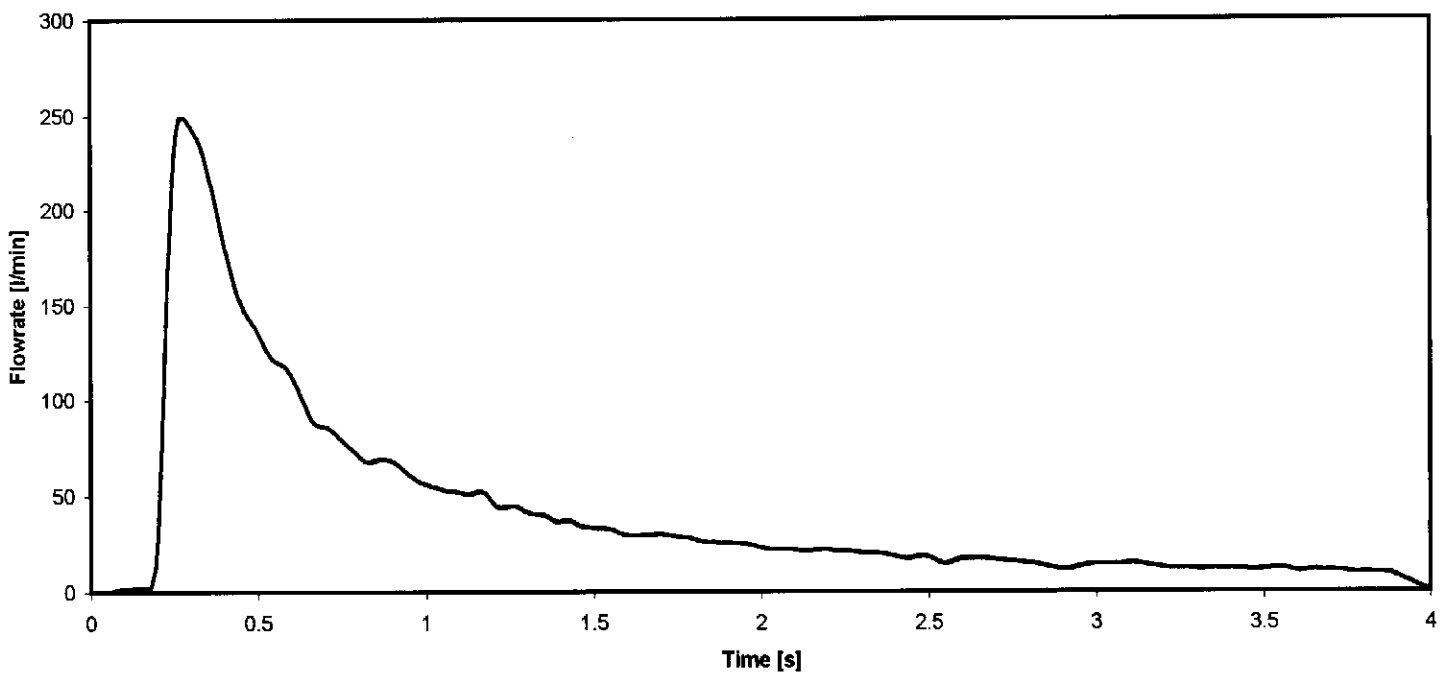


FIGURE 2.3.1
A typical Flow-time waveform

Flow-time waveforms are characterized in terms of the rise time (i.e. the time from 10% to 90% of PEF) and the dwell time (i.e. the duration of the flow in excess of 90% of PEF). In a group of healthy students it was found that the rise time varies from 23 – 84 ms with an average of 41 ms [45]. Dwell time is generally assumed to be in the order of 10 ms.

2.3.1 PEF: Is it prevalent?

This is a legitimate question, and one which has been debated extensively; although not as fiercely contested as the question concerning maximal exercise capacity or maximal oxygen consumption ($\text{VO}_{2\text{max}}$) [46]. Both these debated topics are a result of the absence of “plateau” values which, in the case of PEF, may be described by the work of Hyatt [42] which is summarized in Figure 2.3.2.

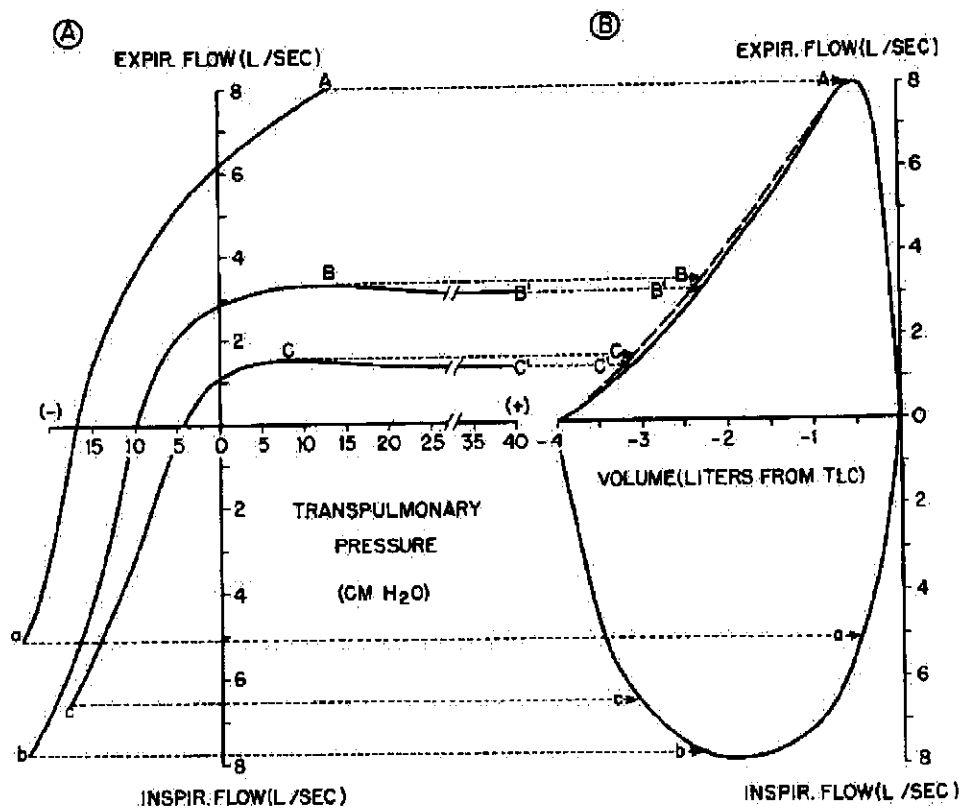


FIGURE 2.3.2
Iso-volumetric Pressure Flow Curve [42]

Figure 2.3.2 was structured from measurement of pressure and flow at pre-defined, fixed lung volumes. (Figure 2.3.2 (a) is therefore the “Iso-volume pressure-flow” curve) At the lower lung volumes (curves marked by B and C) there is clearly a plateau in the V_E values. This means that a certain maximal flow is reached which

cannot be increased by greater effort (increasing the trans-pulmonary pressure through increased muscle contraction).

Curve A, representing the highest volume, however does not exhibit a plateau phase. This is where the argument arises that PEF may not be the maximal possible flow. This is however, still a well-debated topic with no definite conclusions. The possible physiological and pathological factors, which may influence the PEF will be briefly discussed.

2.3.2 Physiological Factors which effect Peak Expiratory Flow (PEF)

The following physiological factors influence PEF to some extent; consequently they are important during measurement and monitoring of PEF:

1. The dimensions of large intra- and extra-thoracic airways, where larger airways have less resistance resulting in higher PEF. The airway sizes are dependent on:
 - a.) Lung volume (which increases during human development), where larger lung volume would result in a larger airway cross sectional area and vice versa.
 - b.) Trans-bronchial pressure could reduce or increase cross sectional area through increased and decreased magnitude respectively. This varying diameter process is interactive as the elastic properties of the lung and the compliance of the airways provide the resistance towards the varying pressure.
 - c.) Flexion or extension of the neck is a contributing factor to the above-mentioned two phenomena.

2. The force generated by the expiratory muscles (abdominal muscles contribute extensively), where a greater force results in higher driving intra-pleural pressures with subsequent higher PEF. Maximum possible force available for expiration is a function of the muscle characteristics, where the force-velocity relationship of muscles is dependent on cross-bridge coupling in the muscle fibres. The latter can be determined through lung inflation, as a greater inflation would result in increased cross-bridge coupling producing a higher attainable force. This effect is optimised for a certain fibre length, and thus a specific lung volume.

3. The “volume history” of the lung. Prolonged extension, for example through a breath held manoeuvre of muscle fibres, result in muscle adaptation with a corresponding decrease in available contraction force.

4. Expiratory muscles may be trained for higher attainable maximum expiratory force, with a subsequent increase in PEF.

5. General observations:

- a.) Males have higher PEF's than females. (Remains the same up to ~15 years in boys and girls. It seems as if the greater muscular power of boys is off set by slightly narrower airways.) Through analysis of epidemiological data a variety of PEF prediction equations exist, which is predetermined by population demographics and descent. There are no prediction equations specifically for the South African population and we therefore use those derived by Schoenberg [48] et al due to the similarities in South African and European

population sample. Schoenberg defined for example, the following equation for white males at age 18 and higher: $\ln(\text{PEF}) = -3.817 + 0.034996 \cdot H$, where PEF is in l-s and H is the subject length in cm.

- b.) Expiratory muscle strength and thus PEF declines slightly with ageing.
- c.) Body position (upright, supine, etc.). When mechanically modelled, the abdomen can be viewed as a container filled with liquid. The viscera float in the peritoneal liquid and the pressure difference between any two levels is given by the difference in height times the specific gravity of the liquid.

In the upright posture and with the respiratory muscles in a relaxed state, the abdomen behaves as a container in which part of its lateral wall is distensible. The pressure in the upper part of such a container is negative. Since the top of this container is also distensible, it will be pulled downward by the gravitational effect of the abdomen contents. However, the hydrostatic pleural forces provide a lifting force in the opposite direction thus preventing any downward movement. The level at which the abdominal pressure is equal to ambient pressure, the 'zero level' [23], depends on the equilibrium among the elastic forces of the abdominal wall, diaphragm, rib cage and lung and the gravitational force of the abdominal contents. It can be estimated that in the erect posture, the zero level at the end of a normal expiration (and at the resting volume of the respiratory system), is about 3 to 4 cm beneath the diaphragmatic dome [23]. The pressure just beneath the dome of the diaphragm is approximately the same as at the lung surface. This suggests that the diaphragm is nearly relaxed. Furthermore, the diaphragm appears not to be under any appreciable elastic tension, the elastic recoil of the lung is being

counterbalanced (at least at the dome of the diaphragm), by the hydrostatic pressure of the abdominal content.

When the subject is in a supine position, the zero level corresponds to the ventral wall of the abdomen. The diaphragm is then distended by the weight of the abdominal contents. It seems probable that the diaphragm balances in this position with its own elasticity the gravitational forces of the abdominal contents. The zero level in the prone position corresponds to the dorsal wall of the abdomen, and when the subject is lying on one side, it is midway between the two sides. The zero level is expected to shift with changes in lung volume, which may also be different for the upright and supine postures.

This shift in the zero level is the main mechanism responsible for the changes in the volume-pressure curve of the respiratory system with posture.

The largest variation in lung function parameters, due to posture, is observed in the resting end-expiratory volume (FRC). The increase in FRC when the subject is in the sitting position, with his arms supported, reflects the influence of the weight and position of the shoulder girdle. As the subject leans forward, the zero level of the abdomen moves downward, since the lower part of the abdomen also becomes flexible. This effect is further exacerbated in the hands-and-knees position, when the zero level is presumably near the ventral wall of a relaxed abdomen. When the prone posture is assumed, the ventral abdominal wall is supported from the outside; the zero level thus moves up

toward the dorsal wall of the abdomen and the FRC decreases. The FRC is smallest in the supine posture (Figure 2.3.3) [23].

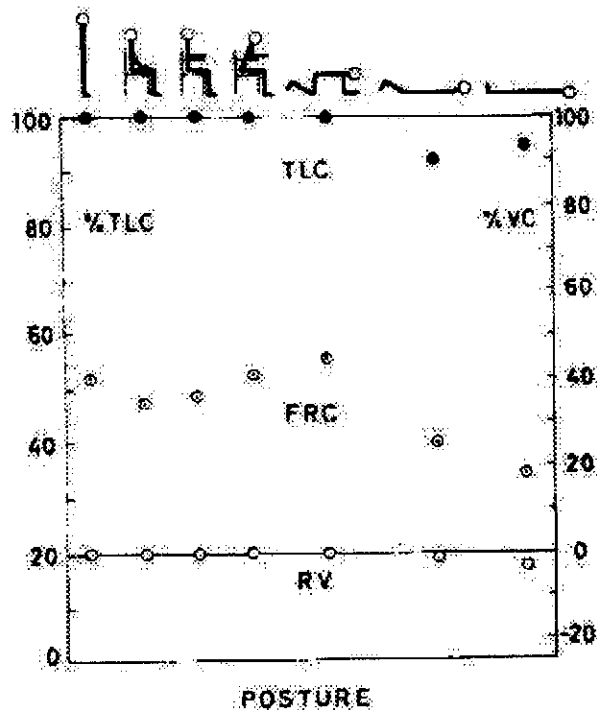


FIGURE 2.3.3
Posture Influencing FRC [23]

PEF is similarly influenced by posture, as FRC. This is because PEF is dependent on VC, which in turn is dependent on FRC, as seen in Figure 2.3.3. If FRC decreases VC decreases which results in a decreased PEF for different postures.

2.3.3 Pathological factors which limit Peak Expiratory Flow

1. The most common influencing factor is a variation in the structure and / or function of the intra-thoracic airways, which precipitates in the form of airway obstruction. Ventilation and breathing, can be greatly impaired by this. Airflow obstruction occurs in association with one or more of three variables:

- diminished elastic recoil of the lungs (i.e. emphysema)

- increased airway resistance (i.e. small airway disease), which may occur in association with long-standing chronic bronchitis
- increased bronchomotor tone as in asthma.

The official definition of asthma (in functional terms) is: “a widespread narrowing of peripheral airways in the lungs, varying in severity over short periods of time either spontaneously or as a result of treatment”. [2] The diagnosis of asthma is not a complex matter and can easily be made with the appropriate physiological measurements. Although airway obstruction is the most obvious physiological disturbance in asthma, the threat to the patient derives from the resulting interference with gas exchange, particularly the development of hypoxemia. The latter is a condition where the ventilation/perfusion (capillary blood supply) ratio is abnormally low, causing the body to enter a stage of shock. Ventilatory control is usually normal in mild asthma. In more severe asthma, however, control may be disturbed: usually alveolar hyperventilation occurs, but in critically severe asthma or some cases of chronic, severe asthma, the patient may experience carbon dioxide retention. Respiratory muscle fatigue and exhaustion may be important factors in ventilatory failure in chronic severe asthma. Hypoxemia has a significant effect on pulmonary circulation and furthermore, treatment aimed at relieving airflow obstruction may also alter pulmonary circulation; this may further adverse effects on arterial saturation. It is therefore justified to follow a preventative course of action towards asthma rather than to depend on the pharmacological treatment of symptoms.

This preventative course of action is implemented through the measurement of defining pulmonary parameters, which have been developed through the years, which quantifies the normality of the lungs.

If frequently measured, a decreasing PEF, may indicate an approaching asthmatic incidence. Due to the obstructive airway nature of the condition, PEF decreases as asthma severity increases. It is thus possible, through regular monitoring of PEF to act preventatively and prevent an asthma attack.

2. Obstruction in the extra-thoracic airways would result in increased airway resistance with a subsequent decrease in PEF.

3. Disease states which limits expansion or which may effect the respiratory muscle functions such a COPD and emphysema patients decrease PEF.

4. Restrictive diseases such as restrictive lung disease causes reduced lung volumes, due to intense elastic recoil of the bronchi. Except in extreme cases, the elastic load in itself does not appear to generate major symptoms at rest, implying acclimatisation to the higher elastic load. A common feature of severe restrictive lung disease is tachypnoea (rapid breathing); this is largely due to the aim of the respiratory control mechanisms, namely to minimise the work of breathing. [20]

The severity of the mentioned obstructive (1) and restrictive (4) conditions is quantified in a mathematical expression of compliance.

$$C_L = \frac{\Delta V}{\Delta P} = \frac{[l]}{[cmH_2O]}$$

Equation 2.3.3.1

This is a quantitative value of the level of effort at which the lung is expanded. This is graphically depicted in Figure 2.3.4 [2].

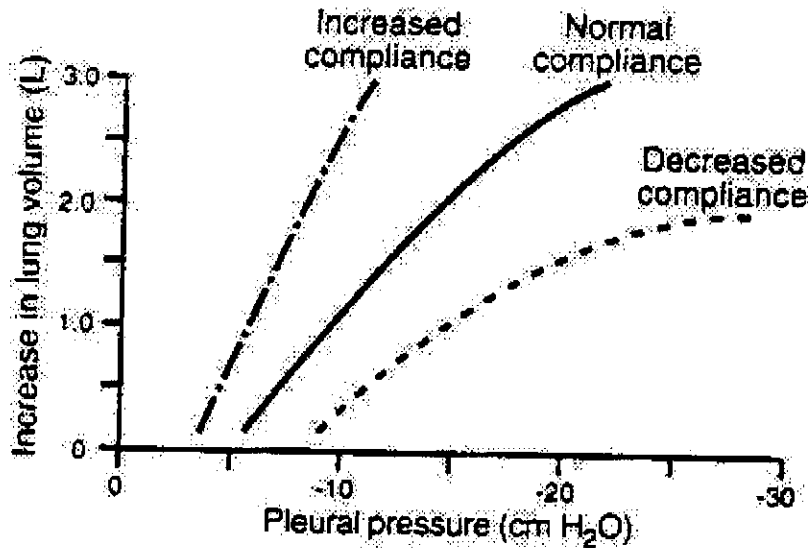


FIGURE 2.3.4
Lung Compliance [2]

2.3.4 Models describing the determinants of maximal flow

Airway obstruction is a physiological condition, which cannot be prevented but, as yet, is not fully understood or defined.

During the process of active expiration, research has indicated that the peak expiratory flow rate (PEF), is effort independent. It is normally achieved within 20% of the forced expiratory vital capacity [1, 2, 3]. The forced expiratory flow limitation may be explained with a schematic (Figure 2.3.5)[2].

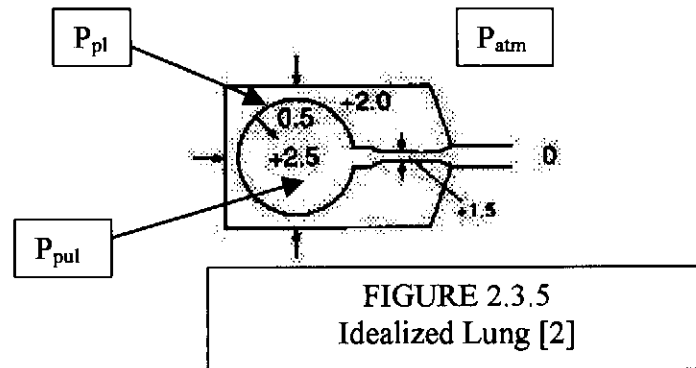


Figure 2.3.5 demonstrates an idealised thorax, consisting of a circle (an alveolar element) lying within a box (the chest wall) and connected to the atmosphere by a tube (the elastic airways). During forceful expiration the expiratory muscles are actively producing a positive pressure of 2 kPa, surrounding the alveoli and airways. The alveoli also possesses elastic recoil, thus resulting in an intrapulmonic pressure of + 2.5 kPa. Due to the resistance to airflow down the airways, there are pressure losses along a gradient, from alveolus to the mouth. At some point the pressure within the airways falls to a level where it is equal to the surrounding intrapleural pressure, this is called the equal pressure point (EPP). Airways downstream from this equal pressure point may compress and close, as the surrounding intrapleural pressure exceeds the pressure within them. The degree of narrowing depends on the stiffness of the airways. Increasing expiratory muscle force, in an effort to overcome the obstruction, will indeed raise the alveolar and therefore the intra-luminal airway pressures. But it will raise the surrounding intrapleural pressure by an equal amount and the obstruction will therefore not be overcome. Thus, in conditions where there is a flow-limiting segment, the driving pressure for expiratory flow becomes the difference between intrapulmonary and intra-luminal pressure at the equal pressure point; the latter can be considered as equivalent to intrapleural pressure.

Therefore, driving pressure for maximum flow = $P_{pul} - P_{pl}$, which in turn is equal to the elastic recoil pressure of the lung (P_L). The equal pressure point results in a maximum achievable expiratory rate and is captured within the laws of gas dynamics.

Mead [3], formulated two hypotheses concerning the limitation of maximum flow. They are:

1. Elastic recoil of the lungs

He postulated that the condition of maximum forced expiratory flow rate may occur, due to the elastic recoil nature of the airways, causing the bronchi to collapse completely beyond the equal pressure point. The obstruction would result in no further airflow, but the intra-luminal pressure would increase from the static to the stagnation pressure as the kinetic pressure head is reduced. Although the increasing pressure can forcefully open the bronchi, establishing airflow again, this would result in an intra-luminal pressure drop, which would again close the bronchi. The above sequence of events results in a pulsated flow distal to the equal pressure point. The lower the frequency of pulsation, the more restricted the maximum expiratory flow rate.

2. Resistance of upstream airways

Flow in a tube can only be sustained if a pressure gradient exists. Therefore, the flow rate is directly proportional to the pressure gradient and is mathematically related the flow resistance:

$$R = \frac{\Delta P}{Q}$$

Equation 2.3.4.1

Due to the low flow rate out of the alveoli, the Reynolds number (Re) is below 2300, indicating laminar flow.

$$\text{Re} = \frac{\rho V d}{\mu} \leq 2300$$

Equation 2.3.4.2

It has been shown that for laminar flow in a tube, the tube's flow resistance is.

[11]

$$R = \frac{\mu \cdot L}{2 \cdot \pi \cdot D^4}$$

Equation 2.3.4.3

Substituting Equation 2.3.4.3 into Equation 2.3.4.1 produces an equation which dictates the rate of flow in the bronchi for a given pressure head as a function of the bronchi's structural parameters. Therefore,

$$Q = \frac{\Delta P \cdot 2 \cdot \pi \cdot D^4}{\mu \cdot L}$$

Equation 2.3.4.4

During a forced expiratory effort, the pressure head is at a maximum (the elastic recoil of alveoli as described), and the diameter has decreased due to bronchiole compression. This reduced diameter affects the flow rate to the fourth power; however, due to the maximum pressure head, a peak expiratory flow rate (PEF) is still produced.

Dawson and Elloit [27], also formulated a hypothesis concerning the mechanism which results in a maximum expiratory flow. They formulated it as follows:

1. Maximum wave speed

The mechanism for flow limitation in a compliant tube is an example of the more general gas dynamic phenomenon of flow limitation at wave speed in a pipe. The speed (c) of a pressure wave in a compliant tube, depends on the density (ρ) of the fluid and the specific compliance of the tube $(1/A)(dA/dP)$, where dA/dP is the rate of change of tube area with pressure. Therefore,

$$c = \frac{1}{\sqrt{\left(\frac{\rho}{A}\right) \cdot \left(\frac{dA}{dP}\right)}} \quad \text{Equation 2.3.4.5}$$

They recognised that maximum flow through a compliant tube is the flow at which flow speed equals wave speed at some point in the tube. The limitation to flow through a compliant tube is analogous to the limitation on the flow of a compressible gas through a nozzle travelling at wave speed. As flow rate is the product of gas speed and tube area, the maximum flow rate derived from Equation 2.3.4.5 is characterised by:

$$\dot{V}_{\max} = \frac{A}{\sqrt{\left(\frac{\rho}{A}\right) \cdot \left(\frac{dA}{dP}\right)}} \quad \text{Equation 2.3.4.6}$$

The only fluid property that appears on the right side of Equation 2.3.4.6 is the fluid density. Flows are allowed for, which the local gas velocity is less than the local wave speed and thus sub-sonic, everywhere in the bronchial tree.

Maximum flow is the lowest flow for which gas velocity equals wave speed at some point in the bronchial tree. The point at which this occurs is the site of flow limitation, or the critical point. In some instances, the critical point is in the trachea, while in others, the critical point appears at the lowest flow in one

of the parallel pathways in a higher generation of the bronchial tree. Flow through these critical pathways are limited by conditions at that critical point, but flow through the other non-critical pathways could increase until critical points occur in them. In all instances, the critical point is dependent on the mechanical properties of the lungs and the range of lung volumes.

These hypotheses lead to important conclusions:

1. Forced expiratory flow is independent of expiratory effort, if total lung volume is more than 60 % of the vital capacity [1, 2, 3]
2. The effective driving pressure for expiratory flow is provided by the elastic recoil of the lung.
3. Any condition which decreases the elasticity of the lung, will result in a decreased pressure head and therefore a decreased PEF.
4. Decreasing the elastic strength of the bronchiole will result in a repositioning of the equal pressure point closer to the alveoli, thereby increasing airway resistance and decreasing PEF.
5. Bronchomotor tonus plays a major role in PEF as it dictates bronchiole diameters, where the latter determines the bronchiole resistance, which has been shown to effect PEF severely.

CHAPTER 3

PEAK FLOW MEASUREMENT

Most of the mechanical peak flow meters commercially available today indirectly measure air flow employing the method of what has become known as “variable orifice measurement”. This chapter will give an overview of the historical development of mechanical peak flow meters and a brief description of the principle of operation.

3.1 Historical background in the development of the mechanical Peak Flow

Meters (PFM)

In 1942 Hadorn [12] attempted for the first time to use peak expiratory flow rate as a physiological index. He measured the flow rate of expiration by means of an aneroid manometer connected across an orifice. No provision was made for recording the maximum deflection of the manometer pointer, except projecting it by eye. Hadorn reported, flow rates in excess of 500 l.min^{-1} .

Wyss [13] used the same type of orifice as Hadorn, but replaced the aneroid manometer with a membrane manometer with a higher frequency response. He used an optical lever to record the pressure deflections photographically. These changes resulted in higher flow rates (720 l.min^{-1}) being registered.

A disadvantage of both methods was that a pressure drop across a simple orifice varies with the square of the flow rate. Therefore at higher flow rates, the pressure drop is considerably increased and in addition, the sensitivity of the method is less at low flow rates. Despite the disadvantage, the manometer was commercialised and

called the “pneumometer”. The pneumometer formed the basis of a number of studies describing the relationship between maximum forced expiratory flow rate and vital capacity [14].

The “pneumometer” was refined by using of a pneumotachograph (a flow resistance with a linear pressure drop/flow rate relationship). Pneumotachographs had the advantage of a low flow resistance [15, 16]. Hereafter, a simpler, more robust and portable instrument, was designed, which was called the “puffmeter” [17, 18]. It was similar in design to the “pneumometer”, but used a robust ceramic grinding wheel as a linear resistance and an aneroid manometer to measure differential pressure. The “puffmeter” had two disadvantages: 1) it had a relatively high resistance to airflow, of about $1 \text{ cm H}_2\text{O}/ \text{l}\cdot\text{min}^{-1}$, and 2) the maximum reading had to be recorded from a rapidly moving hand on a dial.

Wright [21] developed the first peak flow meter, which forms the basis of peak flow meters, as we know them today. The Wright Peak Flow Meter operated differently from its predecessors, with a “variable area orifice meter” concept as described by Wright [5] (Figure 3.1.1).

Wright’s device comprised of a metallic cylindrical cavity, and a radial inlet nozzle (1). A movable vane (2) was pivoted in the centre of the cylinder, fitting closely but without touching the cylinder. A fixed partition (3) extended from one side of the inlet orifice to within a short distance of the bush of the vane. A spiral spring (4) attached to one end of the spindle of the vane tended to rotate the latter towards the inlet orifice with a stop (5) preventing the said spindle from passing the orifice.

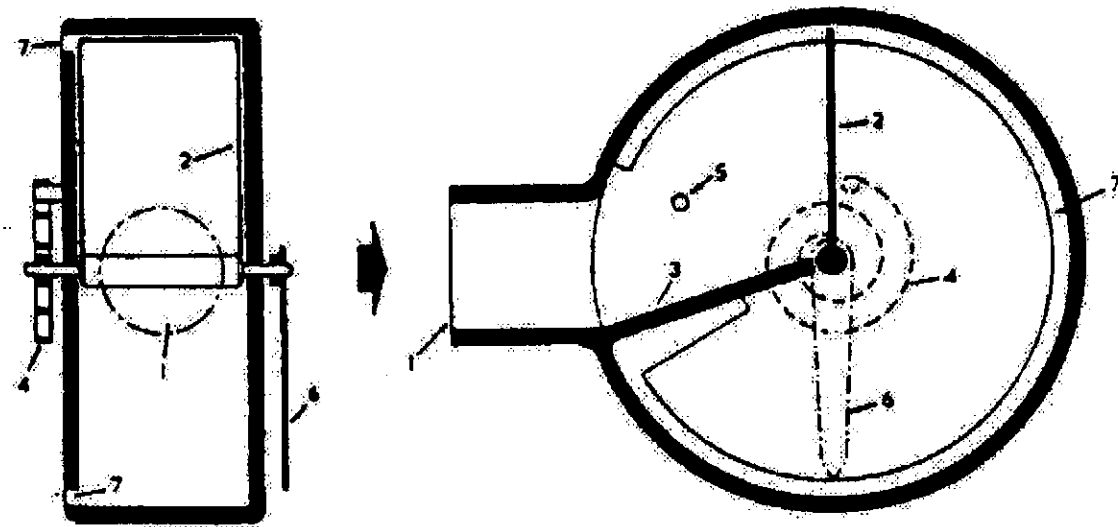


FIGURE 3.1.1
The Wright Peak Flow Meter [5]

A pointer (6) on the other end of the spindle indicated the position of the vane on a dial (not shown) and also served as a counterbalance to the spindle. An annular orifice (7) extended round the periphery of the cylinder at the back, from one side of the inlet orifice to the other side. When air was blown into the instrument it could not escape (except for a small amount, which leaked past the vane) until the vane had moved and uncovered part of the annular orifice. This continued until the uncovered area of the orifice was such that the pressure behind the vane was just sufficient to balance the force of the spring. At this point the vane would come to rest in a position that would indicate the flow rate. Wright's PFM was empirically calibrated and soon became the norm for determining peak expiratory flow rate.

In 1965 Wright refined and patented the above device, patenting what had become commercially known as the mini-Wright peak flow meter (Figure 3.1.2) [6]. The concept took the form of a plastic tubular (1) instrument, with a light spring-loaded

(7) piston (13) and a longitudinal slot (2) as variable orifice, in which a rider (14) was carried as a peak indicator.

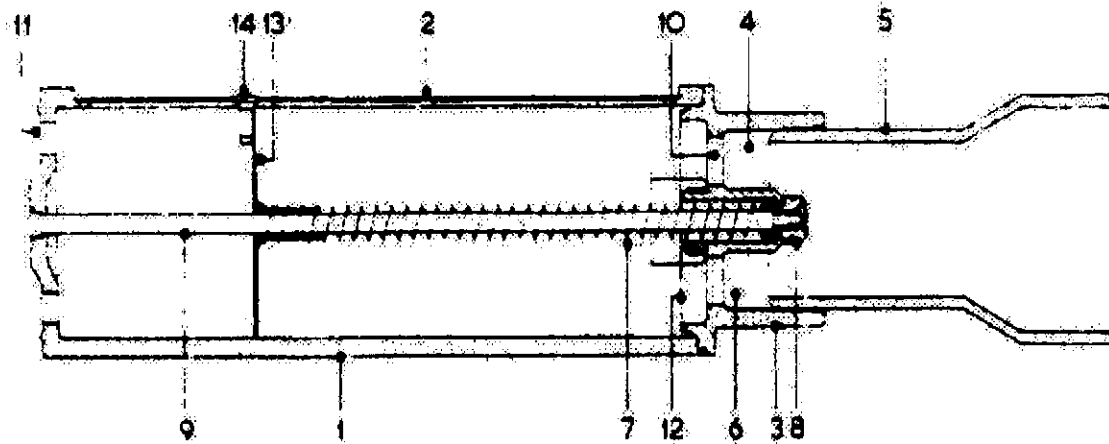


FIGURE 3.1.2
The mini Wright PFM [6]

Clinical tests indicated that readings from the mini-Wright correlated well with those from the first Wright peak-flow meter (PFM) [7] and that its use was acceptable to patients, particularly young children, because of its smaller size. Production of the Mini-Wright device commenced in 1977 and to date remains one of the most popular prescribed peak flow meters.

The only variation to the concept of a piston or vane moving against a variable resistance as a means to determine peak flow rate, was attempted in 1963, the so called “de Bono Whistle” [26]. This was a tube with a longitudinal slot and with a whistle at the end. It fitted inside a standard cardboard mouthpiece, and the length of the uncovered slot was adjusted until the patient could only just activate the whistle. The whistle used in this design belonged to the class of aerodynamic whistles [49]. A major drawback of this whistle class is the absence of a discrete activation point. The

latter is a result of the sonification intensity being dependent on flow rate. Observing audibility was difficult at the end of the scale, producing inaccurate measurements. In addition the evaluation had to be repeated several times, and severe pulmonary patients could only produce one peak expiration.

3.2 Present technology available in Peak Flow Meters

The usefulness of lung function measurements after the diagnosis of asthma and during the continued treatment thereof is increasingly being recognised. Portable and inexpensive peak flow meters are readily available and may be used by the patient at home. A typical Flow-volume curve to evaluate lung function and the accompanying drop in PEF is illustrated in Figure 3.2.1 [2].

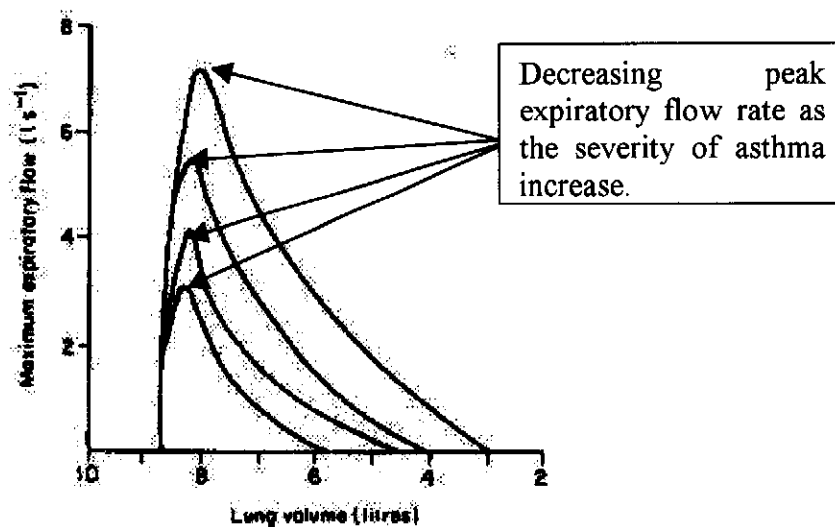


FIGURE 3.2.1
The effect of asthma on PEF [2]

Daily monitoring of PEF may allow patients to respond earlier to signs of deterioration, encourage patients to adhere to recommended therapy and facilitate

review of management by the doctor. Environments or activities, that worsen asthma symptoms, may be identified by daily PEF measurements.

Although the measurement of peak expiratory flow has become an integral part in the management of asthma, PEF monitoring has its limitations. Apart from some peak flow meters being inaccurate, it requires a certain amount of skill from the patient to produce an acceptable maximal expiratory effort. Any small deviation (i.e. coughing, spitting, faking, etc.) from the correct technique of performing the test, may result in unacceptable values. Furthermore, the patients are required to note the absolute peak flow reading on a diary chart, which could result in inaccurate and unreliable records.

In an attempt to address some of the problems associated with portable peak flow devices, a peak flow whistle (Whistle Watch) was developed, more than 35 years after and independent of the "de Bono Whistle". Whereas peak flow meters measure peak flow through the displacement of a plunger restrained by a spring, the Whistle Watch operates through a threshold activated reed whistle to register peak flow.

CHAPTER 4

THE WHISTLE WATCH™ PEAK FLOW MONITOR

Whistle Watch introduces a new technique of asthmatic management through the monitoring of peak flow rate as opposed to measurement thereof. This monitoring is achieved through the implementation of threshold activated whistle technology. This chapter describes how this technology is implemented and managed in the Whistle Watch to produce a novel peak flow monitor.

4.1 Principle of Operation

The Whistle Watch peak flow monitor embodies the principles of a threshold-activated reed whistle and expelling of excess air. The latter is achieved through a variable spiral valve which varies the area of a venting hole, through which excess air is expelled. The functioning of the Whistle Watch can be described using the following diagrammatic illustration. (Figure 4.1.1)

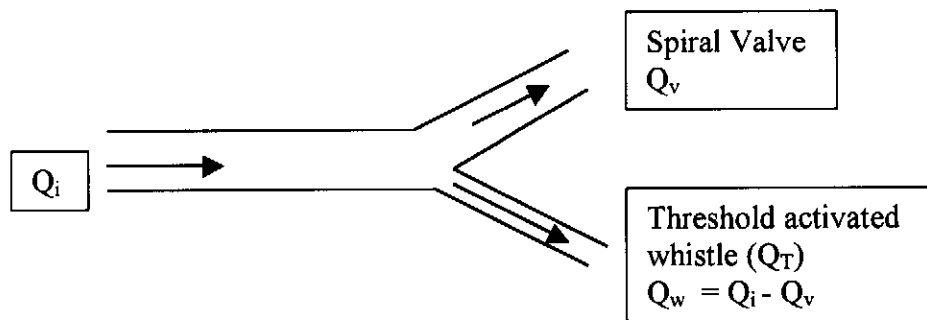


FIGURE 4.1.1
Schematic illustration describing the basic functioning of the Whistle Watch®

From design and experimentation it is known that the whistle activates at a flow rate of Q_T . It is further assumed that the patient's peak expiratory flow is Q_i . (Figure 4.1.1) Adjusting the spiral valve to a set point of Q_v , would vary the vent size in the body of the Whistle Watch in such a manner that an airflow of $Q_w = Q_i - Q_v$ is channeled

through the threshold activating whistle. Should the patient exhale at a level less than Q_i , the whistle will not be activated as $Q_w = Q_i - Q_v < Q_T$. However if the patient blows at level Q_i or more, Q_w would exceed Q_T and the whistle would activate.

4.2 Basic Construction of the Whistle Watch™

The Whistle Watch comprises of two major components: the Whistle Watch-body and the actual whistle. (Figure 4.2.1)

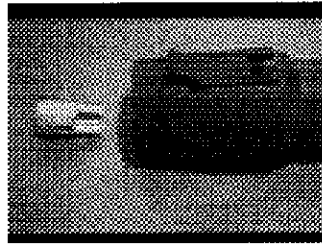


FIGURE 4.2.1
The Whistle Watch® body and whistle

4.2.1 Sub-components of Whistle Watch™-body

The Whistle Watch-body is assembled from 4 components (Figure 4.2.2):

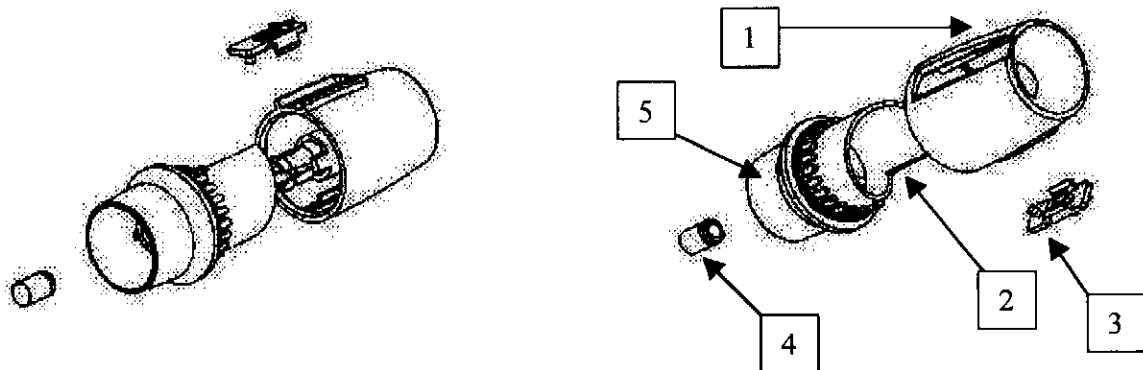
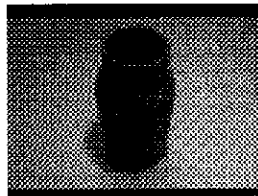


FIGURE 4.2.2
Sub-components of the Whistle Watch® body

- Housing-body (1)
- Revolving spiral valve (2) and mouthpiece (5)
- Locking slider (3)
- Securing pin (4)

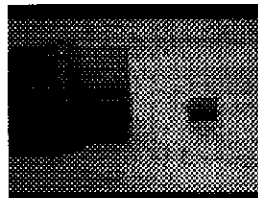
All of the above mentioned components are manufactured from ABS-polymer due to its ultra-violet and temperature stability, biocompatibility and non-toxicity. The assembly procedure is as follow:

Step 1: Take Housing-body

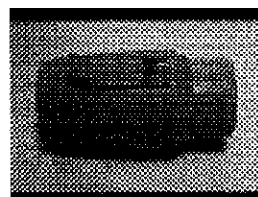


Step 2: Clip Spiral valve into Housing-body

Step 3: Secure assembly through locking of snap fit with Securing pin



Step 4: Snap Locking Slider into position in Housing-body



4.2.2 The threshold activated reed whistle

The whistle (Figure 4.2.3) which is inserted into the Whistle Watch body comprises a body-reed-bed assembly (1) and locking D-piece (3), all manufactured from ABS polymer, and the reed (2) which is punched from polycarbonate sheeting, with an industrial centrifugal punch. ABS polymer was selected for its temperature range, ultra-violet resistance and injection moulding stability. For similar reasons, excluding injection moulding, polycarbonate was chosen.

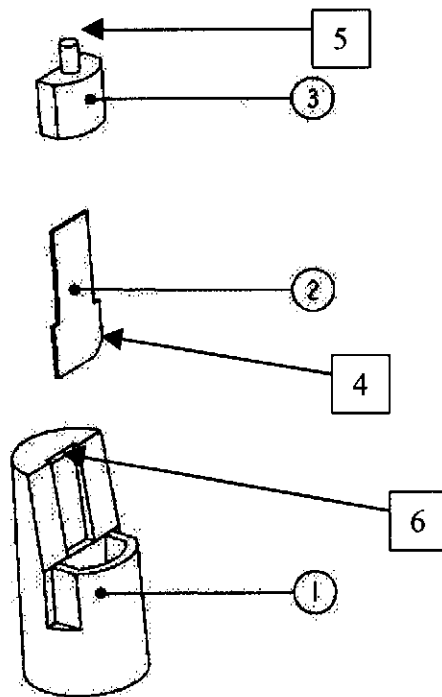


FIGURE 4.2.3
The basic components of the whistle

The assembly procedure is as follow: (Figure 4.2.4)

Step 1: Take the body-reed-bed (1)

Step 2: Insert the reed (2) into the body-reed-bed (1) ensuring that the chamfer on the

T-end (4) is on the right-hand side when facing the reed-hole.

Step 3: Insert and secure the locking D-piece (3) lining semi-circular cross section with semi-circular hole, and insert and secure.

Step 4: Snip the alignment pin (5) of locking D-piece with side-cutter.

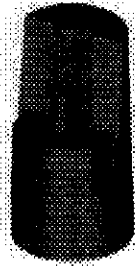


FIGURE 4.2.4
Fully Assembled Whistle

The following description is done with reference to Appendix A. The body has no function other than to encapsulate the reed and to fit into the Whistle Watch assembled body. The reed-bed has an incline of 2° relative to the reed. The latter being 0.25 mm thick with a width of 4.4 mm and a length of 13.1 mm. Tapering on the body facilitates the release of the component from the mould.

Determining of the above mentioned parameters will be discussed later.

CHAPTER 5

LITERATURE REVIEW: MUSICAL INSTRUMENTS

Any reed-driven, woodwind musical instrument can be viewed as having the following subsystems:

1. a performer or musician
2. an air column (cylindrical or conical)
3. a reed valve (single, double or lip)

The Whistle Watch possesses these subsystems with the single major difference being the performer, in this case, an asthmatic patient. When the latter uses the Whistle Watch, the goal is to obtain an indication of his / hers' peak expiratory flow rate, with no importance towards quality of the sound produced. This technique of using sound as a method to present scientific data was coined sonification by Gregory and Kramer [47] and has received much attention during recent years. The research was initiated by reviewing the literature available on reed-driven musical instruments. Summarising the Whistle Watch as a specially designed "reed musical instrument", initiates the review of available literature concerning reed-driven musical instruments. This was a time consuming exercise as most of the literature regarding reed dynamics are contained in doctoral dissertations some of which were never published in scientific or any other journals.

This chapter provides a summary of the literature, which could be harvested. It focuses on the work related to the dynamics of a clarinet reed, which models the Whistle Watch reed valve, the best.

5.1 The onset of oscillation

As described in the introduction, a musical instrument consists of a performer, air column and a reed valve. The performer supplies the blowing pressure, which provides the air flow, which enters the air column through the reed valve aperture. This in itself will not create a musical sound. To induce oscillations, feedback from the air column onto the reed-valve, is imperative. A simplified description of the basic working of a reed “whistle” follows:

“The performer supplies the blowing pressure, forcing the flow of air, through the reed aperture. This creates the pressure difference across the plan surface area of the reed, pushing the elastic reed towards the reed bed. The inherent reed stiffness however, opposes this movement. As the performer however, increases the blowing pressure, the reed moves closer to the reed bed, subsequently setting up Bernoulli forces. The latter supports the performer, and pulls the reed even closer to the reed bed, until the reed finally shuts off against the reed bed, closing the valve.

No music yet!

The described events are executed almost instantaneously, with the closing reed leaving an area of low pressure beyond itself. Air from the atmosphere, which is at a higher pressure, rushes in from the air column and “bumps” against the closed reed. A more scientifically correct expression of the above is “the pressure pulse is reflected at the end of the air column”. If pulses are prevented from running up and down the air column there could be no oscillations, and subsequently no music. Prevention may be accomplished through the insertion of i.e. glass wool into the air column, or using an infinitely long air column. If pulses do however reflect, and are

sufficiently strong, to open the valve, the oscillation cycle repeats itself, and music is produced.”

5.2 The interaction of a reed-valve and the air column: Linear models

The first, and most striking observation, when experimenting with reed whistles is that the frequency of the sound produced differs significantly from the resonance (or natural) frequency of the reed.

Helmholtz [38] was the first to predict this phenomenon in 1862. He defined an “inward striking” reed as one which closes when the blowing pressure is applied. The reed whistle described above is thus an example of an inward striking reed. “Outward striking” reeds were defined as ones where the valve opens when the blowing pressure is applied such as the “lip” reed of a trumpet player. Helmholtz’s [38] linear model of reed and air column interaction, predicted that the playing frequency would always be lower than the reed resonance frequency in the case of an inward striking reed and higher for an outward striking reed. It was therefore, expected that the operating frequency of the Whistle Watch whistle, would be lower than the resonance frequency of the reed.

The natural frequency of a reed can be easily measured as follows:

- Place a sensitive microphone near the reed.
- Strike the reed momentarily.
- Record the resulting pressure signal, which will illustrate the characteristics of a damped simple harmonic motion.

- Execute a Fourier transform on the pressure signal to obtain the natural frequency.

5.3 The reed as a non-linear flow control valve

Backus in 1963 studied the pressure-flow characteristics through an experimental setup seen in Figure 5.1. A long tube filled with fibreglass was attached to the mouthpiece to ensure an escape path for the air with no return or feedback of acoustical signals that could have set the reed into vibration.

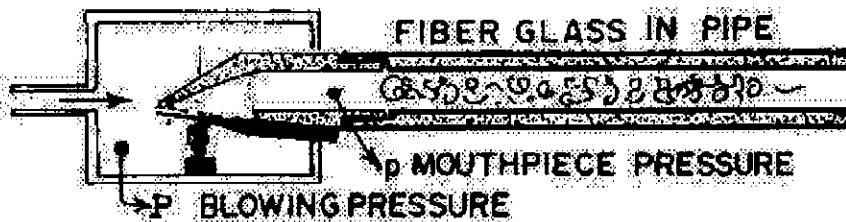


FIGURE 5.1
Benade's Experimental Setup

The results is illustrated in Figure 5.2, where the terminology “embouchure” refers to the amount of damped pressure applied to the reed normally produced by the players lips and teeth.

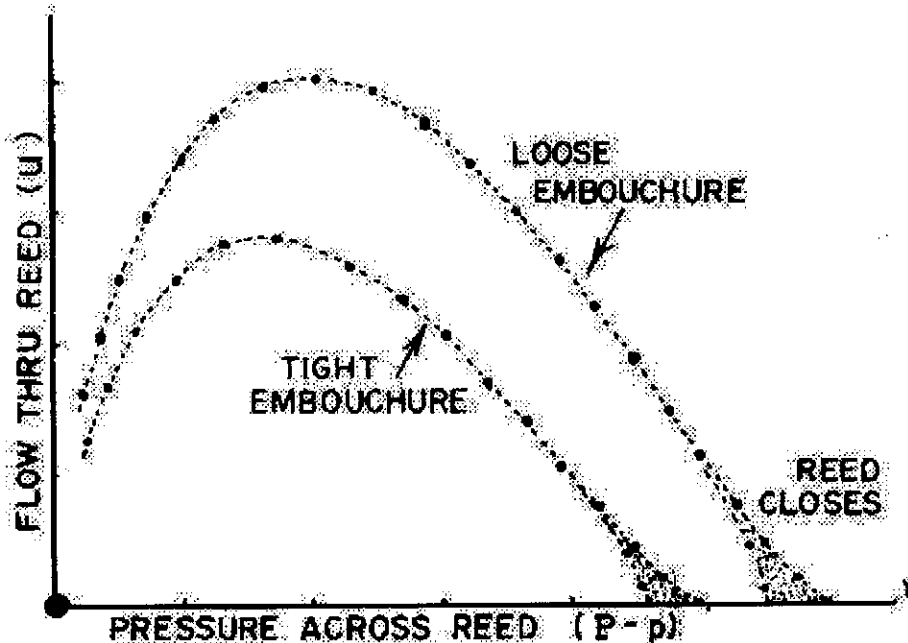


FIGURE 5.2
Aperture Flow versus Reed Driving Pressure

Interpreting Figure 5.2 results in the following observations:

- Initially, the flow through the aperture rises with increasing pressure.
- The reed is pushed progressively closer to the reed bed as P rises, and after the initial increase, the flow rate decreases until the reed is eventually pushed shut against the reed bed.
- For a tighter embouchure the flow rate is less, due to the reduced aperture produced by the closer proximity of the reed to the reed bed.
- A tighter embouchure pressure reduces the pressure required to close the aperture completely.
- The air velocity, past the reed into the mouthpiece tip, increases as the reed nears the reed bed with a resulting Bernoulli force produced, which assists in closing of the aperture. The magnitude of the Bernoulli force is dictated by the inside shape of the mouthpiece tip, which is known as the baffle in the musical fraternity. The shaded region at the end of each flow curve in Figure 5.2 shows how different baffle profiles may alter the required P for reed close off. When the Bernoulli effect is increased the required P is reduced.

Backus proceeded further with his experimentation through the setting of a constant pressure P within the blowing chamber in Figure 5.1, while they created an oscillatory pressure p through the removal of the fibreglass. They made the following 5 observations:

1. Reeds can only oscillate if they receive oscillatory feedback from the air column through pressure p .

2. A reed-valve can sustain only oscillation in an air column if the embouchure and blowing pressure acting on it sets the operating point on the downward slope of Figure 5.2.
3. The high gradient section of the flow versus blowing pressure curve indicates where the flow is sensitively controlled by the mouthpiece pressure p .
4. The reed shut off region is made more sensitive (thus a steeper slope) through the presence of the Bernoulli effect. This fact results in that any increase in blowing pressure or embouchure would move the reed operating point to a steeper slope area with greater flow sensitivity.
5. The player has the ability to decrease ease of play (reduce blowing pressure) at a certain reed operating point through the increase of the embouchure.

Nederveen repeated Backus's experiments in 1968, but used a double reed valve such as generally used in the oboe and bassoon. He formulated a similar non-linear model to Backus, to describe the valving action of a double reed.

5.4 The interaction of a reed-valve and air-column: Non-linear models

The contribution of Arthur H Benade to the field of musical acoustics is un-pared. His work over many years at Case Western Reserve University, lead to many a Ph.D. in this field and probably laid the cornerstone of reed dynamics. Benade and Gans [35] formulated the basic non-linear model, describing the interaction and coupling of the reed valve and air column. Coupling in this sense, also refers to the ease of which oscillations can be induced and maintained into a certain air column. To illustrate this, one can design, through the placement of tone holes, an air column that favours oscillations only at one specific frequency. In other words, the pipe has only one resonance at the frequency where the input impedance is at a maximum. Worman [36]

observed that in a one-resonance pipe, it is difficult to induce stable oscillations. Two- and three-resonance pipes are easier transposed into a state of stable oscillation.

One can therefore say, that the presence of the higher harmonics contributes energy to the system, which enhances stable oscillations. It is this interaction between the harmonics and the fundamental, that reduces the effort to induce stable oscillations into the system. This is what Benade and Gans refer to as the “regeneration function” of the instrument. Benade [35] refers to the resulting oscillations as “regime of oscillations” which he defines as:

“... that state of the collections motion of an air column in which a non-linear excitation mechanism (the reed) collaborates with a set of air-column modes to maintain a steady oscillation containing several harmonically related frequency components, each with its own definite amplitude.”

It was left to Worman [36] to formalize Benade and Gans’s non-linear theorem. Worman’s model was used to predict the characteristics of the clarinet’s frequency spectrum, which closely matched the results from his experimental work. He was also the first to calculate the magnitude of the Bernoulli force acting on the reed and concluded that it only constituted 1.7% of the total force needed to close the reed. The Bernoulli force was then considered to be negligible and excluded from his model. Thompson [24] and later Schumacker [42] expanded Worman’s model to further illustrate the interaction mechanism of the reed valve and air column. Without the presence of non-linearities, music production is not possible. Keefe [8] also illustrated that non-linear air column losses are significant.

5.5 The Air column

Benades earlier work [35] focussed on the influences of tone holes on the input impedance of the air column. Hoekje [22] clearly illustrated that not only is the air column of the instrument important, but that the performer's vocal tract and upper airways, act as a second air column. The reed can thus be seen as a flap valve channelling pressure pulses between an up- and downstream air column. Hoekje illustrated how the second air column significantly influences the sound production.

5.6 Models of woodwind instruments

In this section we give a brief overview of the different mathematical models derived, to describe woodwind instruments. The reader should be aware of the fact that the different groups use different notations. For convenience, the symbols are redefined with the introduction of the different models.

5.6.1 Backus's Model [31]

Backus developed the so-called "Small-Vibration Theory of the Clarinet", which describes and predicts the existence of a threshold blowing pressure for vibrations of restricted reeds with small amplitudes. In developing this theory he first modelled the Clarinet as a whole mathematically with the model in Figure 5.3

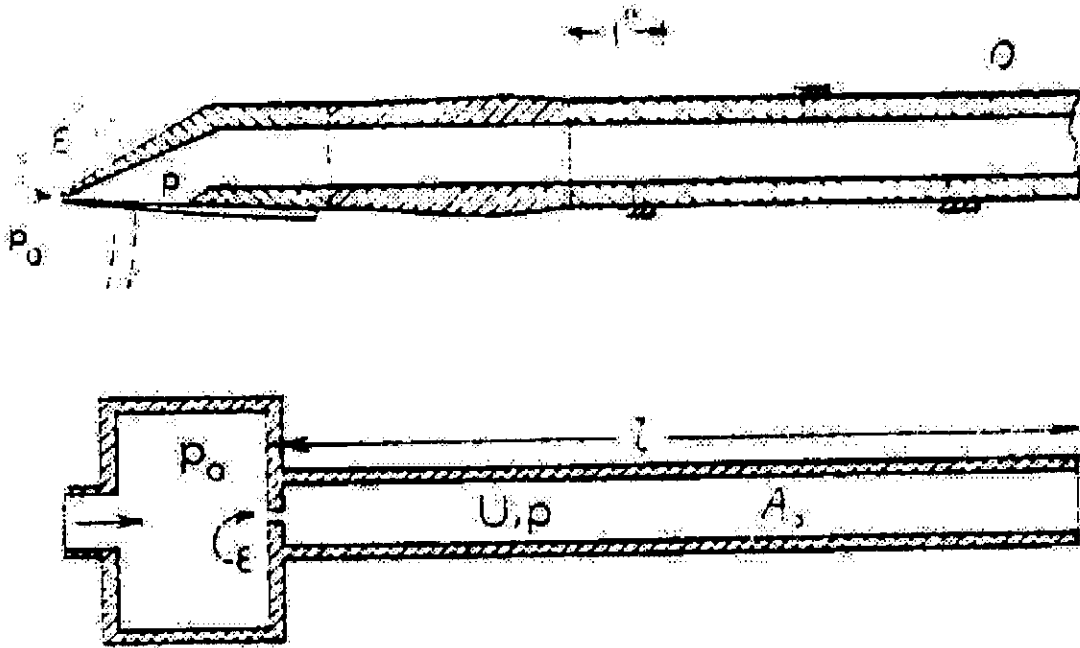


FIGURE 5.3
Backus's Mathematical Model of a Clarinet

Where:

p_0	=	Blowing pressure	[Pa]
ϵ	=	Reed aperture	[m]
l	=	Length to the first open tone hole	[m]
U	=	Volume velocity	[m/s]
A	=	Cross sectional duct area	[m ²]
p	=	Mouthpiece pressure	[Pa]

He then correlated this model with his experimental results to ensure its validity, before transposing and applying it to the clarinet sub-component, the reed, with the constraints of no reed beating¹ or rolling². After manipulation and interpretation the equation for the threshold blowing pressure of a clarinet reed was derived as.

¹ This is defined as a reed that shuts off against the reed bed during oscillation.

² This is defined as a reed of which the body curves during oscillation.

$$p_0 = \frac{1}{2} \cdot \xi_0 \cdot S_r \cdot \left(1 + \frac{\zeta}{\tau}\right) \quad (5.1.1)$$

where

$$\zeta = \frac{k \cdot l}{2 \cdot Q} \quad (5.1.2)$$

and

$$\tau = \frac{\rho \cdot c}{\frac{3}{2} \cdot A_0 \cdot R_0} \quad (5.1.3)$$

In above equations:

p_0	=	Blowing pressure	[Pa]
ξ_0	=	Average reed displacement	[m]
S_r	=	Reed stiffness	[N/m]
k	=	ω/c , reed natural frequency divided by local speed of sound	
l	=	Length to first open tone hole	[m]
Q	=	Q is defined as the sharpness of the tuning and can be determined from the width ΔF of the resonance curve at its -3 dB points. It is also called the quality factor and determined by $Q = F / \Delta F$, where F is the resonance frequency.	
ρ	=	Density of air	[kg/m ³]
c	=	Local speed of sound	[m/s]
A_0	=	Cross sectional duct area	[m ²]
R_0	=	Duct impedance	

This theory was tested against an experimental model shown in Figure 5.4.

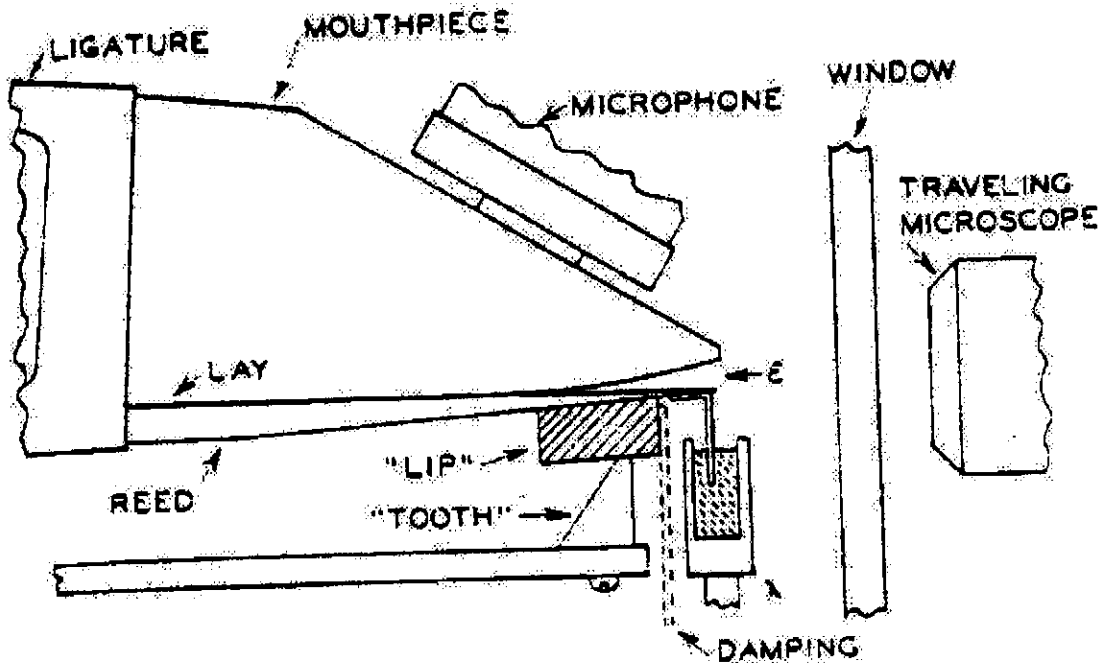


FIGURE 5.4
Backus's Experimental Setup

The travelling microscope was used to determine ξ_0 , while a brass "tooth" and foam neoprene "lip" was installed to generate artificial embouchure. The clarinet was activated through air blown by a household vacuum cleaner. Mouthpiece pressure was measured through an Altec 21-BR microphone.

The model developed tested successfully predicted threshold blowing pressure for small reed amplitude movements.

5.6.2 Worman's Model [36]

Worman expanded through the research of non-linear medium amplitude oscillations, in his Ph.D. titled "Self-sustained non-linear oscillations of medium amplitude in Clarinet-like systems." The main theme of Worman's study was to indicate that no

oscillation of a definite waveform can be sustained if there is no dynamic interaction mechanism between the “reed-plus-mouthpiece” and the main air column. He refers to the reed as a “feedback controlled flow valve”. It should be pointed out again that his study was also on a restricted Clarinet reed. Worman described that the first research done on reeds was by Weber [40] in 1830 when he analysed reeds as undamped harmonic driven oscillators.

Through the development of his non-linear model for medium amplitude oscillations Worman observed and deduced the following observations for the first time:

- Increased blowing pressure, although it decreases the average reed aperture, has little if any effect on the playing frequency.
- Through analysis it is determined that Bernoulli’s effect attribute a maximum of 1.7% to the total driving force of the reed, and has an effect only at high acoustic power levels.

In development of his model, Worman could increase Backus’s small amplitude oscillations through the incorporation of the non-linearities, but this increase was still restricted by the reed not being allowed to beat or roll. In the final form his model could accommodate medium amplitude oscillations. To be able to solve his model he had to assume steady oscillations, which restricted his model applicability.

Worman’s model through Fourier expansion of the fundamental elements around a fundamental frequency (ω), of the form:

$$\frac{P}{z_0} - \sum_{n=0}^{\infty} \frac{P_n}{z_n} \cos(n\omega t + \phi_n + \zeta_n) = \sum_{i,j=0}^{i+j=K} F_{ij}' (-1)^i \left[\sum_{n=0}^{\infty} p_n d_n \cos(n\omega t + \phi_n + \zeta_n) \right]^i \left[\sum_{n=0}^{\infty} p_n \cos(n\omega t + \phi_n) \right]^j \quad (5.1.4)$$

With

$$d_n = |D(n\omega)| \quad (5.1.5)$$

And

$$D(\omega) = \frac{1}{\mu_r \cdot (\omega_r^2 - \omega^2 - i \cdot \omega \cdot g_r)} \quad (5.1.6)$$

Where:

p	=	pressure drop across the reed	[Pa]
z	=	Inlet impedance	
ζ	=	phase shift associated with z	[radians]
δ	=	phase shift associated with D	[radians]
μ_r	=	mass per unit area of the reed	[kg/m ²]
ω	=	oscillating frequency	[Hz]
ω_r	=	natural frequency of the reed	[Hz]
g_r	=	half power band width, damping of the reed	[N·s/m]

5.6.3 Hoekje's Model [22]

Hoekje's research of musical instruments was due to a keen interest and towards a Ph.D. titled "Intercomponent energy exchange and upstream/ downstream symmetry in non-linear self-sustained oscillations of reed instruments".

Hoekje's thesis showed special interest towards the interaction and effect of the upper airways of the musician with the instrument, and the subsequent musical effects produced through manipulation of the upper airways. He reviewed the musician and

instrument as one functional, with the upper airways as the upstream air column and the instrument bore as the down stream air column with the non-linear oscillating reed valve in the middle distributing the energy. The remainder of his thesis focuses on a mathematical expression he derives, which he then implements in the historical theories researched, followed with experimental and practical application. Hoekje's expression is:

$$p = u \cdot (Z_d + Z_u) // Z_r \quad (5.1.7)$$

Where:

p	=	The mouthpiece pressure	[Pa]
Z _d	=	Downstream impedance	
Z _u	=	Upstream impedance	
Z _r	=	Reed impedance	
u	=	Volume flow through the reed valve	[m ³ /s]

Equation 5.1.7 indicates that the roles of the up- and downstream air columns are symmetric. The spectrum of p or u is dependent only on the sum of the air column impedances and so would not change if they were interchanged.

5.6.4 Fletcher's Model [9]

Fletcher's model encapsulates the fundamentals of a simple harmonic oscillating body where the driving force, dictated through Bernoulli's law, is dependent on the oscillation. The derived equations are adjusted through substitution of experimentally determined correction factors, to obtain some correlation between theoretical analysis and empirical testing. [9]

Fletcher's driving force equation:

$$p_0 - p = \left(\left(\frac{2}{\rho} \right)^{\frac{1}{2}} \cdot b \right)^{\frac{-1}{\beta}} \cdot \xi^{\frac{-\alpha}{\beta}} \cdot U^{\frac{1}{\beta}} + \frac{\rho d}{b \xi} \cdot \frac{\partial U}{\partial t} \quad (5.1.8)$$

Where:

p_0	=	Blowing pressure	[Pa]
p	=	Mouthpiece pressure	[Pa]
ρ	=	Density of air	[kg/m ³]
b	=	Breadth of reed aperture	[m]
α	=	Correction factor	
β	=	Correction factor	
ξ	=	Height of reed aperture	[m]
U	=	Acoustic flow rate	[m ³ /s]
d	=	Effective length of small channel between reed and reed-bed	

Fletcher's reed motion equation:

$$m \cdot \left[\frac{\partial^2 \xi}{\partial t^2} + \kappa \cdot \omega_r \cdot \frac{\partial \xi}{\partial t} + \omega_r^2 \cdot (\xi - \xi_0) \right] = s \cdot a \cdot (p_0 - p) \quad (5.1.9)$$

Where

m	=	Mass of reed	[kg]
κ	=	Damping coefficient	
ω_r	=	Resonant frequency	[Hz]
ξ_0	=	Height of reed aperture with no blowing pressure applied	[m]
a	=	Reed free area	[m ²]

s = Either -1 or 1 depending on whether the resonator is an inward reed resonator or an outward lip resonator respectively.

As the whistle is an inward reed resonator $s = -1$. Through inspection of Equation 5.1.8 it may be observed that a maximum blowing pressure (p_0^c) exists where it closes the initial aperture (ξ_0) thus preventing resonance and sound generation. This critical blowing pressure may be mathematically derived as:

$$p_0^c = \frac{m \cdot \omega_r^2 \cdot \xi_0}{a} \quad (5.1.10)$$

Fletcher analysed this system through substitution of Fourier series for each of the acoustical variables ξ , p and U into Equations 5.2.1 and 5.2.2, producing the mode equation. The latter is non-linear, resulting in mixing of the different modes, Fletcher states that “this is important to the behaviour of the instrument”. Fletcher attempted to solve this non-linear mode equation through retaining only the linear components. He found that it gave some insight into the small-signal behaviour, but that even the formal simplified linear solution of the reed admittance (Y_r) was complex and that its meaning was not transparent. He then reverted to typical calculations in which he substituted experimentally determined values into his equations, to prove its correctness, thus once again back to empirical testing.

5.6.5 Keefe's Model [8]

Keefe makes similar assumptions in his theory as Fletcher, assuming the reed to be a simple harmonic resonator where the driving force, predicted through Bernoulli, is dependable on the motion of the reed. His theory is different from Fletcher in the

mathematical approach, where it is not clear from the literature whether or not the constants used in the model are based on actual physical parameters or chosen on the grounds of “mathematical convenience”. The latter could have been done to refine the analytical model to fit the experimental data. The analytical model is given through:

The displacement of the reed:

$$x(t) = S_r^{-1} \cdot u_r(t) \quad (5.1.11)$$

The volume of air per unit time swept out by the reed:

$$u_r(t) = S_t \cdot \left[- \left(g_r \cdot S_r^{-1} + \frac{\sigma \cdot Z_c}{u_t} \right) \cdot u_t(t) - \omega_t^2 \cdot [x(t) - H] - \frac{\sigma \cdot [P_0 - P_h(t) - Z_c \cdot u(t)]}{\mu_r} \right] \quad (5.1.12)$$

The flow rate through the reed tip aperture:

$$u(t) = I_e^{-1}(x) \cdot \left[P_0 - P_h(t) - Z_c \cdot (u(t) - u_t(t)) - C \cdot |u|^\alpha \cdot x^{-\beta} \cdot Sgn(u) \right] \quad (5.1.13)$$

Where:

c	=	Phase velocity of sound	[m/s]
ρ	=	Density of air	[kg/m ³]
S	=	Area of air-column entryway	[m ²]
Z_c	=	$(\rho c)/S$, characteristic impedance at entryway	
S_t	=	Dynamic area of reed	[m ²]
ω_t	=	Reed resonance frequency (rad.s ⁻¹)	[Hz]
f_t	=	Reed resonance frequency (Hz)	[Hz]
μ_t	=	Dynamic mass per unit area of reed	[kg/m ²]
g_t	=	ω_t / Q_t , Half-power bandwidth of reed resonance	[Ns/m]
H	=	Equilibrium opening of reed tip	[m]

l	=	Length of reed tip aperture	[m]
w	=	Width of reed tip aperture	[m]
I_t	=	$(\rho l)/(wH)$, Inertance of reed tip	
C	=	Flow control constant	
α	=	Experimental constant 1.5	
β	=	Experimental constant 2	
P_0	=	Blowing pressure	[Pa]
$r(t)$	=	Reflection function of air column at its entryway	
$P_h(t)$	=	Mouthpiece pressure history function	[Pa]
δ	=	Cane reed (1) or Lip reed (-1)	

Keefe, similar to Fletcher, solved his equations numerically with a computer and experimentally gathered data at discrete points in time, extrapolating to produce a continuous equation in the frequency and time domain. Once again the analytical model was solved through empirical testing.

5.7 This study's contribution

To fully understand this study's contribution it is important first to identify the constraints and unexplored topics in the above literature.

Constraints:

1. The primary focus of all the research done was on musical instruments, with special focus on the Clarinet, with the aim of developing scientifically the "perfect" woodwind instrument.

2. The restricted reed configuration was always evaluated with accommodation for possible player interaction.
3. A constant blowing pressure was always assumed.
4. A defined downstream uniform air column was always present.
5. Oscillations were always assumed and tested at steady state.

Addressing these constraints:

1. The aim of this study is not to develop or predict the “perfect” audible whistle, but to develop an accurate reproducible threshold activated whistle, which may be used in the Whistle Watch, which is an audible peak flow rate monitor for asthmatic patients.
2. The reed configuration could be free or restricted, and is determined by its threshold activating stability and an acceptable signal to noise ratio.
3. The application of the Whistle Watch in the field of peak flow monitoring results in a varying blowing pressure environment of expiration, resulting in research of the effects of varying blowing pressure on the threshold point.
4. The downstream air column is not a uniform duct, but the atmosphere, due to the Whistle Watch geometry.
5. The operating environment is one of varying flow rate in short time durations, of which influence on the threshold set point will be investigated.

Unexplored topics:

1. Although Hoekje investigated the upstream air column, with correlation of the human upper windway, he did not address the effect-defined structures or geometries up stream have on the whistle threshold point.

2. Physical dimensions and properties of the whistle have not been correlated with the threshold activation point.

Addressing these unexplored topics:

1. The effect of defined structures or geometries, as they are encountered with the Whistle Watch body, will be investigated.
2. The whistle will be tested for variations in physical dimension as well as orientation towards the free stream.

CHAPTER 6

THE THRESHOLD ACTIVATED REED WHISTLE

A vibrating system must have a component which stores potential energy and releases it as kinetic energy in the form of motion (vibration) of a mass. The motion of the mass then gives up kinetic energy to the potential energy storing device. It is this interaction between potential and kinetic energy, which sustain a stable oscillation. The oscillating reed of the whistle will be reviewed in this chapter with reference to this vibrational description.

6.1 Descriptive theory:

The following description is applicable to free and restricted reed configurations, with defining parameters:

P	=	Blowing pressure	[Pa]
a_r	=	Reed aperture	[m]
p	=	Mouth piece pressure	[Pa]
u	=	Volume flow rate	[m ³ /s]

As P is applied to the whistle it pushes the reed closer to the reed bed with a subsequent reduction in a_r . This reduction results in an orifice effect with acceleration in the flow through the a_r . A further increasing P results in a further decrease in a_r , and an enlarged pressure drop ($p \ll P$) across the reed. This increasing P produces pulses in p and u in the whistle cavity, where these pulses are transposed into oscillations in the whistle cavity when it is reflected at the downstream air column's open end. This oscillation in the whistle cavity sets a pulsating p , which opposes P , resulting in oscillation (due to p) of the reed around an equilibrium position (due to P) above the

reed bed. This feedback of p is a prerequisite for sustained oscillations of the reed and subsequent sound production.

If the oscillation frequency is within the audible range (20 Hz - 20 kHz), and the amplitude is such that it exceeds the hearing threshold [Figure 6.1.1] it produces the audible sound when the whistle is activated.

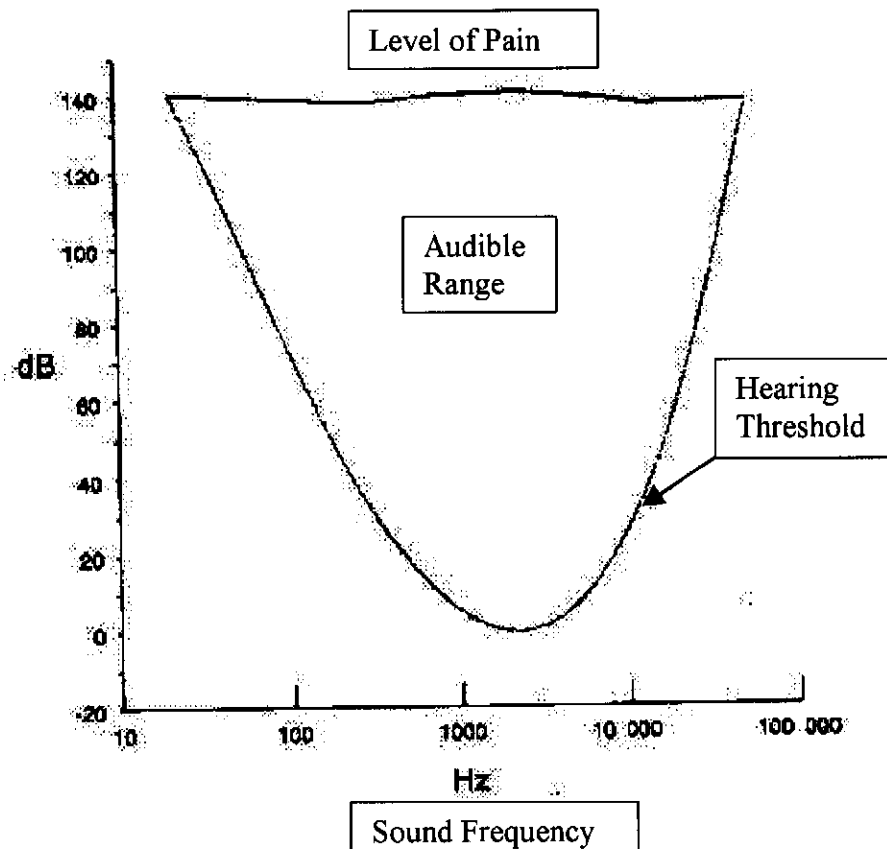


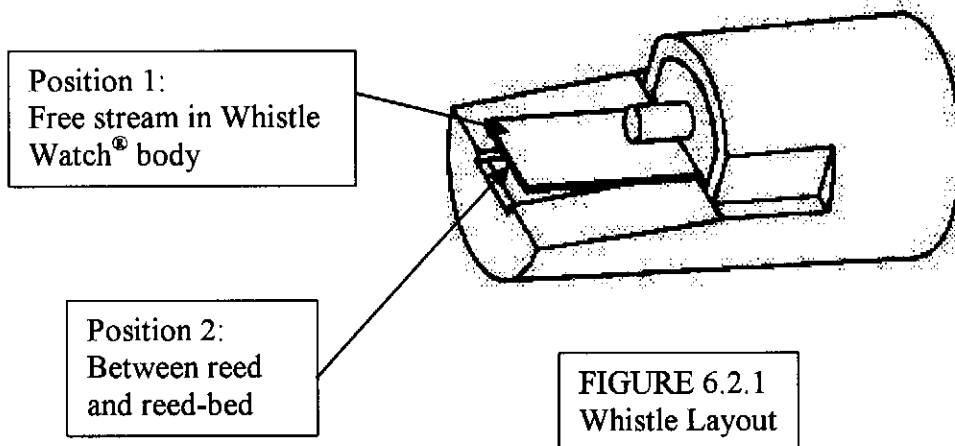
FIGURE 6.1.1
Audible Spectrum

6.2 Analytical theory:

Two fluid mechanics principles are incorporated in the analysis of the whistle:

The first is conservation of mass:

$$Q = A_1 V_1 = A_2 V_2 \quad (6.2.1)$$



The second is The Bernoulli Equation:

$$P_1 + \frac{1}{2}\rho_{air}V_1^2 = P_2 + \frac{1}{2}\rho_{air}V_2^2 \quad (6.2.2)$$

Solving the above equations in terms of the known flow rate, the net pressure difference P_{net} can be calculated as follows:

$$P_1 - P_2 = \frac{1}{2} \times \rho_{air} \times Q^2 \times \left(\frac{1}{A_2^2} - \frac{1}{A_1^2} \right) = P_{net} \quad (6.2.3)$$

A_2 is dependent on time and distance (from the base of the reed). Consequently the above equation should be:

$$P_{net}(x, t) = \frac{1}{2} \times \rho_{air} \times Q^2 \times \left(\frac{1}{A_2^2(x, t)} - \frac{1}{A_1^2} \right) \quad (6.2.4)$$

To determine the net driving force F_{net} of the vibration multiply Equation 6.2.4 with A_{reed} .

$$F_{net}(x, t) = \frac{1}{2} \times \rho_{air} \times Q^2 \times \left(\frac{1}{A_2^2(x, t)} - \frac{1}{A_1^2} \right) \times A_{reed} \quad (6.2.5)$$

The resonance of the reed can be viewed as a cantilever with a time varying but evenly distributed load. Due to the tediousness of deriving vibration equations, the resulting equation will only be stated. For the derivation see Appendix B:

$$\rho_{reed} \times A(x) \times \frac{\partial^2 w(x, t)}{\partial t^2} + \frac{\partial^2}{\partial x^2} \left[E \times I(x) \times \frac{\partial^2 w(x, t)}{\partial x^2} \right] = f(x, t) \quad (6.2.6)$$

The fluid equation must now be substituted into the right side of equation 6.2.6 to describe the complete vibration as follows:

$$\rho_{reed} \times A(x) \times \frac{\partial^2 w(x, t)}{\partial t^2} + \frac{\partial^2}{\partial x^2} \left[E(x) \times I(x) \times \frac{\partial^2 w(x, t)}{\partial x^2} \right] = \frac{1}{2} \times \rho_{air} \times Q^2 \times \left(\frac{1}{A_2^2(x, t)} - \frac{1}{A_1^2} \right) \times A_{reed}$$

Minor constraints prohibiting the solution of the partial differential equation are:

- Non-uniformity of the second moment of inertia;
- Viscous-elastic nature of polycarbonate, implying a non-uniform Young's modulus;
- Varying cross sectional area.

Simplification may be executed through the assumption of uniform and steady characteristics of the above noted properties, resulting in:

$$\rho_{reed} \times A \times \frac{\partial^2 w(x, t)}{\partial t^2} + \frac{\partial^2}{\partial x^2} \left[E \times I \times \frac{\partial^2 w(x, t)}{\partial x^2} \right] = \frac{1}{2} \times \rho_{air} \times Q^2 \times \left(\frac{1}{A_2^2(x, t)} - \frac{1}{A_1^2} \right) \times A_{reed}$$

In this form the equation is exactly the same as Fletcher [9] and Keefe's [8] derived equations. They independently showed that the partial differential equation has no

analytically solution. Fletcher [8] continued and explained that he substituted Fourier series for the time varying components with subsequent elimination of non-linear terms. Solution produced Fletcher states "... is complex, and its meaning is not transparent".

Both Fletcher and Keefe proceeded in mathematical manipulation of the equation to fit empirical steady state tests, as described in Chapter 5. As the greater part of this study is dedicated towards transient phenomena in blowing pressure with practical physiological application, it was decided to abandon the development of restrictive theories. The main focus would be empirical testing with reference to fundamental physics, which predict and govern observed phenomena.

CHAPTER 7

EXPERIMENTAL METHODS

Introduction

This chapter will discuss the experimental setup and methodology used to characterise the whistle. Chapter execution will start through defining the reed activation pressure followed by devising and validating an efficient algorithm for the calculation thereof. Various factors influencing the activation pressure will be investigated. These will include intrinsic factors such as reed dimensions and configurations as well as extrinsic factors such as the manufacturing process and geometry of the experimental apparatus.

The final part of this chapter will focus on the performance of the whistle when inserted into the Whistle Watch body. A set of customised waveforms will be introduced to investigate the influence of different input flow envelopes on the activation pressure.

Whenever there is referred to free and restricted reed configurations in the text, the following dimensions should be assumed:

Reed Properties	Restricted Reed	Free Reed
Reed Length [mm]	13.5	13.1
Reed Width [mm]	4.4	4.0

A reed thickness of 250 μm should always be assumed, except when specifically stated otherwise.

7.1 The Experimental apparatus:

All tests were conducted using a computer controlled single stroke piston pump with the following features: a piston (diameter = 300 mm, stroke = 200 mm) was driven by a wide gauge worm gear (pitch = 5 mm) through a coupling onto a stepper motor¹. (Figure 7.1.1) The stepper motor was controlled by a pulse frequency signal generated by a computer and downloaded via an RS232 serial interface.

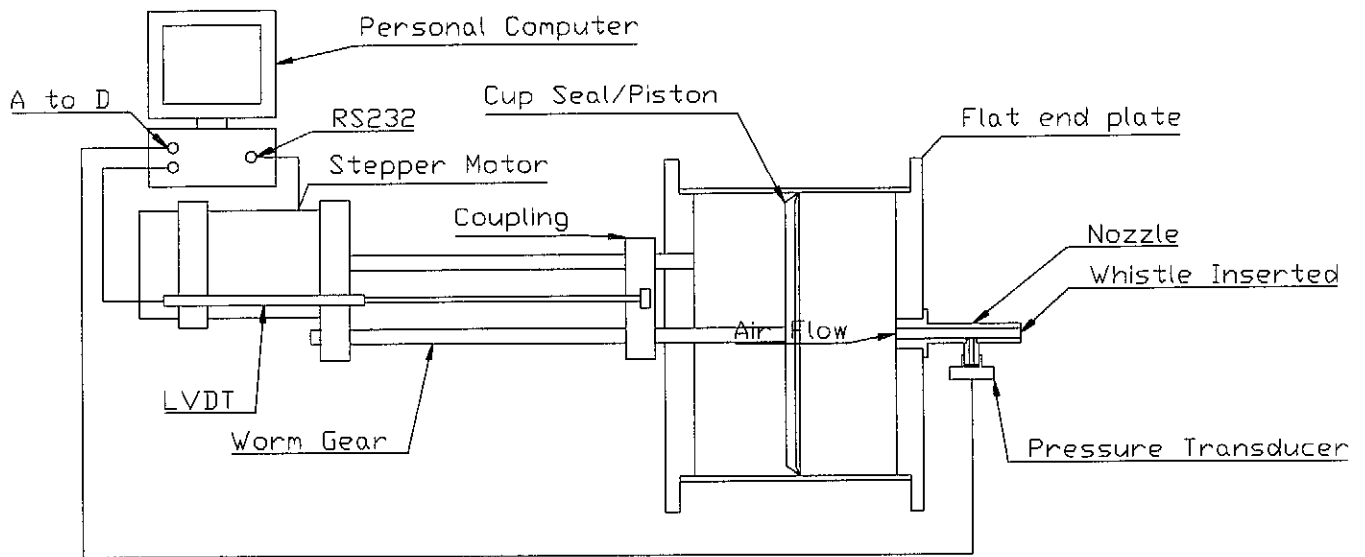


FIGURE 7.1.1
Schematic representation of the mechanical pump

A calibrated² linear variable differential transformer (LVDT³) was fitted to the mechanical pump, to measure the displaced volume (V) of air. The output voltage was sampled through an analogue to digital ISA⁴ card and differentiated with respect to time to produce the corresponding flow rate (Q). A digital filter was used to blank out

¹ Compumotor Sx8 Stepper drive, Stebon Stepper motor SDT-1102-300-275

² The LVDT was factory calibrated. See Appendix C for calibration data

³ RDP type 001-16C-26703 with 100 mm stroke

⁴ 4 Channel ADAS (12 bit resolution), University of Stellenbosch

most of the noise introduced by the differentiation process. Q thus represented the flow rate of the mechanical pump as a result of piston movement. No correction was made for compressibility through the measurement of chamber pressure, as the flow rates at which the whistle operated were relatively low ($< 15 \text{ l.min}^{-1}$). (Appendix D) Using the LVDT as a method of flow measurement as opposed to other more conventional methods (e.g. an orifice plate type of flow meter) will become clear in section 7.2.

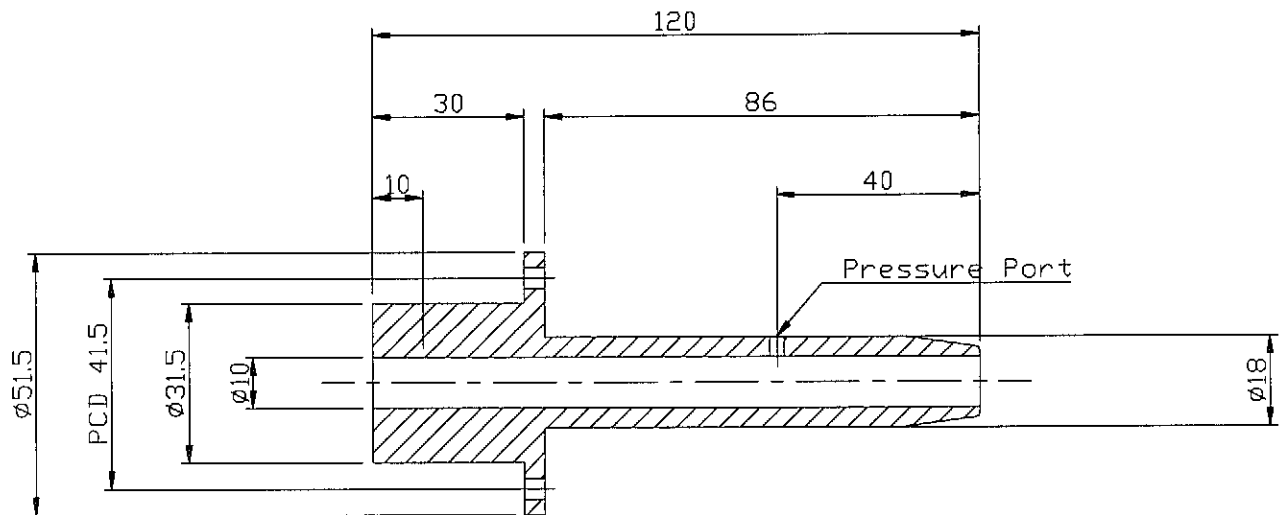


FIGURE 7.1.2
Nozzle Design

A nozzle (Figure 7.1.2) was designed to accommodate the whistles and was fitted to the front plate of the mechanical pump. (Figure 7.1.1) The nozzle design also adhered to the general rule of thumb of fluid mechanics [11]:

- the nozzle entrance had a smooth transition into the required diameter thereby reducing the normal imparted entrance shock to the air flow;

- its length was > 10 times the diameter of 10 mm, thus 120 mm, thus ensuring a adequate mixing length for fully developed flow profile;
- pressure measurement was done upstream of the whistle at 4 times the diameter of 10 mm, thus 40 mm. This prevented any second order effects generated through the resonance of the whistle from influencing the pressure transducer measurement.

Pressure measurement was done using a calibrated¹ pressure transducer² and sampled through the A to D converter. (Appendix C) The pressure signal was digitally filtered using the same filter length as the flow signal to prevent the introduction of any phase difference between the signals.

The computer controlled stepper motor and mechanical pump made it possible to generate a wide range of flow rates (Appendix D) with dynamic characteristics ranging from steady state, ramped increases in flow and customized sinusoidal type of flow envelopes.

For the duration of testing the atmospheric temperature and pressure were recorded. The daily records indicated that the laboratory ambient temperature was constant at 293 K and that the atmospheric pressure did not fluctuate significantly around 756 ± 2 mmHg. It is thus concluded that all experiments were performed under controlled, uniform environmental conditions. Where whistles were compared tests were done on the same day and completed within a time span of 3 hours.

¹ Please see Appendix C for calibration curve and procedure

² Honeywell/ Microswitch 163PC01D36

It is concluded that any effects and trends shown in the remainder of this chapter may not be contributed to laboratory conditions, as it has been relatively constant.

7.2 The influence of nozzle geometry on reed activation pressure

During the pilot study, two types of flow meters, an orifice plate¹ and contracting nozzle², in conjunction with a differential pressure transducer, were used to measure flow through the whistle. The low operating flow range of 0-15 l.min⁻¹ and the physical constraints of the contracting nozzle produced low differential pressure unmeasurable with the differential pressure transducer.

This rendered the contracting nozzle unsuitable. Therefore the orifice plate flow meter was implemented. The Hans-Rudolph flow meter was inserted between the flat end plate and the nozzle containing the whistle (Figure 7.1.1). It was observed that the static activation pressure of the whistle, measured within the nozzle, was markedly different with a flow meter in line as compared to the readings without a flow meter. A further unexpected observation was that the nozzle geometry had a significant influence on the activation pressure. Subsequently the phenomenon was further explored to illustrate the influence of nozzle (upstream) geometry on activation pressure.

Two nozzles similar to the existing testing nozzle were constructed with the exception of a contracting and expansion step insertion in the free stream respectively.

¹ Hans-Rudolph 0-35 l/min

² Custom designed for this thesis: Appendix E

Constricted Nozzle

The initial step length was $L_{\text{step}} = 60$ mm. The step forced the free stream from a $D_{\text{freestream}} = 10$ mm diameter to a $D_{\text{step}} = 6$ mm diameter and releasing eventually into the initial $D_{\text{freestream}} = 10$ mm diameter again. (Figure 7.2.1)

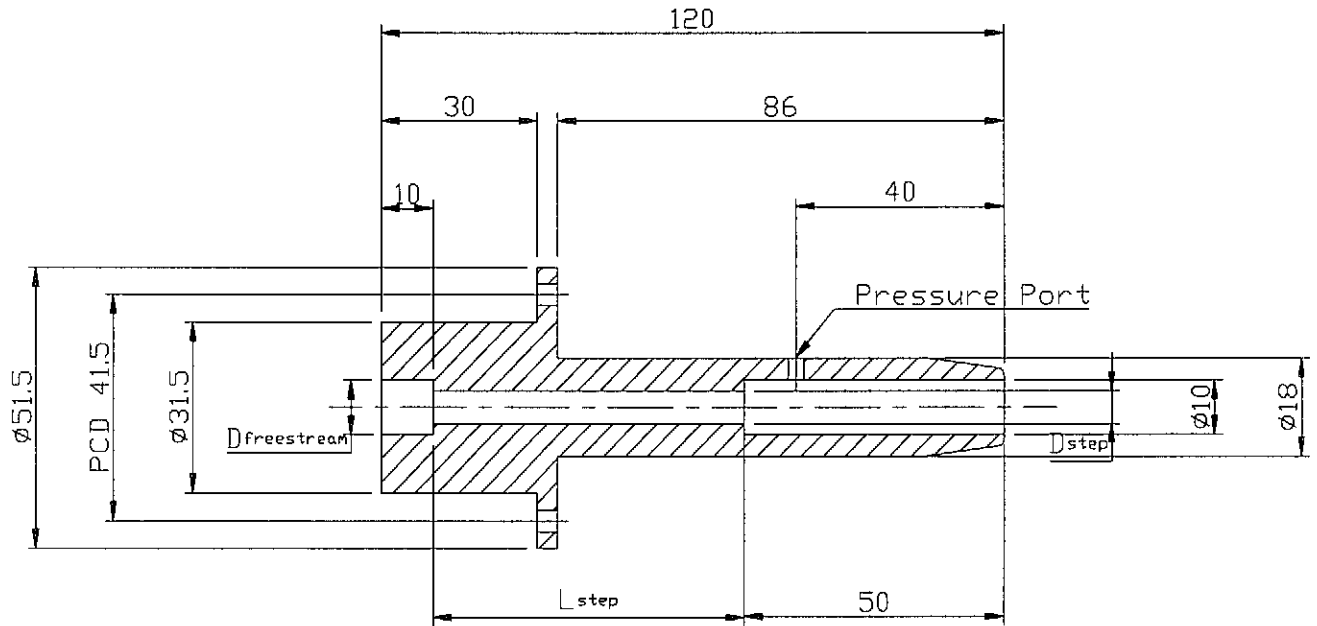


FIGURE 7.2.1
Constricted Nozzle Geometry

The step length (L_{step}) was progressively reduced in steps of 10 mm from the whistle end of the nozzle. This process was repeated until the step was completely removed. Free and restricted reeds were each tested twelve times at each step length.

Expansion Nozzle

The initial step length was $L_{step} = 10$ mm. The step released the free stream from a $D_{freestream} = 10$ mm diameter to a $D_{step} = 14$ mm diameter and forcing eventually into the initial $D_{freestream} = 10$ mm diameter again. (Figure 7.2.2)

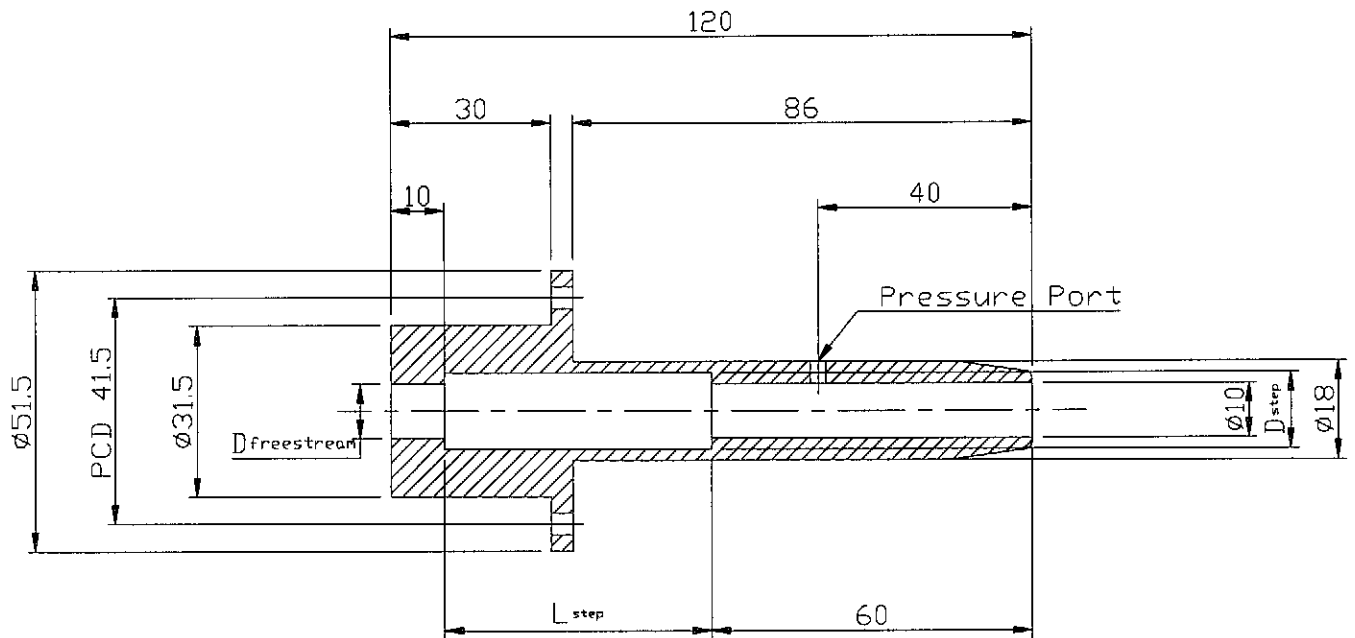


FIGURE 7.2.2
Expansion Nozzle Geometry

The step length (L_{step}) was progressively increased in steps of 10 mm from the calibrator end of the nozzle. This process was repeated until the step was a maximum length of $L_{step} = 50$ mm. Free and restricted reeds were each tested twelve times at each step length.

The maximum step lengths placed the steps in the proximity of the pressure measurement point (Figure 7.2.1&2) with a possible influence on the pressure

measurement. However, the relatively low operating flow rates (0-15 l.min⁻¹) made the positioning acceptable and should leave the pressure measurement unaffected.

7.3 Defining the reed activation pressure

As mentioned in Section 5.6.2, Backus [31] developed an equation to determine the activation pressure of a reed whistle. Backus [31], however does not supply a clear definition of “the threshold blowing pressure”. “The threshold blowing pressure” can either be defined as “*the point where the reed starts to oscillate*” or “*the point at which the sound, produced by the oscillating reed is first heard*”. The first definition is assumed to be more relevant to this thesis than the second. Although the definition as stated sounds fairly simple, it produces problems of its own. As an analogue one can use the definition of the boiling temperature of water. Is it when the first bubble of steam appears? No, science uses a different definition¹ for the “boiling point of water” which differs significantly from “the instant at which boiling starts”. Defining the onset of oscillation would show to be a point between where the “reed starts to oscillate” and “where oscillation becomes audible”. Furthermore, since the reed acts as a pressure activated valve, this pressure would be referred to as the “reed activation pressure” or “ P_{RA} ”.

7.4 Determining the P_{RA}

In order to characterize P_{RA} , a low gradient² ramp-input waveform was used, resulting in a constant acceleration of the plunger (and therefore a second order increase in flow rate). Sampling the pressure signal facilitated in the analysis of the pressure-time

¹ Boiling point of water is when a mixture of liquid water and water vapour (with no air) in equilibrium exist at 1-atm pressure. [32]

² Acceleration of the stepper motor = 0.5 rev/s²

curve comprising of the transition zone ranging from no-activation to full activation of the whistle ending in oscillation termination. (Figure 7.4.1)

The ramp input waveform lasted for approximately 2 seconds and was captured at a sampling rate of 3 kHz which was substantially higher than the reed oscillation frequency (~600Hz), thereby ensuring repeatable and reproducible activation transition zones. An example of a pressure-time waveform of a restricted reed is illustrated in Figure 7.4.2 of which the transition zone is marked and enlarged in Figure 7.4.3.

The reed activation pressure was initially determined through manual evaluation of each pressure-time graph, obtaining the activation pressure and reading off the corresponding flow rate from the flow-time graph. This was extremely time consuming as it had to be repeated twelve times for each whistle to determine the mean activation and standard deviation. Thus it was agreed to automate the process of determining the activation point. Different techniques were considered and put to trial, but failed as activation is a transition zone and not a specific point in time. The technique that proved to be both successful and computationally efficient, was one of determining the standard deviation for each subsequent set of points (e.g. $n = 5$) in the pressure data, then plotting it with respect to time. Where the standard deviation increased significantly, it indicated the transition zone. (Figure 7.4.4)

Pressure vs Time for a Free Reed

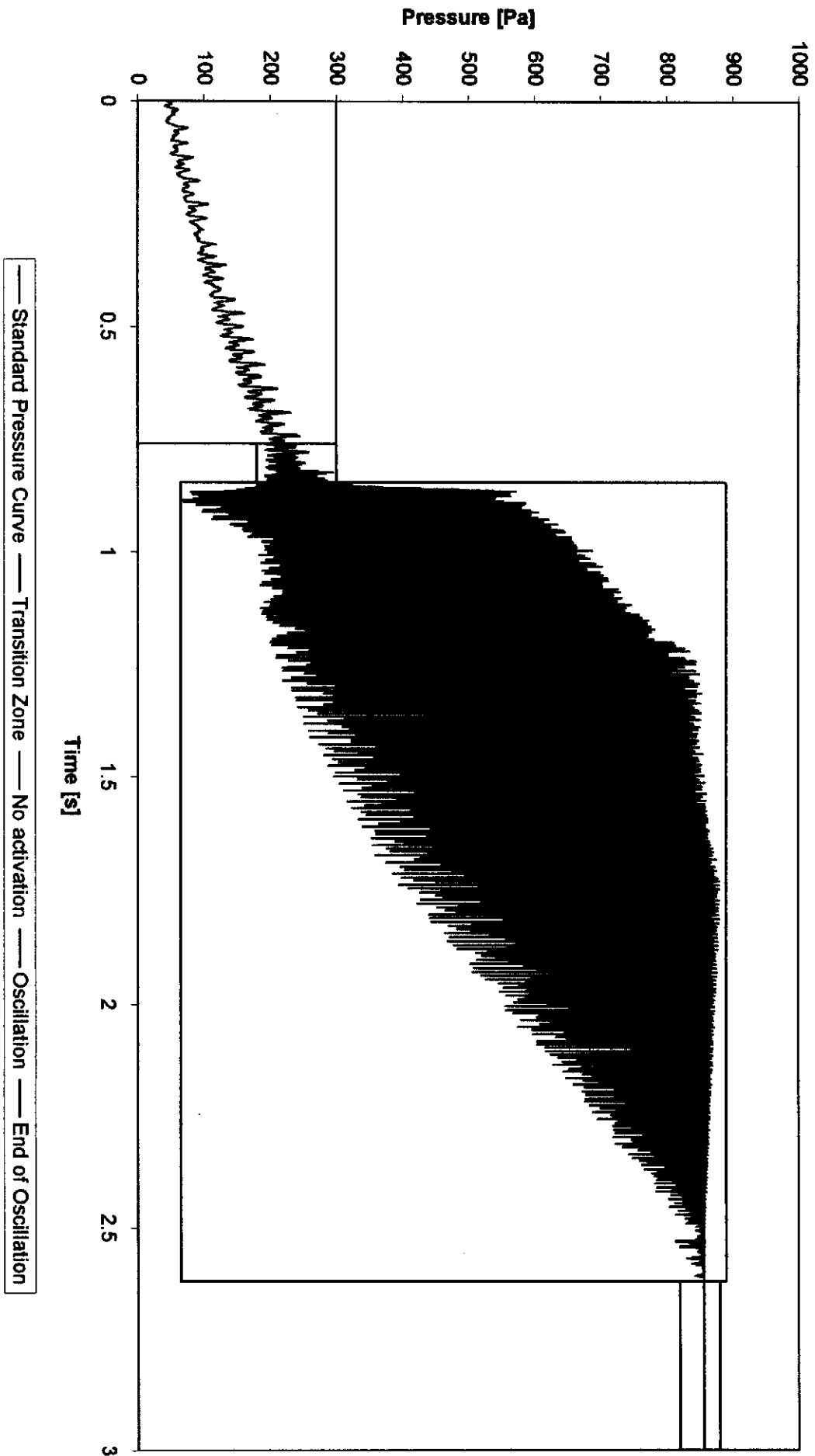
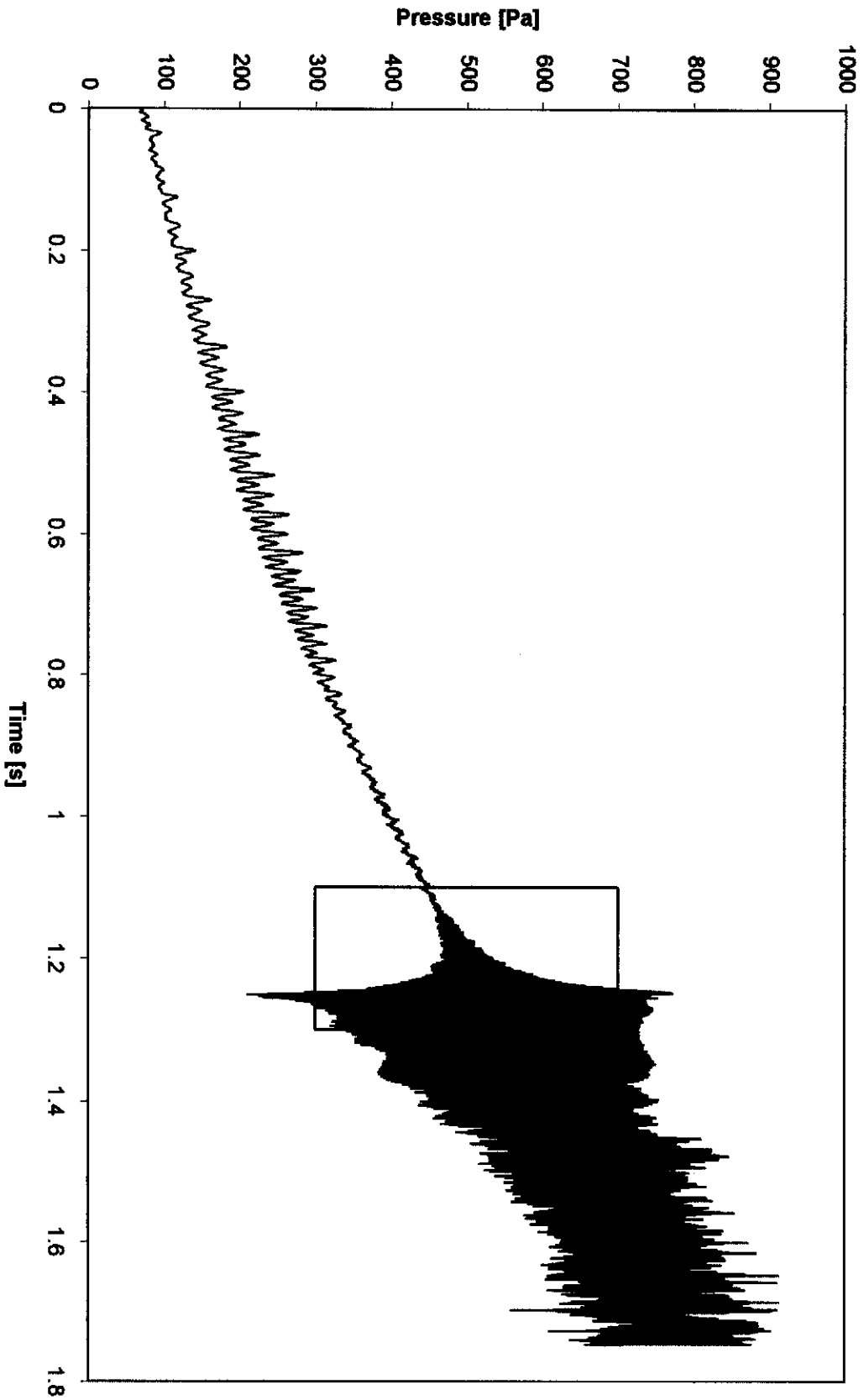


FIGURE 7.4.1

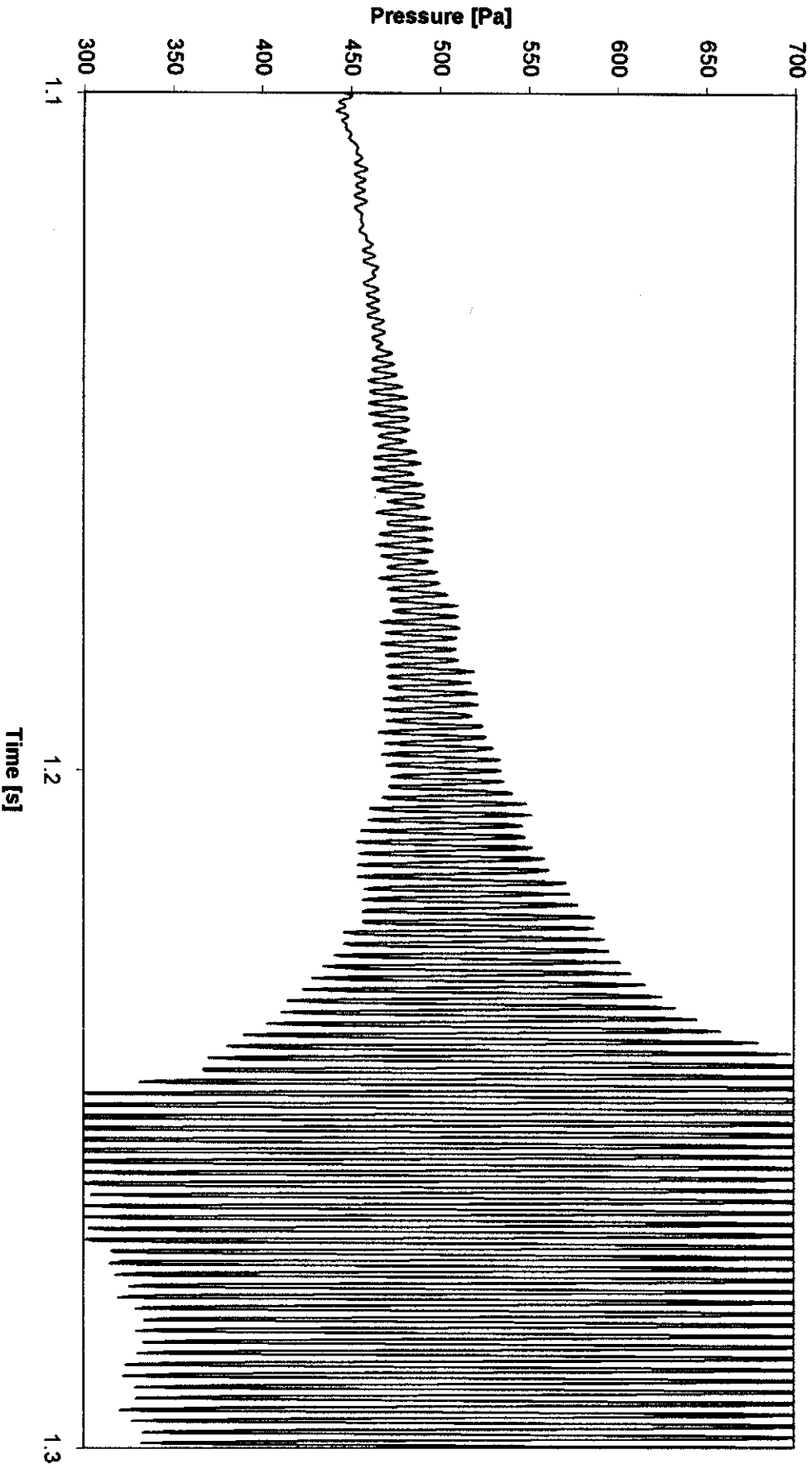
Pressure vs Time for a Restricted Reed



— P3
— Figure 7.4.3

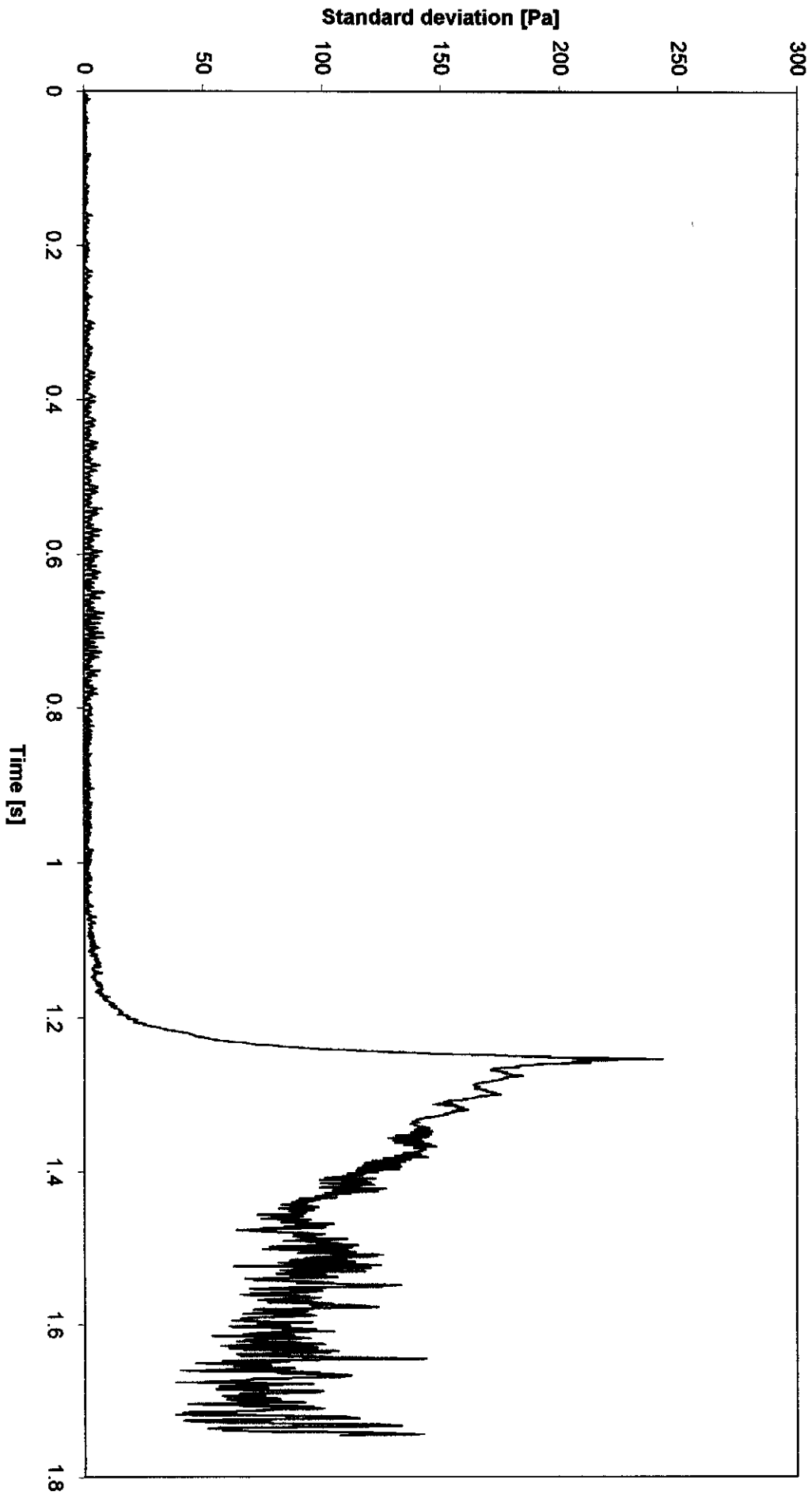
FIGURE 7.4.2

Pressure Transition Zone vs Time for a Restricted Reed
Extracted From Figure 7.4.2



— P3

FIGURE 7.4.3



Standard deviation vs Time

FIGURE 7.4.4

At first it had to be determined how many data points would be adequate for calculating the standard deviation. A minimum value of 5 data points was chosen, and calculations were done with epochs of 5, 7 and 9 points. The higher number of points ($n = 7$, $n = 9$) resulted in the standard deviation curve being too coarse with a resulting low resolution in the transition zone. (Figure 7.4.5&6) It was therefore accepted that 5 data points would suffice to calculate the standard deviation with a acceptable resolution.

Because activation occurred in a transition zone a threshold point of standard deviation had to be determined, which could indicate activation. Threshold values of standard deviation of 0.025, 0.05 and 0.1 were evaluated. Obtaining the maximum value in the calculated standard deviation data and then stepping back in the data until the threshold point (i.e. 0.025, 0.05, 0.1) was encountered for the first time, was marked as the activation point. The latter was then referred back to the pressure data where the reed activation pressure (P_{RA}) was obtained.

The conclusion of the evaluation was that a threshold of 0.05 was adequate as 0.025 projected onto the pressure data before the transition zone and 0.1 too far into it. (Figure 7.4.7&8)

Standard deviation vs Time

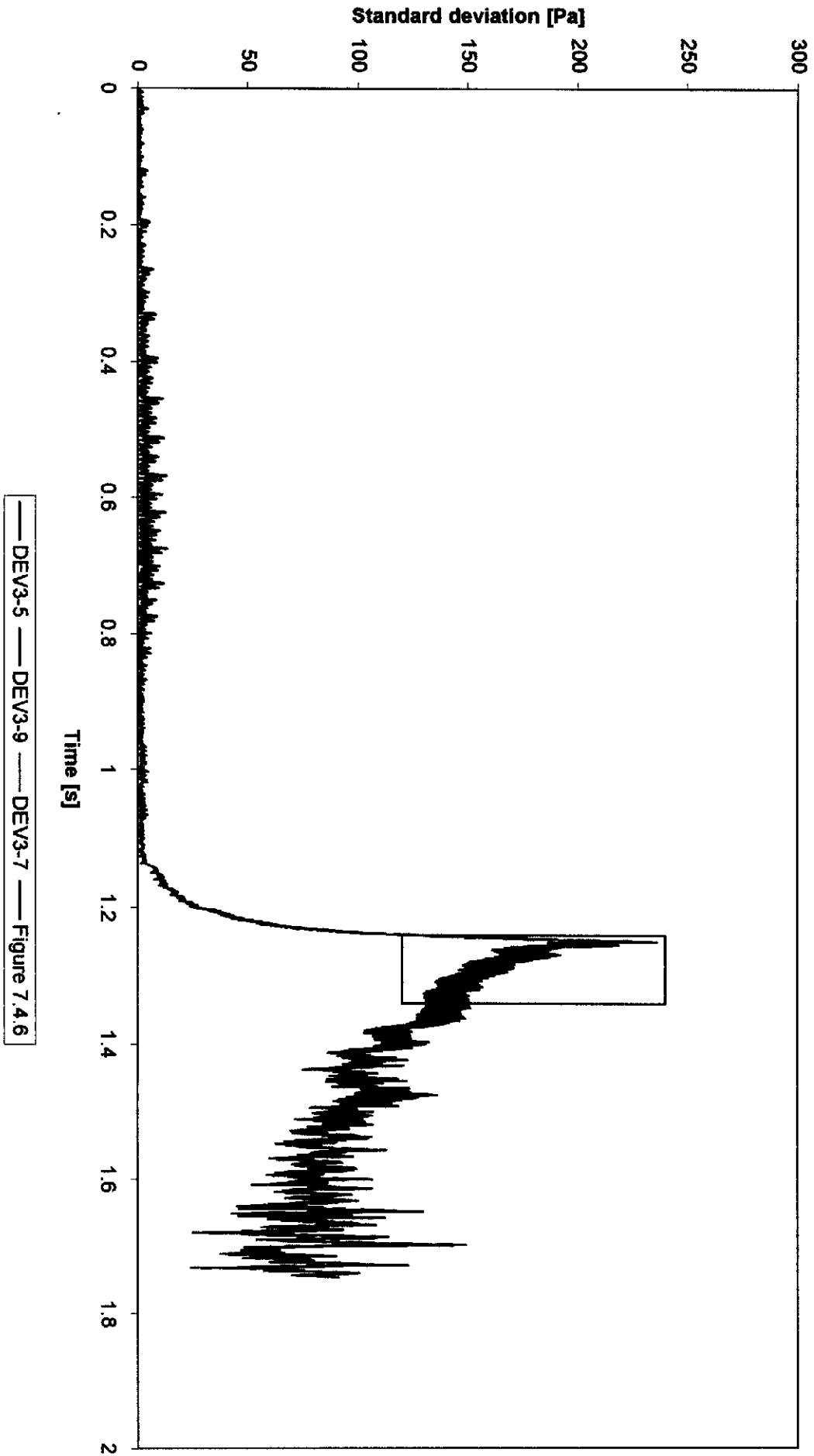
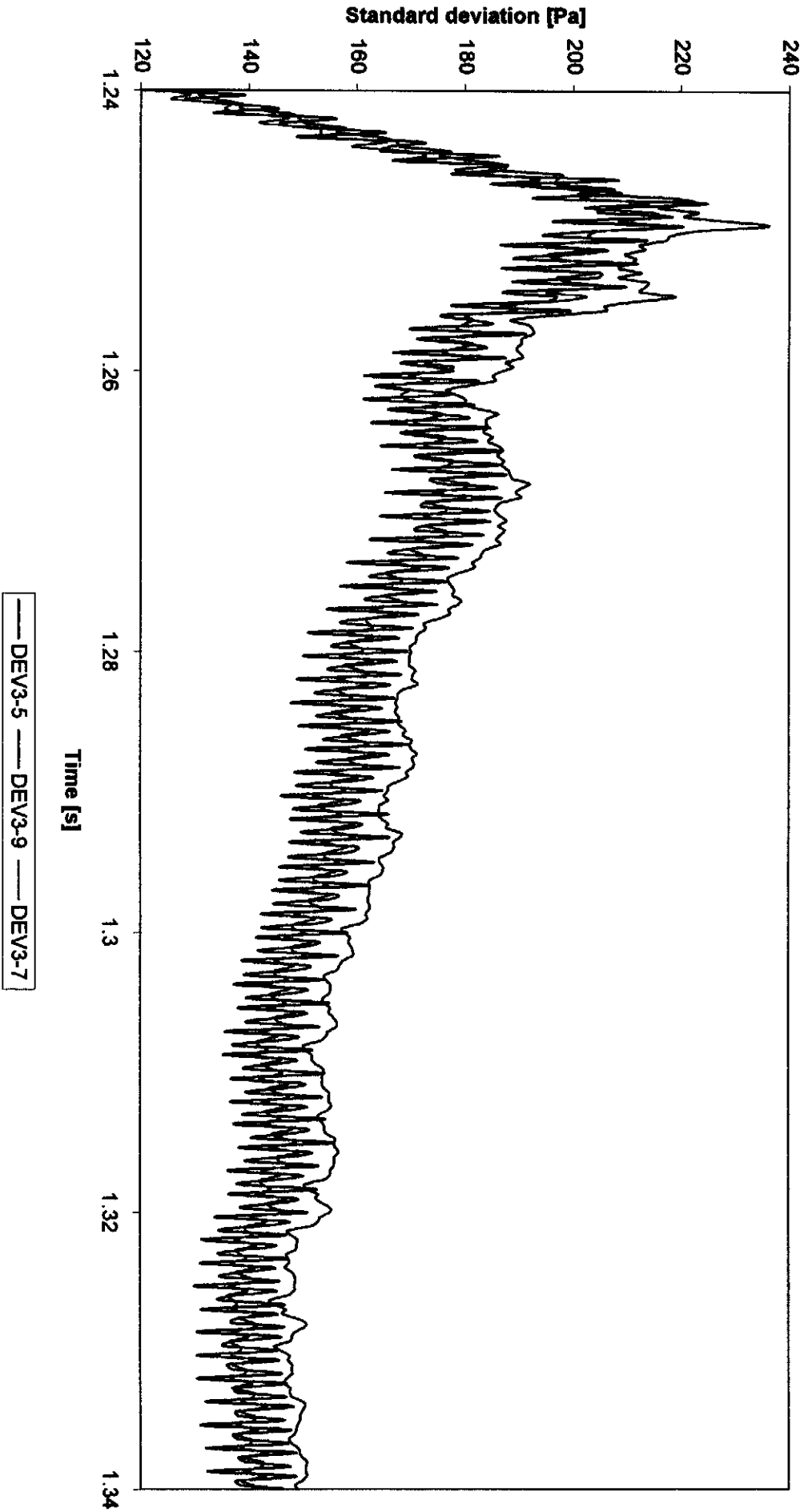


FIGURE 7.4.5



Standard deviation vs Time
Extracted From Figure 7.4.5

FIGURE 7.4.6

Pressure Transition Zone vs Time for a Restricted Reed

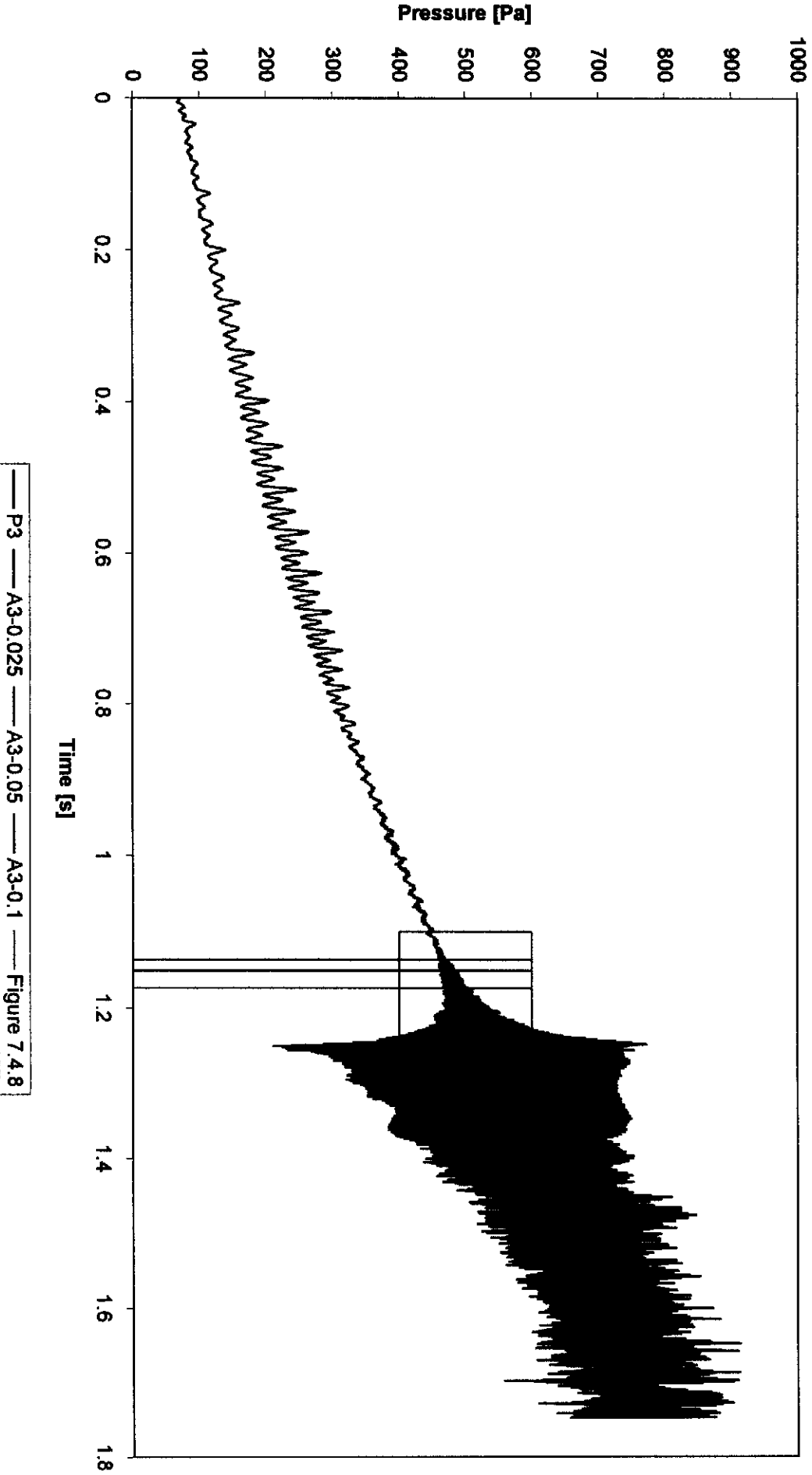


FIGURE 7.4.7

Pressure Transition Zone vs Time for a Restricted Reed
Extracted From Figure 7.4.7

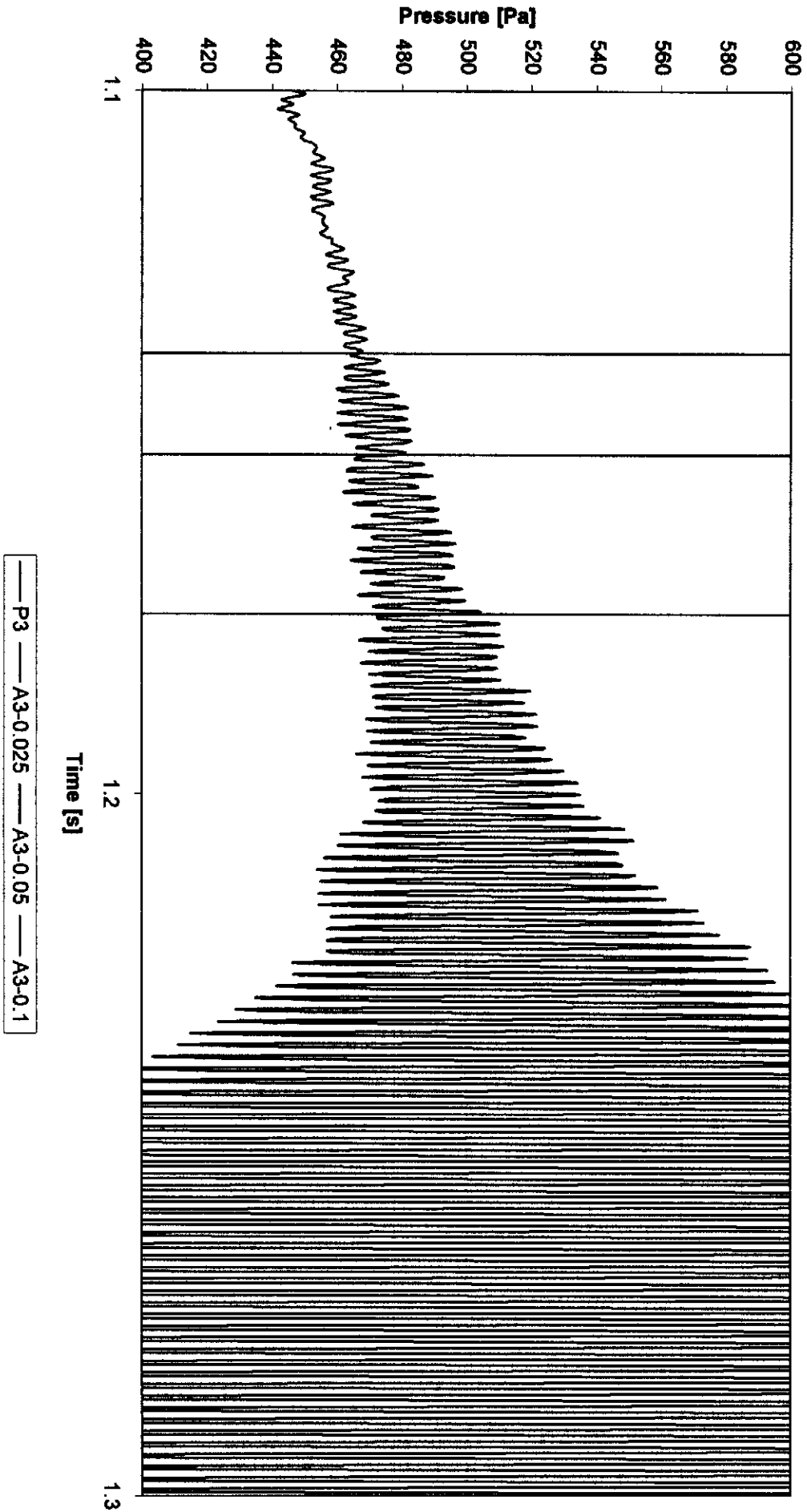


FIGURE 7.4.8

At this point in time the definition of reed activation pressure, as described in Section 7.3, could be redefined as this was a qualitative definition and the technique developed produces a quantitative definition. Reed activation pressure was thus redefined for the purpose of this study as:

The point in time during the onset of reed oscillation where the standard deviation of 5 consecutive pressure points dropped below 0.05 for the first time when searching backwards from the maximum value in the series.

Before this extensive processing was programmed into the sampling program its success had to be evaluated. An algorithm was devised for the calculation process as illustrated in Figure 7.4.9.

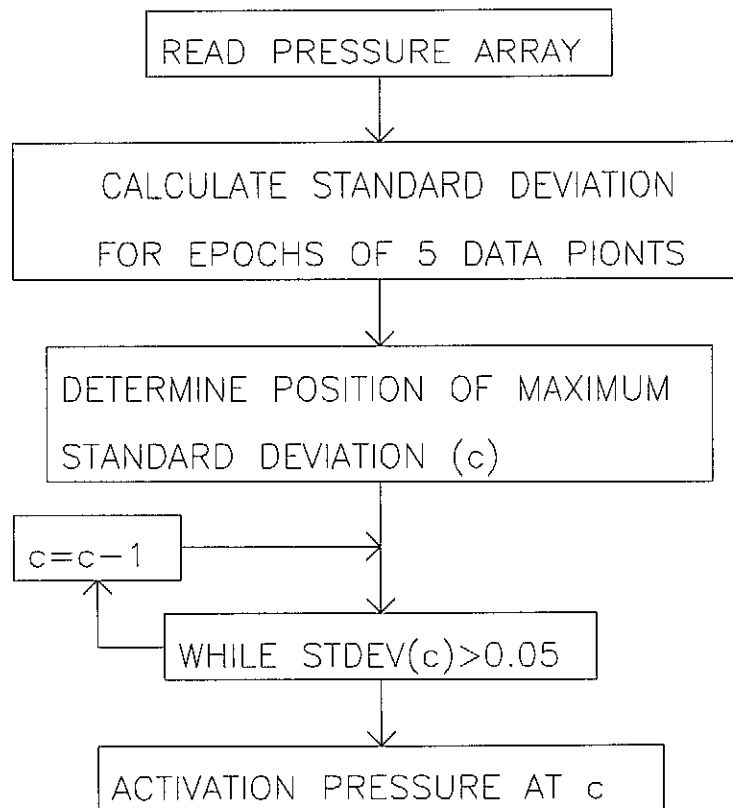


FIGURE 7.4.9
Algorithm for Calculating the Reed Activation Pressure

This algorithm was programmed into the graphical interface of MathCAD¹ 8 professional edition, and then implemented into the electronic circuit analogue software Mathconnex from where the simulation was run. (Appendix F)

Data was sampled on 90 different whistles, each being tested 12 times, resulting in 1080 data sets for which the activation points were found within the Mathconnex simulation. The activation values were determined manually in an Excel² spreadsheet and crosschecked with the values produced by the Mathconnex simulation. The latter proved to be a successful means of automation as every activation point cross-checked correctly.

The next step was to implement the algorithm into the existing Turbo Pascal sampling program. The same whistles, which were used to check the validity of the Mathconnex simulation, were tested after the Turbo Pascal program was updated, again producing 1080 data sets. Actuation values obtained through the Mathconnex and Excel analysis were compared to the results of the Turbo Pascal sampling program. Exact activation points were obtained with the above three programs.

7.5 Validation of the reed activation pressure

The validity of the standard deviation method was tested against the second definition of reed activation as defined in Section 7.3 i.e. “ *the point at which the sound, produced by the oscillating reed is first heard*”. A more formal definition of the above

¹ Mathsoft Inc. Cambridge, Massachusetts, USA

² Microsoft Office '97 International

would be, *“the activation point is where the power in the pressure signal at the oscillating frequency, exceeds a certain pre-defined threshold.”*

This definition was implemented by calculating the Power Spectral Density (PSD) of the pressure signal, which indicate the energy content (or power) at various frequencies. As the reed starts to oscillate one would naturally expect the energy content of the signal to gradually increase at the oscillating frequency.

The DADiSP¹ signal-processing package was used for this analysis using a specified data window of 128 data points. The procedure was as follows:

1. A ramp input was used and the reed activation pressure determined as described in Section 7.4.
2. The 128 data-points preceding the reed activation pressure were then isolated in the pressure signal (Figure 7.5.1) and the linear drift subtracted from the signal.
3. The PSD was then calculated (128Pre).
4. The 128 data-points following the activation pressure were then isolated (Figure 7.5.1) and the linear drift subtracted.
5. The PSD was calculated (128Post).
6. The last data series comprised of choosing 64 points preceding and including the pressure activation point and 64 data-points following (Figure 7.5.1), and the linear drift removed.
7. The PSD were calculated (128Around).

This process was done on both the free and restricted reed whistles to ensure accuracy of activation determination throughout the entire range of testing. Both produced similar results necessitating a mutual discussion of both results.

¹ DADiSP™ Ver1.04C, 1987, DSP INC.

Extract pressure signal

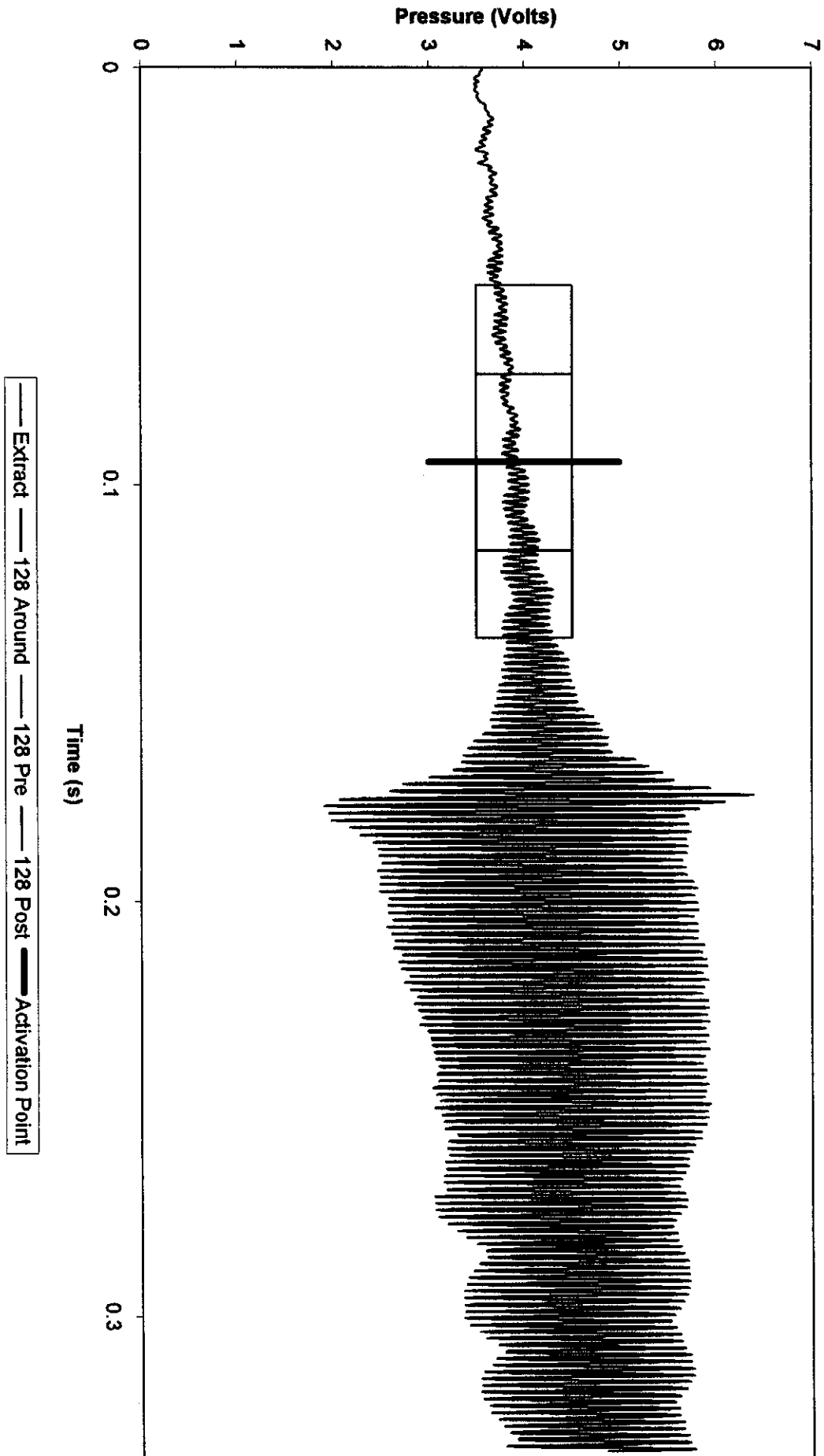
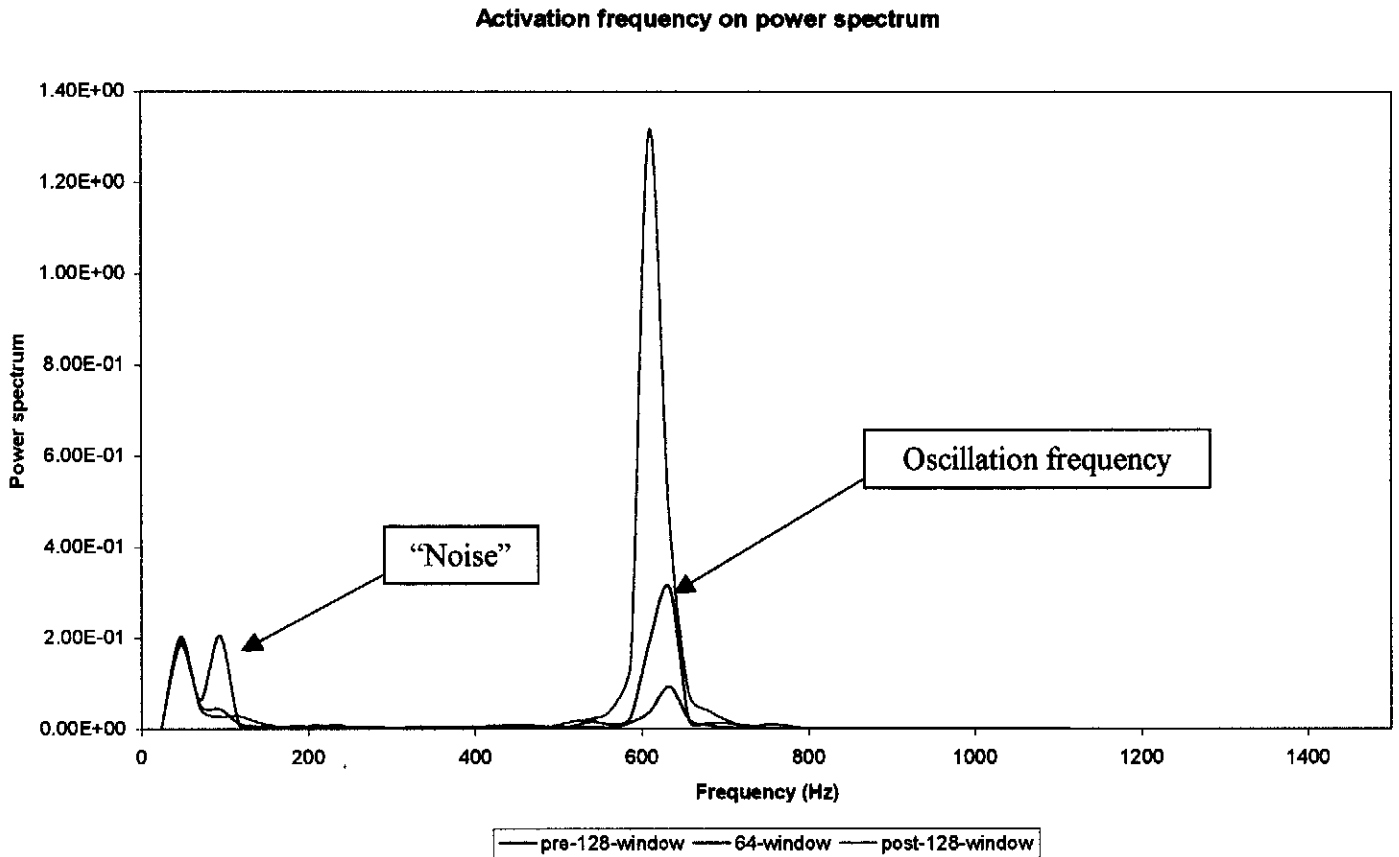


FIGURE 7.5.1

The results of the analysis: (Figure 7.5.2)



**FIGURE 7.5.2
POWER SPECTRUM**

From Figure 7.5.2 it was concluded that the process of activation point determination was correct as indicated by the predominant activation frequency of approximately 600 Hz occurring in the predicted window of activation. The foregoing frequencies are due to the noise in the pressure signal produced by the testing hardware during sampling.

7.6 General characteristics of the reed activation pressure

In order to obtain a perspective of the general behaviour of the whistle near the activation point, sixty whistles were chosen at random consisting of restricted ($n = 30$)

and free reed ($n = 30$) units. Each whistle was tested 12 times with the mentioned ramp-input waveform. Data were captured with the Turbo Pascal program, which incorporated the algorithm for calculating the activation pressure.

7.7 “Sidedness” of the reed

The reeds were produced in a production environment by means of a centrifugal punching press, which uses 250 μm polycarbonate sheeting. Punching was done in the extrusion direction, which ensures homogeneity, as all the polymer chains are orientated in the same direction. The punching is a punch and die process providing a formation of a burr on the punch facing side of the reed. The question was raised whether the whistle activation point is sensitive to the direction of the burr. Subsequently eight whistles were assembled with the burr facing the reed bed and tested 12 times, determining the activation pressure (Figure 7.7.1). Whistles were then disassembled and re-assembled with the burr facing away from the reed-bed, and once again tested 12 times each. These activation points were then compared to the activation points of the downward facing burr tests.

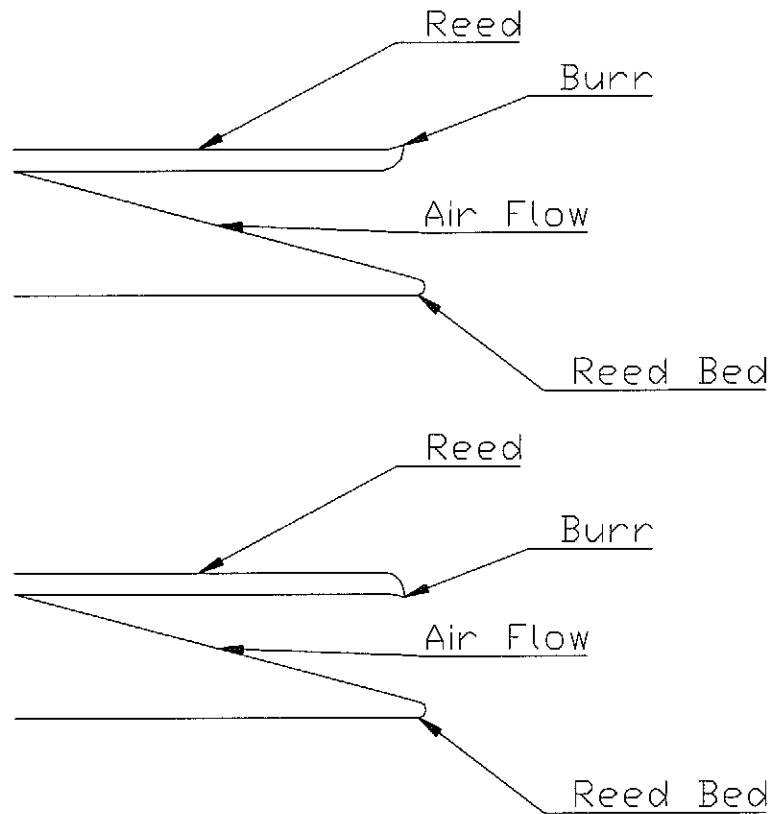


FIGURE 7.7.1
Sidedness of Reed

7.8 The influence of reed dimensions on the P_{RA}

The aim of this series of experiments was to empirically find a relationship between reed dimensions (i.e. width, thickness and length) and the P_{RA} .

7.8.1 The influence of reed width on P_{RA}

Due to the excessive cost and time-consuming nature of spark erosion cutting of different punches, milling of the standard reed was the only way to produce an array of different reed widths. Milling of the reeds however introduced small burrs on the sides of the reeds, which faced the free stream air flow resulting in highly inconsistent testing results. Consequently it was decided, to abandon this series of experiments.

The only other option available with respect to the influence of reed width on P_{RA} was to compare reeds with length = 13.1mm and width = 4.4 mm to a reed with length = 13.1 mm and width = 3.3 mm. It was expected that the wider reed would increase the stiffness and result in higher activation pressure, which was subsequently confirmed through testing.

7.8.2 The influence of reed length on P_{RA}

A series of different reed lengths were produced by milling. The milling was done on the rear end of the reed with the result that the burred side did not face the free stream air flow as it was locked into the body of the whistle. An array of reed lengths were milled from the standard reed (length = 13.5 mm, width = 4.4 mm), covering the range of 13.5-12.5 mm with a resolution of 0.1 mm. The lower range was chosen as this was the shortest reed length, which would be able to produce a significant audible activation. This phenomena is due to the third order stiffness increase of the reed brought about through shortening of the reed. [33] This is illustrated as follows:

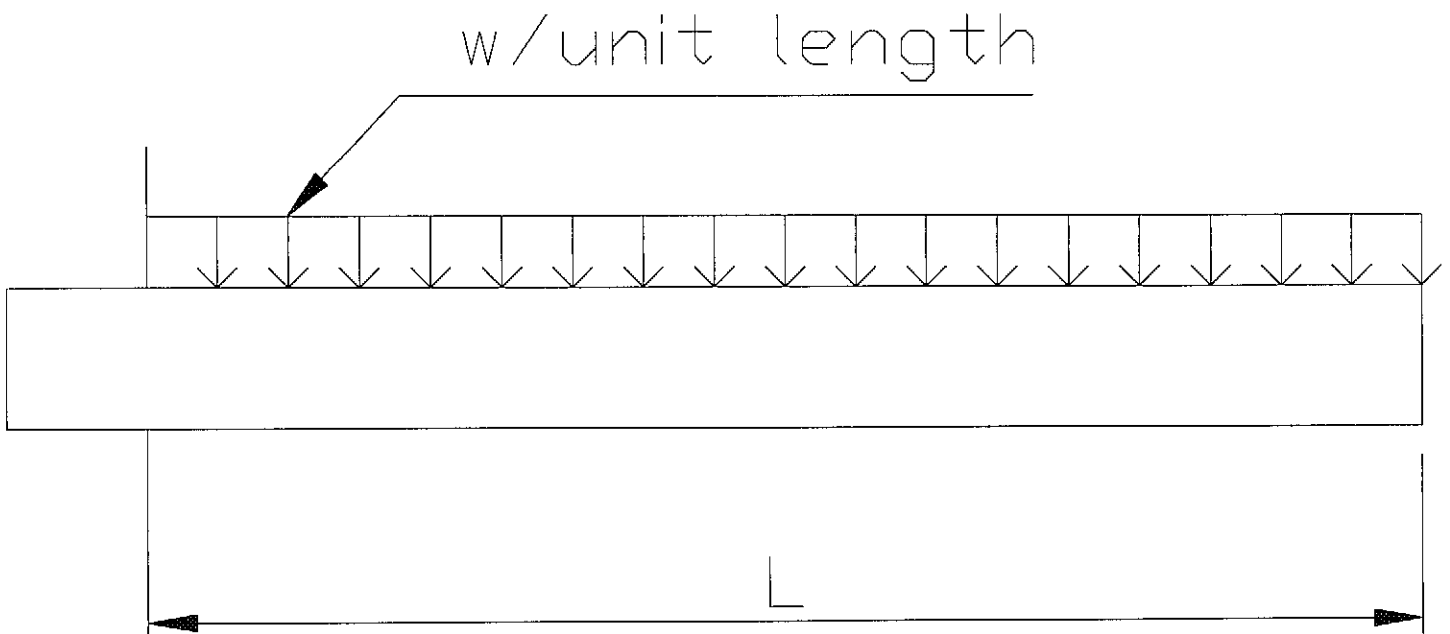


FIGURE 7.8.1
Cantilever

It has been shown [33] that the displacement at the tip of the cantilever shown is:

$$y = \frac{w \cdot L^4}{8 \cdot E \cdot I} \quad (7.8.1)$$

But if $F = w \cdot L$, equation 7.8.1 may be rearranged as follows:

$$F = \frac{8 \cdot E \cdot I \cdot y}{L^3} \quad (7.8.2)$$

Which is of the form $F = k \cdot y$, which is Hook's Elasticity Law, where k is the spring stiffness applying this:

$$k = \frac{8 \cdot E \cdot I}{L^3} \quad (7.8.3)$$

Thus the stiffness (k) of the reed may be described by equation 7.8.3 where:

- y = Displacement [m]
- w = Force per unit length [N/m]
- F = Net force [N]
- k = Stiffness [N/m]
- E = Young's Modulus of Polycarbonate [N/m²]
- I = Second moment of inertia [m⁴]
- L = Reed length [m]
- b = Reed width [m]
- h = Reed thickness [m]

Graphically depicted:

$$E := 4.3 \cdot 10^9 \quad [33]$$

$$b_{\text{rest}} := 4.4 \cdot 10^{-3}$$

$$b_{\text{free}} := 3.3 \cdot 10^{-3}$$

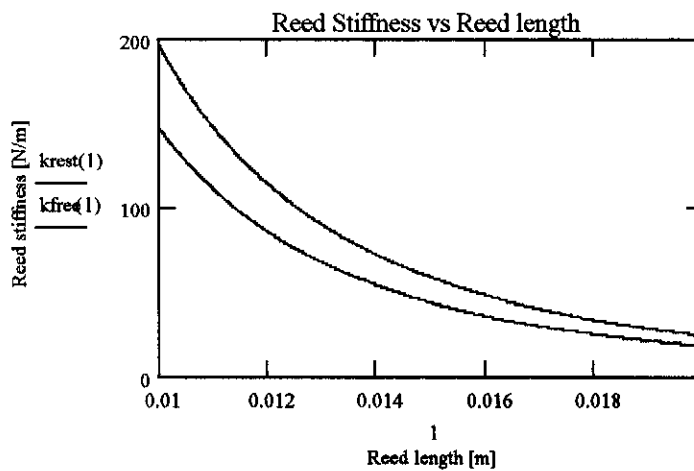
$$h := .25 \cdot 10^{-3}$$

$$I_{\text{rest}} := \frac{(b_{\text{rest}} \cdot h^3)}{12}$$

$$I_{\text{free}} := \frac{(b_{\text{free}} \cdot h^3)}{12}$$

$$k_{\text{rest}}(l) := \frac{(8 \cdot E \cdot I_{\text{rest}})}{l^3}$$

$$k_{\text{free}}(l) := \frac{(8 \cdot E \cdot I_{\text{free}})}{l^3}$$



As stated and graphically supported, the stiffness of the reed is inversely proportional to the third order of reed length, limiting the shortest functional reed length to be a minimum of 12.5 for a restricted reed.

Three whistles were produced for each specific length and the average activation pressure for each length was determined from twelve consecutive test runs.

7.8.3 The influence of reed thickness on P_{RA}

The polycarbonate sheets were only supplied in thickness of 175 μm and 250 μm . The free reed punch of length = 13.1 mm, width = 4.0 mm was used to punch 30, 175 μm and 250 μm reeds respectively. All whistles were assembled and tested with the same ramp input waveform described in Section 7.4. One would expect that the decreased stiffness of the thinner reeds would result in reduced reed activation pressure. This decreased stiffness is depicted in the following calculations, where the same variable definitions as defined in Section 7.8.2 are applicable.

$$E := 4.3 \cdot 10^9 \quad [33]$$

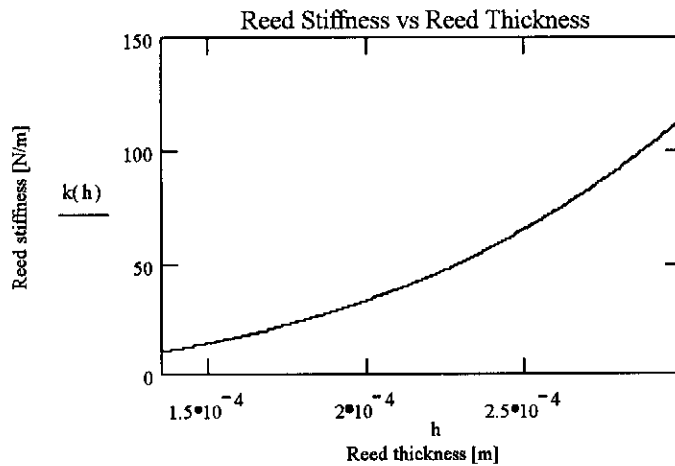
$$b := 3.3 \cdot 10^{-3}$$

$$l := 13.1 \cdot 10^{-3}$$

$$k(h) := \frac{\left[8 \cdot E \cdot \frac{(b \cdot h^3)}{12} \right]}{l^3}$$

$$k(175 \cdot 10^{-6}) = 22.552$$

$$k(250 \cdot 10^{-6}) = 65.75$$



7.9 Functional testing of the Whistle Watch™

The aim of the following series of experiments was to characterise the Whistle Watch as a functional unit. Both the free and restricted reed whistle configurations were inserted into the body of the Whistle Watch and the whistle activation pressure determined at various pre-set flow rates. A secondary objective was to evaluate the response of the Whistle Watch to different input flow envelopes. The latter were considered to be important, due to differing flow envelopes contained within separate asthmatic patients, albeit that they may have the same PEF.

7.9.1 The Requirements of the American Thoracic Society (ATS)

The American Thoracic Society (ATS) prescribes a series of tests for the evaluation of respiratory devices. This body updated their 1979 [29] spirometry recommendations in 1987 [28], through the addition of 26 standard volume-time waveforms, which they recommended for testing of spirometers. Peak expiratory flow values for the waveforms were provided, although they were not originally intended for use in the testing of peak expiratory flow (PEF) meters. Initially they were intended for use in testing of the volume accuracy of spirometers. The latter were tested for a range of volumes, expiratory times, extrapolated volumes and start - end test anomalies.

In 1992, the National Asthma Education Project [30], recommended that ATS Waveform 24 be used to test PEF meters, as it represents an acceptable FVC manoeuvre with a relatively slow rise time, which can be simulated by a mechanical pump. The magnitude of Waveform 24 may be scaled to obtain a range of PEFs typically between 60 and 700 l.min⁻¹. ATS waveform 24 is illustrated in Figure 7.9.1.

Figure 7.9.2 was extracted from Figure 7.9.1 to indicate the rise time (i.e. the time from 10% to 90% of PEF) and the dwell time (i.e. the time from 95% of PEF on the rising edge to 95% of PEF on the falling edge). ATS waveform 24 has a rise and dwell time of 50 ms and 10 ms respectively.

ATS 24 Flow-Time Waveform

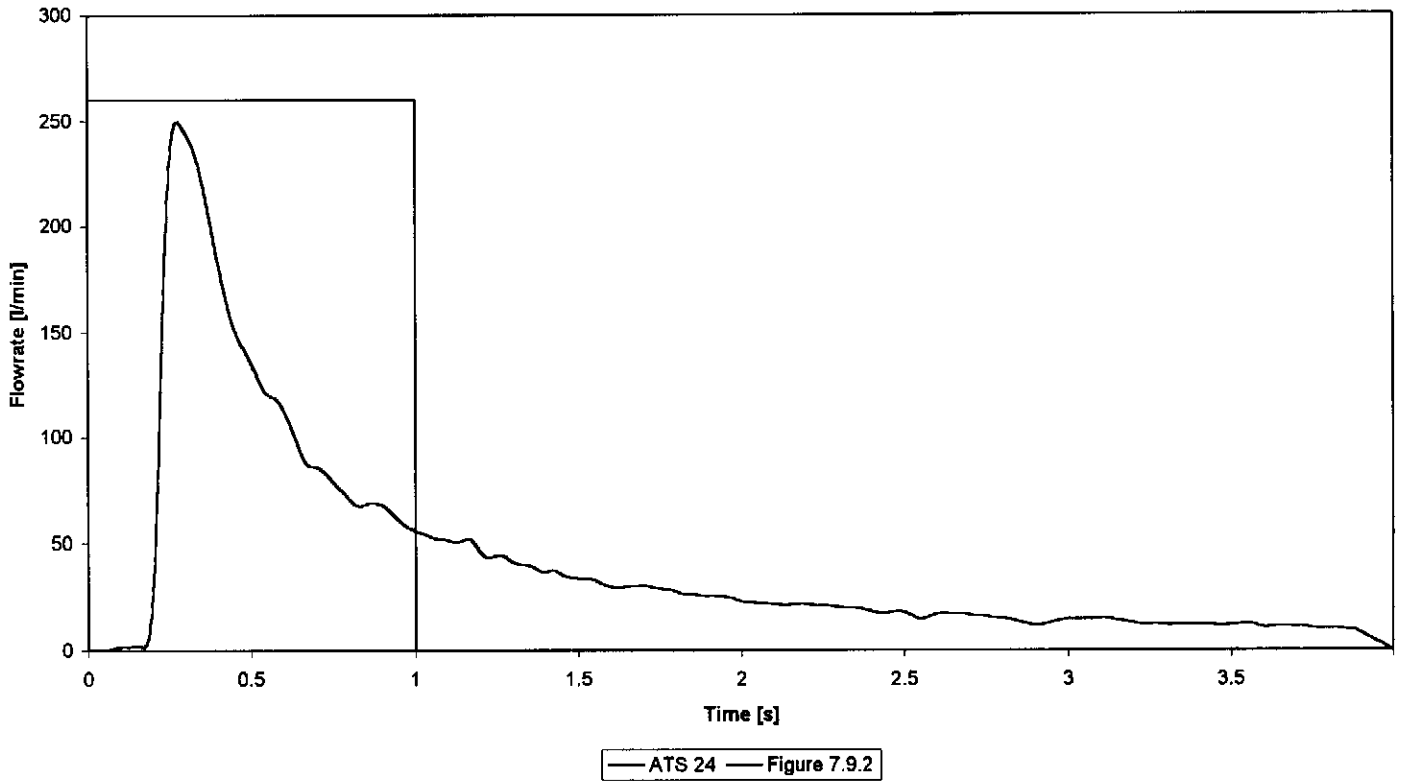


FIGURE 7.9.1
ATS 24 Waveform

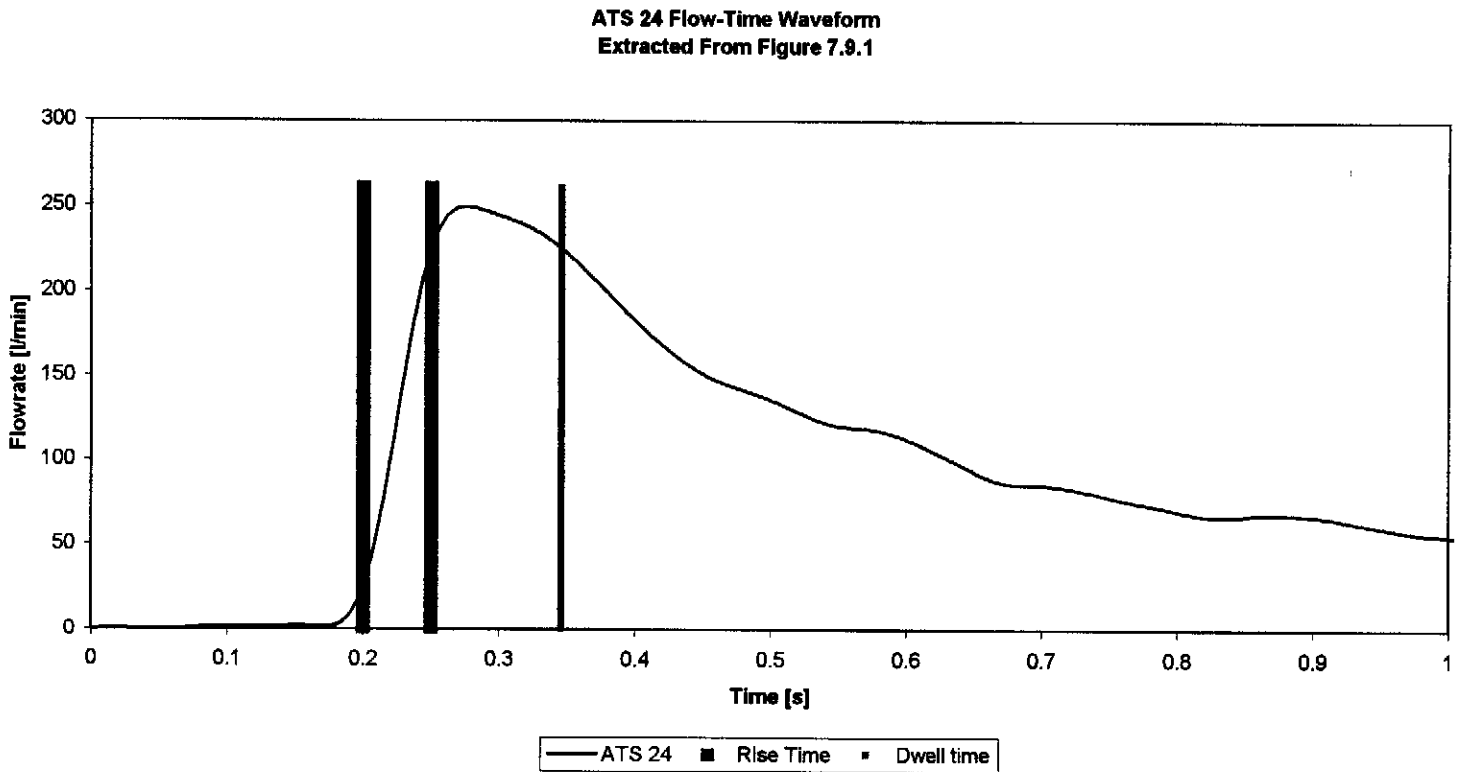


FIGURE 7.9.2
ATS 24 Waveform Extracted From Figure 7.9.1 Indicating Rise and Dwell Time

The ATS 24 flow-time curve, (the norm that the ATS prescribes for the testing of pulmonary devices) was integrated using Gaussian-Quadrature to produce a volume-time curve. The latter was combined with the ATS 24 flow-time curve to produce Figure 7.9.3, an ATS 24 flow-volume curve. A Comparison of Figure 7.9.3 with Figure 3.2.1 (which is a typical expiratory Flow-Volume curve), indicates that the ATS 24 waveform is an acceptable experimental model for simulating forced expiration.

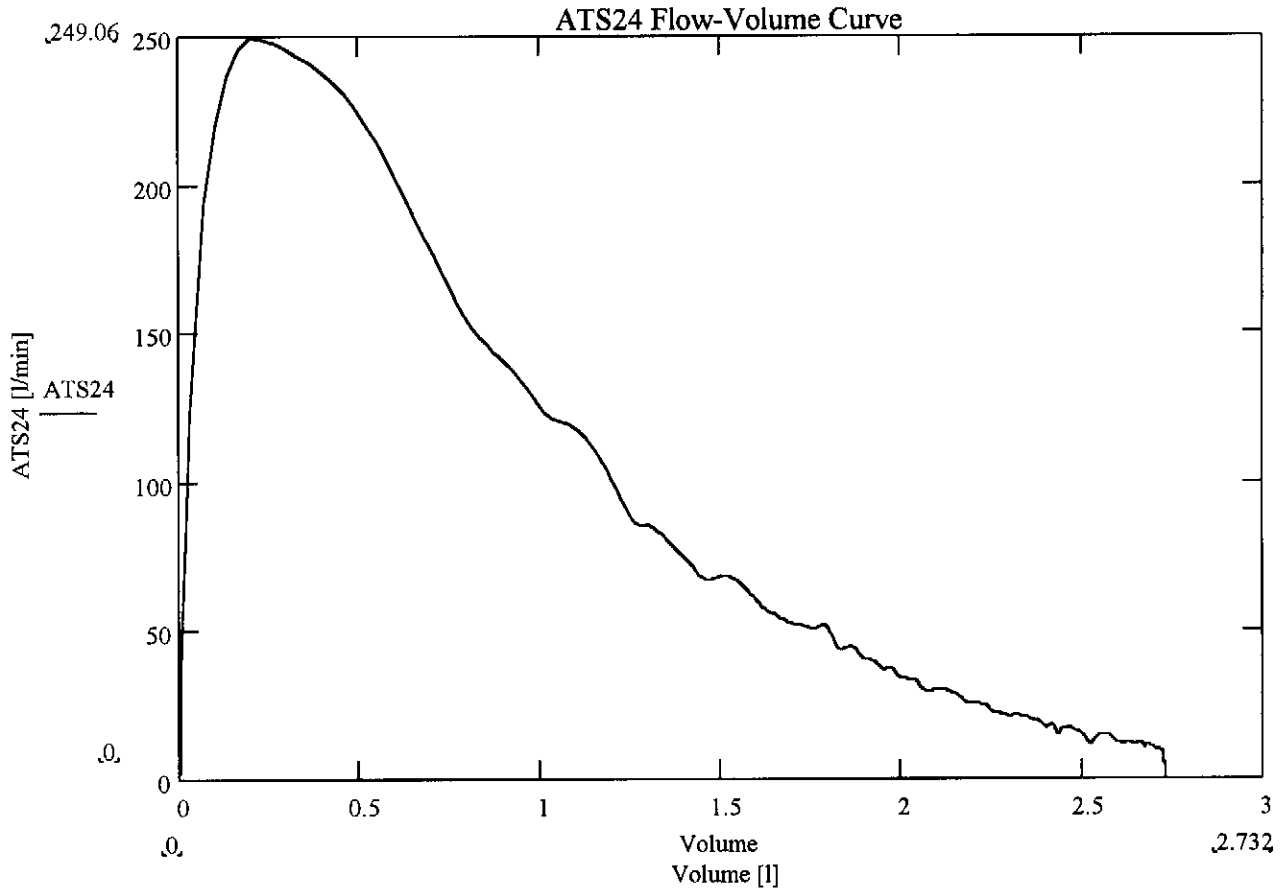


FIGURE 7.9.3
ATS24 Flow-Volume Curve

7.9.2 Customised Impulse waveforms

A process of developing two customised sets of impulse waveforms, straining from the beaten ATS path, was initiated. These waveforms had similar characteristics to the ATS 24, but were designed with the goal to facilitate ease of implementation into the computer controlled stepper motor as described in Section 7.1. Through simple manipulation of the customised waveforms, it was possible to generate different peak flow rates as well as different rise and dwell times.

Impulse 1

Impulse 1 was based on the function $f(x) = \frac{1}{2} \cdot \left(x - \frac{\sin(2 \cdot \pi \cdot x)}{2 \cdot \pi} \right)$, which was developed in MathCAD with the aim to generate an input flow, which has relatively long rise and dwell times. In addition thereto, this would facilitate the implementation onto the mechanical pump, as the impulse waveform's first derivative (flow rate), second derivative (acceleration) and third derivative (jerk) are continuous. Acceleration was initialised from zero for the period of normalisation, to ensure that no shock waves were imparted onto the air column. The above mentioned were the result of:

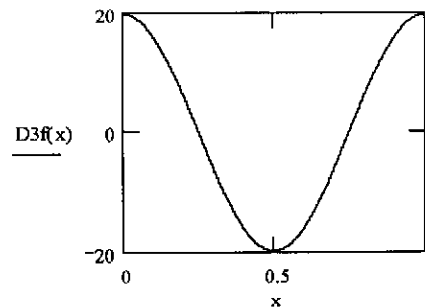
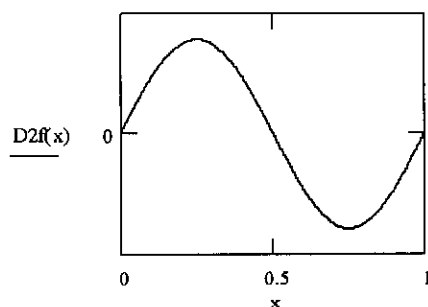
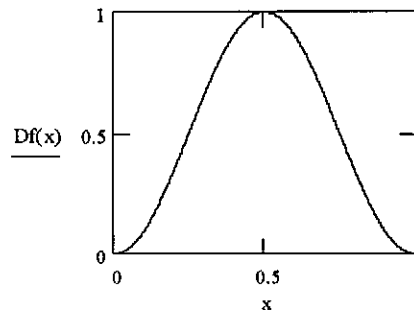
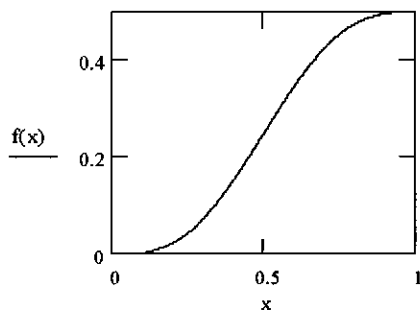
 $j := 0, 0.2.. 1$

$$f(x) := 0.5 \cdot \left(x - \frac{\sin(2 \cdot \pi \cdot x)}{2 \cdot \pi} \right) = \text{Volume}$$

$$Df(x) := \frac{d}{dx} f(x) = \text{Flow rate}$$

$$D2f(x) := \frac{d^2}{dx^2} f(x) = \text{Acceleration}$$

$$D3f(x) := \frac{d^3}{dx^3} f(x) = \text{Jerk}$$



Impulse 2

Impulse 2, based on the following function $f(x) = \frac{1}{2} \cdot \left(x - \frac{\sin(2 \cdot \pi \cdot x)}{2 \cdot \pi} \right)^4$, was generated in a similar manner and complied with all the characteristics of Impulse 1, but with shorter rise and dwell times, as illustrated below:

 $j := 0, 0.2.. 1$

$$f(x) := 0.5 \cdot \left(x - \frac{\sin(2 \cdot \pi \cdot x)}{2 \cdot \pi} \right)^4 = \text{Volume}$$

$$Df(x) := \frac{d}{dx} f(x) = \text{Flow}$$

$$D2f(x) := \frac{d^2}{dx^2} f(x) = \text{Acceleration}$$

$$D3f(x) := \frac{d^3}{dx^3} f(x) = \text{Jerk}$$

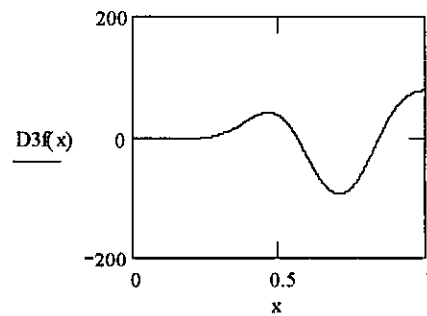
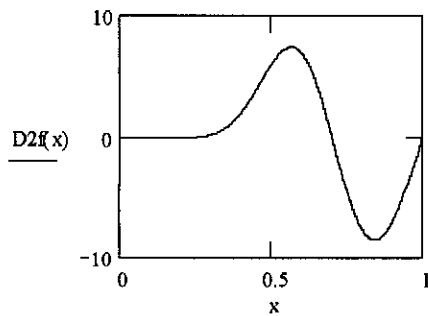
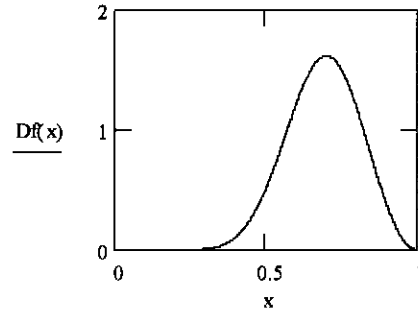
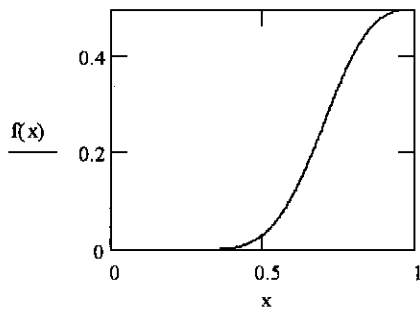


Figure 7.9.4 illustrates the relationship of the custom impulses developed, compared to the ATS 24 waveform.

Flow-Time WaveForm Comparisons

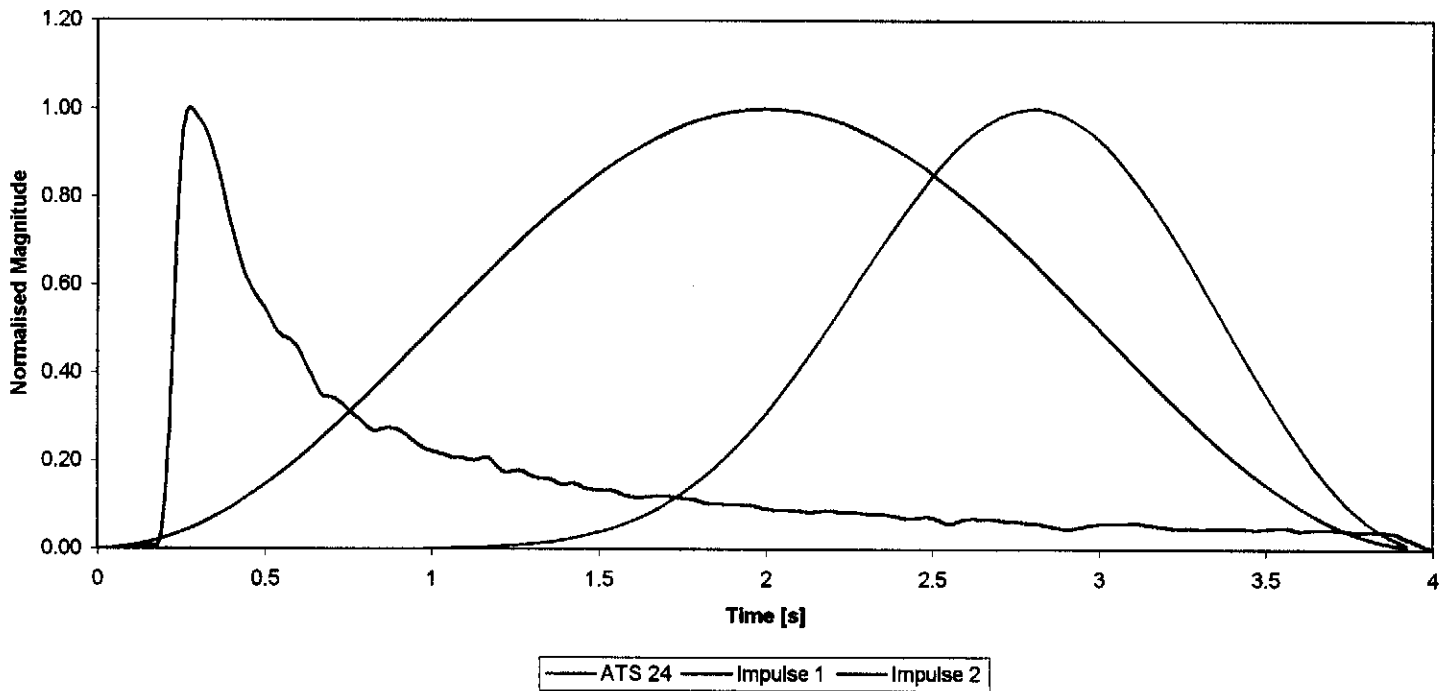


Figure 7.9.4
Waveform Comparison

7.9.3 Time domain changes to the customised Impulse waveforms

Impulse 1 and 2 defines the flow envelopes consisting of 50 data points each, which may be downloaded to the stepper motor and scaled both in time and amplitude (or peak flow). Changing the time interval between consecutive data points could alter the rise and dwell times. The following time intervals were selected; 0.02s, 0.04s, 0.06s and 0.08s and the resulting rise and dwell times have been illustrated in Table 7.9.1 and the corresponding waveforms in Figure 7.9.5 and Figure 7.9.6.

TABEL 7.9.1
Rise & Dwell Times

Time Interval	Impulse 1		Impulse 2	
	Rise Time	Dwell Time	Rise Time	Dwell Time
s	s	s	s	s
0.02	0.3	0.2	0.22	0.12
0.04	0.6	0.4	0.44	0.24
0.06	0.9	0.6	0.66	0.36
0.08	1.2	0.8	0.88	0.48

Normalised Impulse 1 vs Time

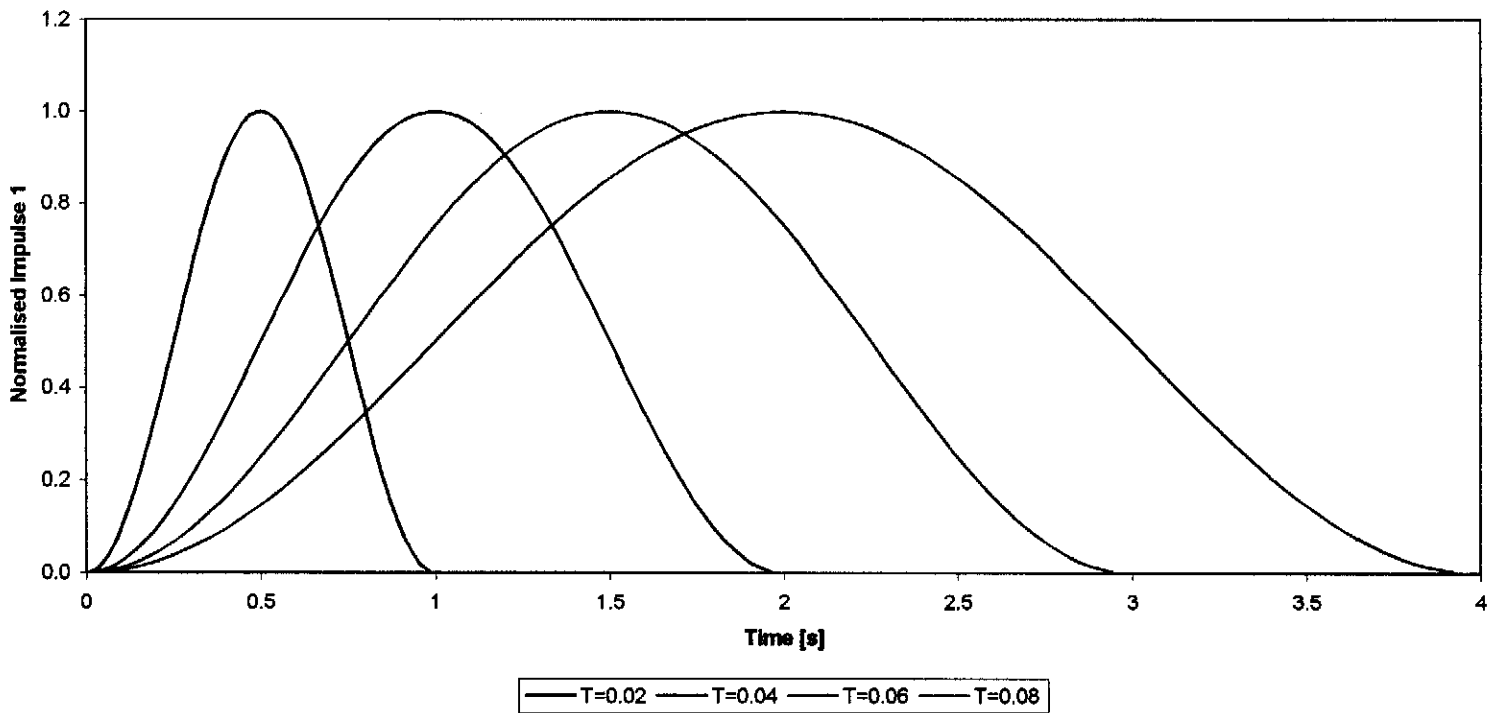


FIGURE 7.9.5
Time domain variations of Impulse 1

Normalised Impulse 2 vs Time

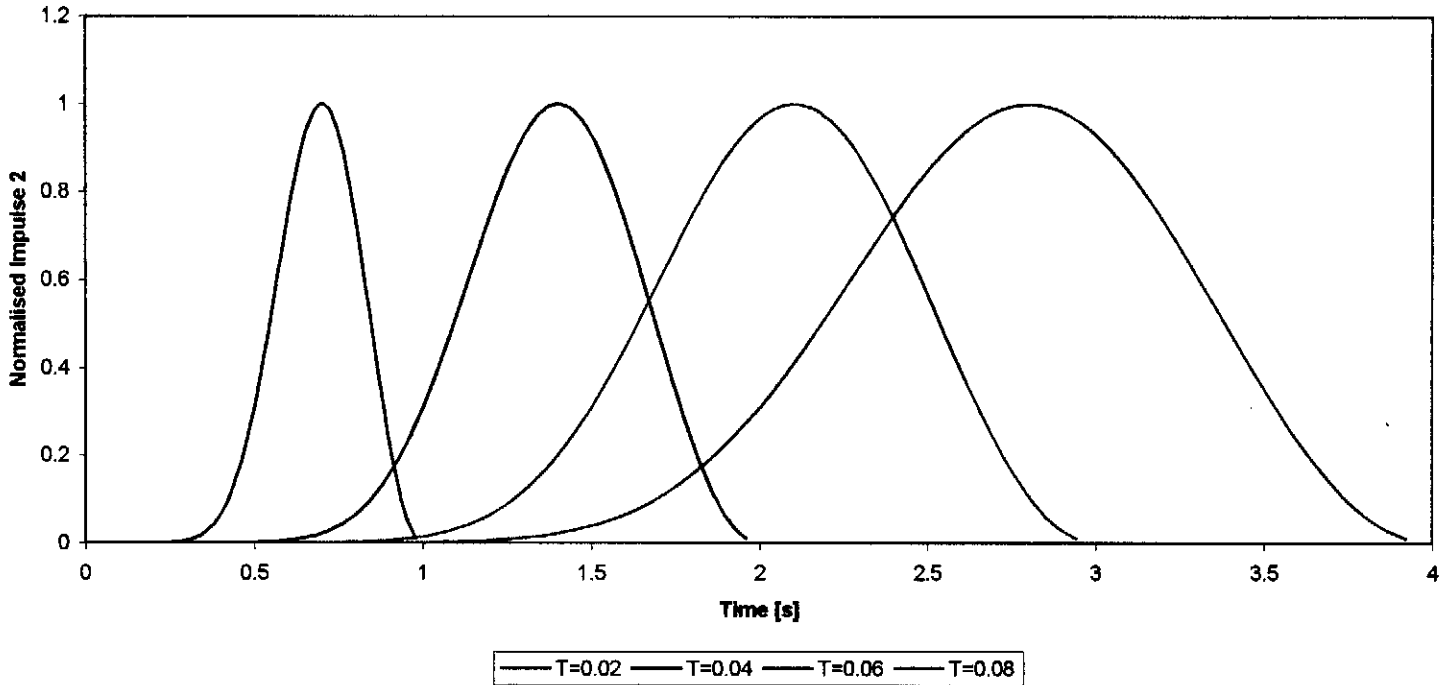


FIGURE 7.9.6
Time domain variations of Impulse 2

7.9.4 Validation of P_{RA} at higher sampling rates

Data capturing was executed in a similar manner, as described in Section 7.4, except for changing the sampling level to 6 kHz. The latter was implemented in accordance with the short Impulse waveforms (0.5s) as apposed to the long ramp input (2s).

The technique of determining the reed activation pressure, as described in Section 7.4, was questioned for the increased sampling frequency. Using the standard ramp input waveform (Section 7.4) and a whistle in two tests, where the sampling frequency was

set at 3 kHz and 6 kHz respectively, pressure data was captured. The technique in Section 7.4 was applied to the pressure data and the activation points were determined, resulting in $P_{RA3kHz} = 535.04 \pm 10.18$ Pa and $P_{RA6kHz} = 541.86 \pm 10.6$ Pa.

A Student's t-test for dependent samples was executed on the activation points, producing a $p = 0.087$, where a $p < 0.05$ indicates a statistical significant difference between compared data sets. Figure 7.9.7 visually compares 3 kHz and 6 kHz sampled data for a specific whistle tested, and the corresponding P_{RA} for each sampling frequency. Figure 7.9.8 is extracted from Figure 7.9.7 for further illustrative purposes.

The Effect of Varying Sampling Rate

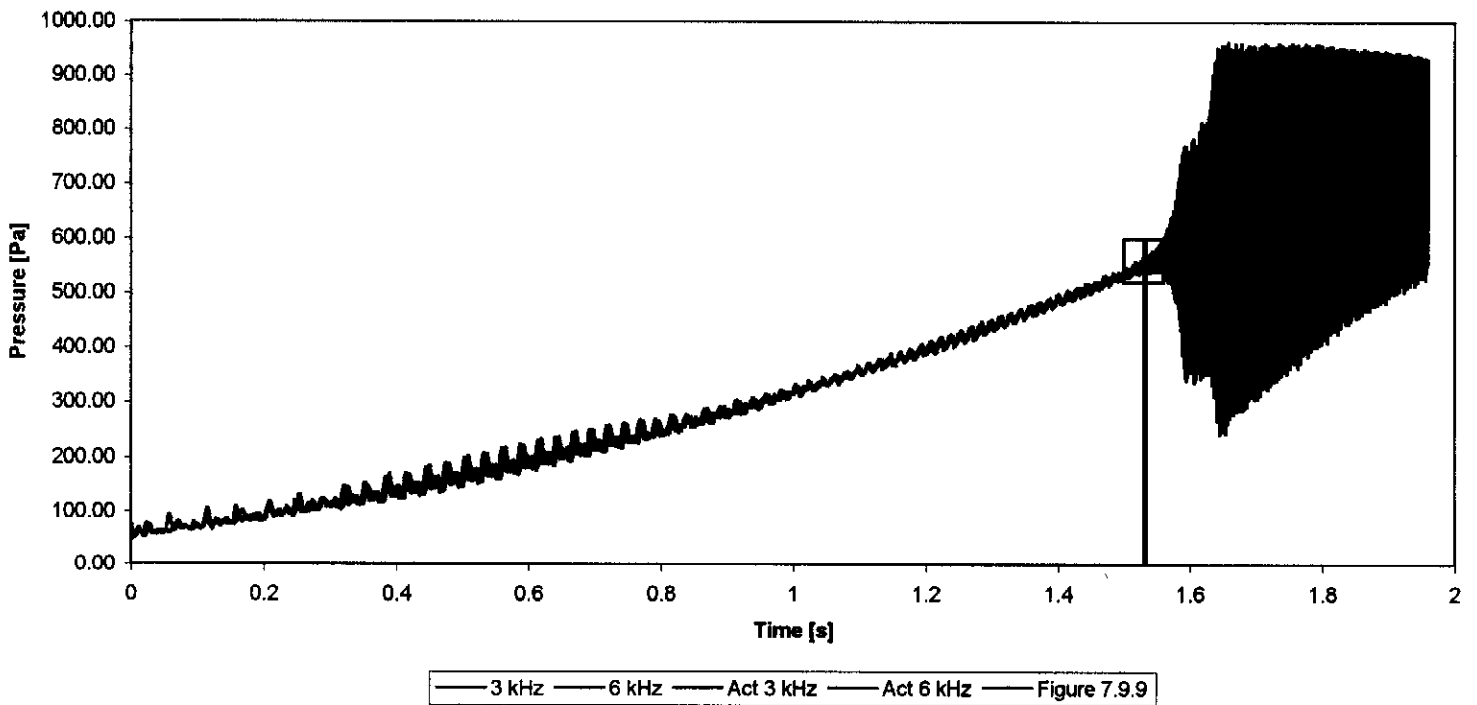


FIGURE 7.9.7
Varying Sampling Frequencies

The Effect of Varying Sampling Rate
Extracted From Figure 7.9.8

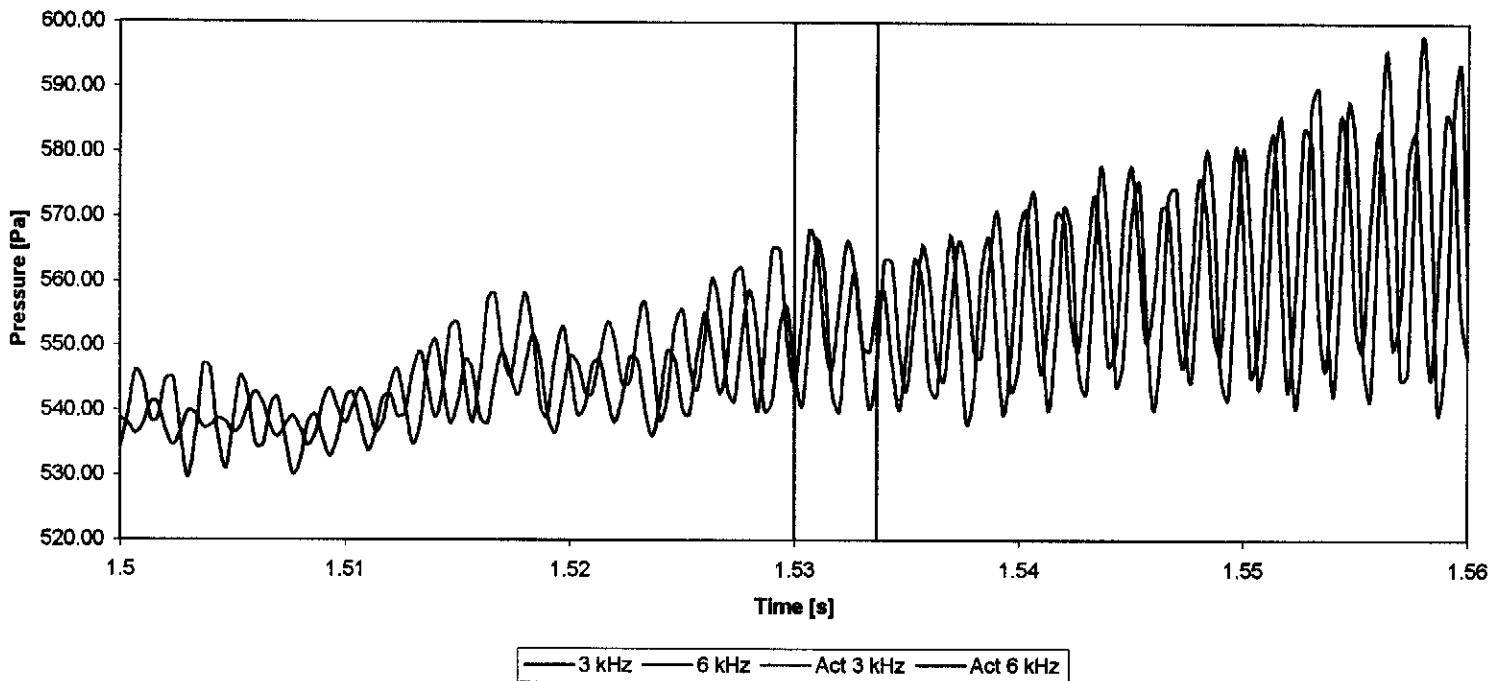


FIGURE 7.9.8
Varying Sampling Frequencies

Results show sufficient support for the conclusion that the technique for determining P_{RA} described in Section 7.4 is in this case independent of the sampling frequency. This experiment and conclusion validated the comparison of P_{RA} determined in the “ideal” nozzle (Figure 7.1.2), sampled at 3 kHz, with the P_{RA} determined in the Whistle Watch, sampled at 6 kHz. The technique of determining P_{RA} with increased sampling rate of 6 kHz was now applied to the customised impulse waveforms, with an example illustrated in Figure 7.9.9.

Pressure vs Time for Impulse 1 on a Restricted Configuration

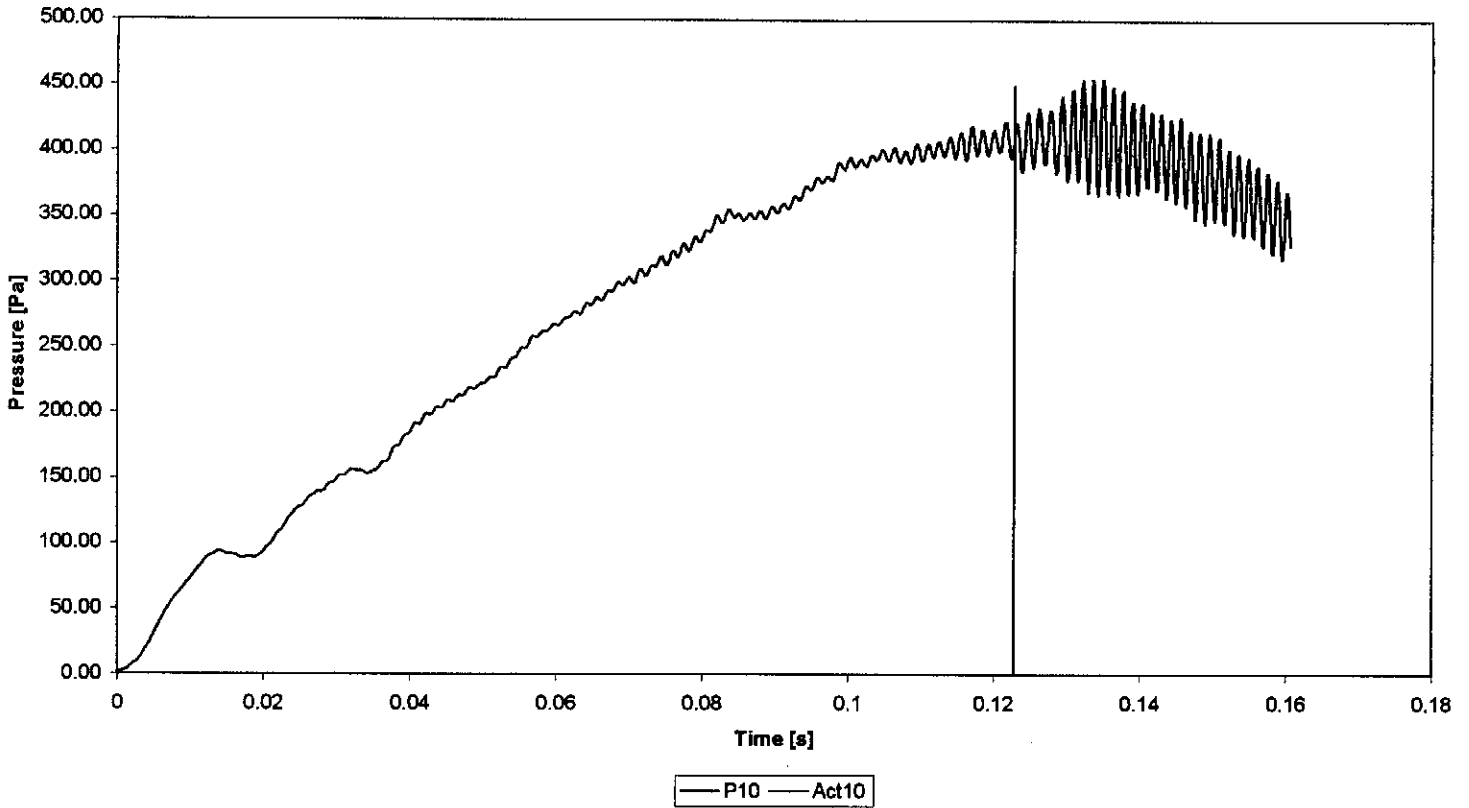


FIGURE 7.9.9
Activation technique at 6 kHz applied to Impulse 1

7.9.5 Test Procedure

A group of restricted ($n = 4$) and free ($n = 4$) reed whistles were selected from respective batches as described in Section 7.6. The whistles in each group were selected to have similar activation pressures and small standard deviations. Whistles were inserted into the pre-set Whistle Watch bodies as shown in Table 7.9.2:

Restricted Reed	Free Reed	Pre-set Whistle Watch
1	1	150 l.min ⁻¹
2	2	200 l.min ⁻¹
3	3	250 l.min ⁻¹
4	4	300 l.min ⁻¹

Table 7.9.2
Whistle Insertion into Pre-set Whistle Watch[®] Body Sequence

This assembly procedure was a permanent fixture, as any attempt to remove the whistles from their taper locks would result in their destruction.

After insertion it was necessary to measure the reed activation pressure of the whistle when encapsulated by the body. Holes were drilled through a non-functional Section of each pre-set Whistle Watch into the whistle location tube, through which blunt syringe needles ($\phi 1.8 \times 40$ mm) (Figure 7.9.10) could be inserted. Needle tips were placed flush with the tube wall, thereby ensuring the measurement of static pressure. (Figure 7.9.11)

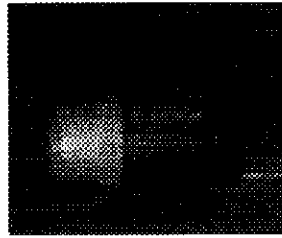


FIGURE 7.9.10
Pre-set Whistle Watch[®] with the inserted syringe needle

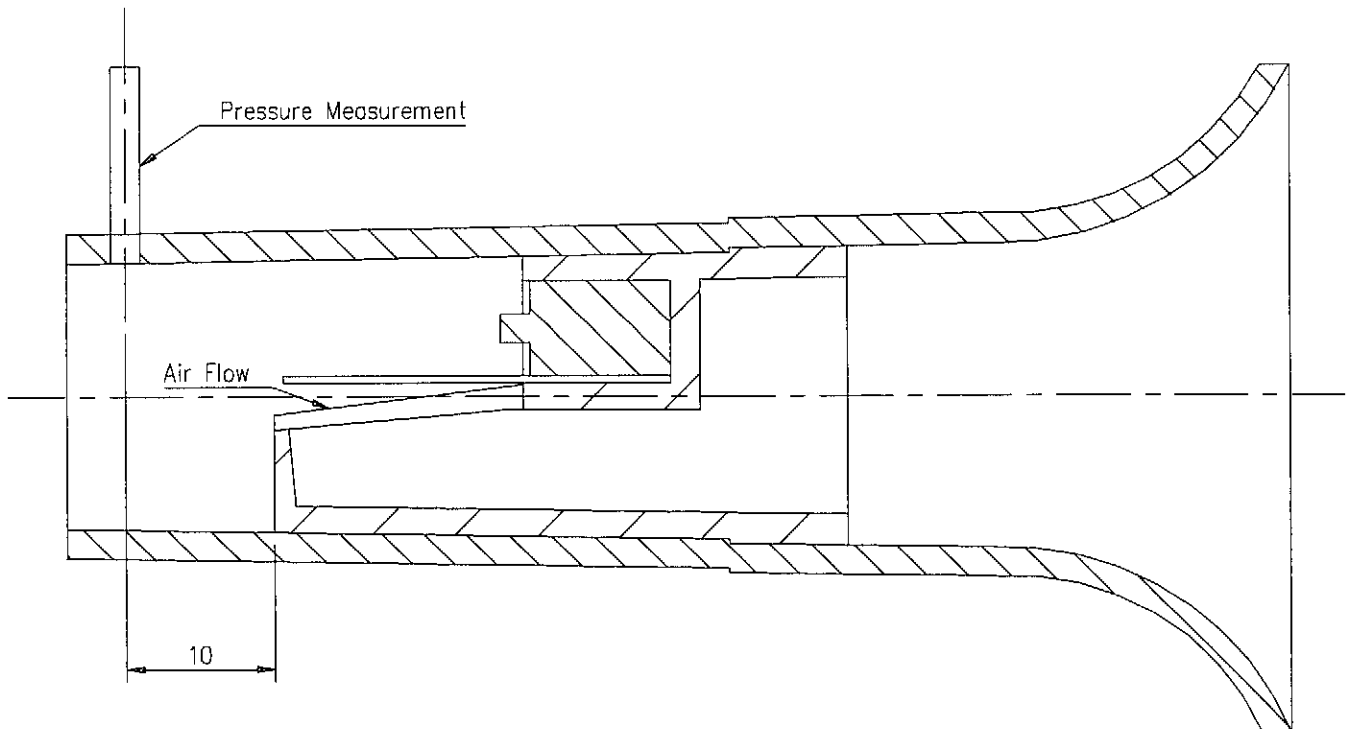


FIGURE 7.9.11
Modified Sectioned Whistle Watch[®], which illustrates where the pressure was measured.

Physical constraints of the Whistle Watch limited the placement of the pressure port at the required 4 location tube diameters, upstream from the whistle. It is therefore possible that second order effects caused by the reed might have influenced the pressure measurement.

The nozzle (Figure 7.1.2) was removed from the mechanical pump and the Whistle Watch was inserted directly into the flat end plate. This configuration was considered to be similar to the way the patient would be using the Whistle Watch, resulting in redundancy of any extension pipe, between the endplate and Whistle Watch, which could facilitate fully developed flow.

CHAPTER 8

RESULTS

This chapter describes the results of the experiments described in Chapter 7. Where applicable, section headings are the same as that of the corresponding experimental procedure in Chapter 7.

8.1 The influence of nozzle geometry on reed activation pressure

The high dependency of P_{RA} on upstream nozzle geometry, is presented in Figure 8.1.1 and Figure 8.1.2, with data plotted as means \pm standard deviation.

Constricted Nozzle

The increasing step length produced a corresponding increase in P_{RA} , with a maximum turning point at $L_{step} = 30$ mm. Step lengths greater than the turning length resulted in a decreasing P_{RA} , with termination at a functional $L_{step} = 60$ mm where P_{RA} is below the initial value. Both free and restricted reeds responded similarly, with the only difference at the longer step lengths (50, 60 mm), where it seems as if the instability in P_{RA} increases for the restricted reed compared to the free reed configuration.

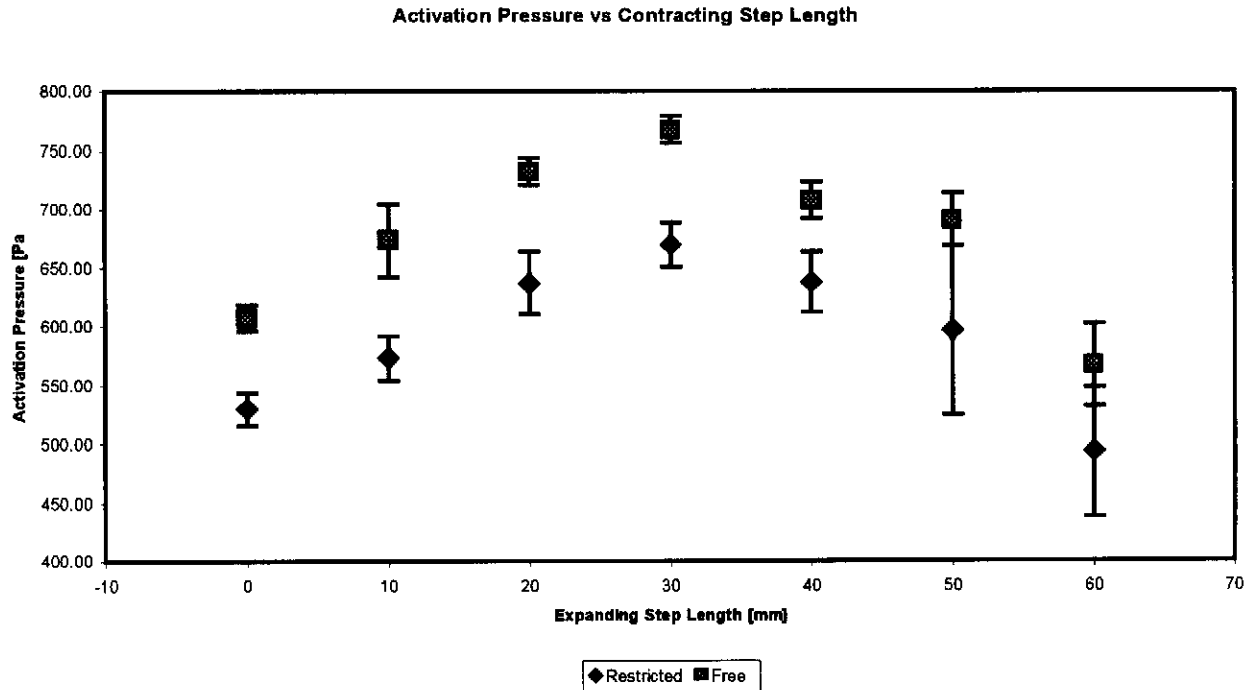


FIGURE 8.1.1
Constricted step length effect on a restricted reed

Expanding Nozzle

The increasing step length produced a corresponding decrease in P_{RA} , with a minimum turning point at $L_{step} = 40$ mm. Step lengths greater than the turning length resulted in an increasing P_{RA} , with termination at a functional $L_{step} = 50$ mm where P_{RA} is below the initial value. Both free and restricted reeds responded similarly.

Activation Pressure vs Expanding Step Length

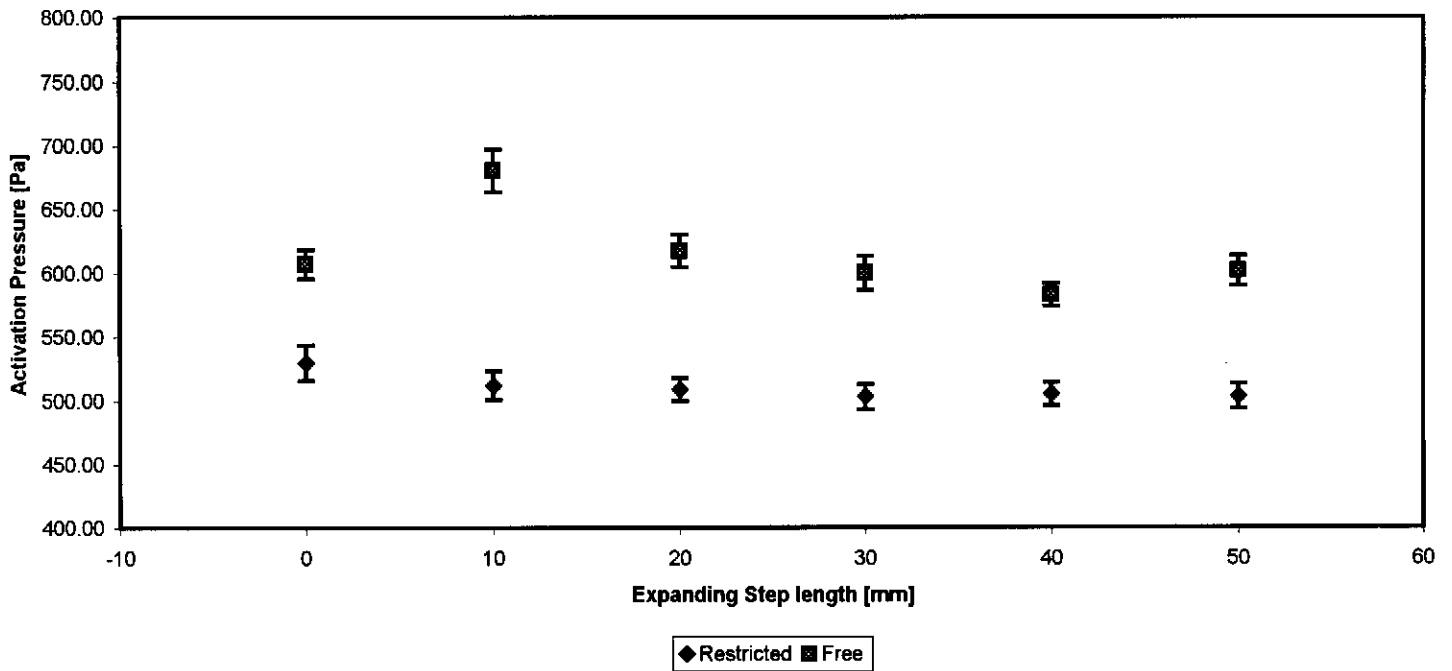


FIGURE 8.1.2
Expanding step length effect on a restricted reed whistle

This behaviour of restricted reeds could not be attributed to measurement error, as both whistles were evaluated in the same manner. This was supported through evaluating pressure measurements taken at different positions in the unstepped length of Figure 7.2.1 and Figure 7.2.2 for the same whistle. These measurements were independent of positioning, and one may therefore assume that the effect is inherent to the specific whistle configuration.

The dependency of P_{RA} on upstream geometry can only be assumed, as no experimental evidence is available for clarification. The two main perceived contributing factors are:

- instabilities induced to the free stream by the step

- altered acoustic coupling between the reed and preceding air column, through changes in the nozzle impedance

1.) Instabilities induced to the free stream by the step:

This factor will be discussed with reference to the constricted nozzle only as the same principles apply to the expanding nozzle, but in reverse.

Figure 8.1.3 is an extracted view of the constricted section of the geometrically modified nozzle (Figure 7.2.1). It illustrates what effect the constricted section has on the free stream.

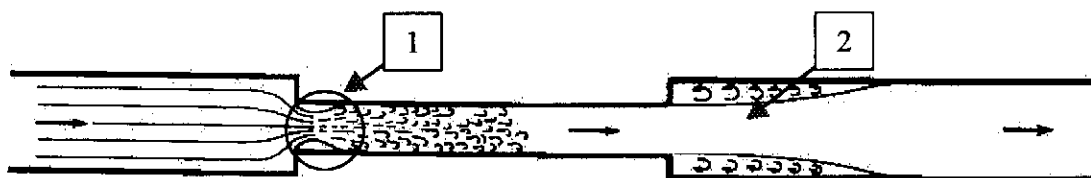


FIGURE 8.1.3
Extracted view of constricted section of geometry nozzle

To understand the instabilities induced to the free stream by the step it is important to review the fluid mechanics of a constricted section.

The sudden contraction results in a marked drop in pressure due to the increase in velocity and to the loss of energy in turbulence. The central stream at 1 is surrounded by air, which is in a state of turbulence but has very little forward motion. This increased turbulence and vortex motion are carried over and amplify the sudden expansion effects, which follow. At the sudden expansion (2), there is a rise in pressure due to a decrease in velocity and a state of excessive turbulence. Figure 8.1.2 shows that the effect of the sudden

expansion is greater than the contraction. This is due to the inherent instability of flow during expansion, where the diverging paths of the flow tend to encourage the formation of eddies within the flow. The eddy magnitude and quantity are amplified through the dimensional constrains of the nozzle. It is this eddy forming effect of the contraction, which introduces the instabilities to the free stream.

This theory was put to practice in setting up of a computational fluid dynamics model in Flo++. The pressure and velocity distribution in both the constricted and expanding nozzle at various step lengths were modelled. The proceeding discussion will be executed with reference Appendix G, which encapsulates the results of the CFD modelling. The pressure and velocity distribution presented in Figure G.1 and Figure G.2 respectively was constructed for the testing nozzle of Figure 7.2.1 for a flow rate of $15 \text{ l}\cdot\text{min}^{-1}$. These figures will be used as a benchmark to review the figures of the constricted and expanding nozzles at various step lengths.

Expanding nozzle

The first observation made is that the pressure patterns and magnitudes obtained at various step lengths are similar to Figure G.1. The velocity patterns and magnitude on the other hand varies greatly from one step length to the other. Worman [36] pointed out that Bernoulli forces, which is comprised of velocities, contribute only 1,7% towards the activation of the whistle. This fact together with the CFD result, leads to the conclusion that velocity is the major contributing factor, which effects the whistle activation in

an expansion nozzle, but only to a small extent. The latter is observed in Figure 8.1.2.

Constricted nozzle

The observed effects are reversed with the constricted nozzle as oppose to the expanding the nozzle. The velocity pattern and magnitude for each step length is similar to Figure G.2, whereas the pressure pattern and magnitude varies extensively. It is the varying pressure gradients within the constricted section, which reflects at the end of the contraction, superimposing pulsating pressure onto the blowing pressure. The unsteady ramp input envelope should be kept in mind when any conclusions are made, as well as the varying flow resistance of the whistle during activation. This culmination of different contributing factors increases the complexity of the analysis to such an extent that no clear conclusions can be made to describe the phenomena observed in Figure 8.1.1.

Summarising, the CFD could only underline that the identified factor of instabilities in the free stream contributes extensively to the effects observed in Figures 8.1.1 and Figures 8.1.2.

2.) Altered acoustic coupling between the reed and preceding air column through changes in the nozzle impedance:

With any change in diameter, the air column's acoustic impedance would be altered, which may cause a shift in oscillation frequency. Hoekje [22] clearly illustrated how a change in upstream geometry (in his case the clarinet players windway) caused a shift in the playing frequency. Not only will it influence the

frequency but also the “ease” with which oscillations can be introduced into the down stream air column as pointed out by Worman [36] and Benade and Gans [35].

Both indicated factors could influence the general behaviour as depicted in Figure 8.1.1 and Figure 8.1.2 as well as the observed increase in the standard deviation of the restricted reed at certain step lengths. The relative contribution of the above-mentioned factors, however remains to be determined through proper experimentation. The reason for the free reed activating a relatively higher pressure than the restricted reed is its increased reed stiffness, which is manifested in its length.

The phenomena observed in Figure 8.1.1 and Figure 8.1.2 with their contributing factors, is important to consider when the whistle is placed into the Whistle Watch body. Complex internal structure of the Whistle Watch (as well as the patient’s windway) would cause the P_{RA} to precipitate at a different set point compared to the “ideal” nozzle.

8.2 General characteristics of the reed activation pressure

Activation fluctuations for restricted and free reed configurations are presented as Bland & Altman¹ plots in Figure 8.2.1 and 8.2.2 respectively. The whistle with the lowest coefficient of variance (COV) in each group was chosen (as defined by the Bland & Altman definition) to be the “golden standard whistle” for that specific group, from which the Bland & Altman plots were constructed.

The mean activation pressure for the restricted reed (506.68 ± 38.93 Pa) was lower than that of the free reed (579.94 ± 31.19 Pa). This was expected as the minor stiffness advantage the restricted reed has (80.1 versus 79.6 N/m), was cancelled by the dominating surface area of the free reed (59.4 versus 52.4 mm²). The greater surface area has a dual influence in lowering the P_{RA} :

1. For a given blowing pressure, an increased surface area results in an increase in net driving force.
2. In addition it introduces a higher form drag on the reed tip (the Bernoulli effect as investigated by Worman [36] described in Section 5.1.3) when compared to the narrower free reed.

Comparing Figure 8.2.1 to 8.2.2 it is noticed that with the exception of one data point in each group, the data are within ± 2 standard deviations from the mean. Through closer evaluation it is found, in both configurations that 73% of the cases are within one standard deviation of the mean. Two major contributing factors to the spread in data for both configurations are:

1. The process of manual assembly of the whistles.
2. The punching process imparting irregularities to the reeds.

The first factor may be minimised to an extent, through automation, but the second factor should be seen as inherent reed characteristics. A further minor effect, may be the technique used for determining P_{RA} .

¹ Choose the whistle with the lowest coefficient of variance as the golden standard and plot the remaining whistles' deviation from it.

A second observation from Figures 8.2.1 and 8.2.2 is that the restricted reed configuration generally results in a larger spread of the activation pressure. No obvious explanation for this behaviour exists, since the same assembly procedure and quality control were executed on each batch. Difference in the quality of the free and restricted reed's punch-die sets, were ruled out to an extent as both sets were new and produced by the same high quality manufacturer. This behaviour of free reeds producing smaller standard deviation was however observed throughout this study.

The above observations have practical implications pertaining to the accuracy and quality control of the Whistle Watch. It firstly indicates that the accuracy limits of the Whistle Watch should be referred to as a percentage of the mean activation pressure, and every whistle should be tested for compliance with these limits. Secondly, it seems that the free configuration would provide more consistent results than a restricted configuration.

Bland&Altman Plot For Restricted Reed Configuration

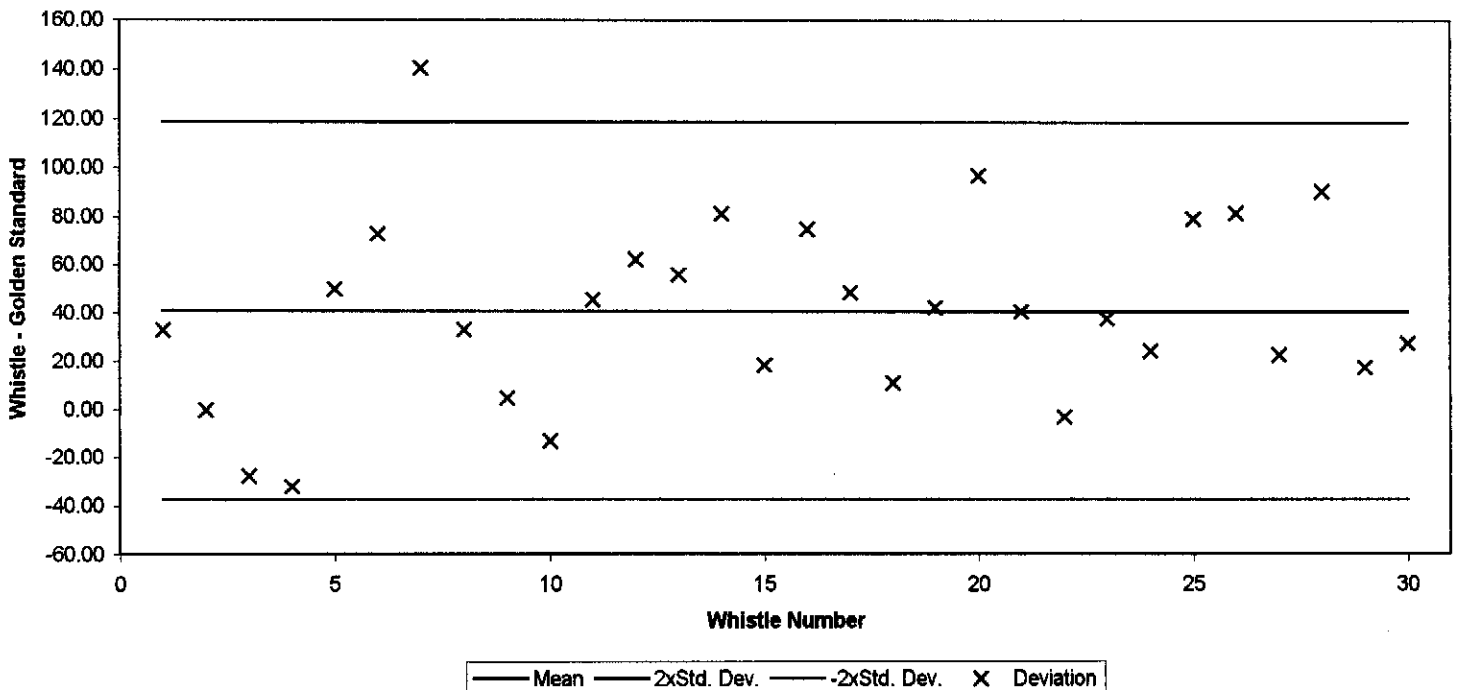


FIGURE 8.2.1
Restricted Reed

Bland&Altman Plot For Free Reed Configuration

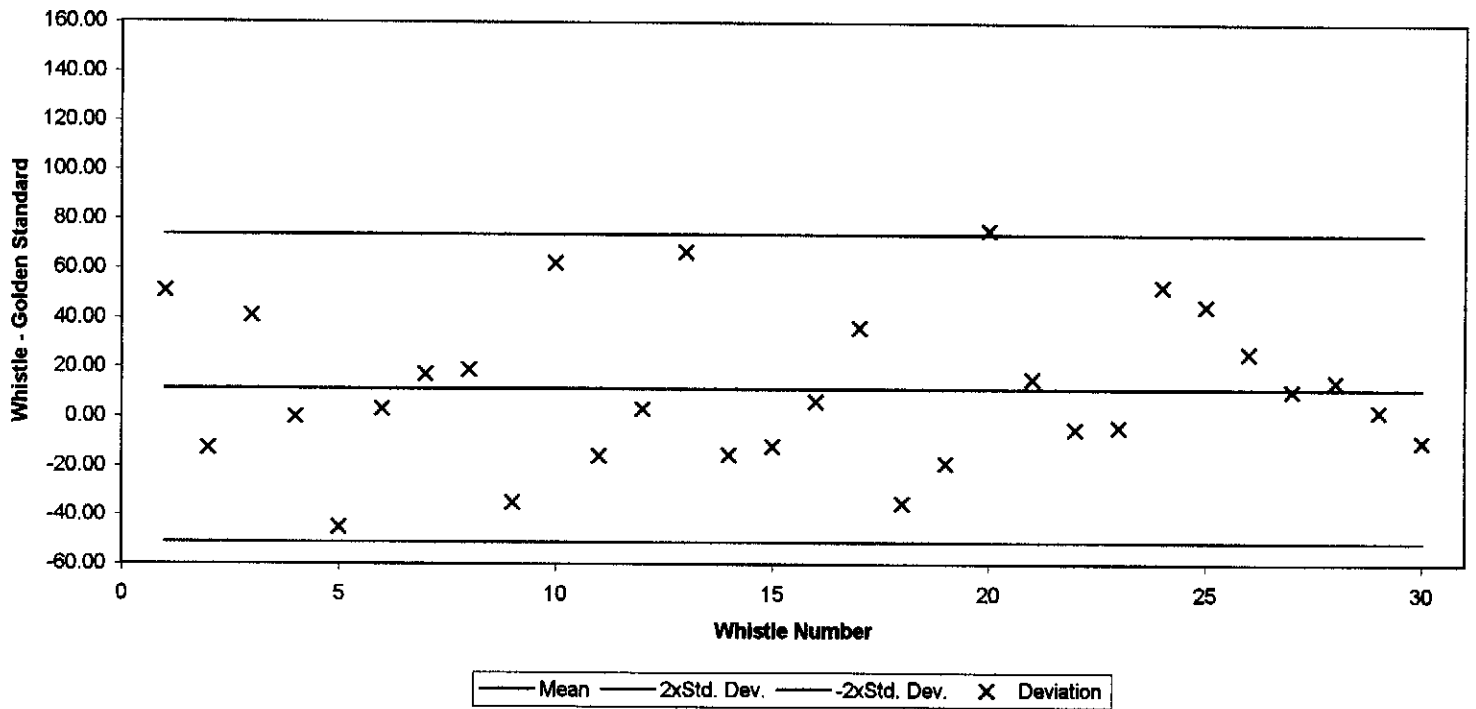


FIGURE 8.2.2
Free Reed

8.3 "Sidedness" of the reed

Results from the 8 whistles evaluated are summarised in Table 8.3.1 as mean and standard deviations. Data was analysed using the Student t-test for dependent samples where a $p < 0.05$ indicated a statistically significance between the data sets compared.

Differences were found in 6 of the 8 whistles (75%) between up and downward facing burrs, while whistles 1 and 28 did not produce significant differences ($p > 0.05$). A reason for this may be the manual (by hand) method of assembly and disassembly of the whistles. It may also be that the burrs produced by the punching process were not as prominent on these whistles as the rest.

There was no clear pattern in the results (for example that downward facing burrs always activated at a lower pressure as compared to upward facing burrs). It was however concluded that P_{RA} is orientation sensitive, and care should be exercised during the assembly process to ensure that all reeds have the same orientation.

T-test comparison for Sidedness					
Whistle Number	Down Burr [Pa]		Up Burr [Pa]		t-Test
	Mean	Std. Dev.	Mean	Std. Dev.	p
1	498.82	15.84	491.62	12.27	0.27
7	606.4	20.59	503.62	14.04	0.002*
11	511.59	18.5	555.93	17.99	0.004*
14	547.34	15.72	519.23	15.9	0.005*
16	541.18	20.39	480.64	10.66	0.002*
19	508.24	18.03	631.62	21.6	0.001*
25	545.53	13.67	567.6	13.5	0.001*
28	547.97	12.93	556.56	12.7	0.175

TABLE 8.3.1
T-test comparison for Sidedness
* p < 0.05

8.4 The influence of reed dimensions on the P_{RA}

8.4.1 The influence of reed width on P_{RA}

The data accumulated for the only two accurate reed widths available (Section 7.8.1) is listed in Table 8.4.1 as means and standard deviations. It may be seen from Table 8.4.1 that the wider reed has a higher P_{RA} , and through calculating the mean of the three whistles in each batch and expressing it as a ratio, shows the wider reed activating $\pm 10\%$ higher.

Reed Width	Whistle 1 P_{RA} [Pa]		Whistle 2 P_{RA} [Pa]		Whistle 3 P_{RA} [Pa]	
	Mean	Std. Dev.	Mean	Std. Dev.	Mean	Std. Dev.
4.4	610.79	15.86	565.46	21.11	582.37	16.01
4	534.08	16.7	533.65	13.93	523.69	9.95

TABEL 8.4.1
The influence of reed width on the activation pressure

The reason for this higher P_{RA} may be due to increased reed stiffness, which may be supported through calculation. Backus's [31] equation (Equation 5.1.1, Section 5.6.1) indicates a linear influence of reed stiffness on the threshold blowing pressure:

$$p_0 = \frac{1}{2} \cdot \xi_0 \cdot S_r \cdot \left(1 + \frac{\zeta}{\tau}\right) \quad (8.4.1)$$

Thus applied to reed widths mentioned above, produces

$$\frac{p_{04.4}}{p_{03.3}} \propto \frac{S_{r4.4}}{S_{r3.3}} \quad (8.4.2)$$

where S_r , the reed stiffness, is expressed in Section 7.8.2 as:

$$k = \frac{8 \cdot E \cdot \frac{b \cdot h^3}{12}}{l^3} \quad (8.4.3)$$

Substituting Equation 8.4.3 into Equation 8.4.2 for reed stiffness of 4.4 and 3.3 mm respectively, and simplifying.

$$\frac{p_{04.4}}{p_{03.3}} \propto \frac{b_{4.4}}{b_{3.3}} = \frac{4.4}{3.3} \quad (8.4.4)$$

Equation 8.4.4 indicates that the P_{RA} increase is proportional to the increase in reed width of 33%. This increase corresponds with the experimentally observed increase in P_{RA} , therefore it may be concluded that reed stiffness is the major contributing factor. A further minor antagonistic element is the increased plan surface area. The latter effects the reed through reduction in the equilibrium reed aperture, when the reed oscillates. For a constant blowing pressure an increase in plan surface area results in an increased net driving force. The relative contribution of this effect in reducing the effect of increased stiffness, is not clear from present data or existing literature. Similarity in magnitude of the theoretical predicted increase in P_{RA} (due to increased reed width), with the experimental increase observed; underlines that in the range of

reed widths from 4.0 to 4.4 mm the increase in P_{RA} may be predicted by the stated theory. The reed width range of operation for this theory may be extended through further experimentation in order to determine what antagonistic effect the plan surface area has on reed stiffness changes.

8.4.2 The influence of reed length on P_{RA}

The P_{RA} 's for the different batches ($n=3$) in the array of reed lengths (width = 4 mm) are illustrated in Figure 8.4.1, as means \pm standard deviation. There is a clear downward trend starting at ± 750 Pa @ 12.5 mm and decreasing towards ± 450 Pa @ 13.5 mm. P_{RA} dependency towards reed geometry is high, as a 1 mm decrease in reed length resulted in a 40 % reduction in P_{RA} .

Activation Pressure vs Reed Length for a Restricted Configuration

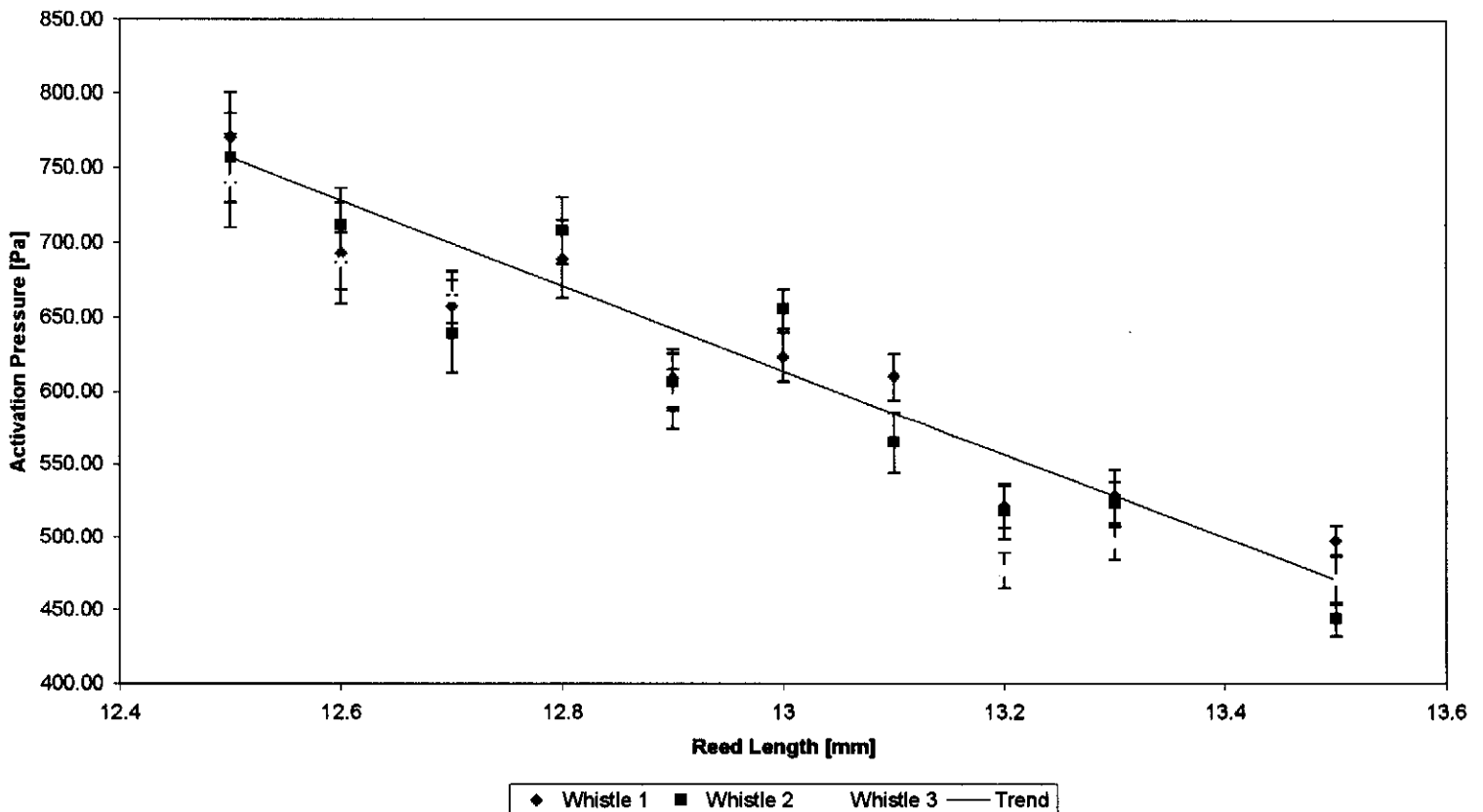


FIGURE 8.4.1
Activation pressure variation vs varying reed length.

This downward trend may be attributed to the reed properties, which vary with decreased reed length:

1. Decreased reed stiffness
2. Increased plan surface area

1. Decreased reed stiffness

Backus's equation for P_{RA} (Equation 5.1.1, Section 5.6.2) indicates the linear effect of reed stiffness as follows:

$$p_0 = \frac{1}{2} \cdot \xi_0 \cdot S_r \cdot \left(1 + \frac{\zeta}{\tau}\right) \quad (8.4.5)$$

Thus applied to reed lengths produces

$$\frac{P_{04.4}}{P_{04}} \propto \frac{S_{r4.4}}{S_{r4}} \quad (8.4.6)$$

S_r , reed stiffness, is expressed in Section 7.8.2 as:

$$k = \frac{8 \cdot E \cdot \frac{b \cdot h^3}{12}}{l^3} \quad (8.4.7)$$

Substituting Equation 8.8.7 into Equation 8.8.6 for reed stiffness of 13.5 and 12.5 mm respectively, and simplifying.

$$\frac{P_{013.5}}{P_{012.5}} \propto \frac{l_{12.5}^3}{l_{13.5}^3} = \left(\frac{12.5}{13.5}\right)^3 \quad (8.4.8)$$

Equation 8.4.8 indicates that a change in P_{RA} , due to a change in reed length, is inversely proportional to the cube of the reed length ratio. A decrease of 20% in P_{RA} is predicted by a reed length increase of 1 mm, this prediction contributes 50% to the experimentally observed decrease.

2. Increased plan surface area:

It can only be speculated, whether the increase in plan surface area for a 1 mm reed length increase has the remaining 20% decreasing effect on P_{RA} , as no experimental data or literature are available for clarification. The literature [8, 9, 31, 35, 36] points out that an increase in plan surface area results in a subsequent decrease in reed aperture for a constant blowing pressure (due to the higher net driving force) and vice versa.

This initial quantitative study of reed length influence on P_{RA} can only be clarified through a new formulated study, with high levels of expenditure towards punch-die sets for every reed length. The new study would be time consuming due to the number of whistles required for functional statistical analysis. It can only be concluded that P_{RA} is highly dependent towards reed length, with a decreasing trend due to an increase in reed length.

8.4.3 The influence of reed thickness on P_{RA}

Figure 8.4.2 presents the data of the thinner 175 μm reed tested, in the Bland & Altman format, with the whistle at the lowest coefficient of variance (COV), again selected as the golden standard. The results are similar to that of the 250 μm free reed (Figure 8.2.2) with 73% of the tested whistles within one standard deviation of the mean.

Bland&Altman Plot For 175 μm Free Reed Configuration

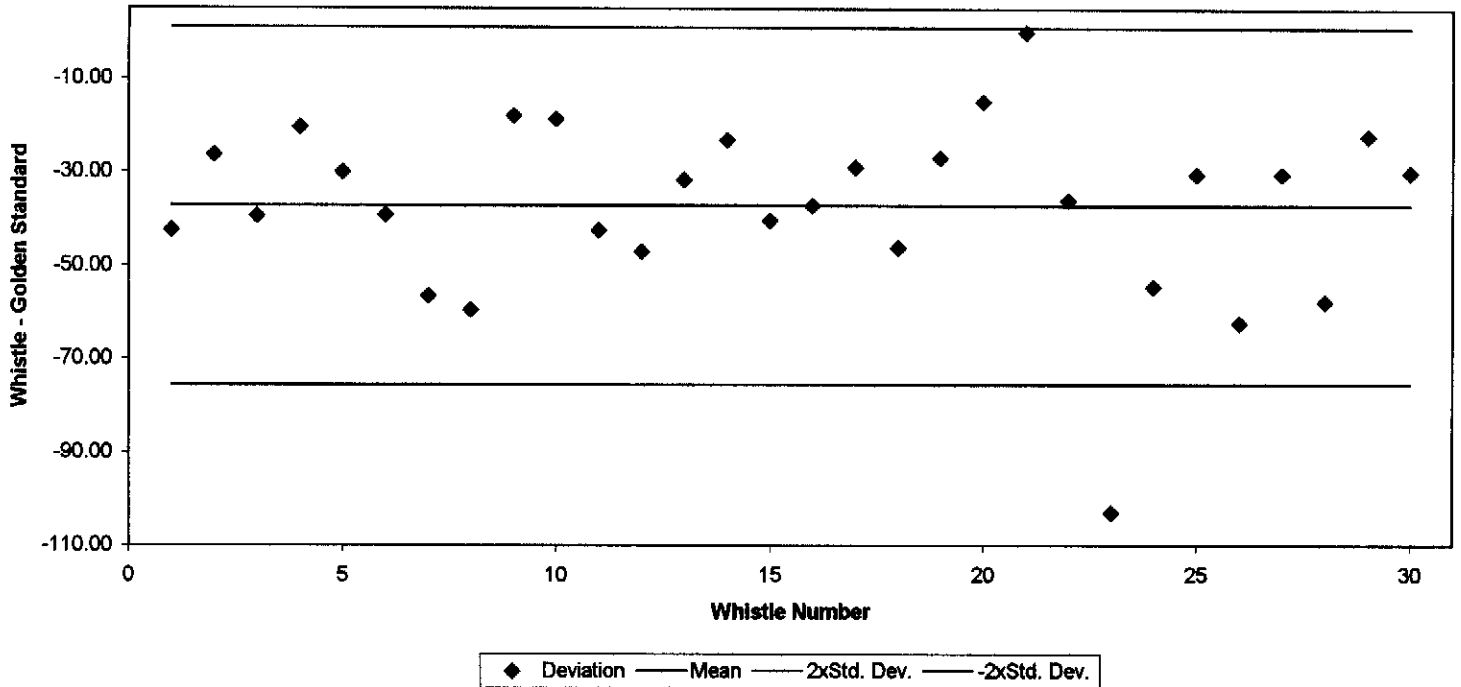


FIGURE 8.4.2
Activation pressure for 175 μm free reed

The mean activation pressure of the thinner 175 μm reed was significantly ($p < 0.05$ in the t-student test) lower (62%) than that of the 250 μm reed as listed in Table 8.4.2.

The lower P_{RA} was anticipated due to the decreased stiffness.

	175 μm	250 μm	p
Mean Activation pressure for 30 whistles	225.42	579.94	0.001*
Standard Deviation	19.15	31.19	

TABEL 8.4.2
Influence of reed thickness on activation pressure

The anticipation may be illustrated similar to the method used in Section 8.4.1, to investigate reed width and length influence on P_{RA} .

Again, from Backus [31]:

$$p_0 = \frac{1}{2} \cdot \xi_0 \cdot S_r \cdot \left(1 + \frac{\zeta}{\tau}\right) \quad (8.4.9)$$

Thus applied to the two reed thicknesses produces

$$\frac{P_{0175}}{P_{0250}} \propto \frac{S_{r175}}{S_{r250}} \quad (8.4.10)$$

S_r , reed stiffness, is expressed in Section 7.8.2 as:

$$k = \frac{8 \cdot E \cdot \frac{b \cdot h^3}{12}}{l^3} \quad (8.4.11)$$

Substituting Equation 8.4.11 into Equation 8.4.10 for reed stiffness of 175 and 250 μm respectively, and simplifying.

$$\frac{P_{0175}}{P_{0250}} \propto \frac{h_{175}^3}{h_{250}^3} = \left(\frac{175}{250}\right)^3 \quad (8.4.12)$$

Equation 8.4.12 indicates that the P_{RA} decrease is proportional to the cube of the decrease in reed thickness of 66%. This decrease corresponds with the experimentally observed decrease in P_{RA} .

This single comparison of reed thickness indicates the high sensitivity of P_{RA} towards reed thickness, as a 30% reduction in reed length resulted in a 62% reduction in P_{RA} . This sensitivity has significant practical implications towards the accuracy of the Whistle Watch as a peak flow monitor. Extensive quality control with narrow tolerance levels should be executed on the polycarbonate sheeting from which the whistle reeds are to be punched, to ensure homogeneity in the cross sectional thickness of the sheeting.

Reed geometry summary

The predictions, results and observations of Section 8.4 may be summarised in table format as illustrated in Table 8.4.3.

	Predicted	Experimentally Observed
Width	33%	10%
Length	20%	40%
Thickness	66%	62%

TABLE 8.4.3
Summary of reed geometry results

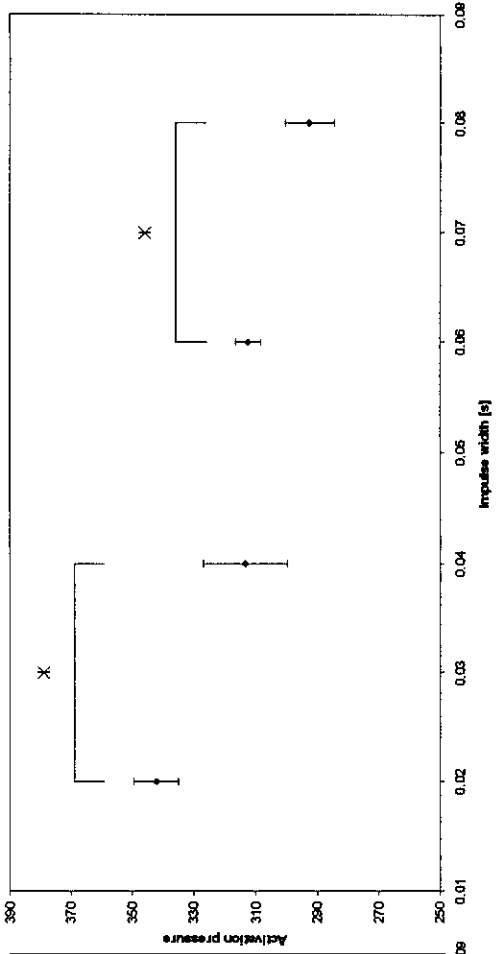
The similarities between the predicted and experimentally observed effect of reed width and thickness on P_{RA} are noted. This lends credibility to the respective hypotheses, implemented into Backus's equation 5.1.1, which explains the effect of reed width and thickness has on P_{RA} .

The predicted and experimentally observed effect of reed length on P_{RA} , points out that the formulated model does not consider all effects involved in reed length phenomena.

8.5 Functional testing of the Whistle Watch™

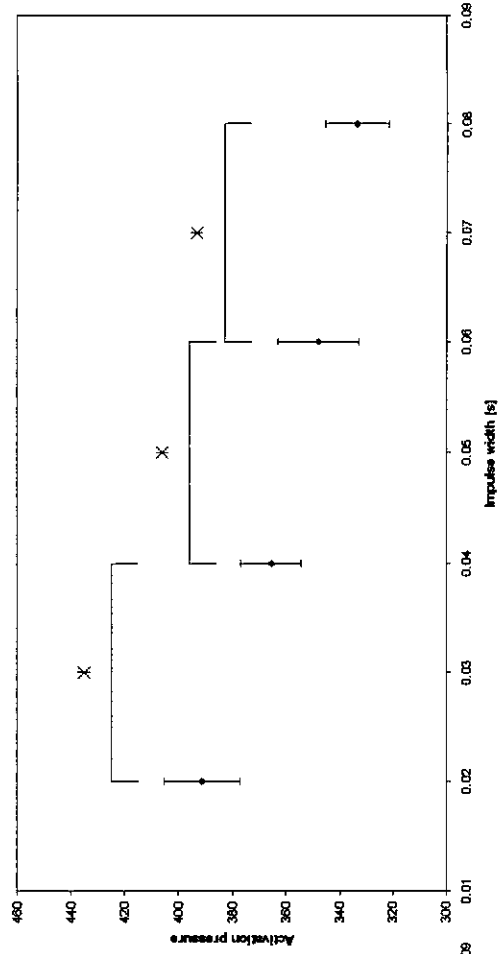
The influence of different pulse widths and rise times, of the customised input waveforms (I and II), on the P_{RA} , at various pre-set peak flow rates (150, 200, 250, 300 l.min⁻¹), are illustrated in Figures 8.5.1 to 8.5.4.

Activation pressure vs Impulse I width for a Restricted Reed
200 U/min



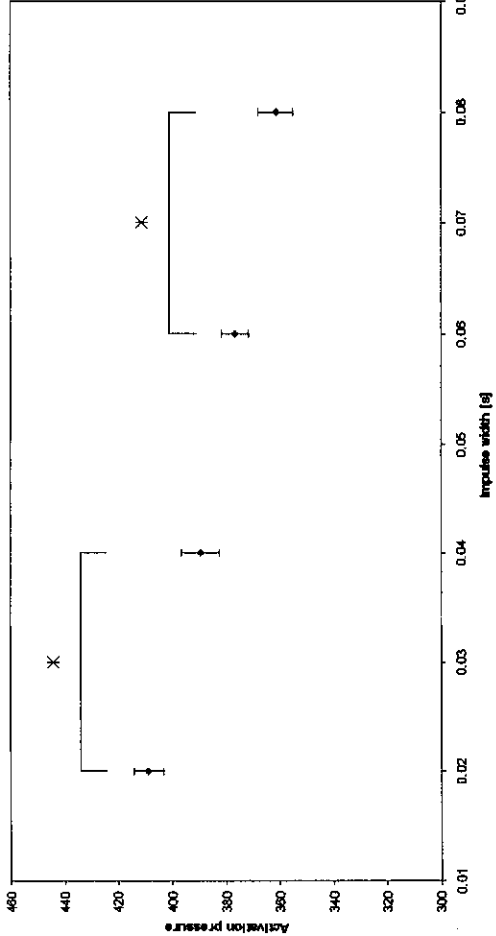
A

Activation pressure vs Impulse I width for a Restricted Reed
300 U/min



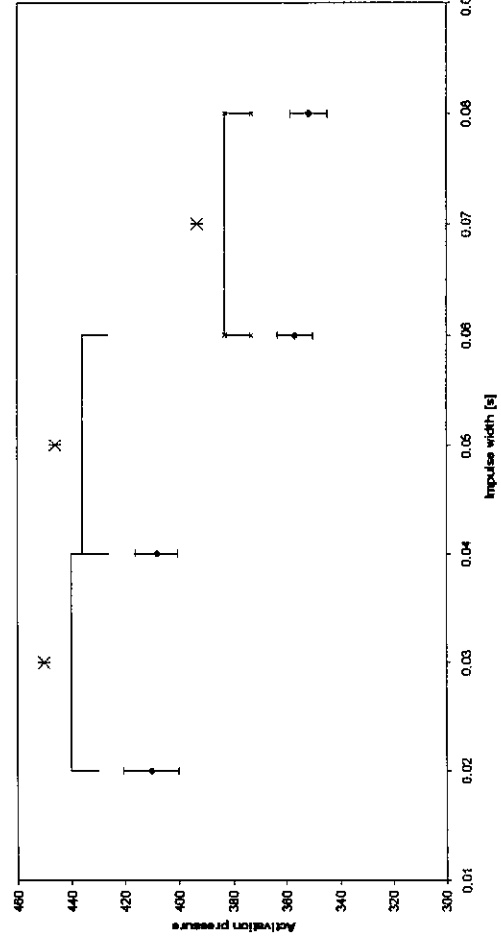
B

Activation pressure vs Impulse I width for a Restricted Reed
150 U/min



C

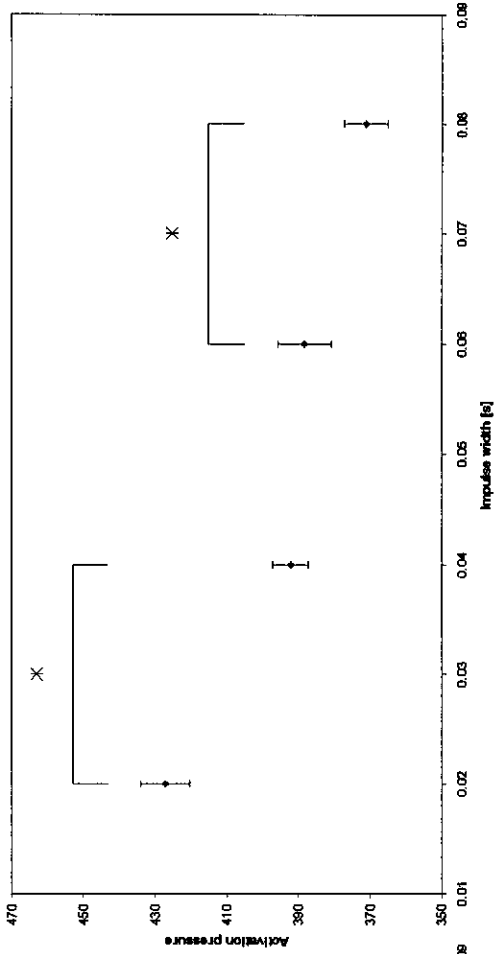
Activation pressure vs Impulse I width for a Restricted Reed
250 U/min



D

FIGURE 8.5.1

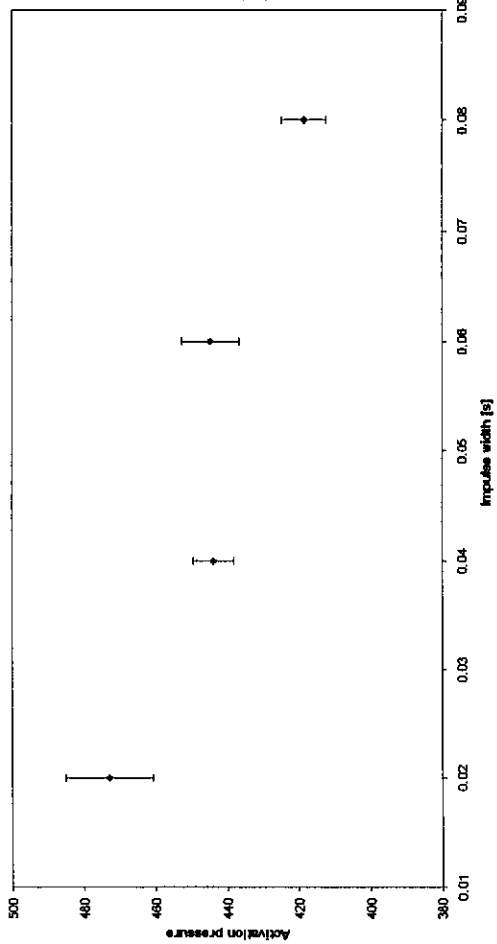
Activation pressure vs Impulse II width for a Restricted Reed
200 l/min



B

D

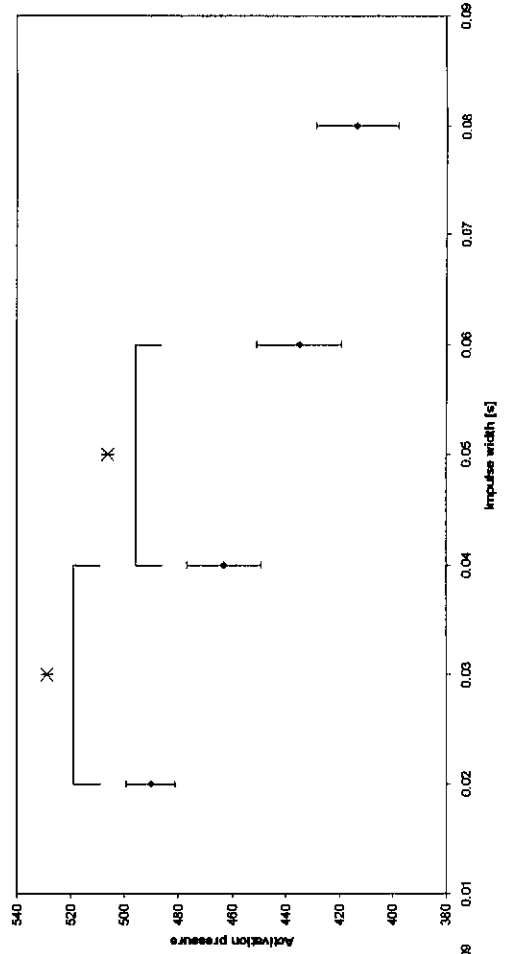
Activation pressure vs Impulse II width for a Restricted Reed
150 l/min



A

C

Activation pressure vs Impulse II width for a Restricted Reed
300 l/min



Activation pressure vs Impulse II width for a Restricted Reed
250 l/min

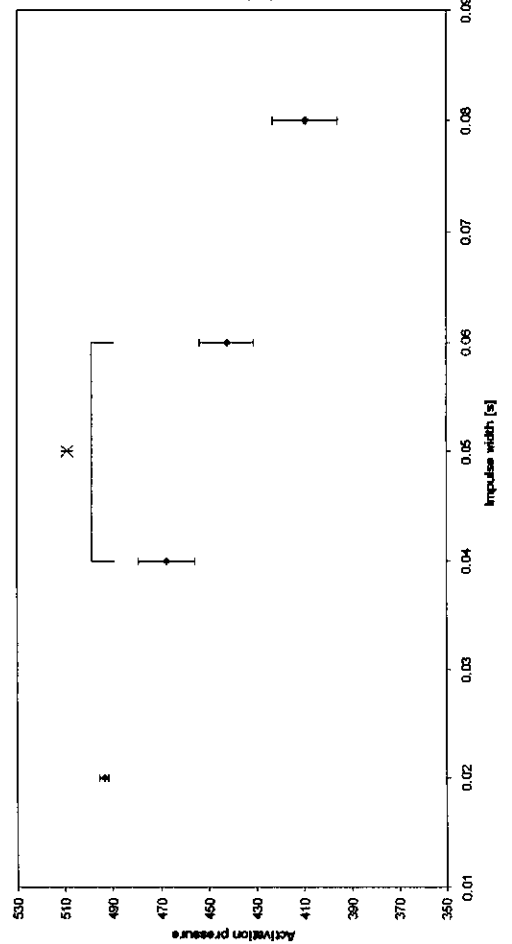


FIGURE 8.5.2

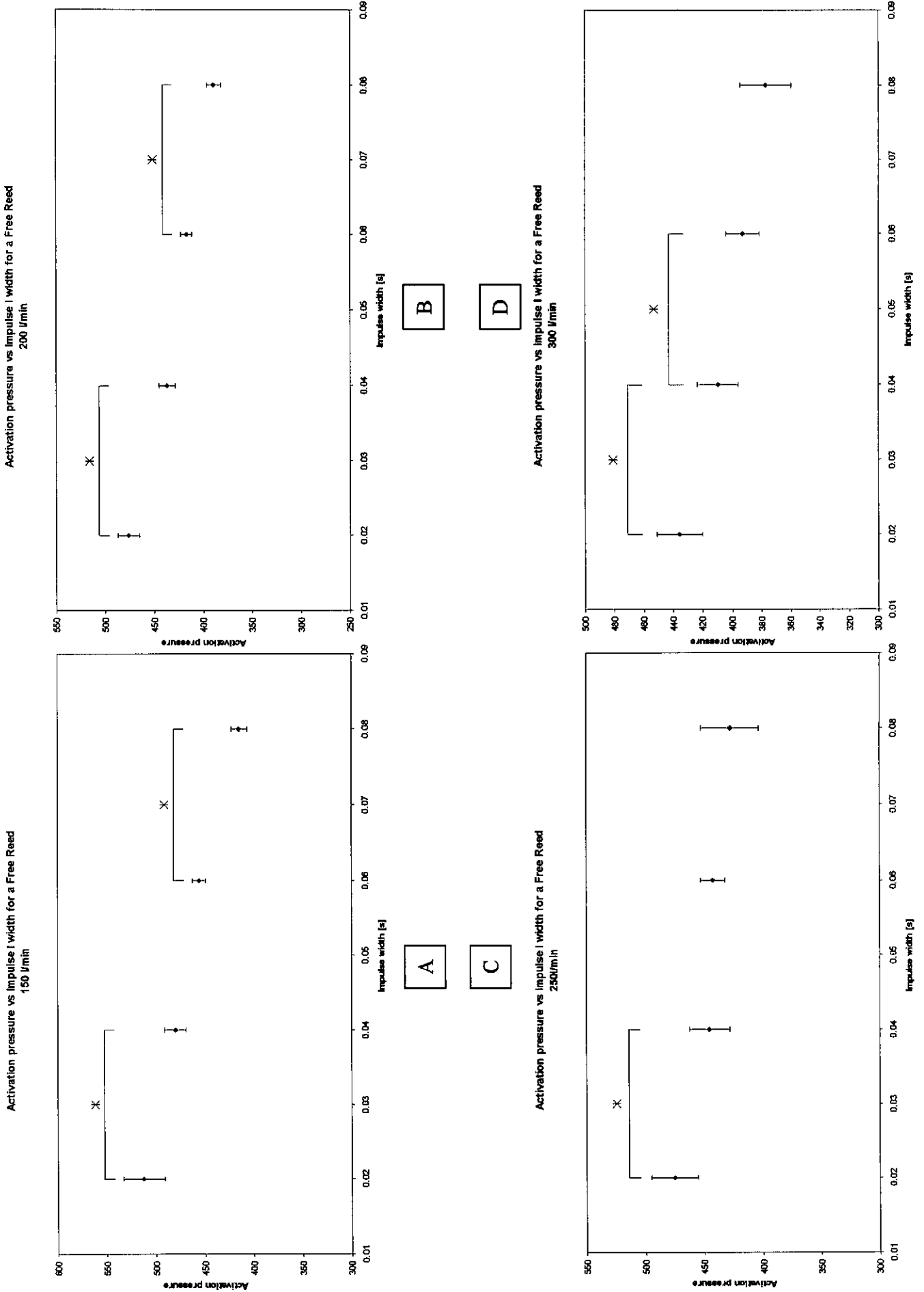
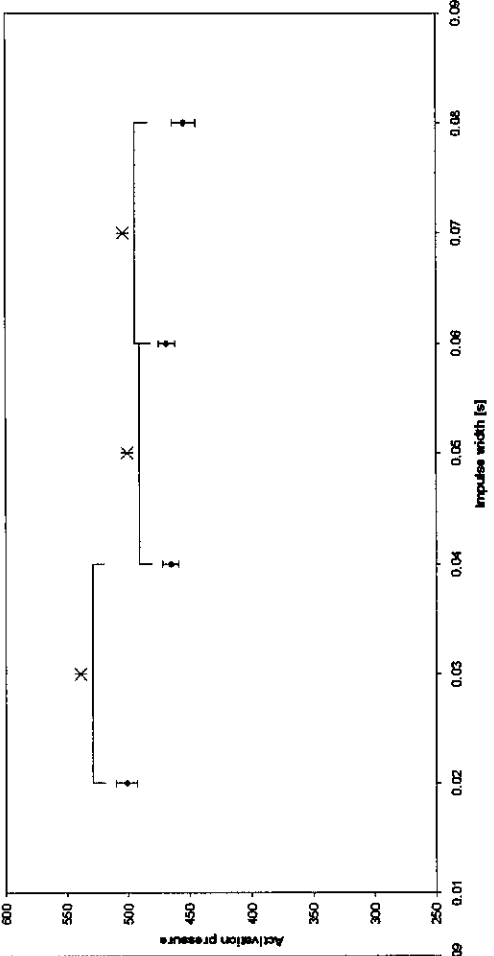


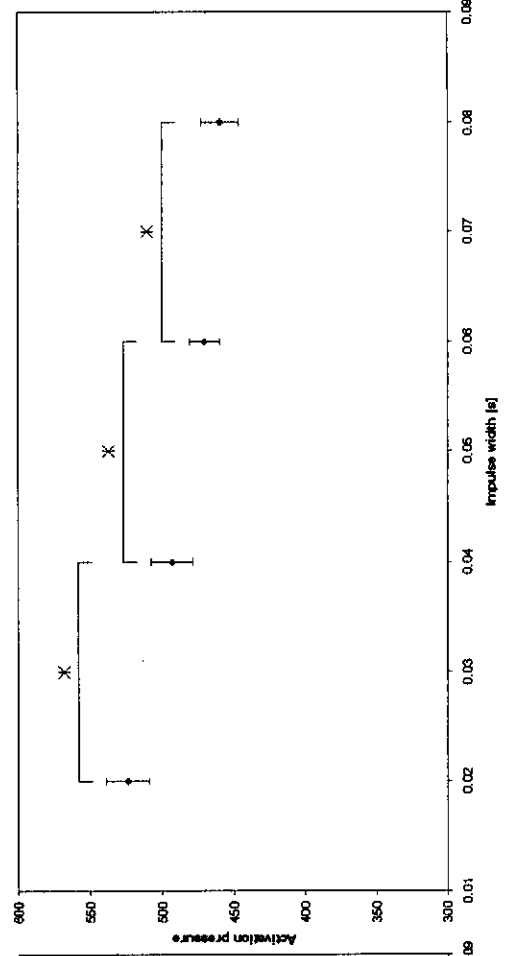
FIGURE 8.5.3

Activation pressure vs Impulse II width for a Free Reed
200 l/min



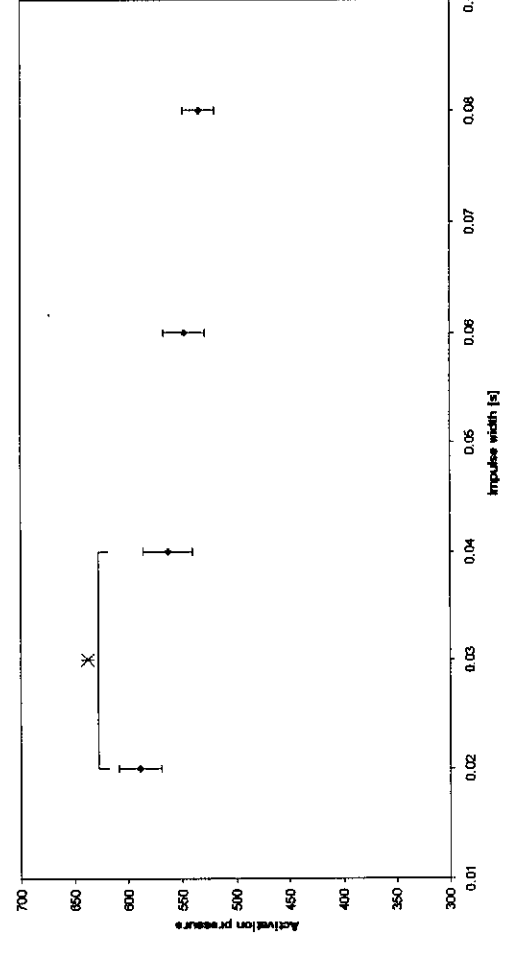
A

Activation pressure vs Impulse II width for a Free Reed
300 l/min



B

Activation pressure vs Impulse II width for a Free Reed
250 l/min



C

FIGURE 8.5.4

The data was analysed using an ANOVA test, with statistical significant differences indicated by * ($p < 0.05$). A general observation is the gradual decrease in P_{RA} for corresponding increases in pulse width and rise time. This phenomenon is present in both the free and restricted reed configurations, which were each subject to variations in Impulse I and II. The relatively higher rate of increase of P_{RA} for the free reed configuration may be observed.

A characteristic of a non-linear system, is the dependency of the output towards the type of input. This dependency is observed in the foregoing figures and was expected, as most woodwind models available and developed in Chapter 5 are non-linear. Although this dependency is a known and observed fact no existing woodwind models addresses it. It also influences the accuracy of the Whistle Watch, because if two patients with similar PEF values, but with different flow envelopes used the device, the slower rise time and larger dwell time envelope would appear to have the lower PEF. A possible reason for the peculiar behaviour is described below.

8.5.1 Energy absorbing characteristics of the reed

In an attempt to clarify the above observed behaviour, the product of the integrals, to the point of activation, of the pressure- and flow-time curves for Impulse I and II were compared. This comparison is illustrated in Figure 8.5.5 and 8.5.6 for free and restricted configurations respectively.

The integration was executed by a developed Mathcad routine (Appendix H), which numerically integrated the pressure and flow data to the activation point with respect to time through the implementation of the Trapezoidal rule and then multiplying the

results. The integrated pressure data has the dimensions of “impulse per unit area” $[\text{N}\cdot\text{s}\cdot\text{m}^{-2}]$ and the flow that of volume $[\text{m}^3]$, which produces a multiplication product of $[\text{J}\cdot\text{s}]$. This was done for 3072 test curves and representative data of free and restricted reeds are presented in the following:

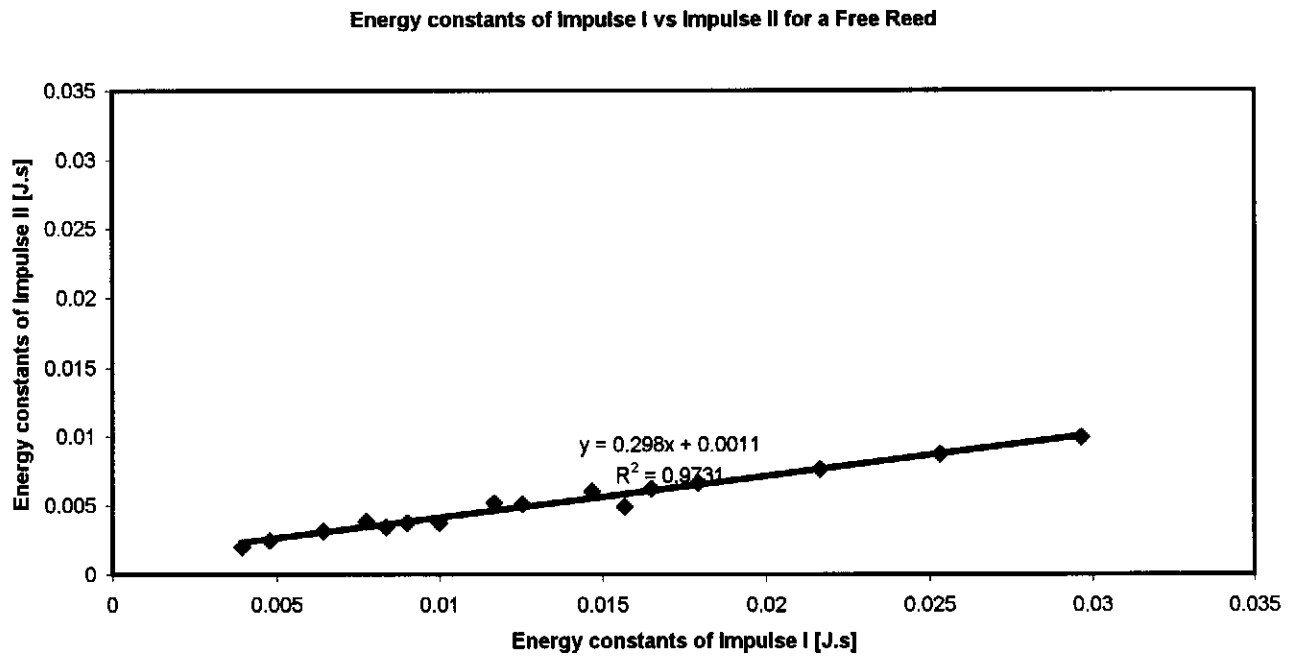


FIGURE 8.5.5
Integral comparisons for free reed

Energy constant for Impulse II vs Impulse I for a Restricted Reed

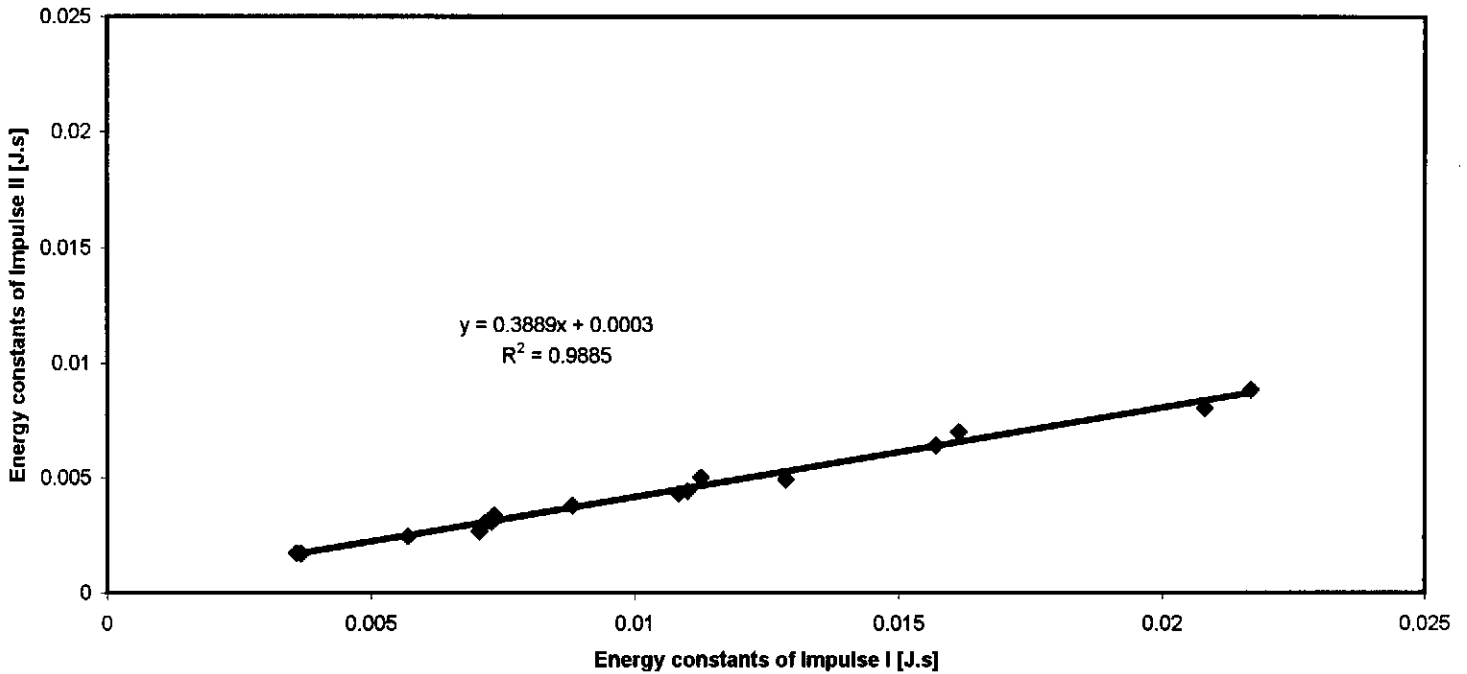


FIGURE 8.5.6
Integral comparisons for restricted reed

Interpretation of observed phenomenon illustrated in Figure 8.5.5 and Figure 8.5.6, one has to start by the evaluation of the units of the new property created, which is Joules-second. The latter is the same units as Planck's constant (h) for Quantization of Energy. Reviewing Quantum mechanics Planck and Einstein [41] have shown that molecules emit or absorb energy in discrete units of light energy called quanta or photons. They do so by "jumping" from one quantum state to another, where the quantum states refer to integer multiples of the fundamental molecular frequency. If the molecule "jumps" one quantum, i.e. from no oscillation to the fundamental frequency (f), the photon energy absorb is expressed through:

$$E = h \cdot f \quad (8.5.1)$$

Where:

E = Energy absorb to transpose from one quantum to the next

h = Planck's constant [J·s]

f = Oscillating frequency

Equation 8.5.1 may be adapted in its exact form for application to the observed phenomenon.

Redefining:

E = Energy absorb by the reed to transpose into a state of oscillation.

h = The energy constant generated through multiplication and integration.

f = The reed oscillating frequency.

The reed oscillating frequency remains constant for a constant up- and downstream impedance, as in the case when the data was compiled to generate Figures 8.5.5 and 8.5.6. Thus the only varying independent component of Equation 8.5.1 is the energy constant (h).

This hypothesis is supported through an observation by Idogawa [43] in one of his studies of a clarinet with all the tone holes closed blown artificially. He recorded through a unique experimental setup, shown in Figure 8.5.7 and Figure 8.5.8, mouthpiece pressure, reed opening and volume flow rate from the artificial mouth into the instrument.

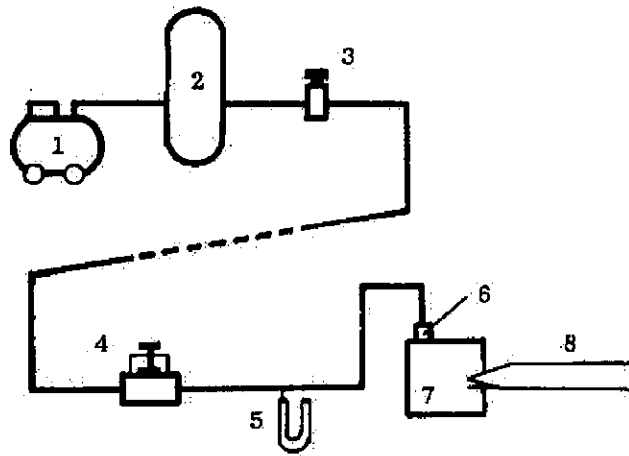


FIGURE 8.5.7 [43]

Idogowa's Artificial Clarinet Blower

(1) compressor, (2) reservoir, (3) pressure reducing valve, (4) bleed type pressure regulator, (5) manometer, (6) air connector, (7) blowing chamber, (8) clarinet

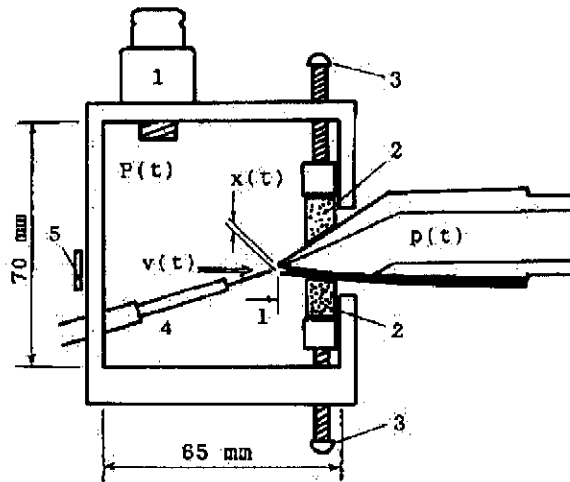


FIGURE 8.5.8 [43]

Idogowa's Detailed Blowing Chamber

(1) air connector, (2) artificial lips, (3) adjusting screw, (4) probe of the hot wire anemometer, (5) photodiode

He observed several different vibratory states over a complete range of blowing pressures, he had tested. The states were stable within their respective regions, but sudden transitions took place from one state to the other when the blowing pressure was varied beyond the stable region. A further observation made, was that multiple vibratory states were excitable in some ranges of the blowing pressure. The state excited was dependent upon the manner in which the blowing pressure was varied.

The experiment was repeated for different lip adjustments with similar observations. These observations are not sufficient proof of the validity of the hypothesis, but purely indicate the possible existence thereof. A validation of the hypothesis would involve an experimental setup as in Figure 8.5.7 and Figure 8.5.8 where the whistle is tested with different blowing pressure envelopes. Through measurement of the blowing pressure, mouthpiece pressure and flow rate the input and output energies may be determined. Subtracting these two energies would produce the amount of energy absorbed by the reed (E). Implementing the above-mentioned calculations an energy constant (h) for the specific blowing pressure envelope should be obtained, and from there the oscillating frequency of the reed may be determined. If the hypothesis is valid the calculated frequency should be the same as the measured frequency.

It is further noted that the slopes of both regression lines of Figures 8.5.5 and 8.5.6 are less than one, indicating that Impulse II activates the whistle with less energy for a given reed oscillating frequency than Impulse I. The reduced rise and dwell time of Impulse II (Section 7.9.2) with respect to Impulse I, implicates a higher rate of energy transferral to the reed and downstream air column.

It is thus concluded that if the reed is subjected to a higher rate of energy transferral, due to reduced rise time, less energy is required to transpose the reed into a state of oscillation, thus activation. This phenomenon has not been addressed in previous literature, where constant blowing pressures were assumed. The functionality of the Whistle Watch as a peak flow monitor, is also effected by this phenomenon, as variations are encountered in the rise time of forced expiratory envelopes.

8.6 General Characteristics of the whistle

During testing of the whistle's general characteristics were observed, which related well with published results.

8.6.1 Hysteresis

Figure 8.6.1 and 8.6.2 show the effect of hysteresis of the whistle, where it has the ability to continue to oscillate at lower pressures than the threshold blowing pressure, after the onset of oscillation. This phenomenon was also observed by Hoekje [22], who highlighted this with reference to the reed flow control valve as an “energy exchanger”. He concurred with previous literature, that oscillation can only be sustained for products of reed transconductance and input impedance greater than 1. He proceeded in proving the reed's ability to extract energy from the downstream air column, which functions as a source of energy. The latter is added to the drained energy of the upstream air column (due to reducing blowing pressure), resulting in prolonged oscillation below the threshold blowing pressure.

8.6.2 Critical blowing pressure

As described in Chapter 5 Worman [36], Backus [31] and Fletcher [9] derived expressions for the critical blowing pressure of a Clarinet. This critical blowing pressure, is that pressure at which the reed shuts off against the reed bed with termination of oscillation and sound production. Benade [35] made reference to this critical blowing pressure and summarised the effect, which was studied and noted in Section 5.1.1.

Histerese effect for different time domains of Impulse I for a Restricted Reed

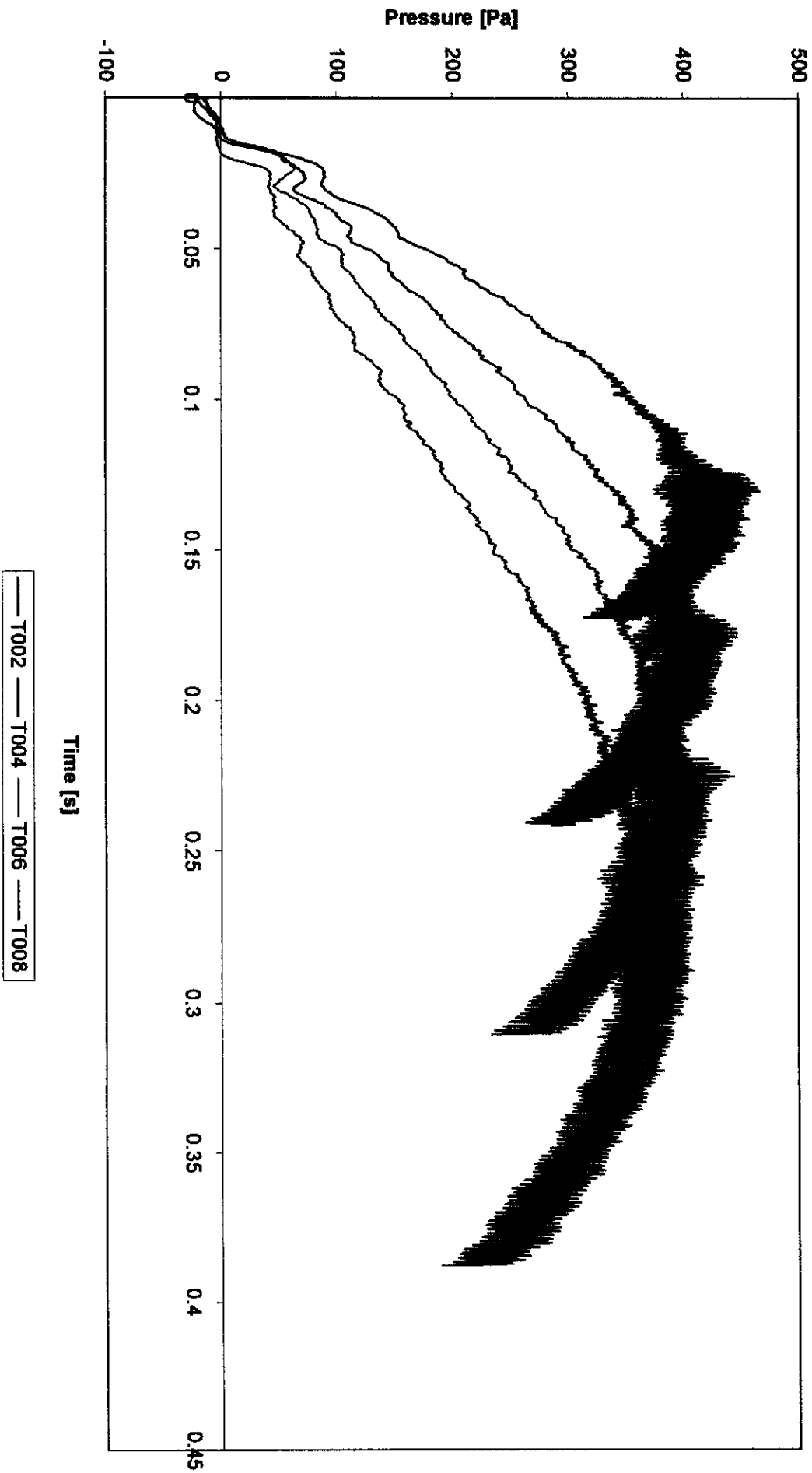


FIGURE 8.6.1

Histerese effect for different time domains of Impulse II for a Restricted Reed

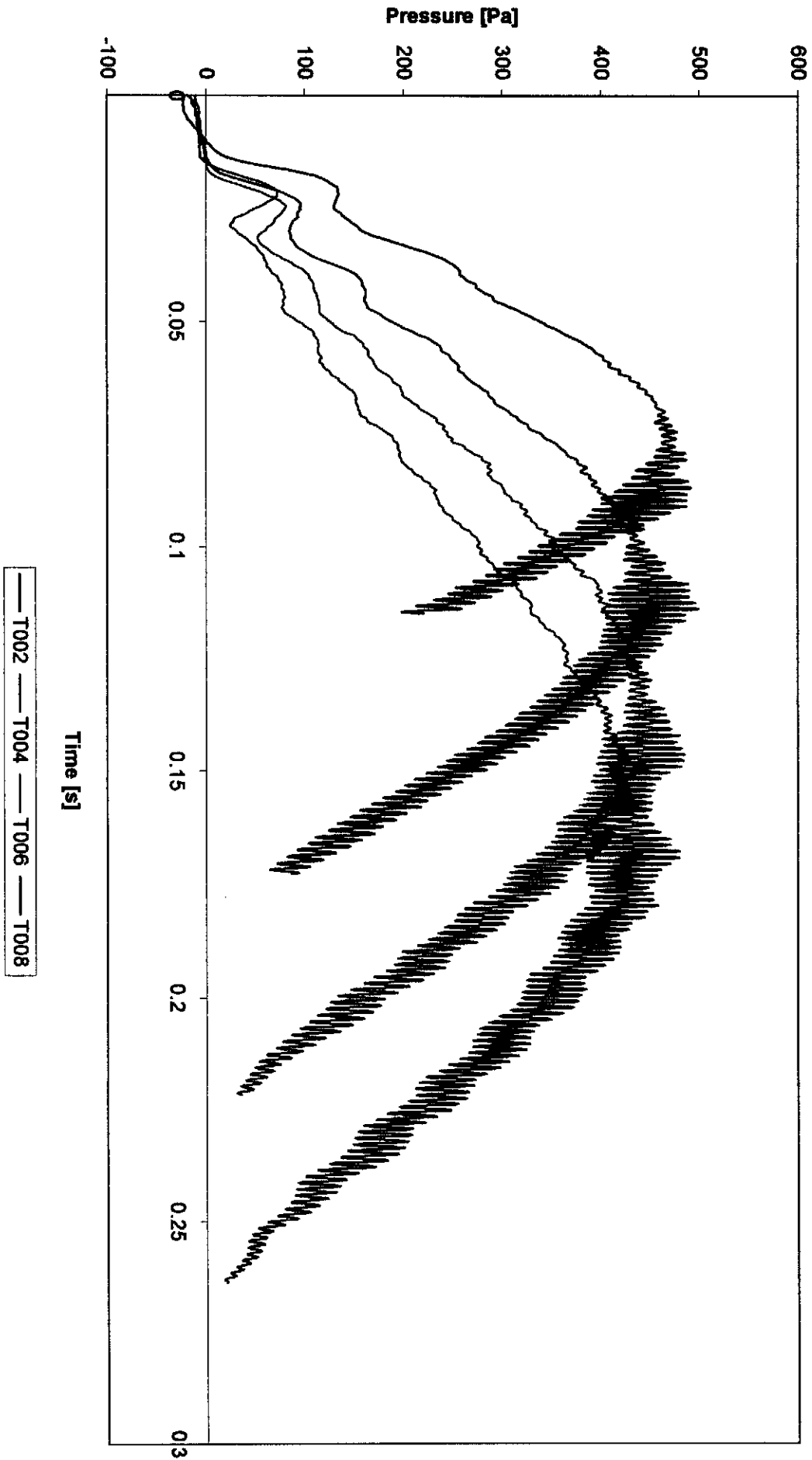


FIGURE 8.6.2

Pressure vs Time for a Free Reed

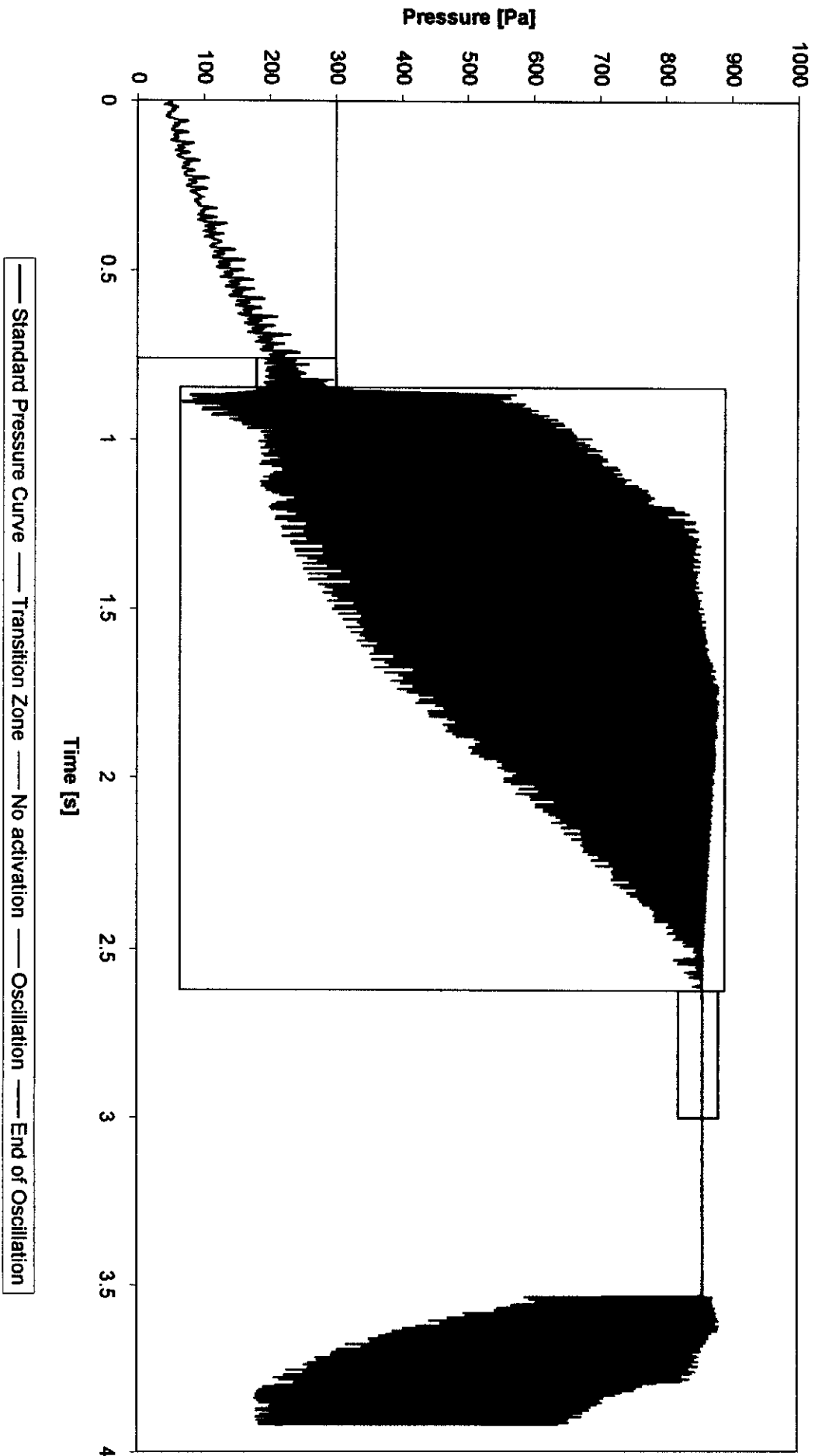


FIGURE 8.6.3

This critical blowing pressure was observed with the free and restricted configuration whistles, and is shown in Figure 8.6.3. At the termination of Figure 8.6.3 it may be seen that oscillation is initialised again when the blowing pressure becomes sub-critical.

8.6.3) Free versus Restricted Reed Stability

A further observation made during the testing of the whistles was the dominating stability of the free reed versus the restricted reed. This is illustrated in Figure 8.6.4. Figure 8.6.5 is normalised from the latter for closer inspection. The following is observed concerning the free reed when compared to the restricted reed:

- higher activation pressure
- shorter transition zone
- narrower onset of oscillation
- reduced amplitude of oscillation


The practical implication is that the free reed configuration is better suited for use in the Whistle Watch as it results in more stable and accurate threshold activation than a restricted reed configuration.

8.6.4) Oscillatory effects

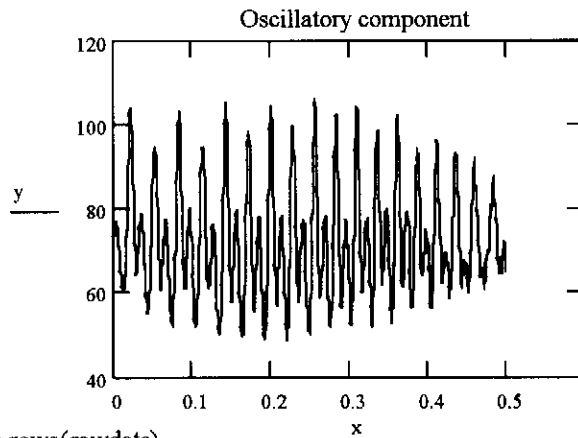
Figure 8.6.6 depicts a typical pressure-time curve of a restricted whistle when tested with a ramp input waveform. A super imposed oscillation preceding the transition zone is observed in the extraction block of Figure 8.6.7. This oscillatory pressure may be attributed to the incremental acceleration of the stepper motor (25 000 increments/rev), which via the plunger, imparts shock waves to the chamber air.

This may be proofed through a Fourier evaluation of only the oscillatory component of Figure 8.6.7 as follows:

```

:= 
C:\VFFFT-data.csv
y := rawdata<0>
x := | s←0
      | t←0
      | while s<rows(y)
      |   | carrys ← t
      |   | t←t +  $\frac{1}{3000}$ 
      |   | s←s + 1
      | carry

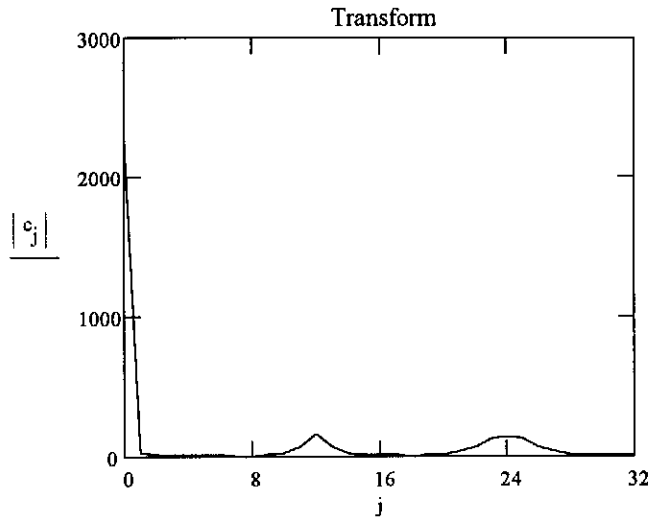
```



```

r := rows(rawdata)
n := trunc( $\frac{\ln(r)}{\ln(2)}$ )
sub := 2n
x := submatrix(rawdata, 0, sub - 1, 0, 0)
c := fft(x)
N := last(c)
j := 0..N
N = 512

```



Thus the primary oscillatory frequency is 2500 Hz, but the corresponding flow rate at this point in time is $\sim 2,5$ l/min = $4,167 \cdot 10^{-5}$ m³/s. The latter may be converted into revolutions per second of the stepper motor through:

$$\text{rev/s} = \frac{\text{volumeflowrate}}{\text{plungerarea} \cdot \text{pitch}} = \frac{4,167 \cdot 10^{-5}}{\frac{\pi \cdot .3048^2}{4} \cdot 5 \cdot 10^{-3}} = 0.114 \quad (8.6.1)$$

As stated there are 25 000 steps in each revolution of the stepper motor, and consequently a speed of 0.114 rev/s equals an incremental acceleration frequency of 2855 Hz. This is on par with the experimentally observed oscillatory frequency.

Comparative Transition Zones for Restricted and Free Reeds

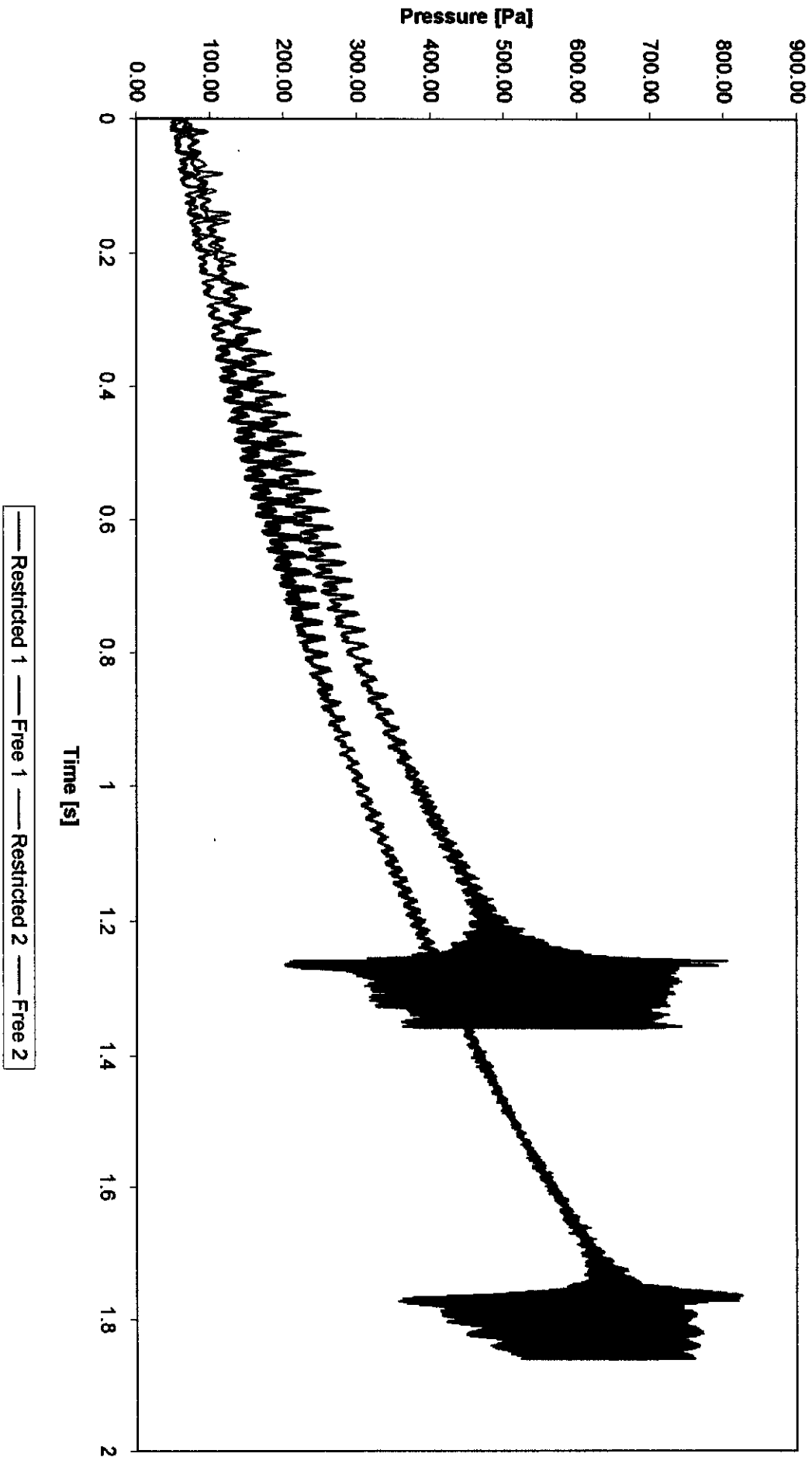


FIGURE 8.6.4

Normalised Transition Zones for 2 Free and Restricted Reed Configuration

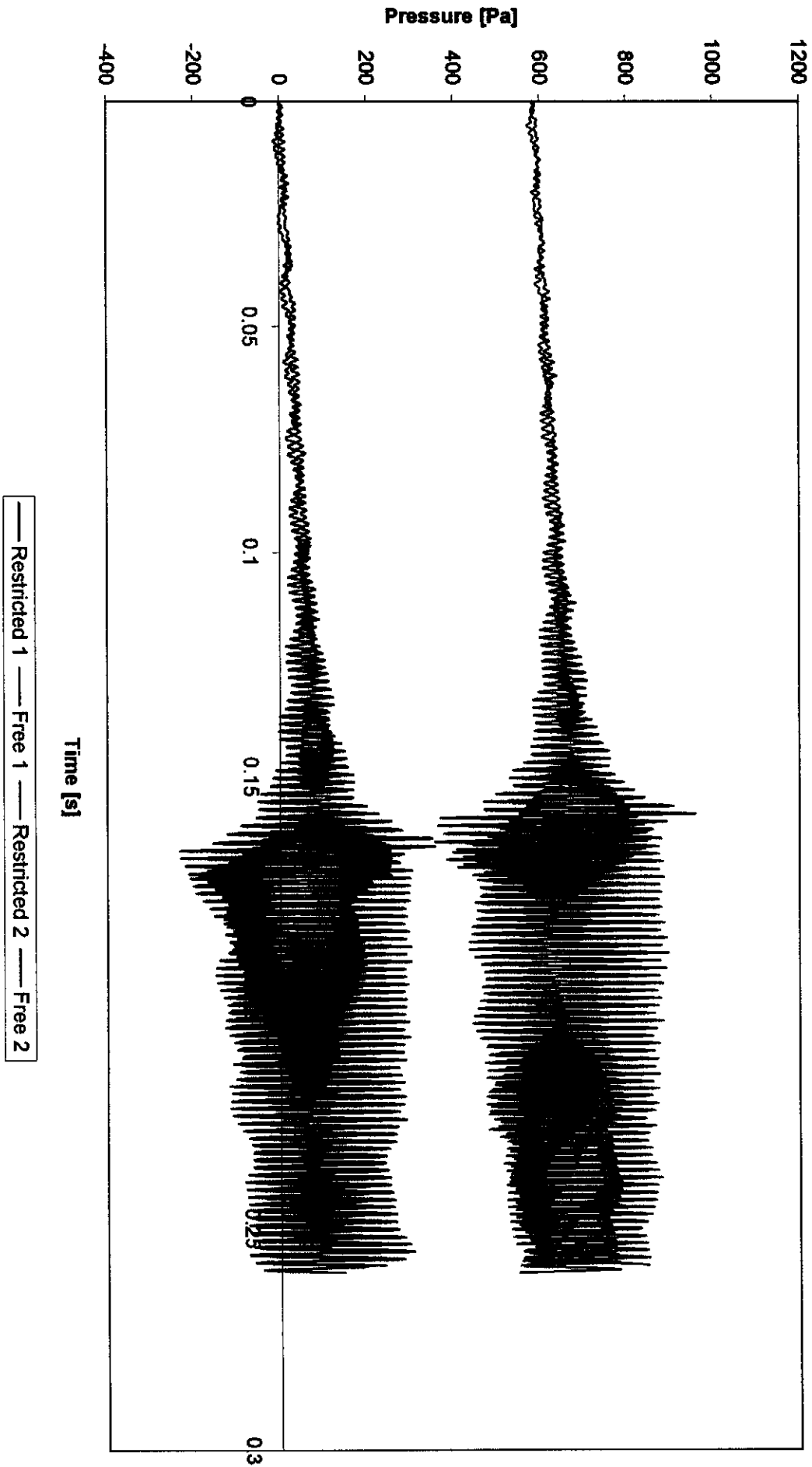


FIGURE 8.6.5

Pressure vs Time for a Restricted Reed

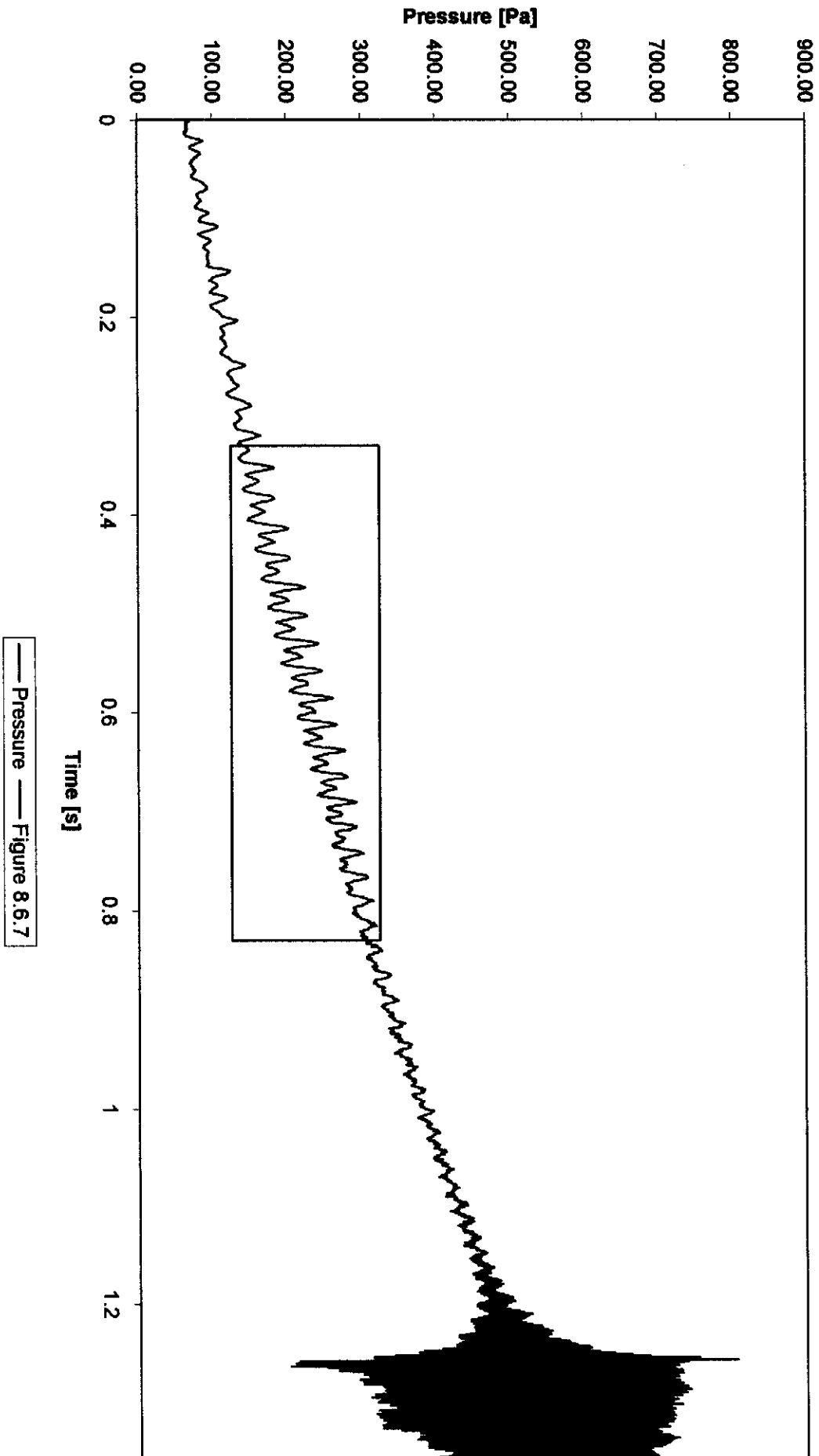
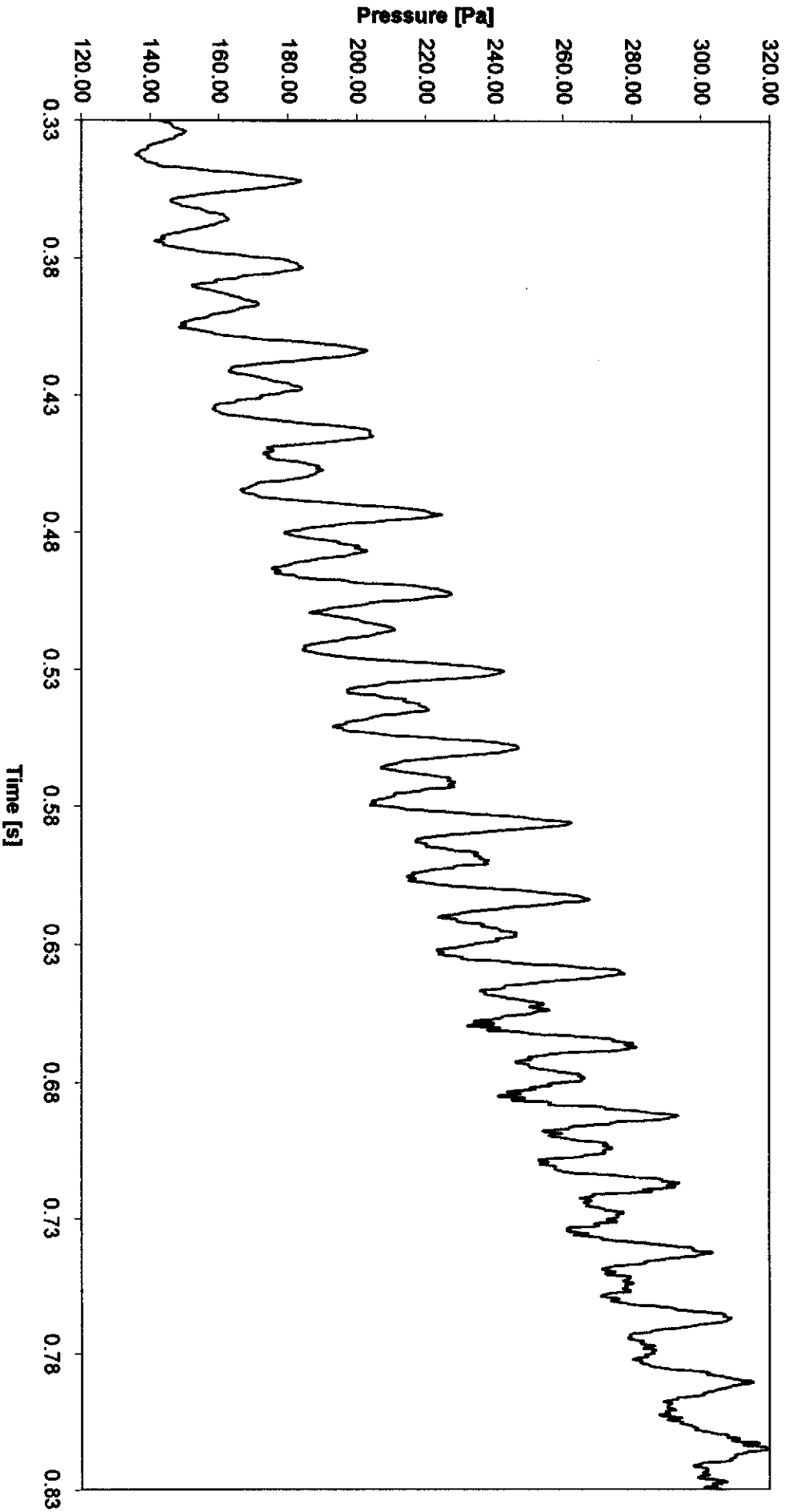


FIGURE 8.6.6



Pressure vs Time for a Restricted Reed
Extracted from Figure 8.6.6

FIGURE 8.6.7

CHAPTER 9

CONCLUSION

9.1 Summary of findings and conclusion

The technique developed of determining reed activation pressure accurately and consistently, with no human intervention, has far reaching practical application in the production environment. If this technique was implemented in the form of “GO NO-GO” system in the production environment, it would eliminate current subjectiveness. The latter is manifested in the current setup of a human tester executing a “GO NO-GO” opinion based upon a measurement read from an analogue pressure gauge. The technique would also find relevance in future studies concerning threshold whistles.

This study has contributed to the mosaic of theories of woodwind musical instruments, through highlighting the sensitivity of the Whistle Watch to upstream geometry. Increased quality control of the Whistle Watch bodies can now be motivated, thereby ensuring accurate peak flow monitoring.

Experimentation on the orientation sensitivity of the reed and highlighting the inherent property of the whistle to activate within a statistical spread, restated the importance of proper assembly control of the whistles to ensure an accurate product.

The effects of reed dimensions on activation pressure have been exposed as a complex unexplored field, with applications in designing the optimum stable whistle, with a specific threshold. A possible application of the latter would be in an

inspiratory peak flow monitor, which could indicate sufficient minimum inspiratory flow rate for effective ventilation and nebulisation.

A major constraint of existing models and literature in assuming constant blowing pressures has been defined, as the non-linear reed valve is highly sensitive towards different input waveforms, and moreover, to their rise times. This effect has a practical application pertaining to the accuracy of the Whistle Watch, as the whistle configuration and design chosen, should have a minimum susceptibility towards varying rise times.

9.2 Future studies

Future studies for master and doctoral theses could be aimed at:

- Characterising the effect of defined upstream geometries on reed activation pressure.
- Correlating reed geometry with activation pressure.
- Testing of further variations of input waveforms on activation pressure.
- Developing a new mathematical model, accommodating unsteady oscillations.

REFERENCES

- [1] Bone R.C., Pulmonary and critical care medicine. Chicago: Mosby, 1992.
- [2] Brewis R.A.L., Gibson G.J. and Geddes D.M., Respiratory Medicine. London: Bailliere Tindal, 1990.
- [3] Crystal R.G., The Lung: Scientific Foundation. New York: Raven Press, 1991.
- [4] Tortora G.J. and Anagnostakos N.P., Principles of Anatomy and Physiology Sixth Edition. New York: Harper & Row Publishers, 1990.
- [5] Wright B.M. and McKerrow C.B., Maximum Forced Expiratory Flow Rate as a measure of Ventilatory Capacity. British Medical Journal Nov. 21: 1041-1047, 1959.
- [6] Wright B.M., A miniature Wright peak-flow meter. British Medical Journal 2: 1627-1628, 1978.
- [7] Oldham H.G., Bevan M.M. and Mcdermott M., Comparison of the new miniature Wright peak flow meter with standard Wright peak flow meter. Thorax 34: 807-809, 1979.
- [8] Keefe D.H., Physical Modeling of Wind Instruments. Computer Musical Journal 16, 4: 57-73, 1992.
- [9] Fletcher N.H., Air flow and sound generation in musical wind instruments. Annual Revised Fluid Mechanics 11: 123-146, 1979.
- [10] Selkurt E.E., Physiology fifth edition. Boston: Little Brown, 1984.
- [11] White F.M., Fluid Mechanics (third edition). New York: McGraw-Hill, 1994.
- [12] Hadorn W., Schweiz Medical War Script 23, 946, 1942.
- [13] Wyss F., Helv. Medical Act 17: 516, 1950.
- [14] Hildebrandt G., O. Hanke, Ärztl. Wschr. 11: 439, 1956.

- [15] Silverman L., Whittenberger J.L., *Methods in Medical Research* 2: 104, 1950.
- [16] Lilly J.C., *Methods in Medical Research* 2: 113, 1950.
- [17] Goldsmith J.R., *American Revised Tuberculosis* 78: 180, 1958.
- [18] Young A.C., *Journal of Applied Physiology* 8: 562, 1956.
- [19] Weibel E., *Morphometrics of the lung*, *Handbook of Physiology*. Baltimore: Waverly Press, Section 3: Volume 1: 304, 1964.
- [20] Otis A.B., *The work of breathing*. In: *Handbook of Physiology*. Baltimore: Waverly Press, Section 3, Volume 1, p 463, 1964.
- [21] Linford A., *Flow Measurement and Meters*. London: Spon., 1949.
- [22] Hoekje P.L., *Intercomponent Energy Exchange and Upstream/ Downstream Symmetry in Non-linear Selfsustained Oscillations of Reed Instruments*. Ph.D. Case Western Reserve University. 1986.
- [23] Agostoni E., *Action of respiratory muscles*. *Handbook of Physiology*. Baltimore: Waverly Press, Section 3, Volume 1, 387, 1964.
- [24] Thompson S.C., *The effect of the reed resonance on woodwind tone production*. *Journal of Acoustical Society of America*. 66. 1299. November 1979.
- [25] Quargir Ph.H., *Peak expiratory flow: conclusions and recommendations of a working party of the European Respiratory Society*. *European Respiratory Journal*. 10:524, 25-85, 1997.
- [26] de Bono E.F. , *Lancet*. 2, 1146, 1963.
- [27] Dawson S.V., Elliott E.A. *Wave-speed limitation on expiratory flow- a unifying concept*. *Journal of Applied Physiology: Respiratory Environmental Exercise Physiology*. 48:498-515,1977.

- [28] American Thoracic Society Statement. Standardisation of spirometry – 1987 update. *American Revised Respiratory Disease*. 136: 1285-1298, 1987.
- [29] American Thoracic Society Statement. Standardisation of spirometry – 1979 update. *American Revised Respiratory Disease*. 136: 831-838, 1979.
- [30] National Asthma Education Program. Expert panel report on diagnosis and management of asthma. National Institutes for Health Publication No. 92-2113A, October 1992.
- [31] Backus J., Small-Vibration Theory of the Clarinet. *The Journal of the acoustical society of America*. 35: p 305-313, 1963.
- [32] Cengel Y.A., Boles M.A., *Thermodynamics an engineering approach*. McGraw-Hill: p 22, 1994.
- [33] Benham P.P., *Mechanics of Engineering Materials*. Longman Group Limited: p 188, 1996.
- [34] Shigley J., *Mechanical Engineering Design*. McGraw-Hill: p 325, 1989.
- [35] Benade A., *Fundamentals of Musical Instruments*. Oxford University Press: p 433 – 447, 1990.
- [36] Worman W.E., *Self-sustained Non-linear oscillations of medium amplitude in Clarinet-like Systems.*, Ph.D. thesis, Case Western Reserve University. 1971.
- [37] Nederveen C., *Acoustical Aspects of Woodwind Instruments.*, Frits Knuf, Amsterdam, p 28-37, 1969.
- [38] Helmholtz H., *Sensations of Tone.*, p388-397, 1877.
- [39] Bouasse H., *Instruments a Vent.*, Librairie Delgrave, Paris, 1929.
- [40] Weber W., *Akustik, Mechanik, und Wärmehre*, Berlin, p 206-256, 1892.
- [41] Serway R., *Physics for scientist and engineers.*, third edition, Saunders College Publishers, 1992.

- [42] Hyatt, Handbook of Physiology. Volume II Section III , p 1381-1397.
- [43] Idogawa T., Non-linear vibrations in the air column of a clarinet artificially blown. Journal Acoustical Society of America. 93 (1), p 540-551, 1993.
- [44] Quanjer P.H. et. al. : Peak expiratory flow: conclusions and recommendations of a working party of the European Respiratory Society. European Respiratory Journal. 10 (24); 2 –8, 1997.
- [45] Pederson O.F., Naeraa N., Lyager S., Hilberg C. and Larsen L. A device for evaluation of flow recording equipment. Bull European Physiopathology Respiration. (19) p 515-520, 1983.
- [46] Terblanche E., New Insights Into Stochastic Exercise Testing. , Ph.D. thesis, University of Stellenbosch. 1996.
- [47] Kramer G., Auditory Display: Sonification, Audification and Auditory interfaces. Addison Wesley, 1- 78, 1994.
- [48] Schoenberg J.B., Beck G.J. and Bouhny A., Respiration Physiology vol (33) p 367- 393. 1978.
- [49] Aerodynamic Whistles: Chanaud R.C., Scientific American, p 40 –46, 1986.

APPENDIX A

APPENDIX B

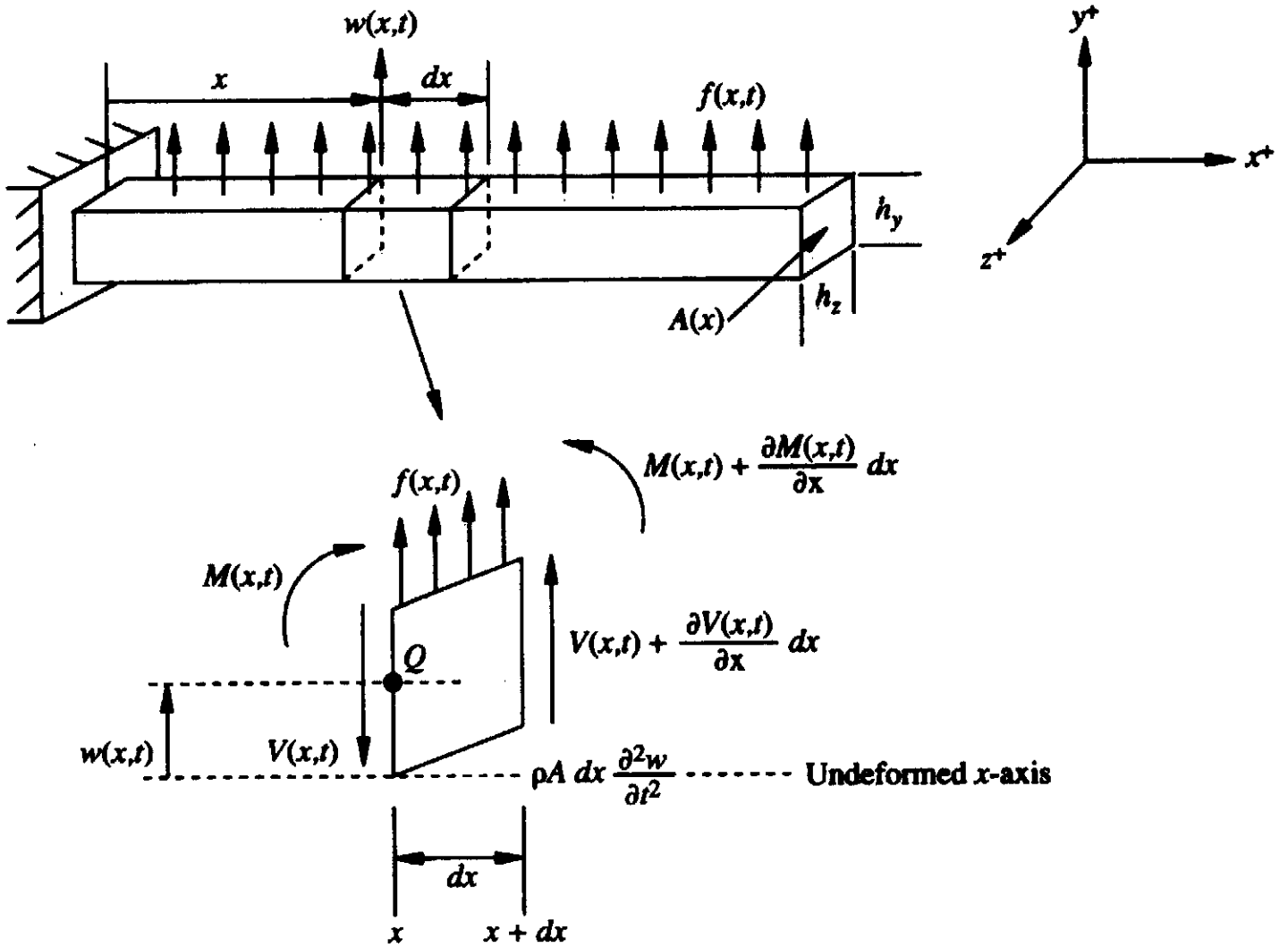


FIGURE B.1
Derivation of cantilever equation

APPENDIX C

C.1) The pressure transducer calibration procedure:

The pressure transducer¹ was calibrated against a Betz² water manometer (Figure C.1) which is accurate to 2 mmH₂O. A syringe was connected to the high pressure point of the manometer whilst the transducer was connected to the low pressure point. Pressure was increased in steps of 2 mmH₂O from 0 to 86 mmH₂O. At each step the pressure transducer output was captured through an analogue to digital 12 bit ISA card to the hard drive of a personal computer, and the Betz manometer reading noted. Upon reaching the maximum pressure, the pressure was decreased in the same manner, once again capturing the transducer output and noting the corresponding Betz reading.

The mean of both Betz and transducer readings respectively was calculated for the up and down procedure combined. The latter was done to compensate for any minor histereses effects present in the pressure transducer. A least square regression was constructed of the mean (up - down) transducer values versus the mean (up -down) Betz values.

¹ Honeywell / Microswitch 163PC01D36

² Van Essen University in the Netherlands, range 0 – 500 mmH₂O

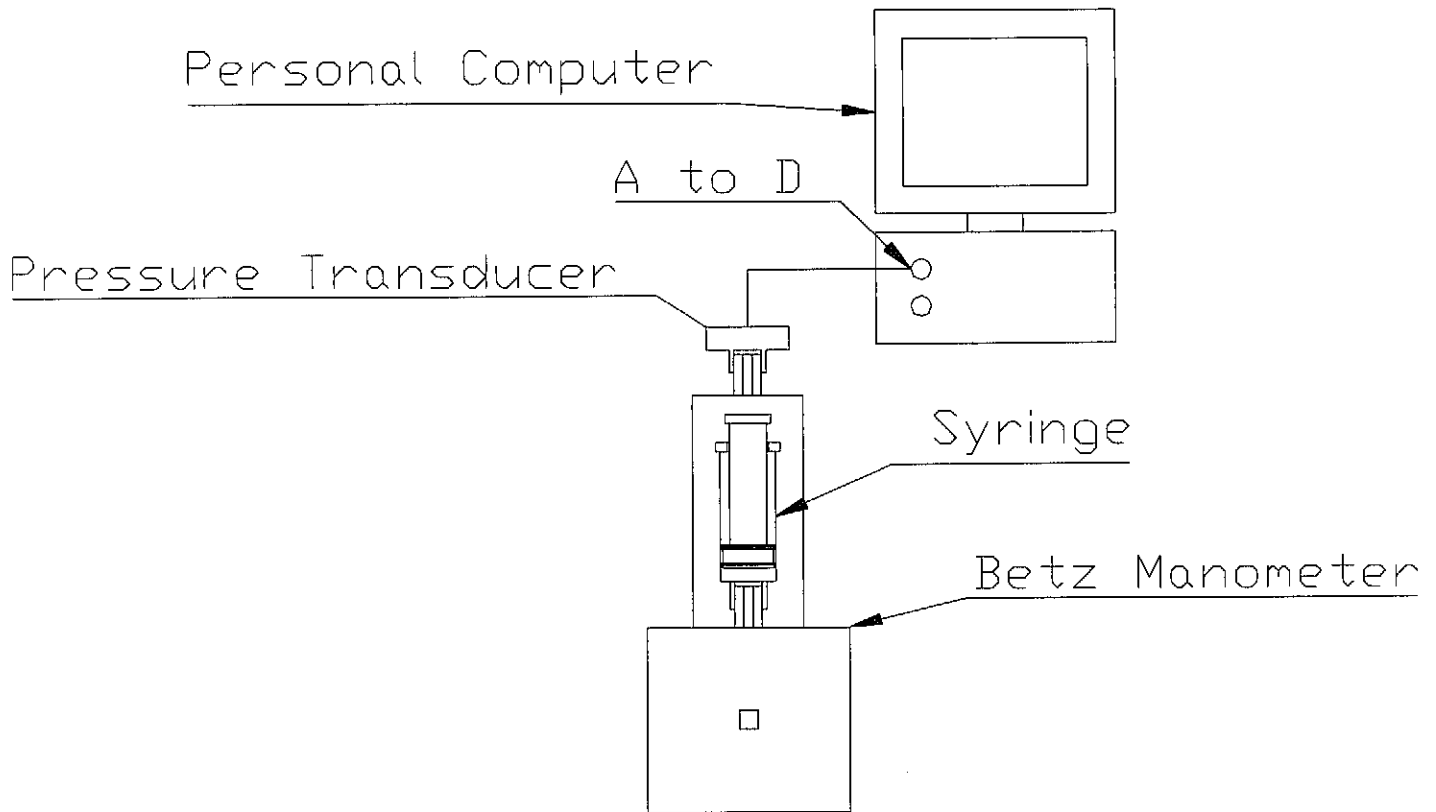


FIGURE C.1
Pressure Transducer Calibration

Calibration was repeated on two consecutive days, noting the atmospheric temperature and pressure for each day. The later was found to be constant (294.2 K and 756.5 mmHg) resulting in acceptable comparison between the two day's calibration curves. The following was generated on the days stated. (Figure C.2 and Figure C.3)

19 January 1999:

- Regression: $y = 125.33x - 8.4643$
- Coefficient of determination: $R^2 = 0.9948$

20 January 1999:

- Regression: $y = 129.31x - 20.387$
- Coefficient of determination: $R^2 = 0.9987$

C.3
Calibration Curve on 19/01/99

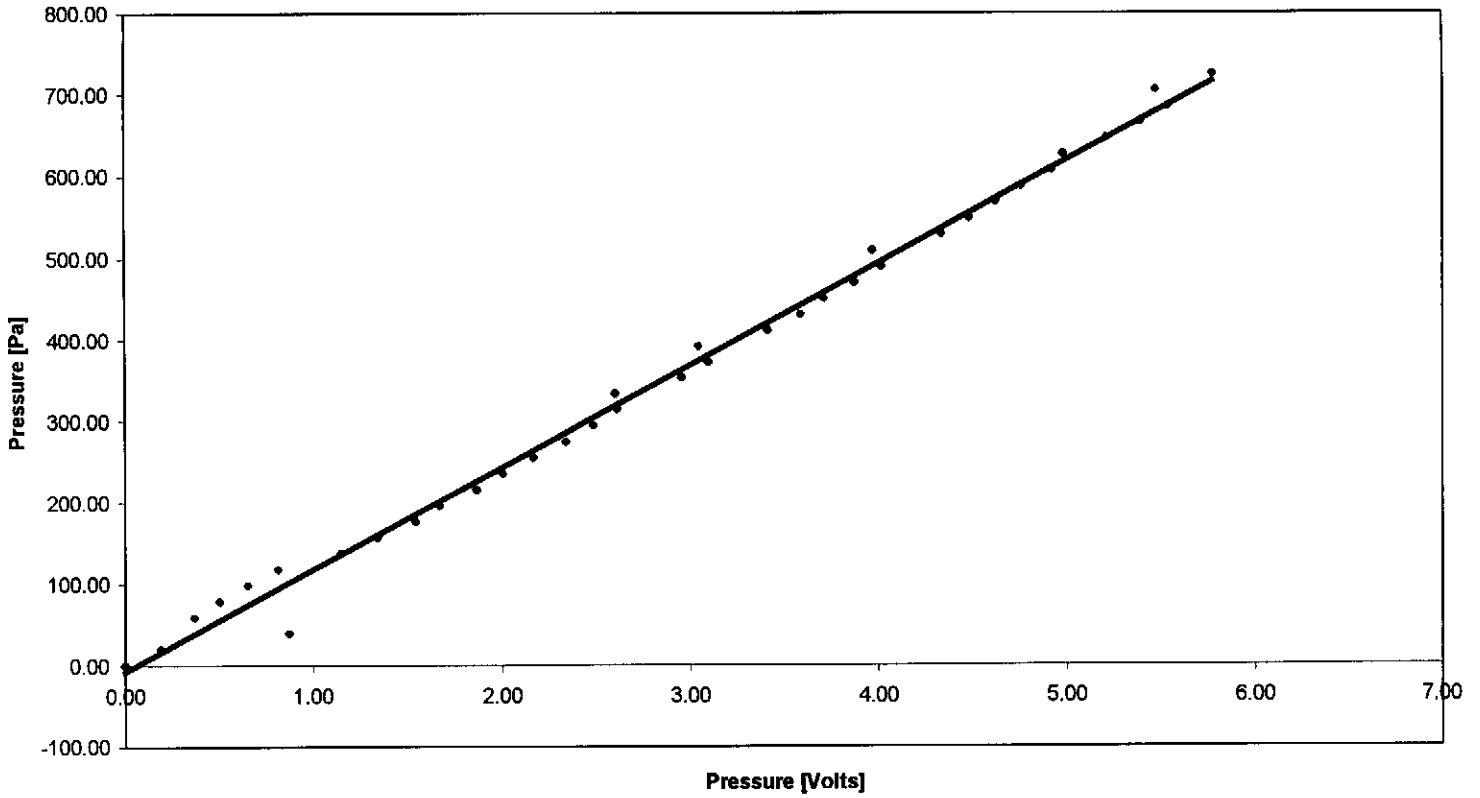


FIGURE C.2
Pressure Transducer Calibration on 19/01/99
Calibration Curve on 20/01/99

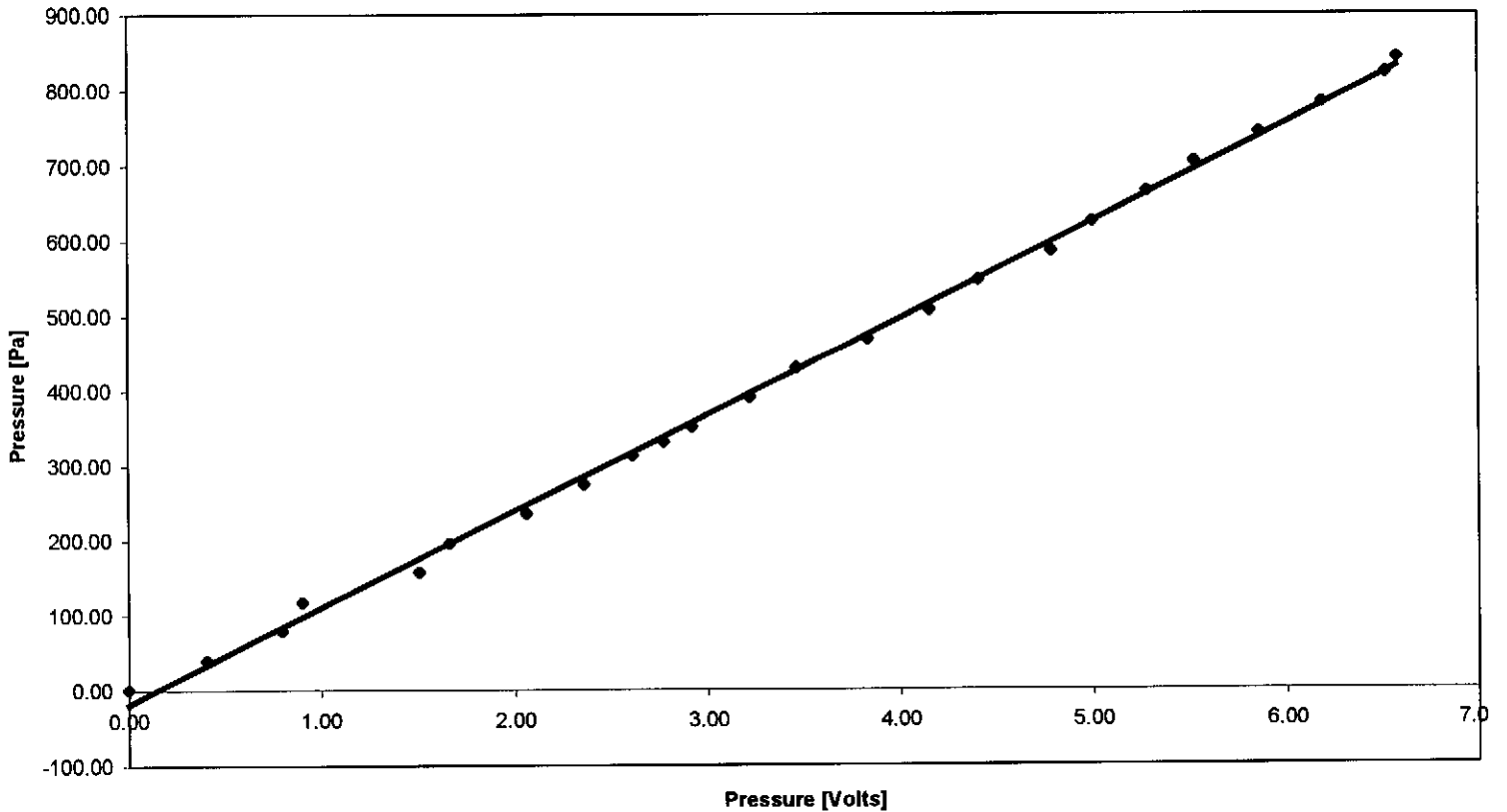


FIGURE C.3
Pressure Transducer Calibration on 20/01/99

C.4

Comparison of Calibration Curves

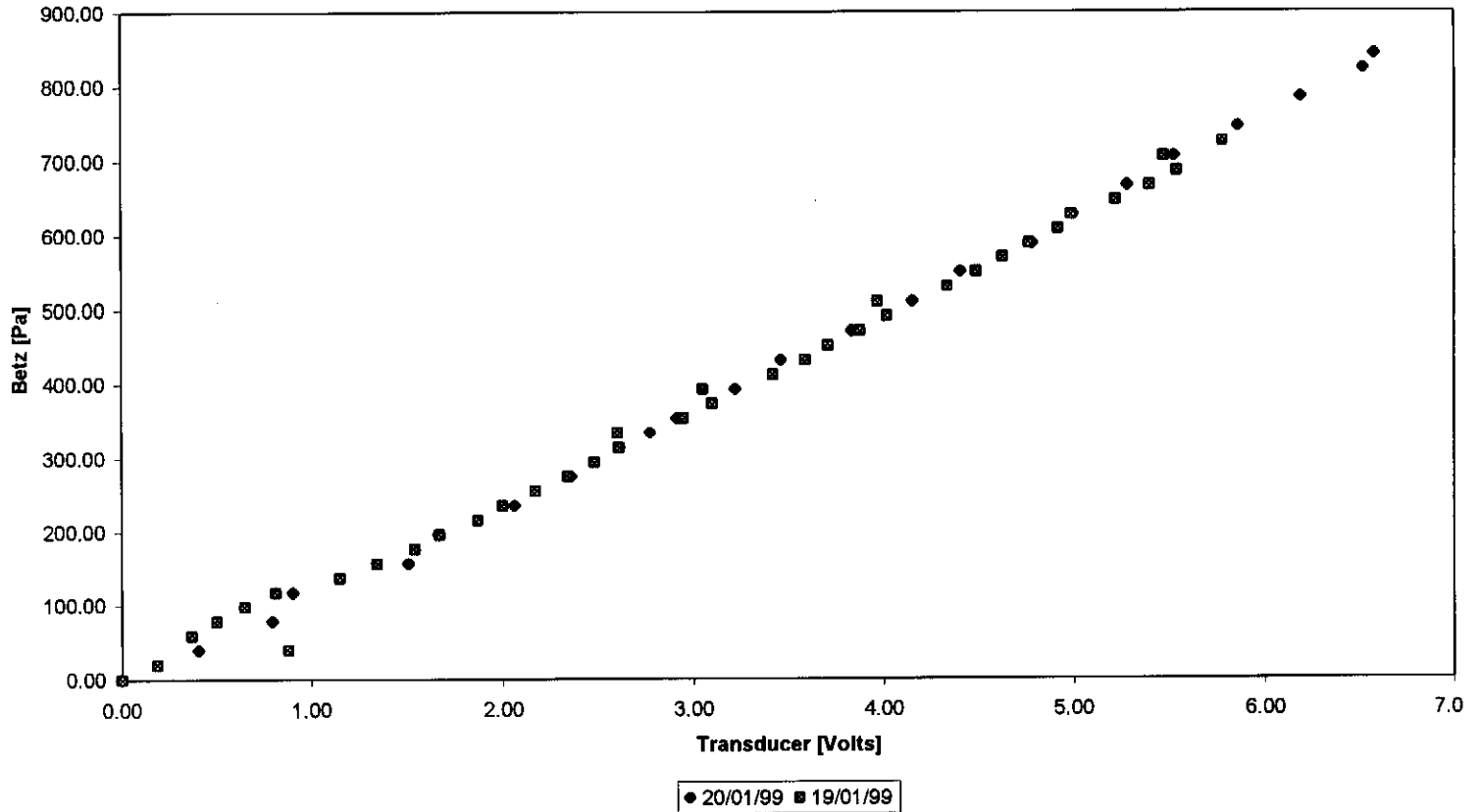


FIGURE C.4
Pressure Transducer Calibration Comparison

From Figure C.4 it may be seen that the calibration generated on day two was on par with the calibration generated on day one. This confirms the success of the calibration. Less data were captured on 20/01/99 as this was a benchmark correlation for 19/01/99. The data points could not be combined in one regression as they were two discrete data sets accumulated during two days. It was decided to use the second day's calibration equation as it's correlation coefficient is the closest to unity, indicating the better correlation of the two.

C.2) Linear Variable Differential Transformer (LVDT) Calibration

The LVDT was calibrated at the factory with a slope coefficient of 102.65 mV/mm.

This value was incorporated into determining the incremental real time volume produced by the mechanical pump as follows:

$$Volume = \frac{\frac{\pi}{4} \cdot D^2 \cdot pitch}{LVDT \cdot pitch} = \frac{\frac{\pi}{4} \cdot 0.3048^2 \cdot 5 \cdot 10^{-3}}{102.65 \cdot 5 \cdot 10^{-3}} = 7.108 \cdot 10^{-3} [m^3 \cdot mV^{-1}]$$

This volume was then differentiated with respect to time to produce the flow rate generated by the mechanical pump.

APPENDIX D

D.1) The design of the mechanical pump

The method used to generate artificial expiratory lung profiles, had to accommodate the high human attainable flow rates (up to 800 l/min) in short rise times (~8 ms). A pneumatic pump is limited by the compressible nature of air and cannot achieve the required flow rates in the required time. Using a reservoir of compressed air controlled by an electronic throttling valve is unsuitable as it has a high internal energy level, which fluctuates with varying ambient and operating conditions, resulting in inconsistent waveforms. The mechanical pump in Figure D.1 was the only viable cost effective option which adhered to the stringent requirements.

An existing mechanical pump was available for testing, but produced inconsistent waveforms. The problem was identified as its' volume of approximately 80 liters, as well as the large dead space incorporated in an oversize contracting nozzle. These factors contributed to considerable compressibility losses due to the elastic nature of air, which resulted in greatly reduced flow rates than perceived. A further shortcoming was the inefficient plunger design, which had provided blowby when exposed to high flow resistance. These shortcomings resulted in the pump not being able to produce the 26 standard ATS waveforms for testing peak expiratory flow meters. A further defect encountered during research and development of new pulmonary products, were the fluctuations in readings for constant plunger displacement. This was due to the inflexibility of the coupling between motor and shaft, and the stepper motor being accelerated instantaneously, which imparts shock waves to the air, causing irregular activation of the products being evaluated.

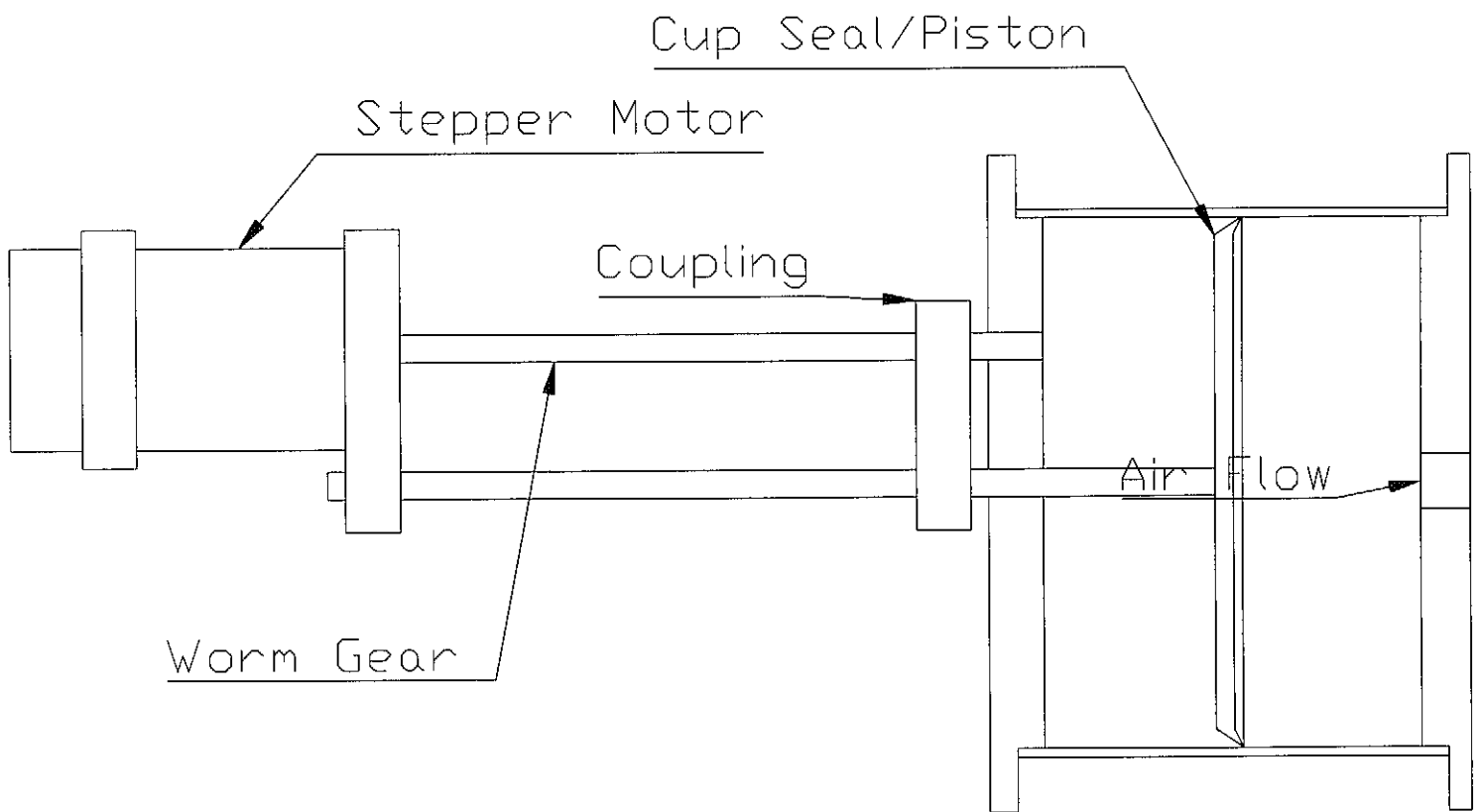


FIGURE D.1
Mechanical Pump

All of the above mentioned precipitated the decision for the design and building of a new mechanical pump with the following design criteria:

- Minimize leakage losses
- Minimizing compressibility losses
- Produce PEF of 1200 l/min in 50 ms in ATS 24 waveform with minimum shock waves

1. Minimize leakage losses

Purchasing of a high pressure (7 bar) pneumatic cup seal (Chesterton Seals¹) with outer diameter of 300 mm.

2. Minimizing compressibility losses

After an extended search for a large enough diameter pipe to accommodate the cup seal, a piece of steel pipe was acquired. Due to its length and required surface finish, the pipe had to be machined to 300 mm inner diameter and ground smooth by a specialist. In order to reduce dead space to a minimum, a square finish was assembled onto the end of the pipe and plunger assembly. The need for a minimum dead space is a result of the compressible nature of air. The latter may be explained through describing the testing procedure.

The flow rate measured by the linear variable differential transformer (LVDT) is not the flow rate delivered by the mechanical pump as a certain amount of this flow rate is absorbed in the elastic nature of air (back pressure). The LVDT flow rate must be compensated for with the amount of flow rate lost in the chamber (V_{comp}) due to compression, this is done through calculating V_{comp} :

$$V_{comp} = P_{comp} \cdot V_{pump} / (P_{atm} - P_{H_2O}) \quad \text{Equation D.1.1}$$

Where:

P_{comp} = Back pressure in chamber

V_{pump} = Instantaneous volume in chamber

P_{atm} = Atmospheric pressure

P_{H_2O} = Water vapor pressure

Incorporating equation D.1.1 into the actual flow rate (V_p) equation produces:

¹ AW Chesterton CO. Stoneham, Massachusetts USA

$$V_p = V_{total} - V_{pump} - V_{comp} \quad \text{Equation D.1.2}$$

Where

V_p	= Actual mechanical pump flow rate
V_{total}	= Total chamber volume
V_{pump}	= Instantaneous volume in chamber
V_{comp}	= Volume lost due to gas compression

It should be pointed out that a decrease in instantaneous volume through the reduction of dead space will decrease the volume lost due to air compression, Equation D.1.1, with a subsequent increase in actual mechanical pump flow rate, Equation D.1.2. Thus the square finish for minimum dead space reduces the volume loss in the chamber.

3. Produce PEF of 1200 l/min in 50 ms in an ATS 24 waveform:

To produce 1200 l/min in 50 ms, the mass of the piston was used to determine the acceleration force required. It was an iteration process of combining the required force with an estimated back pressure, to produce a required torque-revolution curve which was smaller than the curve of the existing stepper motor. The power screw thread was designed using the following deduced [34] equation:

$$T = \frac{F_{total} d_m}{2} \left(\frac{l + \pi \mu d_m}{\pi d_m - \mu l} \right) + \frac{F \mu d}{2}$$

T	=	Torque [N.m]
F	=	Load [N]
d_m	=	Mean thread shaft diameter [m]
l	=	lead [m]
μ	=	Friction coefficient
d	=	driving collar diameter [m]

Producing a required torque curve illustrated in Figure D.2

Required Torque vs Speed Profile

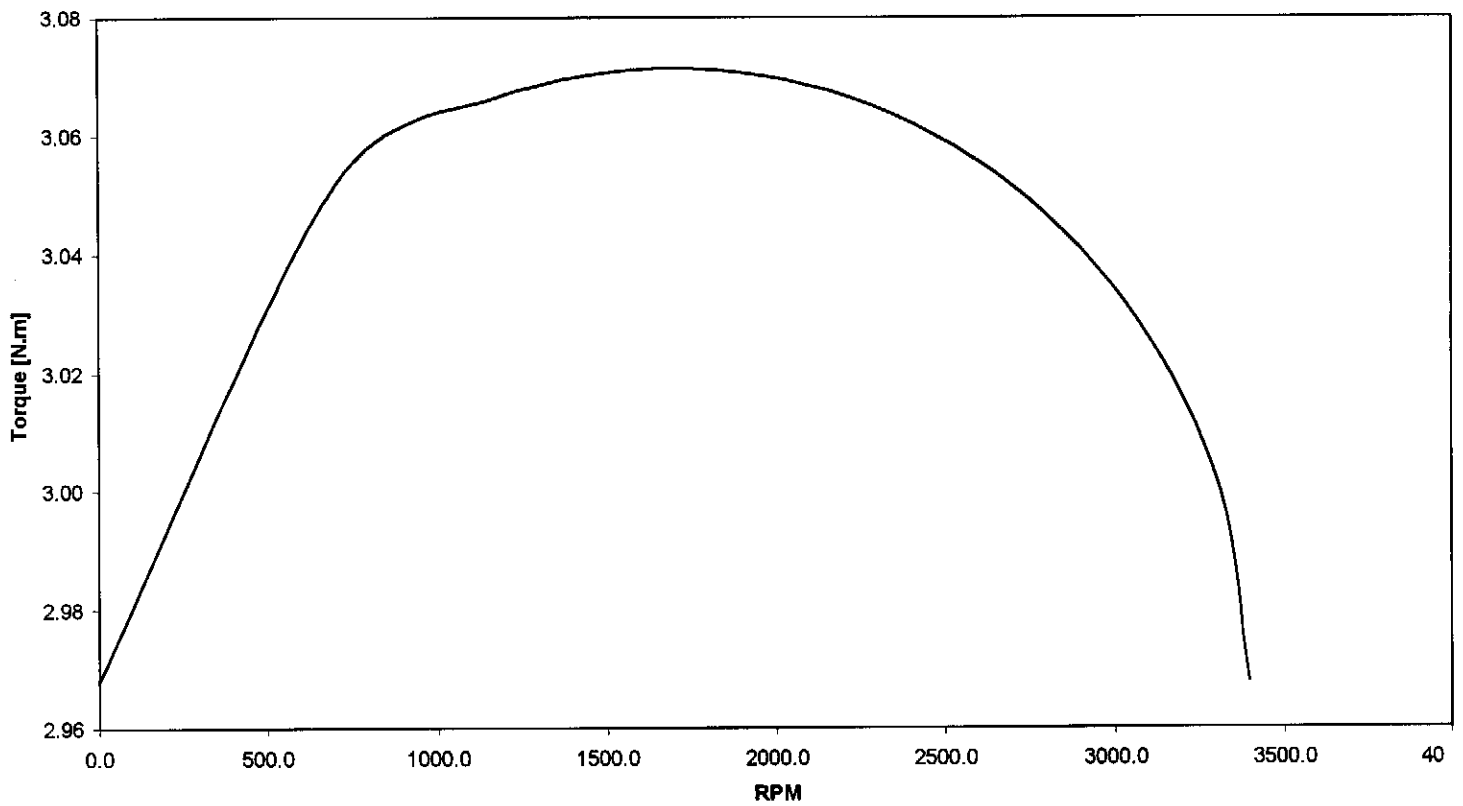


FIGURE D.2
Required Torque Curve

It was concluded that the existing stepper motor and controller would be adequate the need of the required torque curve which would produce 1200 l/min at 20kPa in 50 ms.

APPENDIX E

E.1) Contracting nozzle design:

The design of the contracting nozzle was initiated by the need, for a flow rate measurement technique, which would minimise the preceding flow resistance to the whistle. The solution was a contracting nozzle design (venturi-like), that was subscribed by Bernoulli's equation. The nozzle had to be designed with a final contracted diameter, which could house the whistle.

The following initial calculations were done to determine the feasibility of the nozzle and it's operating range and limits.

Design nozzle for maximum flow rate (20 l/min) as limiting factor:

$$\text{MaxQ} := 20$$

$$\rho := 1.2$$

$$\mu := 1.8 \cdot 10^{-5}$$

$$D1 := 20 \cdot 10^{-3}$$

$$D2 := 10 \cdot 10^{-3}$$

$$A1 := \frac{\pi \cdot D1^2}{4}$$

$$A2 := \frac{\pi \cdot D2^2}{4}$$

Thus the Reynolds number is:

$$\text{ReIn} := \frac{\left(\rho \cdot \frac{\text{MaxQ}}{60 \cdot 10^3} \cdot D1 \right)}{\mu}$$

$$\text{ReIn} = 1.415 \cdot 10^3$$

$$\text{ReOut} := \frac{\left(\rho \cdot \frac{\text{MaxQ}}{60 \cdot 10^3} \cdot D2 \right)}{\mu}$$

$$\text{ReOut} = 2.829 \cdot 10^3$$

Thus the flow through the nozzle is laminar as ReIn and ReOut is in the range of 2300

$$V_{out} := \frac{MaxQ}{60 \cdot 10^3 \cdot A_2}$$

$$k := 1.4$$

$$R := 287$$

$$T := 298$$

$$a := \sqrt{k \cdot R \cdot T}$$

$$Ma := \frac{V_{out}}{a}$$

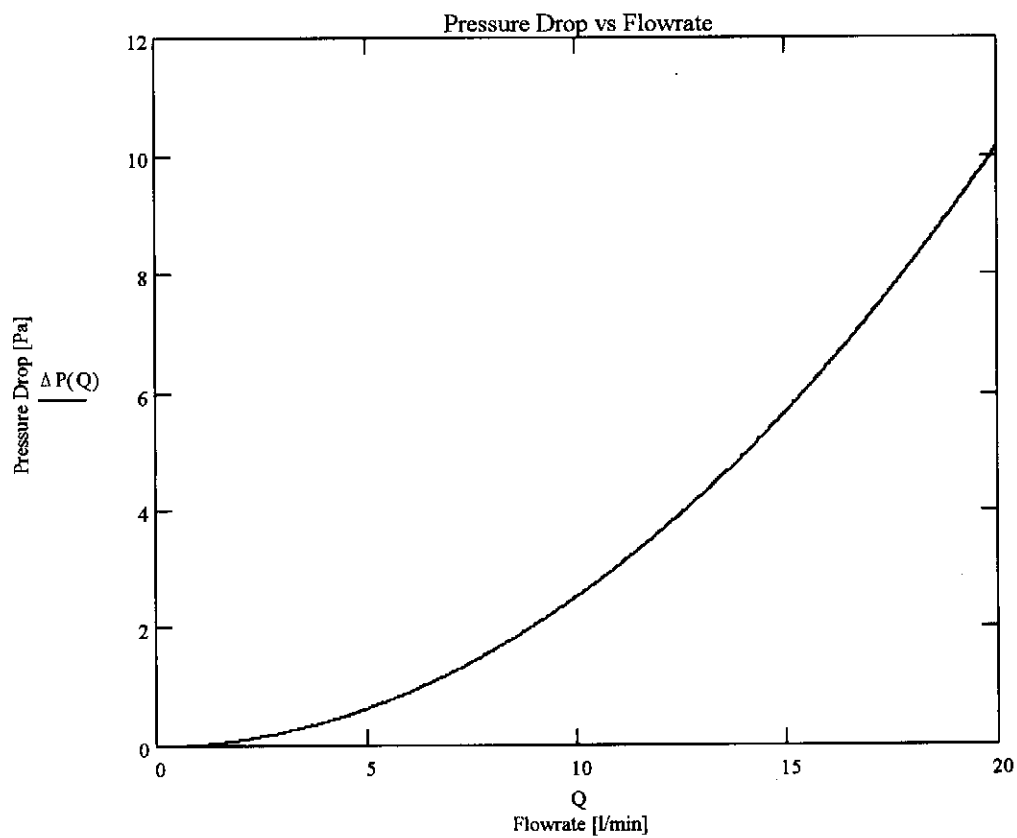
$$Ma = 0.012$$

Thus completely incompressible flow as $Ma \ll 0.3$

$$\Delta P(Q) := \frac{\rho}{2} \cdot \left(\frac{Q}{60 \cdot 1000} \right)^2 \cdot \left[\frac{(A_1^2 - A_2^2)}{(A_1 \cdot A_2)^2} \right]$$

$$\Delta P(0) = 0$$

$$\Delta P(20) = 10.132$$



The above calculations transposed into the actual contracting section design, presenting an ellipse with the long axis, 5 times the short axis. (Figure E.1)

Elliptical profile long axis 25 short axis 5

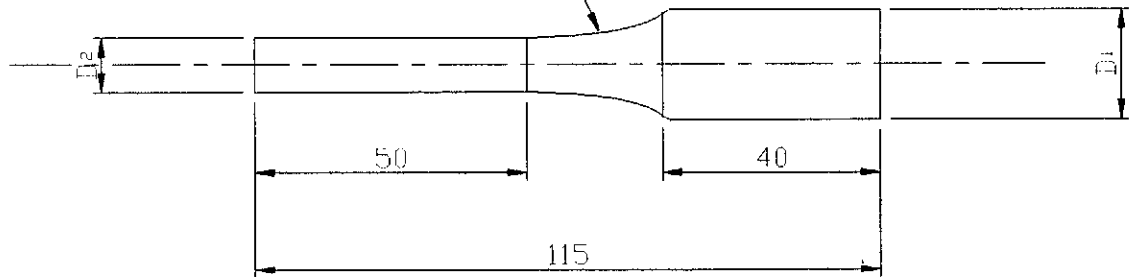


FIGURE E.1
Profile of the Contracting Nozzle

A program was written in Matlab to determine and draw the axial velocities at each station (Figure E.2) as well as the streamlines (Figure E.3).

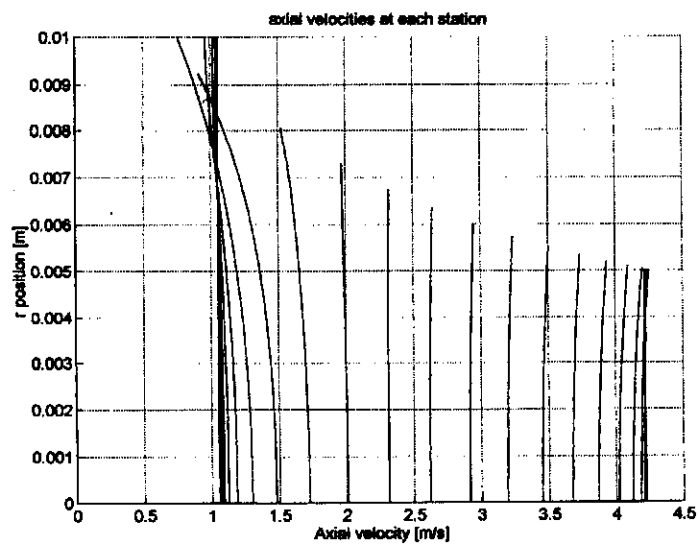


FIGURE E.2
Axial Velocities

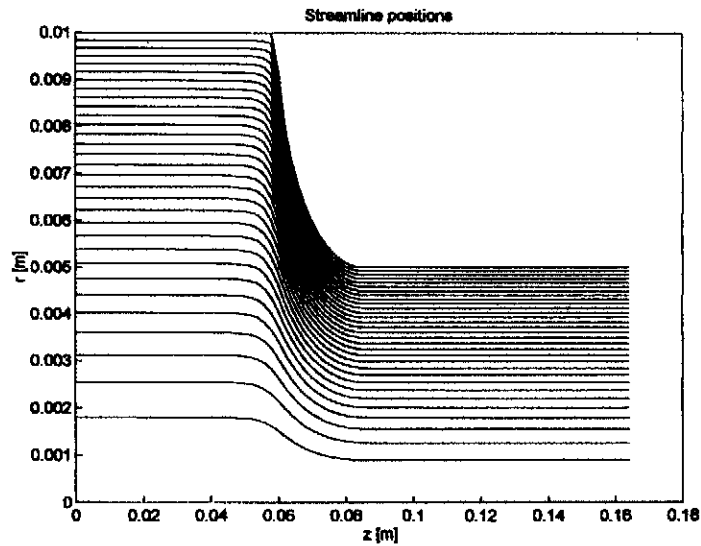


FIGURE E.3
Stream lines

At this point in time it was decided to evaluate the nozzle more extensively and a Computational Fluid Dynamics (CFD) model was developed in Flo++.

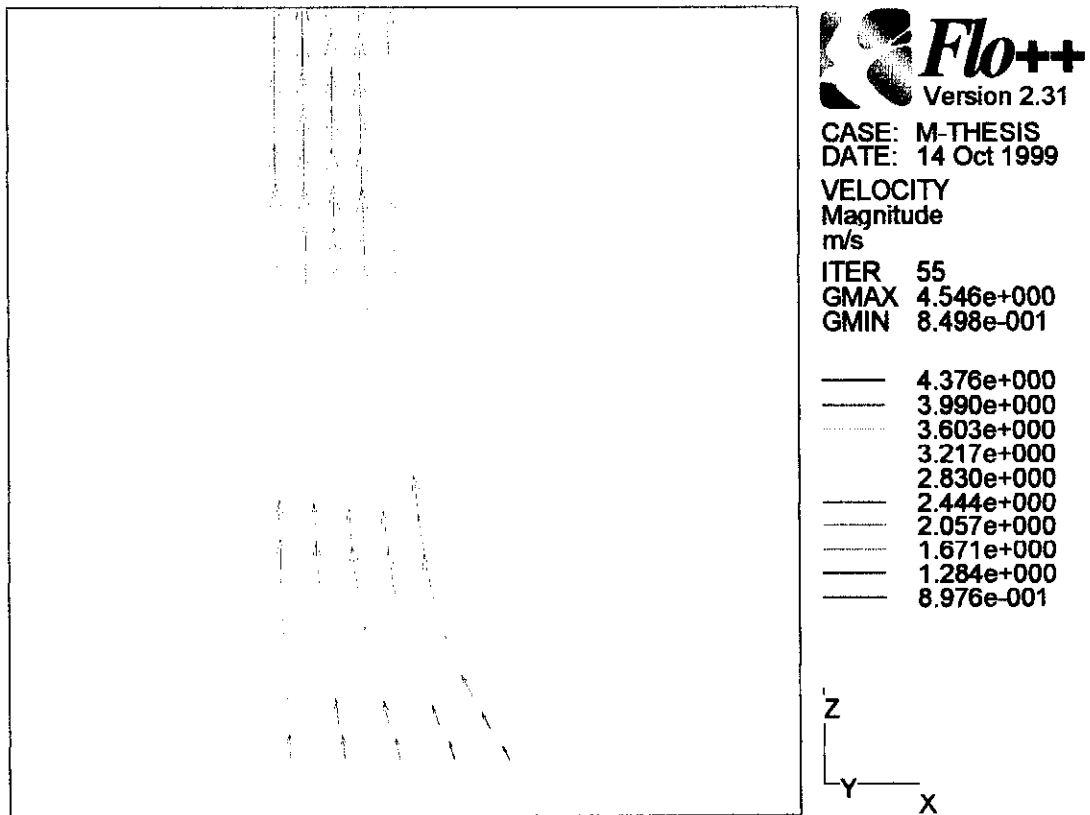


FIGURE E.4
Velocity-Vectors

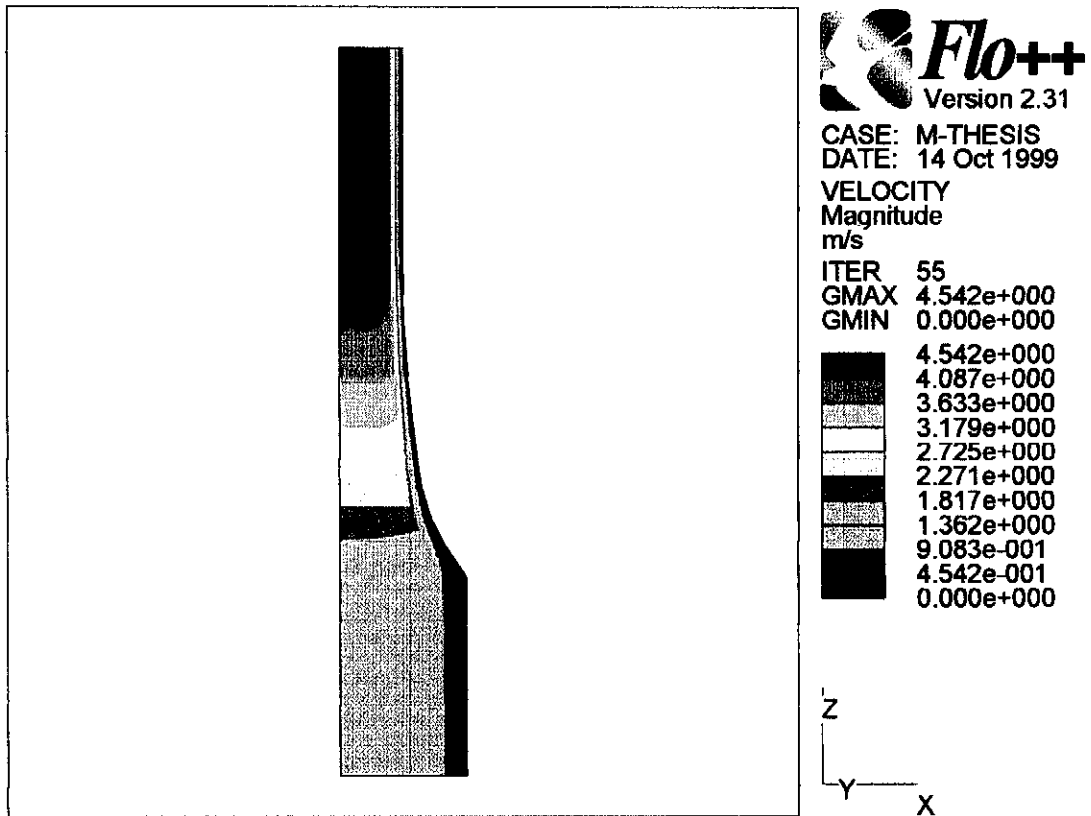


FIGURE E.5
Velocity-Profile

Figures E.4&5 show that the velocity profile and distribution is fully developed at the maximum operating flow rate of 20 l/min with no abnormalities, indicating a successful profile.

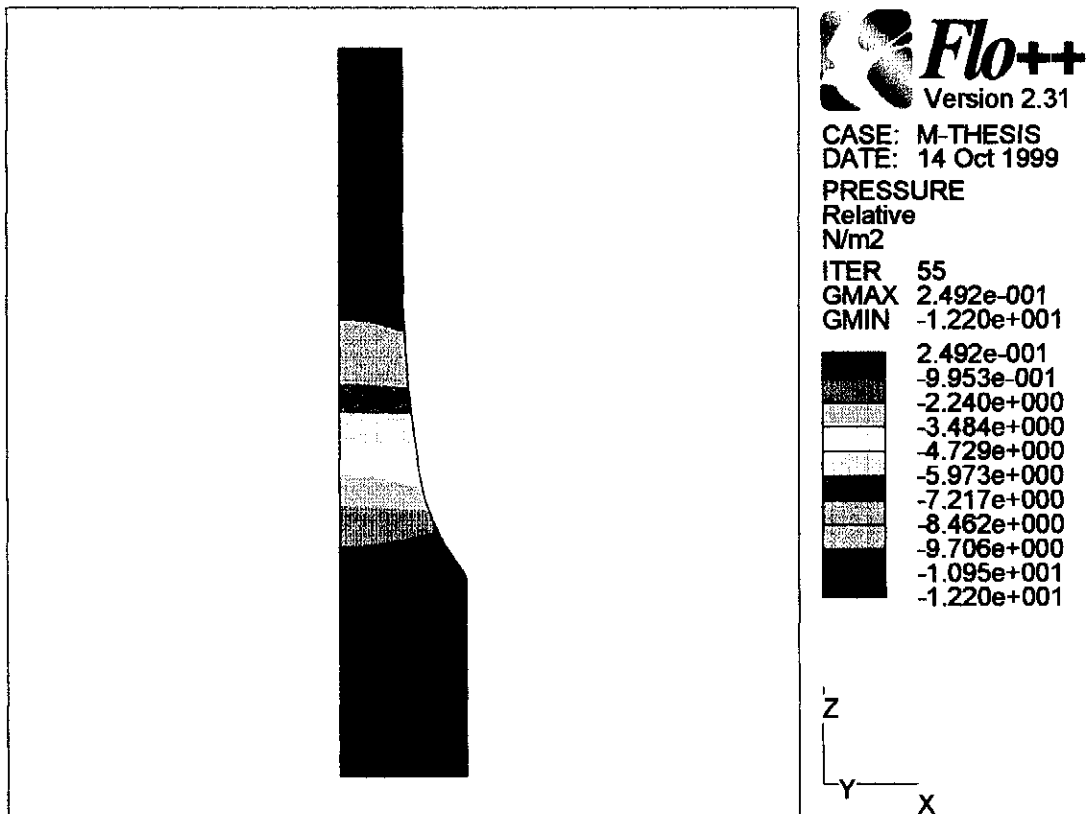


FIGURE E.6
Static pressure Distribution

Figure E.6 confirms that measuring the static pressure 4 diameters up and down stream of the contracting section, would ensure stable measurement, as these pressure distributions are fully developed. These pressure measurements had to be implemented into the Bernoulli's relationship.

In conclusion, the contracting nozzle was successfully designed for the application it has been intended for, as far as the principles of fluid dynamics are concerned.

APPENDIX F

Data augmenting program

The following program was compiled to augment six files sampled from the tests executed with a ramp input waveform for a specific whistle. It compiles one global database of flow and pressure data for manipulation by activation point determining program.

:= 
C:\Processing\12511.prn

:= 
C:\Processing\12512.prn

:= 
C:\Processing\12611.prn

:= 
C:\Processing\12513.prn

:= 
C:\Processing\12613.prn

:= 
C:\Processing\12612.prn

```

grouped := | r ← 0
           | while r < 6000
           |   newr,0 ← file1r,0
           |   newr,1 ← file1r,1
           |   newr,2 ← file2r,0
           |   newr,3 ← file2r,1
           |   newr,4 ← file3r,0
           |   newr,5 ← file3r,1
           |   newr,6 ← file4r,0
           |   newr,7 ← file4r,1
           |   newr,8 ← file5r,0
           |   newr,9 ← file5r,1
           |   newr,10 ← file6r,0
           |   newr,11 ← file6r,1
           |   r ← r + 1
           | new
toptrimmedvalue = | r ← 0
                  | j ← 1
                  | while | groupedj,0 | ≤ | groupedr,0 |
                  |   | r ← r + 1
                  |   | j ← j + 1
                  |   |
                  |   j
toptrimmedvalue = |
columns := cols(grouped)
toptrimmed := | c ← 0
              | while c < columns
              |   r ← toptrimmedvalue
              |   j ← 0
              |   while r < 6000
              |     | trimj,c ← groupedr,c
              |     | j ← j + 1
              |     | r ← r + 1
              |     | c ← c + 1
              |   trim
row := rows(toptrimmed) - 1

```

```

bottomtrimmedvalue= c← 1
                    j← 0
                    while c < columns
                      r← row
                      while toptrimmedr,c < 10
                        r← r - 1
                        value← r
                        j← j + 1
                        c← c + 2
                      value
trimvalue= min(bottomtrimmedvalu)
bottomtrimmed= c← 0
              while c < columns
                (r← 0)
                while r < trimvalue
                  (trimr,c ← toptrimmedr,c)
                  r← r + 1
                c← c + 1
              trim

```


 C:\Processing\test2.xls
 bottomtrimmed

Reed activation pressure program

This program is the reed activation pressure determining program. It incorporates the developed algorithm, where the standard deviation of 5 epochs points are determine. The maximum is found in the standard deviation array, with a subsequent reverse search for values smaller than 0.05 and then cross correlating it to the pressure to determine the reed activation pressure. For an input it uses the global database compiled by the augmenting program, and consequently can determine six activation points at a time.

```
:= 
C:\..\raw1.txt
```

```
columns:= cols(rawdata)
row := rows(rawdata)
deviation:= c←0
           j←0
           while c< columns
             r←0
             while r<(row-5)
               temparray← submatrix(rawdata,r,(r+4),c,c)
               between← stdev(temparray)
               collectiver,j← between
               r←r+1
             j←j+1
             c←c+2
           collective
columns2:= cols(deviation)
row2 := rows(deviation) - 1
maxvalue:= c←0
           while c< columns2
             temparray2← submatrix(deviation,0,row2,c,c)
             between2← max(temparray2)
             collective2c← between2
             c←c+1
           collective2
maxposition:= c←0
             while c< columns2
               r←0
               while deviationr,c≠maxvaluec
                 r←r+1
               collective3c←(r+1)
               c←c+1
             collective3
```

```

cutposition:= | c ← 0
               | while c < columns2
               |   evaluate ← submatrix(deviation, 0, maxpositionc, c, c)
               |   r ← (rows(evaluate) - 1)
               |   while evaluater > 0.1
               |     r ← r - 1
               |     betweenc ← (r + 1)
               |     c ← c + 1
               | between
activationpoints:= | c ← 0
                  | x ← 1
                  | k ← 0
                  | while c < columns
                  |   pos ← cutpositionk
                  |   small ← submatrix(rawdata, (pos - 4), (pos + 4), x, x)
                  |   flowrate ← mean(small)
                  |   carrierk,0 ← rawdatapos,c
                  |   carrierk,1 ← flowrate
                  |   k ← k + 1
                  |   x ← x + 2
                  |   c ← c + 2
                  | carrier

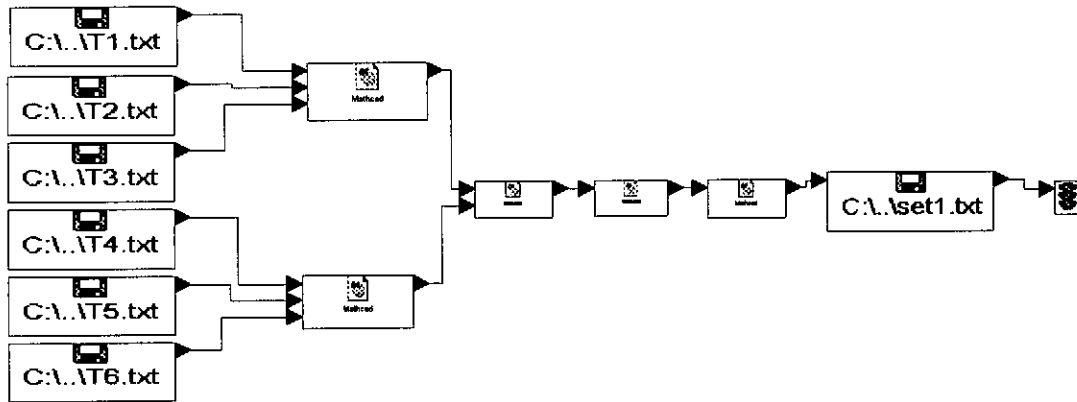
```



C:\..batch4.xls
activationpoints

Mathconnex Simulation

The above to programs was integrated into a Mathconnex electronic circuit board simulation to speed up the processing of data.



Turbo Pascal Compiled Program

After the preceding program was tested successful the theory was implemented into a Turbo Pascal program. The latter facilitated in faster testing procedure, as the activation pressure was determined for each test post to the data acquisition. The Turbo Pascal program, which follows is the mentioned program, and was compiled from the initial Turbo Pascal sampling program with integration of the theory of the MathCAD Reed Activation Pressure program.

```

PROGRAM mov4;
{Download a sequence to the SX-8}
{Add start/stop from DtoA board}
{09/05/1999}
{Add the algorith to calculate the activation point}
{14/05/1999}
USES dos,crt,async2,ASA_Drv,rtgsub,graph,rtstdhdr,rtfft,
      rtgwin,rtchart,rtgcommo;

Const
  FileLength = 21;
  AantalToetse =12;
{AtoD constants start here}
  BaseAdress      = $360;
  PointerLength   = 6000;(*600*)
  MaxSampleArray  = 6000;(*600*)
  InitialSampleRate = 3000; {Hz} (*1000*)
  ADChi           = $362; (* ADC hi bytes and Int line *)
  DAC0            = $364;
  DAC1            = $366;
  PressureAtoDCalFactor = 0.004887;
  BeginPosition   = 2.6;
{Filter constants start here}
  CutOffFreqF     = (24)/InitialSampleRate;    {Hz}
  CutOffFreqP     = 800/InitialSampleRate;    {Hz}
  FilterOrder     = 123;    {Digial Filter size. See QuinnCurtiss}
  FilterWindow    = 2;    {Type of filter window See QuinnCurtiss}
type
longArray=array[1..MaxSampleArray] of RealType;
VAR
  err, cport      : Integer;
  HexArray        : ARRAY[1..FileLength] OF STRING[30];
  i,
  LoopCounter     : Integer;
  FileVarIn,FileVarOut : Text;
  LoopQuit        : boolean;
  Infile          : STRING[15];
{AtoD variables start here}
  Dat             : ADData;
  deltaT          : Real;
  Vector1         : pointer;
  SampledArray    : ARRAY[1..4,0..PointerLength] OF Integer;
  Head,Tail       : integer;
  adsample2,
  adsample3       : Real;
  OkToCapture     : Boolean;
  PressureFileData,
  FlowFileData    : ^longArray;(*ARRAY[1..MaxSampleArray] of Realtye;*)
  FileCounter     : Integer;
  EndOfExperiment : Boolean;
  PressureData    : rtvaluearraytype;
{Filtering variables start here}
  FilterCoeff     : ARRAY[0..FilterOrder] of REAL;
  filteredFlowFileData : ^longArray;(*ARRAY[1..MaxSampleArray] of Realtye;*)
{QC vertoon veranderlikes begin hier}
xAxis : ^longArray;(*array[1..MaxSampleArray] of realtype;*)
teller : integer;
FileName : String[10];
Str1,Ofile,OutFile : String[20];
{ActivationVariables start here}
ActivationTeller,Maxteller: integer;

```

```

Mean,SumMeanDiff,MaximumPressureStdev:real;
ActivationFound:Boolean;
ActivationPressure,ActivationFlow,ActivationPoint:real;
ActFile,ActOutFile : string[20];
FileVarAct : text;
(=====)
{This is the ISR for each sample at samplerate}
Procedure GetInterruptSample;
interrupt;

begin
  inline ($FA);           { Stop Intrr. }
  asm
    mov di,offset DAT
    mov cx,4
  @2:
    mov dx,BaseAdress
    in al,dx               {Read low byte}
    mov bl,al
    mov dx,BaseAdress+2
    in al,dx               {Read high byte}
    and al,0FH
    mov bh,al
    and al,08H
    jz @3
    sub bx,1000H
  @3:
    mov [di],bx           {Store channel A/D data}
    inc di
    inc di
    loop @2
  end;
  SampledArray[1,Head] := Dat[0];
  SampledArray[2,Head] := Dat[1];
  SampledArray[3,Head] := Dat[2];
  SampledArray[4,Head] := Dat[3];
  inc(Head,1);
  IF (Head>MaxSampleArray) then Head := 0;
  port [$20] := $20;      { Herstel 8259 }
  inline ($FB);
end;(GetInterruptSample)
(=====)

{Set up the AtoD board}
Procedure SetUpASAboard(InterruptAddress:Pointer; InterruptRate:integer);
{Load all interrupts and timers for ASA board}

Begin
  ASA_TimerControl(BaseAdress,$34);           {Mode 2}
  ASA_WriteTimerCounter(BaseAdress,0,round(250000/InterruptRate));
  {Initial value @250kHz clock = 4Mhz/16}
  {ASA timer setup as follows.....
  4Mhz osc / 16 = CLKSEL2 (250kHz)
  JMPR P5 - Out0,3 to U10,5 !CONVST
  - CLKSEL2,6 to CLK0,1
  }
  getintvec(13, Vector1);           {Old pointer for IRQ5 }
  setintvec(13, InterruptAddress);  {IRQ5 --> ISR of GetInterruptSample}
end;(SetUpASAboard)

(=====)

```

```

{Starts the interrupt process ISR at IRQ5 }
Procedure Init_Interrupt;

begin
  port [$21] := port [$21] and $DF;    { Stel 8259 vir IRQ5 }
  port [$20] := $20;                  { Herstel 8259 }
  inline ($FB);                        { Steun ondr. }
end;{Init_Interrupt}
{=====}
{ Stops the interrupt process ISR at IRQ5 }
Procedure Stop_Interrupt;

begin
  port [$20] := $20;                  { Herstel 8259 }
  inline ($FA);                       { Stuit ondr. }
end;{top_Interrupt}
{=====}
{Collecting samples at the specified sampling rate}
Procedure ServiceTheSample;
begin
  IF Head<>Tail then {Check cyclic buffer counters}
    begin
      adsample2 :=(SampledArray[2,tail])*PressureAtoDCalFactor;
      adsample3 :=(SampledArray[3,tail])*PressureAtoDCalFactor;
      If OkToCapture = True then
        begin
          PressureFileData^[FileCounter]:=adsample2;{Volt}
          FlowFileData^[FileCounter]:=adsample3;    {Volt}
          Inc(FileCounter);
        end;
      inc(Tail,1);
      IF (Tail>MaxSampleArray) then Tail:=0;
      IF (FileCounter>MaxSampleArray) then EndOfExperiment:=true;
      IF (FileCounter>MaxSampleArray) then FileCounter:=1;
    end;
end;{ServiceTheSample}
{=====}
{DtoA: Ouputs the Analogue voltage }
Procedure SNA(K,S : integer); {K->kanaal nommer, S->getal}
begin
  {K=0 ->start}
  {K=1 ->stop}
  if S > 511 then S := 511;
  { if S < -512 then S := -512;}
  if S < 0 then S := 0;
  S := (S + 512) shl 6;
  if K = 0 then begin
    port[DAC0+1] := hi(S);
    port[DAC0] := lo(S);
  end
  else begin
    port[DAC1+1] := hi(S);
    port[DAC1] := lo(S);
  end;
end; {SNA}
{=====}
(*
Procedure FindTheStart;
var
  CurrentPosition : real;
  Som : real;

```

```

begin
  CurrentPosition:=0;
  Writeln('Bepaal die huidige posisie...');
  OkToCapture := True;
  EndOfExperiment:=False;
  tail:=head-1;
  FileCounter:=1;
  Som:=0;
  repeat
    ServiceTheSample;
  until EndOfExperiment;
  OkToCapture := False;
  FOR i:=1 to MaxSampleArray do
    begin
      Som:=Som+FlowFileData[i];
    end;
  CurrentPosition:=Som/MaxSampleArray;
  Writeln('Die huidige posisie is ',CurrentPosition:3:1);
  If CurrentPosition > BeginPosition then
    begin
      Writeln('Beweeg vorentoe...');
      writelnCom(CPORT, 'PS', ERR);
      writelnCom(CPORT, 'IN1A', ERR);
      writelnCom(CPORT, 'IN2C', ERR);
      writelnCom(CPORT, 'LD3', ERR);
      writelnCom(CPORT, 'MC', ERR);
      writelnCom(CPORT, 'TR10', ERR);
      writelnCom(CPORT, 'H+', ERR);
      writelnCom(CPORT, 'Q1', ERR);
      writelnCom(CPORT, 'RM0300', ERR);
      writelnCom(CPORT, 'T20', ERR);
      writelnCom(CPORT, 'Q0', ERR);
      writelnCom(CPORT, 'TR01', ERR);
      writelnCom(CPORT, 'C', ERR);
    end;
  If CurrentPosition < BeginPosition then
    begin
      Writeln('Beweeg terug...');
      writelnCom(CPORT, 'PS', ERR);
      writelnCom(CPORT, 'IN1A', ERR);
      writelnCom(CPORT, 'IN2C', ERR);
      writelnCom(CPORT, 'LD3', ERR);
      writelnCom(CPORT, 'MC', ERR);
      writelnCom(CPORT, 'TR10', ERR);
      writelnCom(CPORT, 'H-', ERR);
      writelnCom(CPORT, 'Q1', ERR);
      writelnCom(CPORT, 'RM0300', ERR);
      writelnCom(CPORT, 'T20', ERR);
      writelnCom(CPORT, 'Q0', ERR);
      writelnCom(CPORT, 'TR01', ERR);
      writelnCom(CPORT, 'C', ERR);
    end;
  {Pulse the START switch}
  SNA(0,256);
  delay(100);
  SNA(0,0);
  OkToCapture := True;
  EndOfExperiment:=False;
  tail:=head-1;
  FileCounter:=1;
  repeat

```

```

    ServiceTheSample;
until (adsample3>BeginPosition-0.1) and
    (adsample3<BeginPosition+0.1);
OkToCapture := False;
{Pulse the STOP switch}
SNA(1,256);
delay(100);
SNA(1,0);
{Maak die buffers skoon}
FOR i:=1 to MaxSampleArray do PressureFileData[i]:=0;
FOR i:=1 to MaxSampleArray do FlowFileData[i]:=0;
FOR i:=1 to MaxSampleArray do FilteredFlowFileData[i]:=0;
end;
*)
{-----}
PROCEDURE ReadInputFile;
BEGIN
    Writeln('Busy reading the file...');
    assign(FileVarIn,infile);
    reset(FileVarIn);
    FOR i:=1 TO FileLength do readLN(FileVarIn,HEXARRAY[i]);
    close(FileVarIn);
END;
{-----}
Procedure StelCommPoortOp;
begin
    cport := 0; {0->comm1, 1->comm2}
    opencom(CPORT,9600,'N',1,8,err);
    SETHARDhANDSHAKE(CPORT,0);
end;
{=====}
(*
Procedure MoveThePistonBack;
begin
    writeln('Moving piston back to START');
    writelnCom(CPORT,'PS',ERR);
    writelnCom(CPORT,'IN1A',ERR);
    writelnCom(CPORT,'IN2C',ERR);
    writelnCom(CPORT,'LD3',ERR);
    writelnCom(CPORT,'MC',ERR);
    writelnCom(CPORT,'TR10',ERR);
    writelnCom(CPORT,'H-',ERR);
    writelnCom(CPORT,'Q1',ERR);
    writelnCom(CPORT,'RM0300',ERR);
    writelnCom(CPORT,'T20',ERR);
    writelnCom(CPORT,'Q0',ERR);
    writelnCom(CPORT,'TR01',ERR);
    writelnCom(CPORT,'C',ERR);
{Pulse the START switch}
SNA(0,256);
delay(100);
SNA(0,0);
OkToCapture := True;
EndOfExperiment:=False;
tail:=head-1;
FileCounter:=1;
repeat
    ServiceTheSample;
until (adsample3>BeginPosition-0.1) and
    (adsample3<BeginPosition+0.1);
OkToCapture := False;

```

```

(Pulse the STOP switch)
  SNA(1,256);
  delay(100);
  SNA(1,0);

{Maak die buffers skoon}
  FOR i:=1 to MaxSampleArray do PressureFileData[i]:=0;
  FOR i:=1 to MaxSampleArray do FlowFileData[i]:=0;
  FOR i:=1 to MaxSampleArray do FilteredFlowFileData[i]:=0;
end;
*)
{-----}

Procedure GetFilterData(CutOffFreq:real);

VAR
  filtcoef : realpnter;

begin
  getmem(Filtcoef,sizeof(realtype)*FilterOrder);
  RTFirFreqSample(Filtcoef,CutOffFreq,FilterOrder,0,0,FilterWindow);
  FOR i := 0 to FilterOrder-1 DO FilterCoeff[i] := getpntreal(Filtcoef,i);
  freemem(Filtcoef,sizeof(realtype)*FilterOrder);
end;
{-----}
Procedure DoThePressureFiltering;      {All the filtering is done here}
VAR n,m : integer;
begin
  {filter die druk}
  for n:=0 to MaxSampleArray do filteredFlowFileData^[n] := 0;
  For n:= (FilterOrder-1) to MaxSampleArray do
    begin
      for m:=0 to (FilterOrder-1) do
        begin

filteredFlowFileData^[n]:=filteredFlowFileData^[n]+(FilterCoeff[m]*PressureFileD
ata^[n-m]); {digital filter formulae}
          end;
        end;          {end of filtering section}
      for n:=0 to MaxSampleArray do PressureFileData^[n]:=filteredFlowFileData^[n];
    end;
  {-----}
Procedure DoTheFlowFiltering;      {All the filtering is done here}
VAR n,m : integer;
begin
  {filter die vloei}
  for n:=0 to MaxSampleArray do filteredFlowFileData^[n] := 0;
  For n:= (FilterOrder-1) to MaxSampleArray do
    begin
      for m:=0 to (FilterOrder-1) do
        begin

filteredFlowFileData^[n]:=filteredFlowFileData^[n]+(FilterCoeff[m]*FlowFileData^
[n-m]); {digital filter formulae}
          end;
        end;          {end of filtering section}
      for n:=0 to MaxSampleArray do FlowFileData^[n]:=filteredFlowFileData^[n];
    end;
  {-----}
PROCEDURE WriteFiles;

```

```

BEGIN
  str(LoopCounter, str1);
  OFile:='c:\mav\rrs40'+str1;
  OutFile:=OFile+'.txt';
  assign(FileVarOut, OutFile);
  Writeln('Saving to ', Outfile);

  (*
  Writeln('Wat is die naam van die lee^r?');
  Readln(FileName);
  ASSIGN(FileVar, 'c:\mav\'+'+FileName+'.prn');
  *)
  Rewrite(FileVarOut);
  Writeln(FileVarOut, 'Pressure', ',', ',', 'Flow', ',', ',', 'StdDev');
  FOR i:=1 to MaxSampleArray do
  writeln(FileVarOut, PressureFileData^[i]:3:3, ',', ',', FlowFileData^[i]:3:3
  , ',', ',', FilteredFlowFileData^[i]:3:3);
  Close(FileVarOut);
END;
{-----}
  (*
  Procedure DisplayPressureAndFlow;

  begin
  {Flow = rtstat[1]}
  rtsetwindowoptions(rtstat[1], rt_resize or rt_maximize or rt_hide or rt_iconize
  or rt_savewinimage or rt_3dborder or rt_3dinner);
  rtsetpercentwindow(rtstat[1], 0.01, 0.1, 0.99, 0.5);
  rtsetwin2plotratio(rtstat[1], 0.15, 0.15, 0.15, 0.15);
  rtsetViewBackground(rtstat[1], 7);
  rtscalePlotArea(rtstat[1], 0, 0, MaxSampleArray, 50);
  rtsetxyintercepts(rtstat[1], 0.0, 0.0);
  setcolor(5);
  rtdrawyaxis(rtstat[1], 10, 0);
  rtlabelyaxis(rtstat[1], 5, 0, 0);
  rtdrawxaxis(rtstat[1], 100, 0);
  rtlabelfxaxis( rtstat[1], 1, 0, 0);
  For i:= 1 to MaxSampleArray do xAxis^[i]:=i;{*deltaT;}
  *)

  (* rtLinePlotData(rtstat[1], @xaxis, @FlowFileData, MaxSampleArray, 14, 0); *)
  (*
  rtLinePlotData(rtstat[1], @xaxis, @FlowFileData, MaxSampleArray, 0, 0);
  setcolor(14);
  rttitlexaxis(rtstat[1], 'Time (s)');
  rttitleyaxis(rtstat[1], 'Flow');
  {Pressure = rtstat[2]}
  rtsetwindowoptions(rtstat[2], rt_resize or rt_maximize or rt_hide or rt_iconize
  or rt_savewinimage or rt_3dborder or rt_3dinner);
  rtsetpercentwindow(rtstat[2], 0.01, 0.6, 0.99, 0.99);
  rtsetwin2plotratio(rtstat[2], 0.15, 0.15, 0.15, 0.15);
  rtsetViewBackground(rtstat[2], 7);
  rtscalePlotArea(rtstat[2], 0, 0, MaxSampleArray, 10);
  rtsetxyintercepts(rtstat[2], 0.0, 0.0);
  setcolor(5);
  rtdrawyaxis(rtstat[2], 1.0, 0);
  rtlabelyaxis(rtstat[2], 1, 1, 0);
  rtdrawxaxis(rtstat[2], 100, 0);
  rtlabelfxaxis( rtstat[2], 1, 0, 0);
  rtLinePlotData(rtstat[2], @xaxis, @PressureFileData, MaxSampleArray, red, 0);
  *)

```



```

setcolor(14);
rtttitlexaxis(rtstat[2], 'Time (s)');
rtttitleyaxis(rtstat[2], 'Pressure');
REPEAT
    rtprocesswindowoptions;
UNTIL KEYPRESSED;
readln;
rtClearWindow(rtstat[1]);
rtClearWindow(rtstat[2]);
rtCloseGraphics(1);
end;
*)
{-----}
PROCEDURE OpenTheActivationFile;

BEGIN
{} ActFile:='c:\mav\arrs40';
ActOutFile:=ActFile+'.txt';
assign(FileVarAct,ActOutFile);
Rewrite(FileVarAct);
Writeln(FileVarAct, 'Teller', ',', ',', 'Pressure', ',', ',', 'Flow');
Close(FileVarAct);
END;
{-----}
PROCEDURE WriteTheActivationFile;

BEGIN
{} ActFile:='c:\mav\arrs40';
ActOutFile:=ActFile+'.txt';
assign(FileVarAct,ActOutFile);
Writeln('Saving to ',ActOutfile);
Append(FileVarAct);

Writeln(FileVarAct,ActivationTeller, ',', ',', ActivationPressure:3:3, ',', ',', ActivationFlow:3:3);
Close(FileVarAct);
END;
{-----}
Procedure DetermineTheActivationPoint;

begin

{CalculateTheStandardDeviation}
for teller:=1 to MaxSampleArray do filteredFlowFileData^[teller]:=0;
ActivationPressure:=0;
ActivationFlow:=0;
ActivationTeller:=0;
For teller:= 1 to (MaxSampleArray-5) do
begin
    mean:=(PressureFileData^[teller]+
            PressureFileData^[teller+1]+
            PressureFileData^[teller+2]+
            PressureFileData^[teller+3]+
            PressureFileData^[teller+4])/5;
    SumMeanDiff:=
        (PressureFileData^[teller]-mean)*(PressureFileData^[teller]-mean)+
        (PressureFileData^[teller+1]-mean)*(PressureFileData^[teller+1]-mean)+
        (PressureFileData^[teller+2]-mean)*(PressureFileData^[teller+2]-mean)+
        (PressureFileData^[teller+3]-mean)*(PressureFileData^[teller+3]-mean)+
        (PressureFileData^[teller+4]-mean)*(PressureFileData^[teller+4]-mean);
    filteredFlowFileData^[teller]:=sqrt((SumMeanDiff/5));

```

```

end;

{FindTheMaximumValue}
MaximumPressureStdev:=0;
MaxTeller:=0;
For teller := 1 to MaxSampleArray-20 do
  begin
    if PressureFileData^[teller] >= MaximumPressureStdev
      Then
        Begin
          MaximumPressureStdev:=PressureFileData^[teller];
          MaxTeller:=teller;
        end;
    end;
  end;

{FindTheActivationPoint}
ActivationFound := false;
ActivationPoint:=0.05;
For teller:=MaxTeller DownTo 1 do
  Begin
    If FilteredFlowFileData^[teller] <= 0.05
      then
        If ActivationFound = false
          Then
            begin
              ActivationTeller:=teller;
              ActivationFound:=True;
            end;
        end;
  end;

ActivationPressure:=PressureFileData^[ActivationTeller];
ActivationFlow:=
  (FlowFileData^[ActivationTeller+1]+
  FlowFileData^[ActivationTeller+2]+
  FlowFileData^[ActivationTeller+3]+
  FlowFileData^[ActivationTeller+4]+
  FlowFileData^[ActivationTeller+5]+
  FlowFileData^[ActivationTeller-1]+
  FlowFileData^[ActivationTeller-2]+
  FlowFileData^[ActivationTeller-3]+
  FlowFileData^[ActivationTeller-4]+
  FlowFileData^[ActivationTeller-5])/10;
WriteTheActivationFile;
end;
(=====)

(=====)
Procedure CalculateParameters;

begin
{Covert to volume: gebruik filteredFlowFileData array hiervoor}
For teller:=0 to MaxSampleArray do
  filteredFlowFileData^[teller]:=abs((FlowFileData^[teller]-
FlowFileData^[1])*(1/0.10265)*(0.365/5));{liter}
{Convert to flow}
FlowFileData^[1]:=0;
For teller:=2 to MaxSampleArray do
  FlowFileData^[teller]:=(filteredFlowFileData^[teller]-
filteredFlowFileData^[teller-1])/deltaT*60;{liter/min}

GetFilterData(CutOffFreqF);

```

```

DoTheFlowFiltering;
GetFilterData(CutOffFreqP);
DoThePressureFiltering;
DetermineTheActivationPoint;
WriteFiles;

{display data}
{
rtopenrtg(detect,0,defaultgraphdir,3,1);
DisplayPressureAndFlow;
*}
end;
{=====}
PROCEDURE DownloadTheFile;
  Begin
    For LoopCounter:= 1 to AantalToetse do
      begin
        Writeln('Downloading.....');
        For i:=1 to FileLength do writelnCom(CPORT,hexarray[i],ERR);
      {Sample the data}
      {Pulse the START switch}
        SNA(0,256);
        delay(20);
        SNA(0,0);
      Delay(1000);
        Writeln('Sampling.....');
        OkToCapture := True;
        EndOfExperiment:=False;
        tail:=head-1;
        FileCounter:=1;
        repeat
          ServiceTheSample;
        until EndOfExperiment;
        OkToCapture := False;
        delay(6000);
      {Pulse the STOP switch}
        SNA(1,256);
        delay(100);
        SNA(1,0);
        delay(1000);
      {Claculate the Parameters}
        CalculateParameters;
      (*      MoveThePistonBack;*)

        end;
      end;

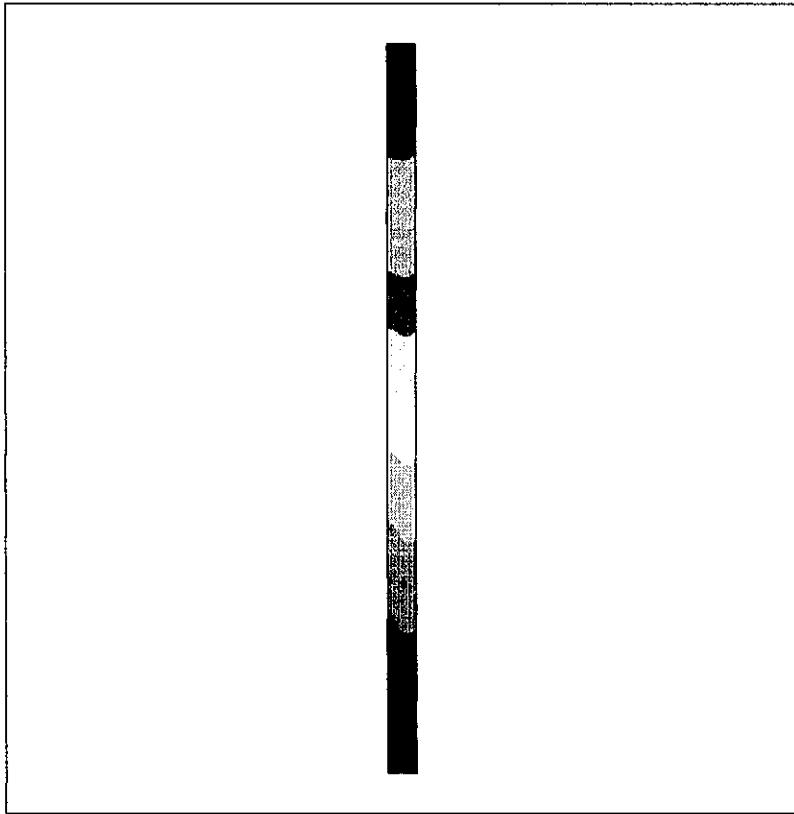
  {=====Main Program=====}
BEGIN
  ClrScr;
  OpenTheActivationFile;
  Writeln('Press <ENTER> to start the test');
  Readln;
  new(PressureFileData);
  new(FlowFileData);
  new(FilteredFlowFileData);{Set up the AtoD card}
  new(xAxis);
  deltaT:=1/InitialSampleRate; {stel vir die monster tempo}
  SetUpASAbord(@GetInterruptSample,InitialSampleRate); {Setup sample interval}
  Init_Interrupt;          {Init all vectors and Interr.Controller}
  ASA_ReadAtoD(BaseAdress,Dat);    {clears the ASA buffer}

```

```
{Make sure the START/STOP switches are off}
{0->start}
{1->stop}
  SNA(0,0);
  SNA(1,0);
{Clear the buffers}
  FOR i:=1 to MaxSampleArray do PressureFileData^[i]:=0;
  FOR i:=1 to MaxSampleArray do FlowFileData^[i]:=0;
  FOR i:=1 to MaxSampleArray do FilteredFlowFileData^[i]:=0;
  StelCommPoortOp;
(*
  FindTheStart;
*)
{}
  InFile:='c:\mov.prg';
  writeln(Infile);
  ReadInputFile;
  DownloadTheFile;
  closecom(cport);
  Stop_Interrupt;
Dispose(PressureFileData);
Dispose(FlowFileData);
Dispose(FilteredFlowFileData);
Dispose(xAxis);
END.
```

APPENDIX G

G.1



CASE: M-THESIS
DATE: 19 Nov 1999

PRESSURE
Relative
N/m²

ITER 210
GMAX 7.669e-002
GMIN -7.381e+001

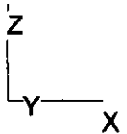
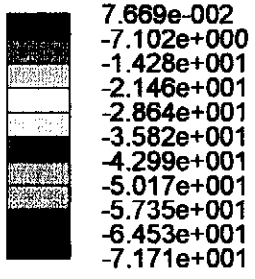
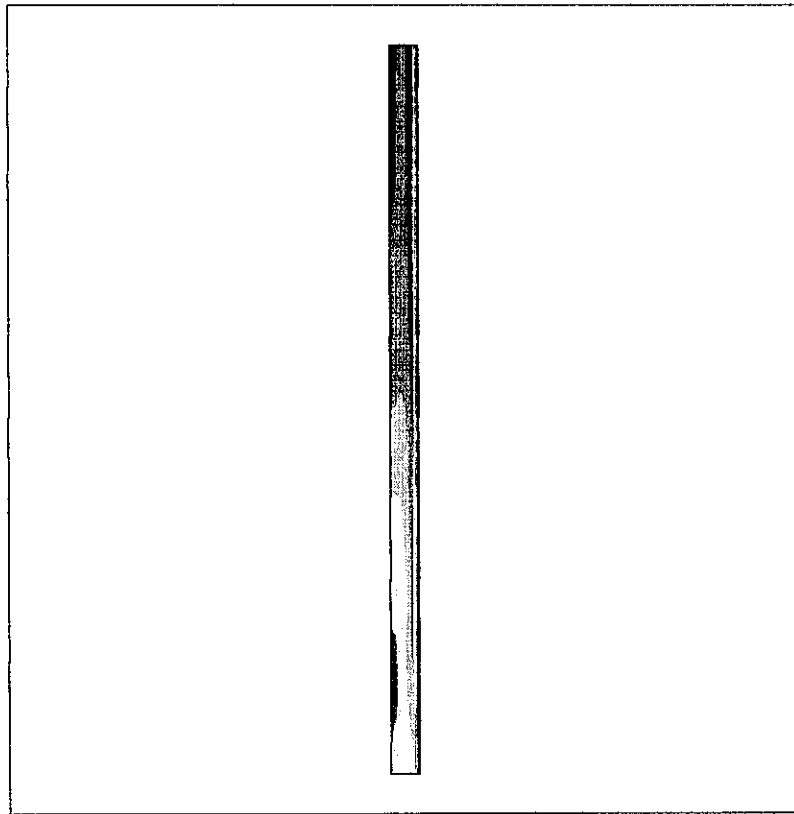


FIGURE G.1
Pressure Distribution in Testing Nozzle



CASE: M-THESIS
DATE: 19 Nov 1999

VELOCITY
Magnitude
m/s

ITER 210
GMAX 4.399e+000
GMIN 0.000e+000

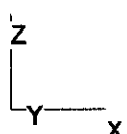
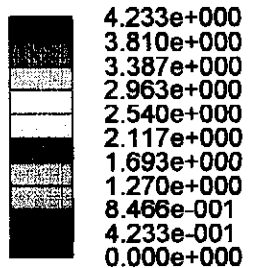
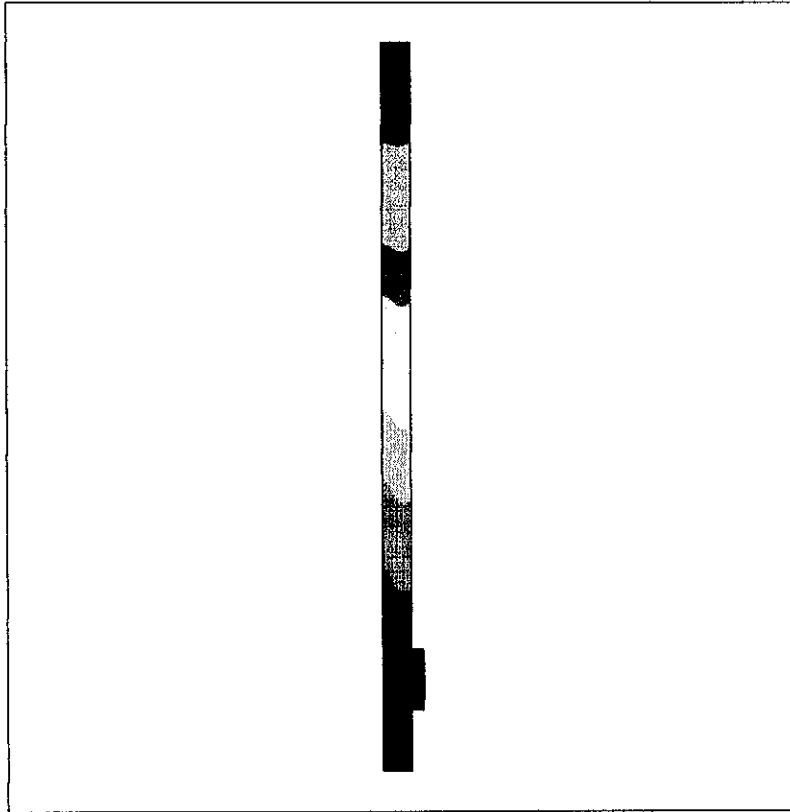


FIGURE G.2
Velocity Distribution in Testing Nozzle



CASE: M-THESIS
DATE: 19 Nov 1999

PRESSURE
Relative
N/m²

ITER 197
GMAX 7.674e-002
GMIN -6.643e+001

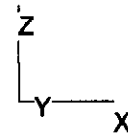
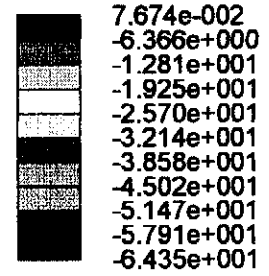
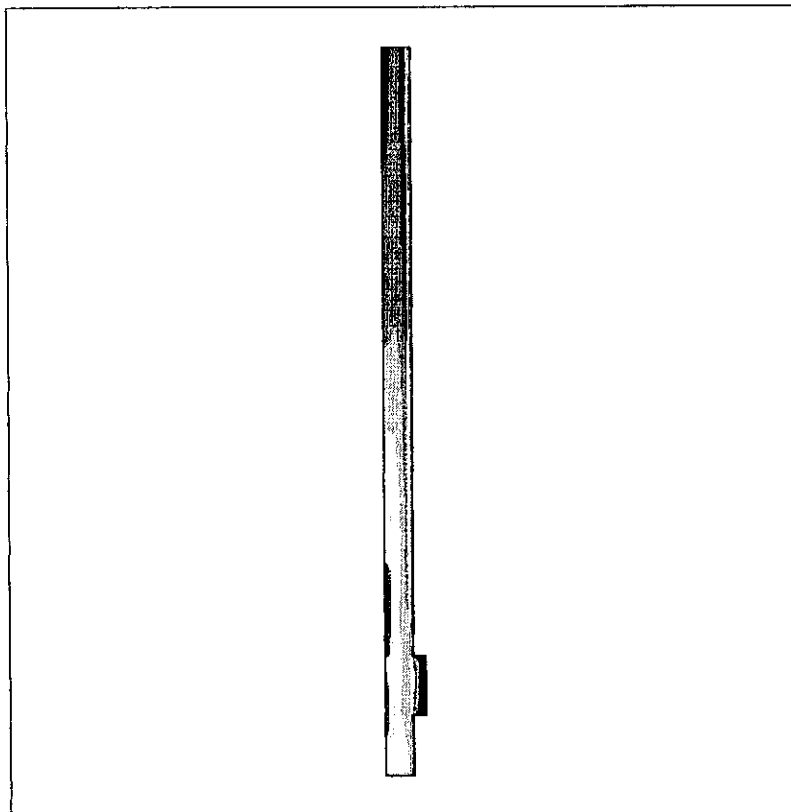


FIGURE G.3
Pressure Distribution in Expansion Nozzle ($L_{step} = 10$ mm)



CASE: M-THESIS
DATE: 19 Nov 1999

VELOCITY
Magnitude
m/s

ITER 197
GMAX 4.400e+000
GMIN 0.000e+000

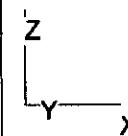
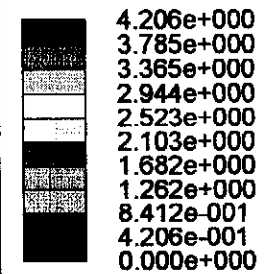


FIGURE G.4
Velocity Distribution in Expansion Nozzle ($L_{step} = 10$ mm)

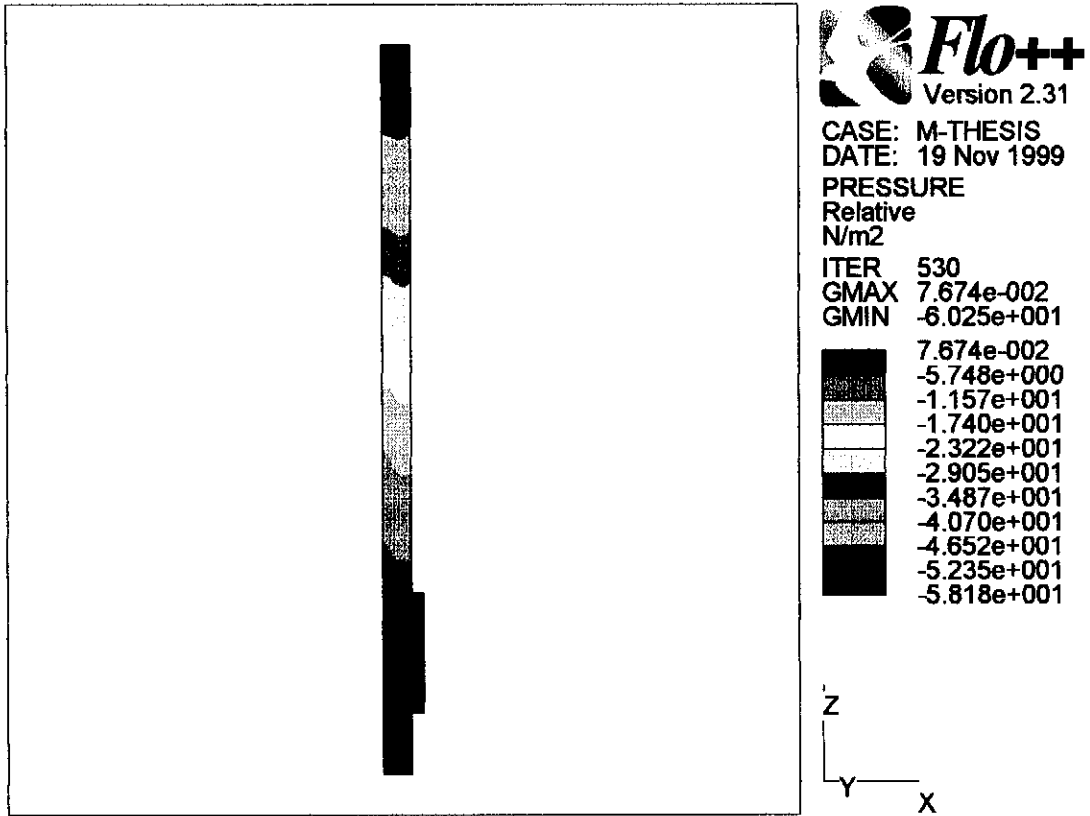


FIGURE G.5
Pressure Distribution in Expansion Nozzle ($L_{step} = 20$ mm)

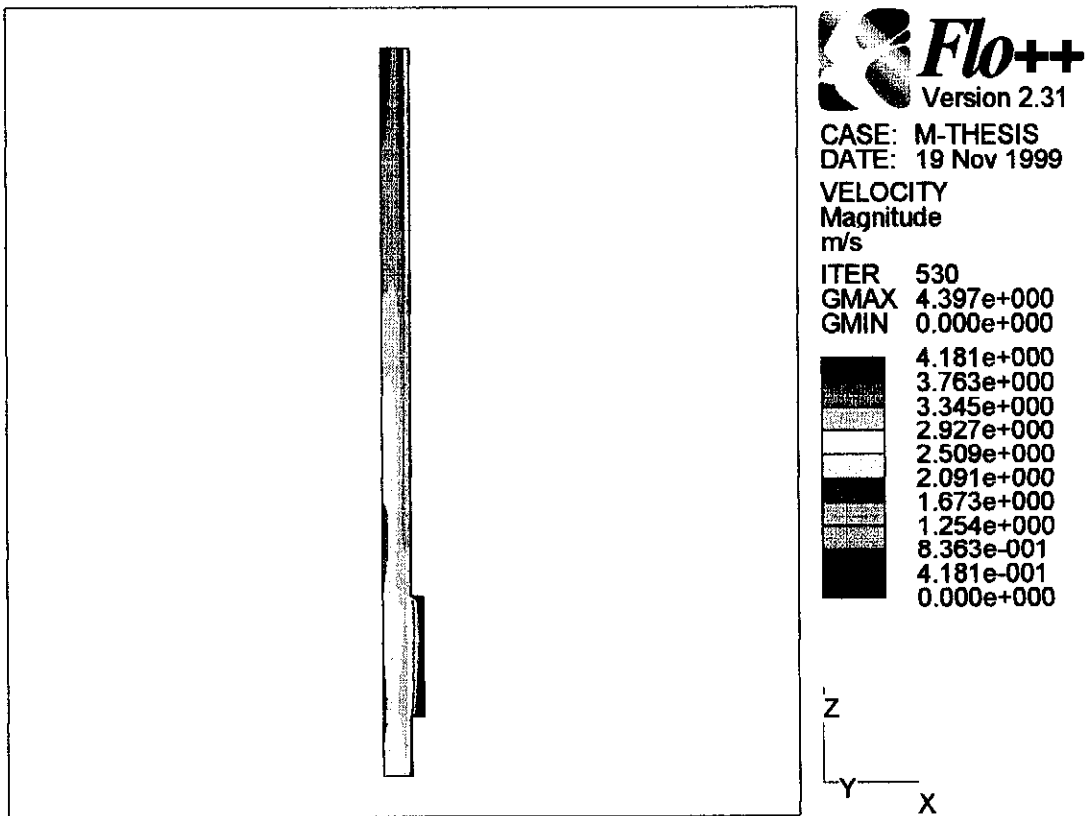


FIGURE G.6
Velocity Distribution in Expansion Nozzle ($L_{step} = 20$ mm)

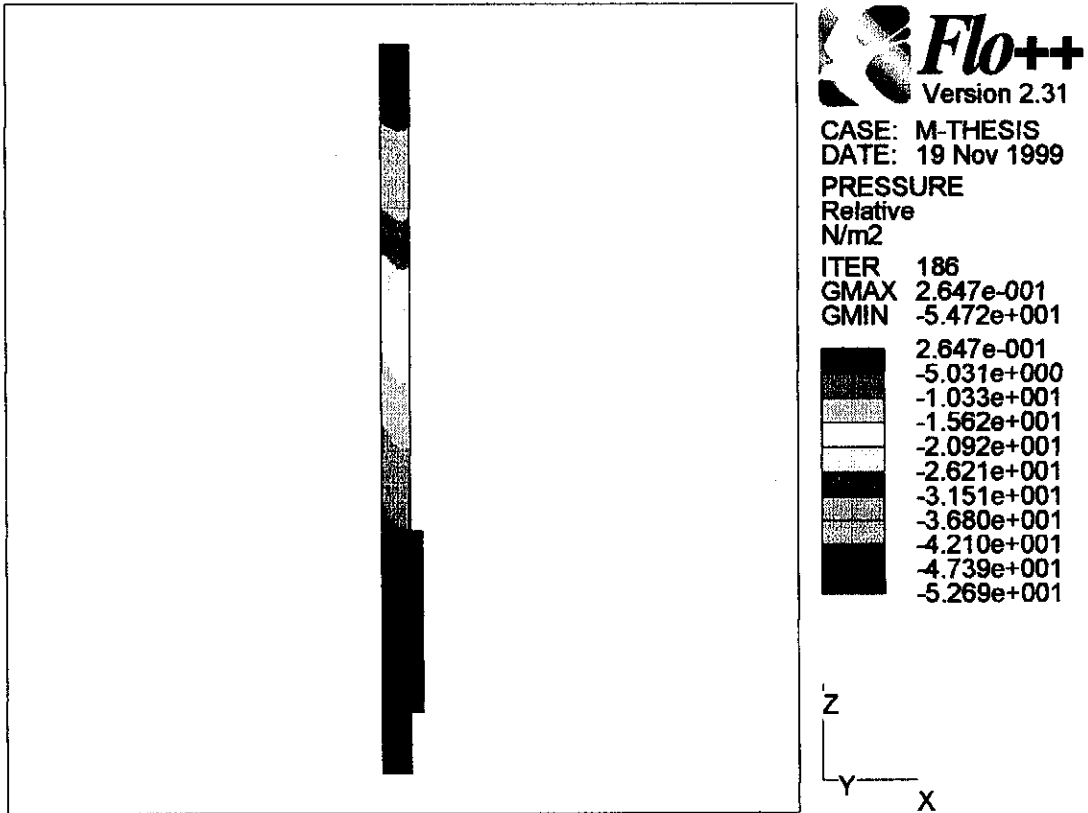


FIGURE G.7
Pressure Distribution in Expansion Nozzle ($L_{step} = 30$ mm)

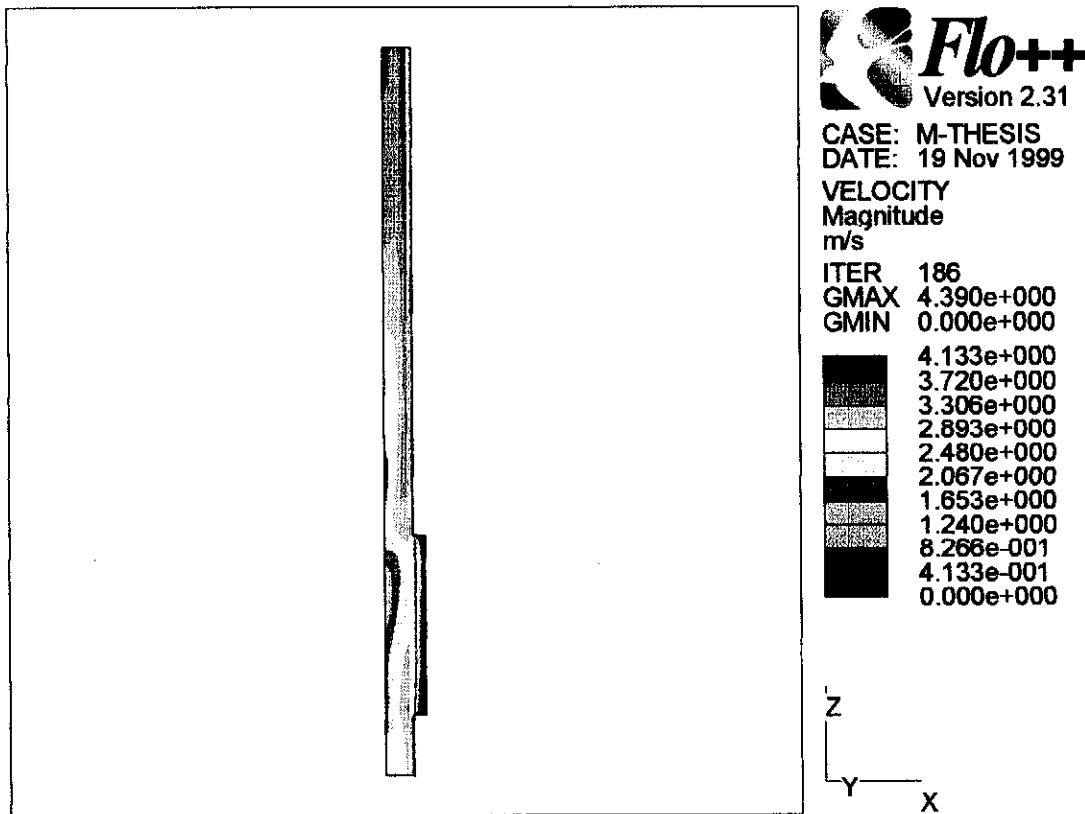


FIGURE G.8
Velocity Distribution in Expansion Nozzle ($L_{step} = 30$ mm)

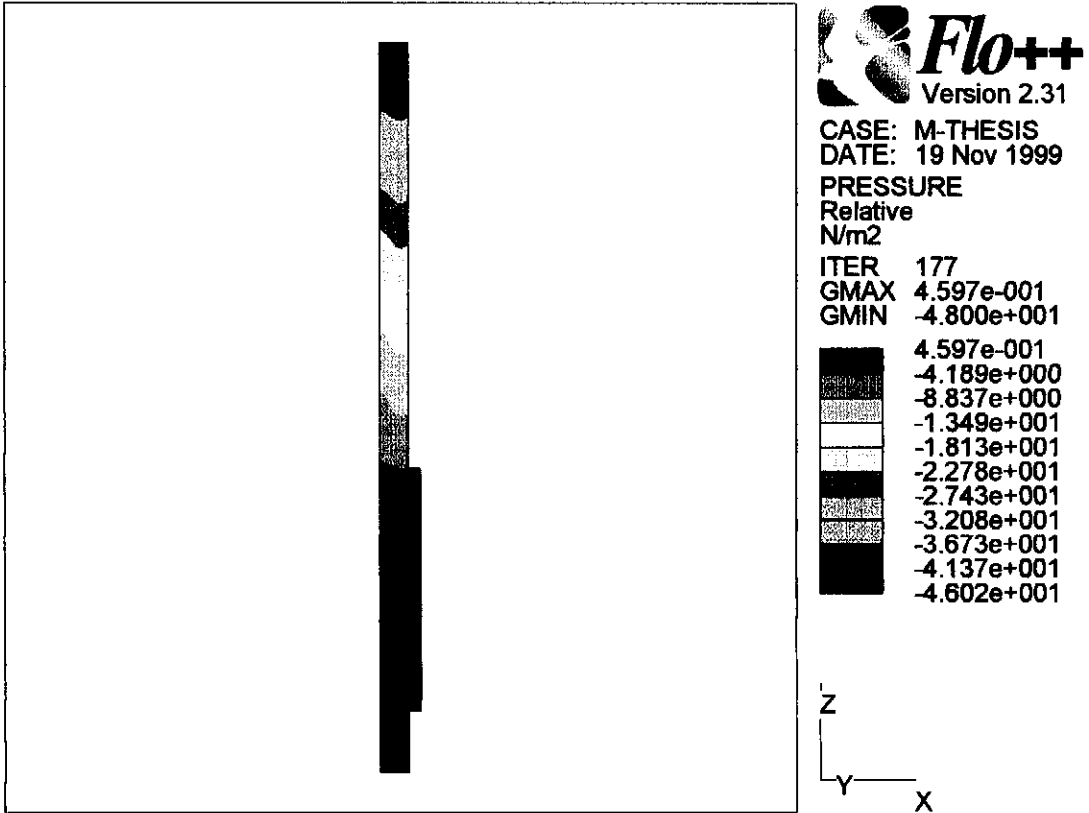


FIGURE G.9
Pressure Distribution in Expansion Nozzle ($L_{step} = 40$ mm)

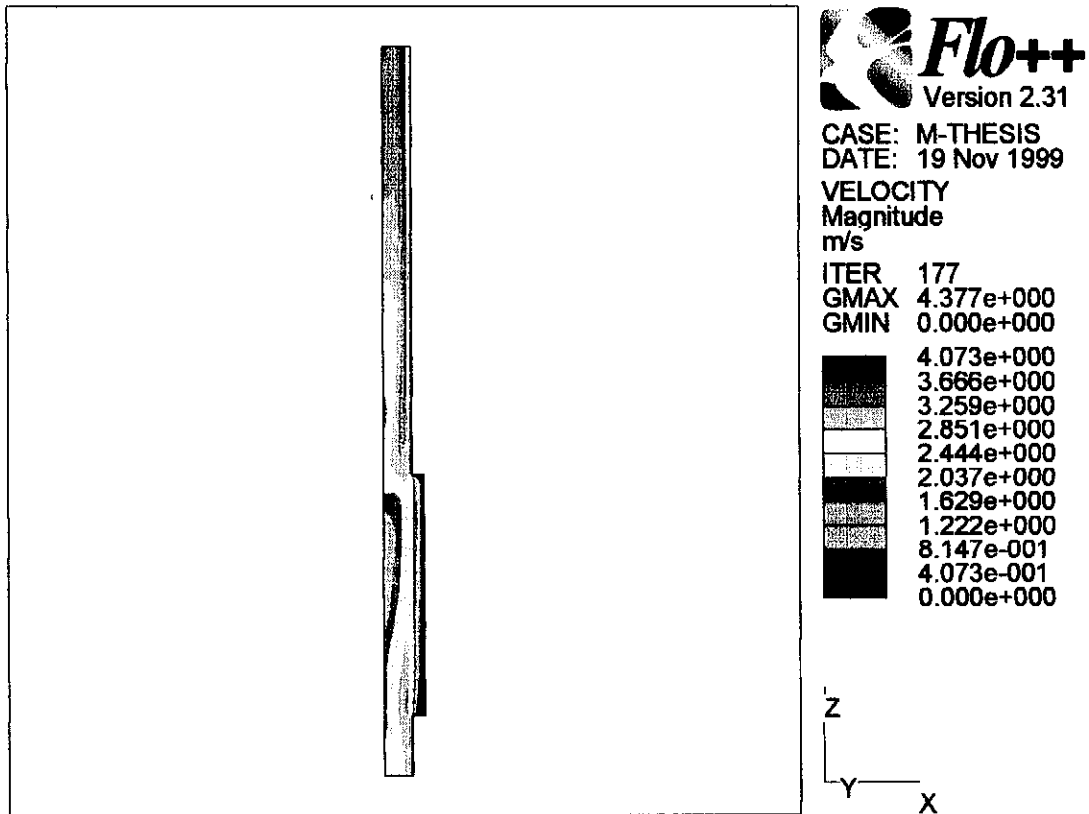


FIGURE G.10
Velocity Distribution in Expansion Nozzle ($L_{step} = 40$ mm)

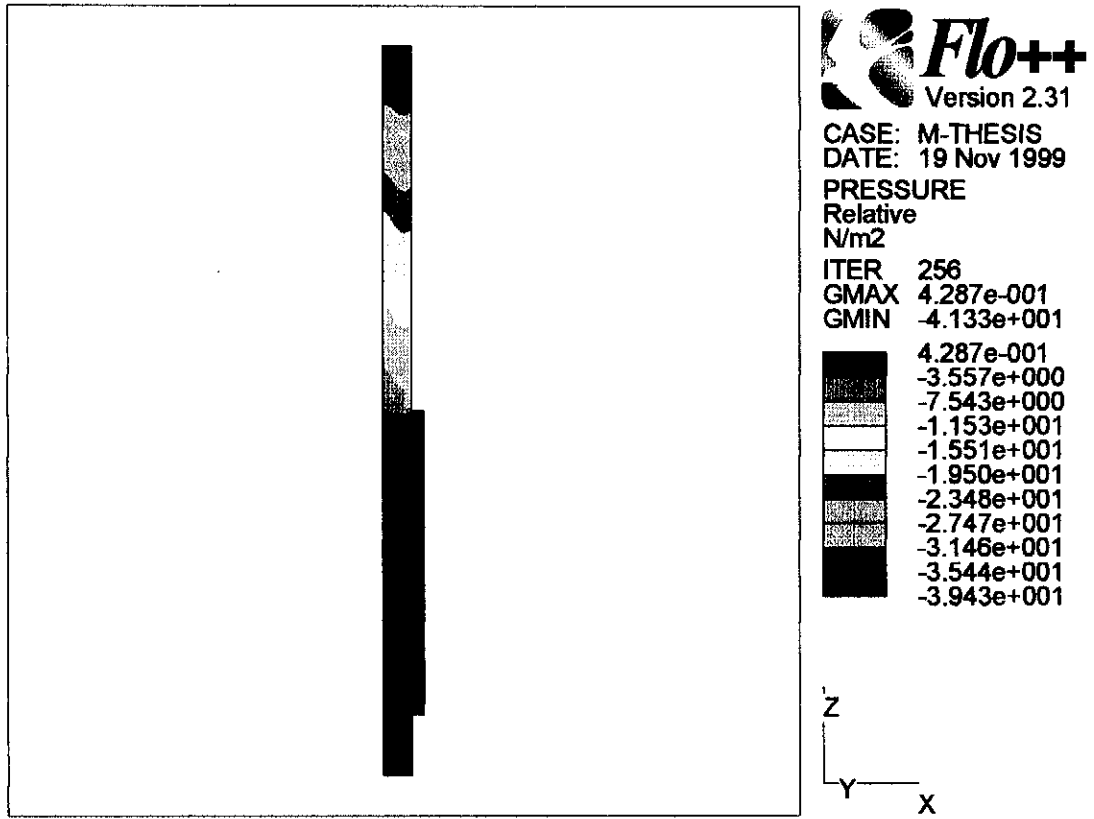


FIGURE G.11
Pressure Distribution in Expansion Nozzle ($L_{step} = 50$ mm)

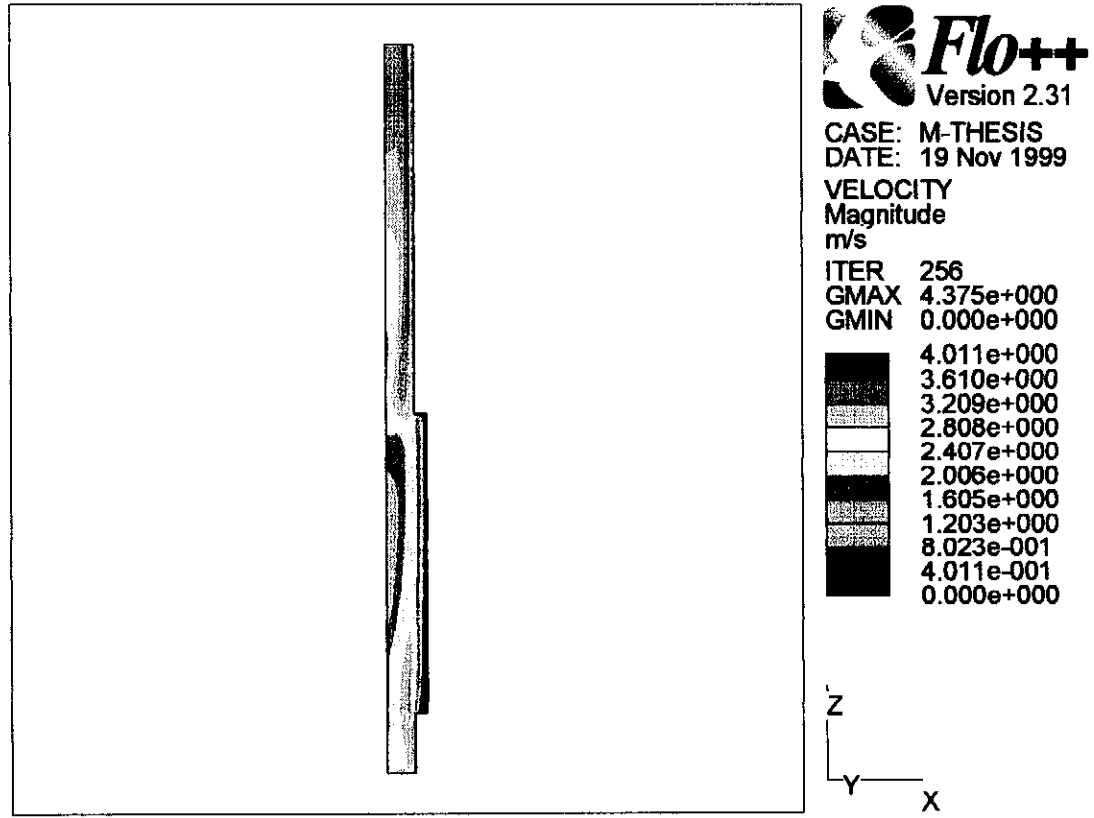


FIGURE G.12
Velocity Distribution in Expansion Nozzle ($L_{step} = 50$ mm)

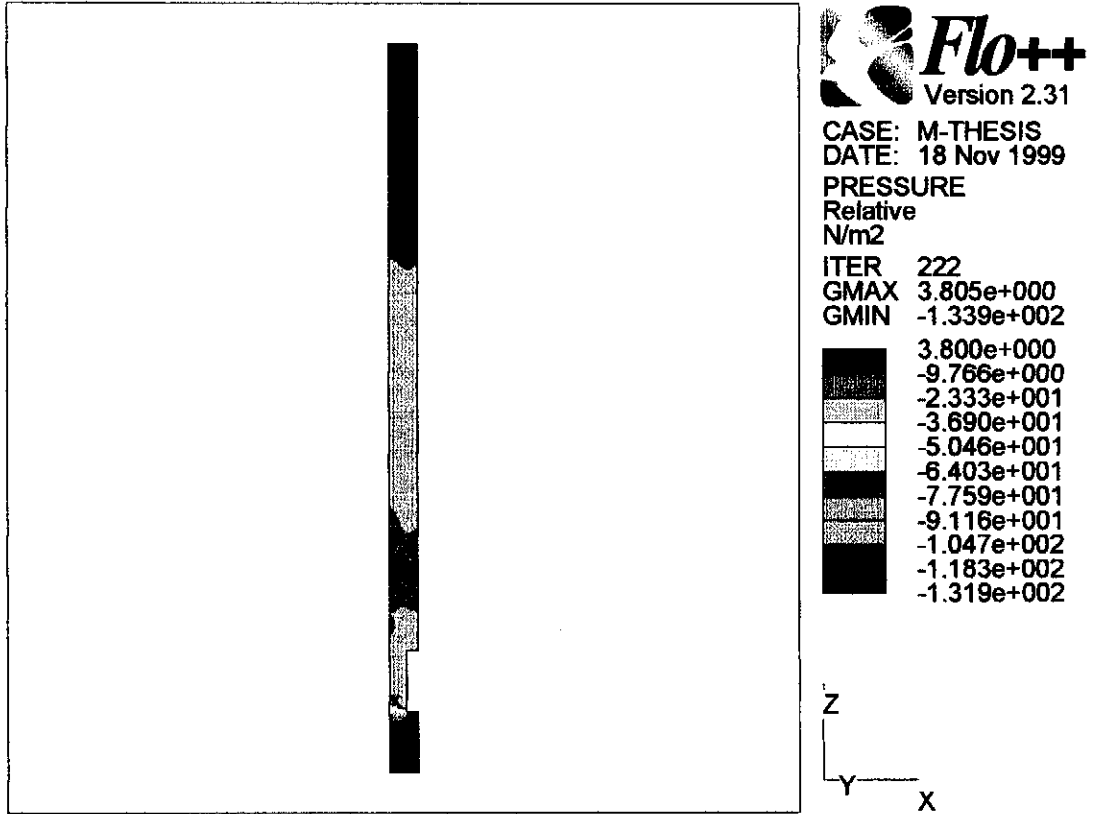


FIGURE G.13
Pressure Distribution in Contracting Nozzle ($L_{step} = 10$ mm)

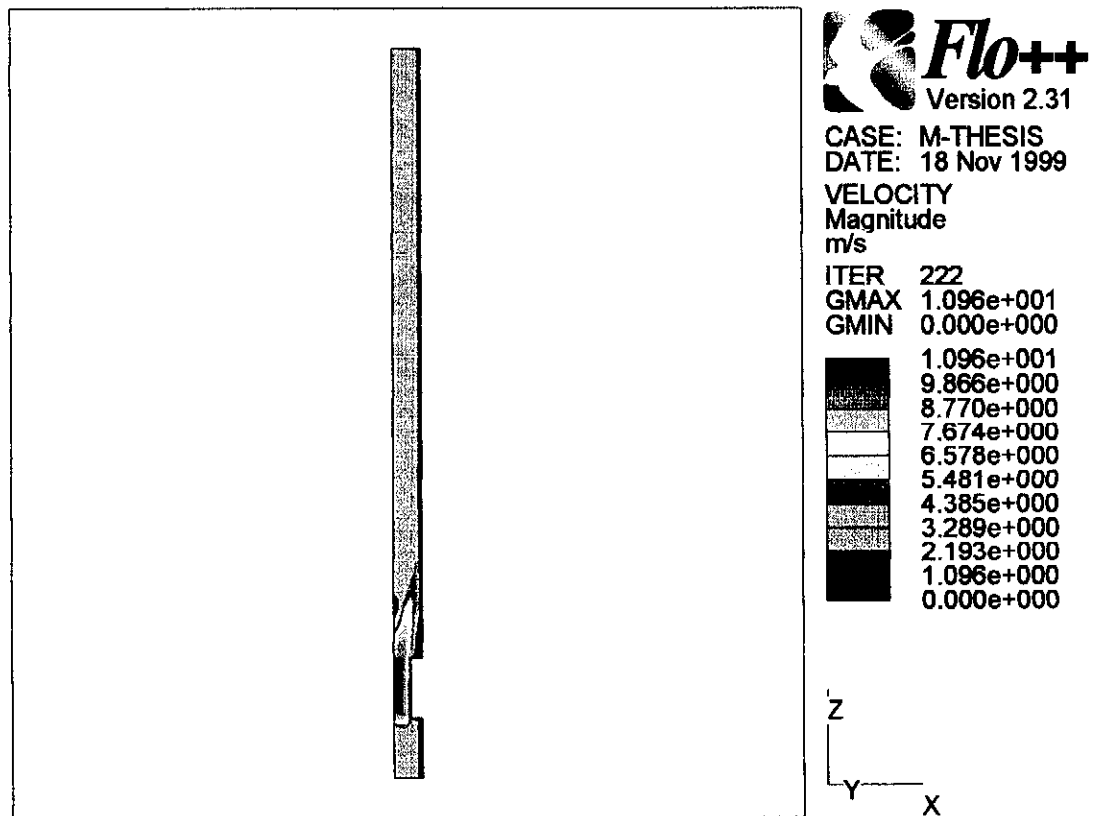


FIGURE G.14
Velocity Distribution in Contracting Nozzle ($L_{step} = 10$ mm)

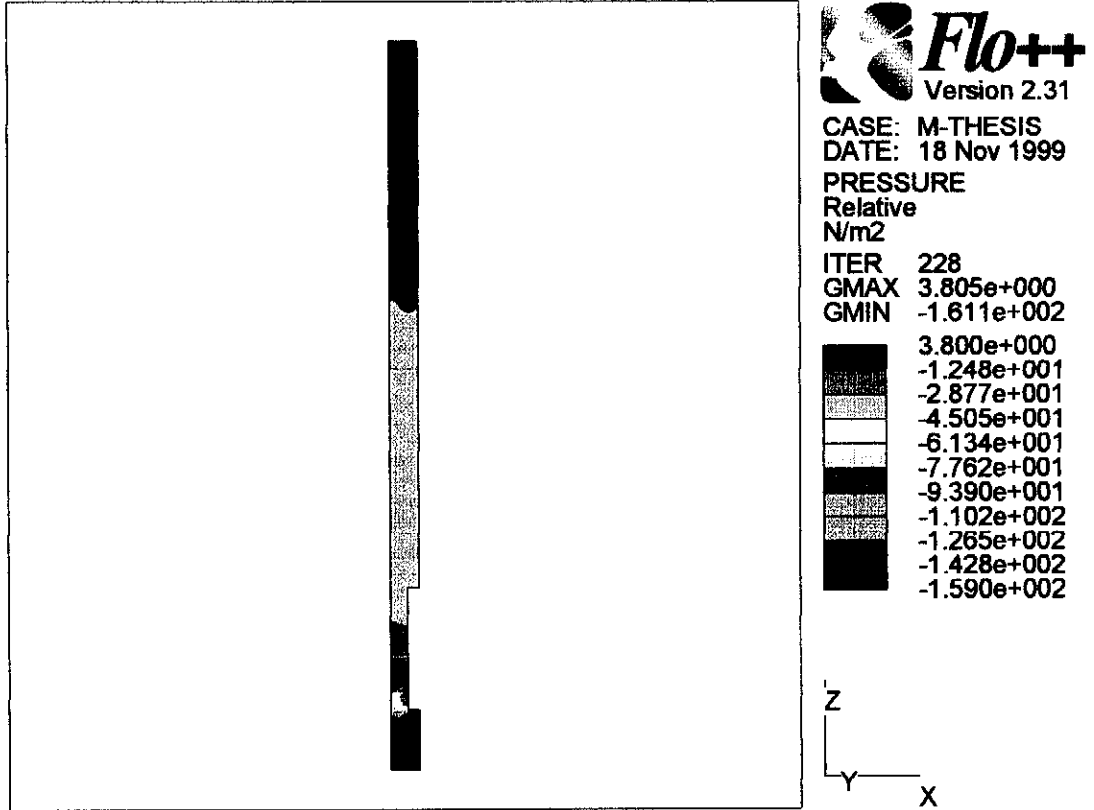


FIGURE G.15
Pressure Distribution in Contracting Nozzle ($L_{step} = 20$ mm)

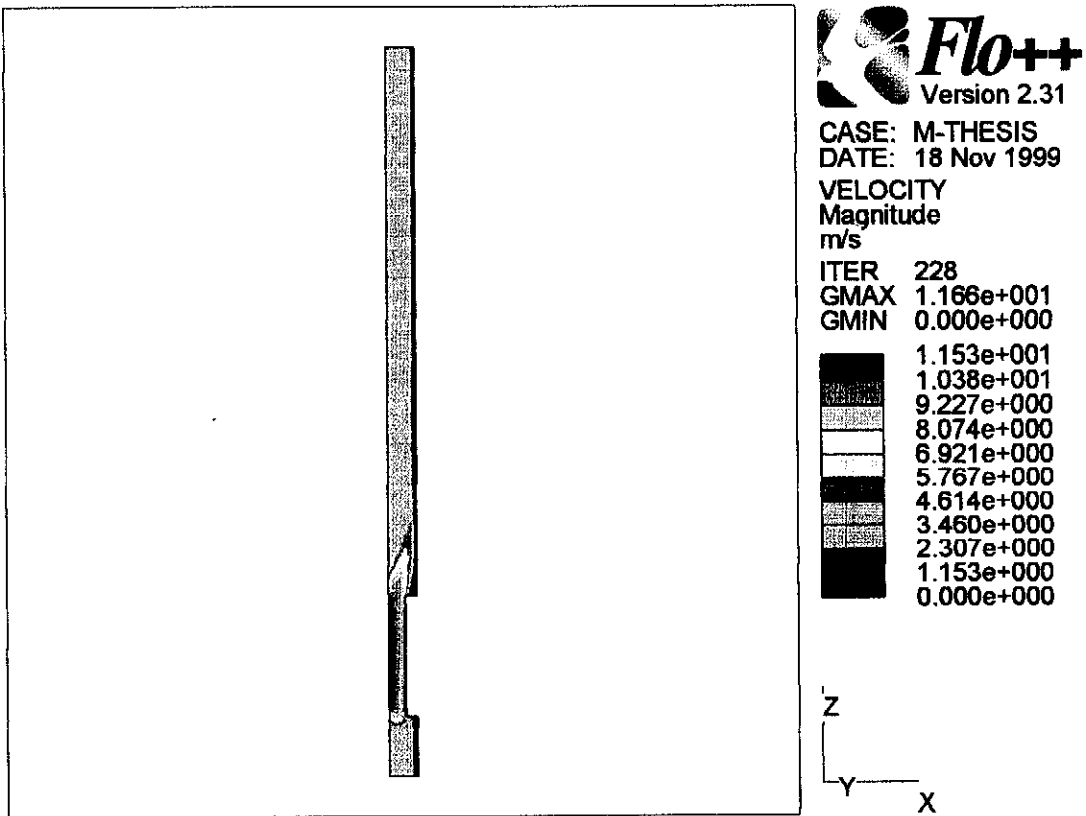


FIGURE G.16
Velocity Distribution in Contracting Nozzle ($L_{step} = 20$ mm)

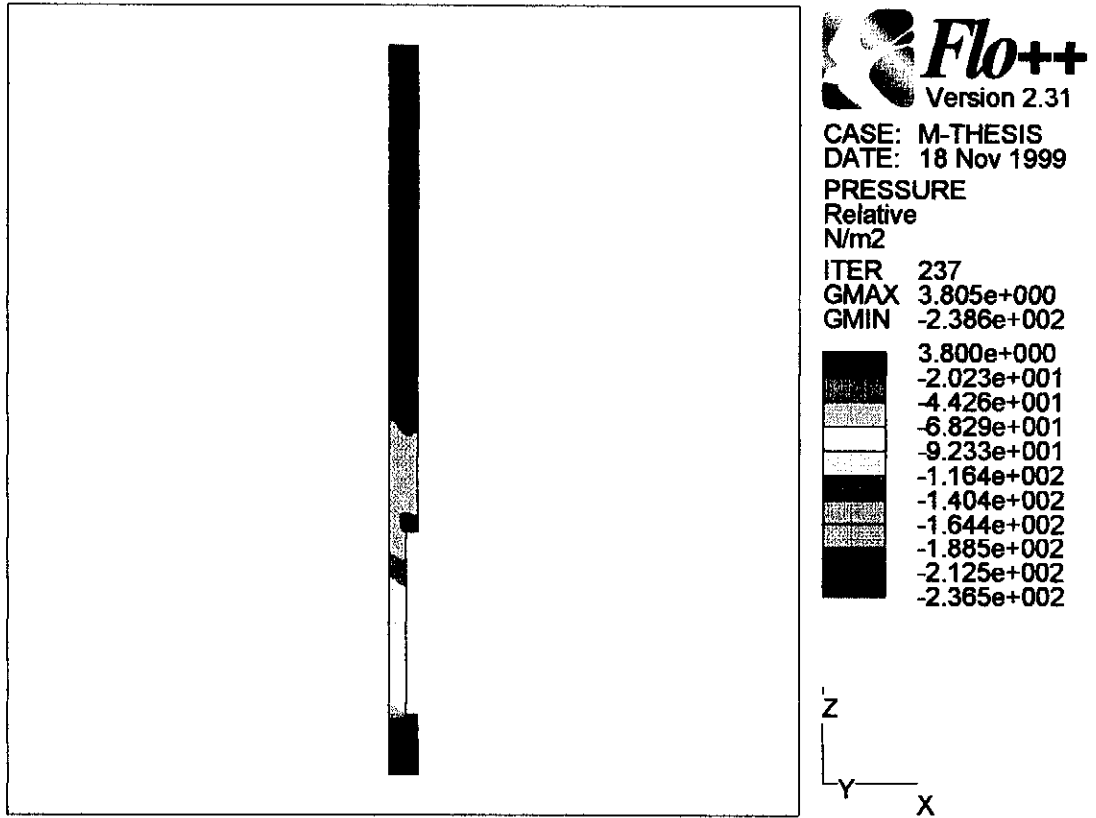


FIGURE G.17
Pressure Distribution in Contracting Nozzle ($L_{step} = 30$ mm)

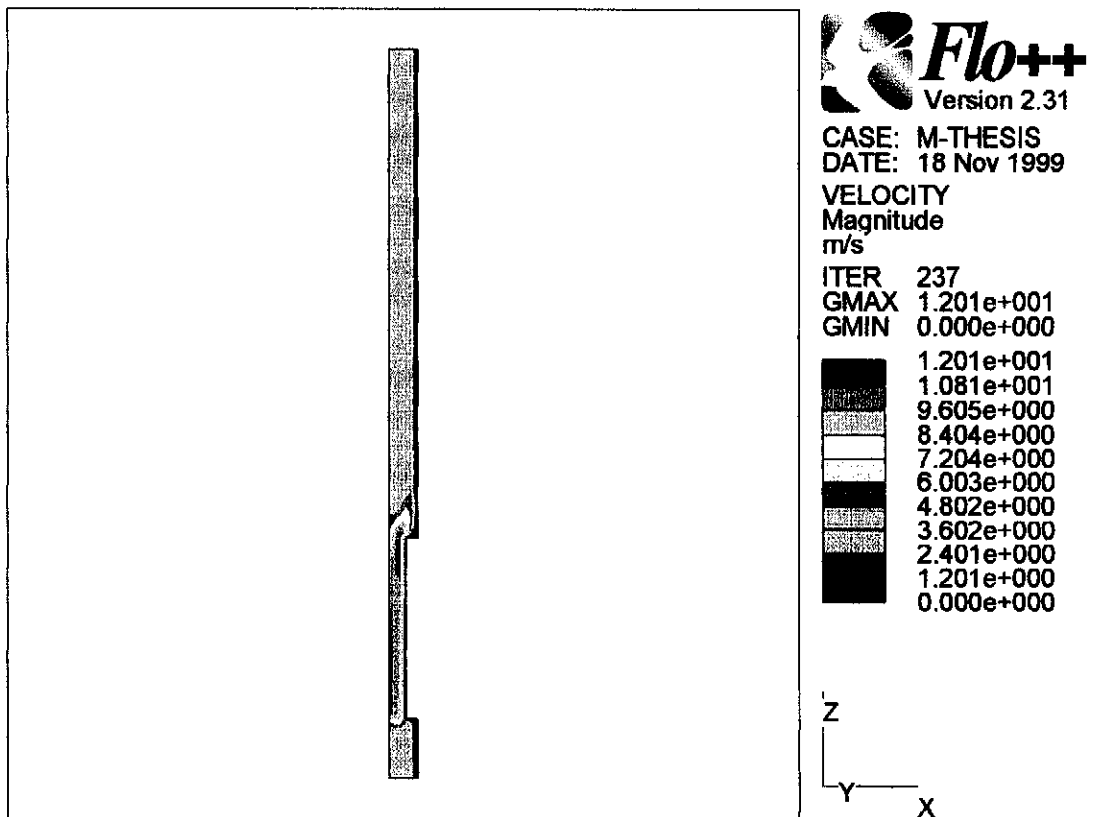


FIGURE G.18
Velocity Distribution in Contracting Nozzle ($L_{step} = 30$ mm)

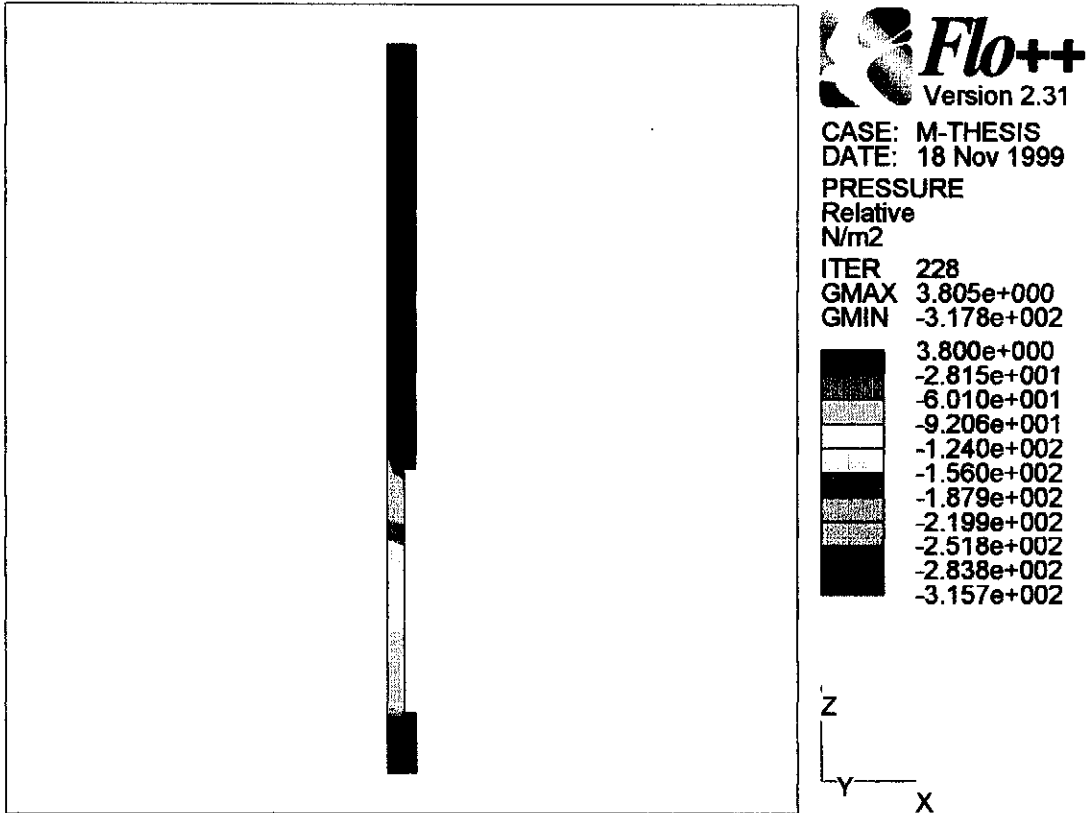


FIGURE G.19
Pressure Distribution in Contracting Nozzle ($L_{\text{step}} = 40 \text{ mm}$)

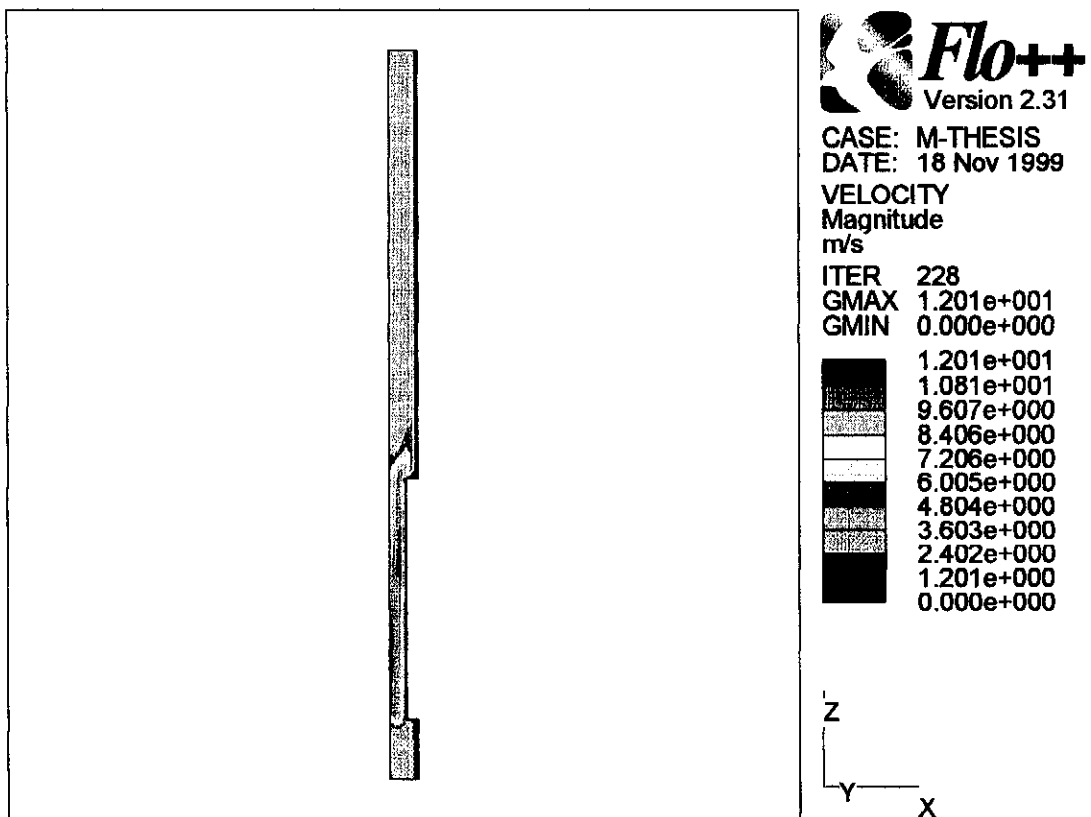


FIGURE G.20
Velocity Distribution in Contracting Nozzle ($L_{\text{step}} = 40 \text{ mm}$)

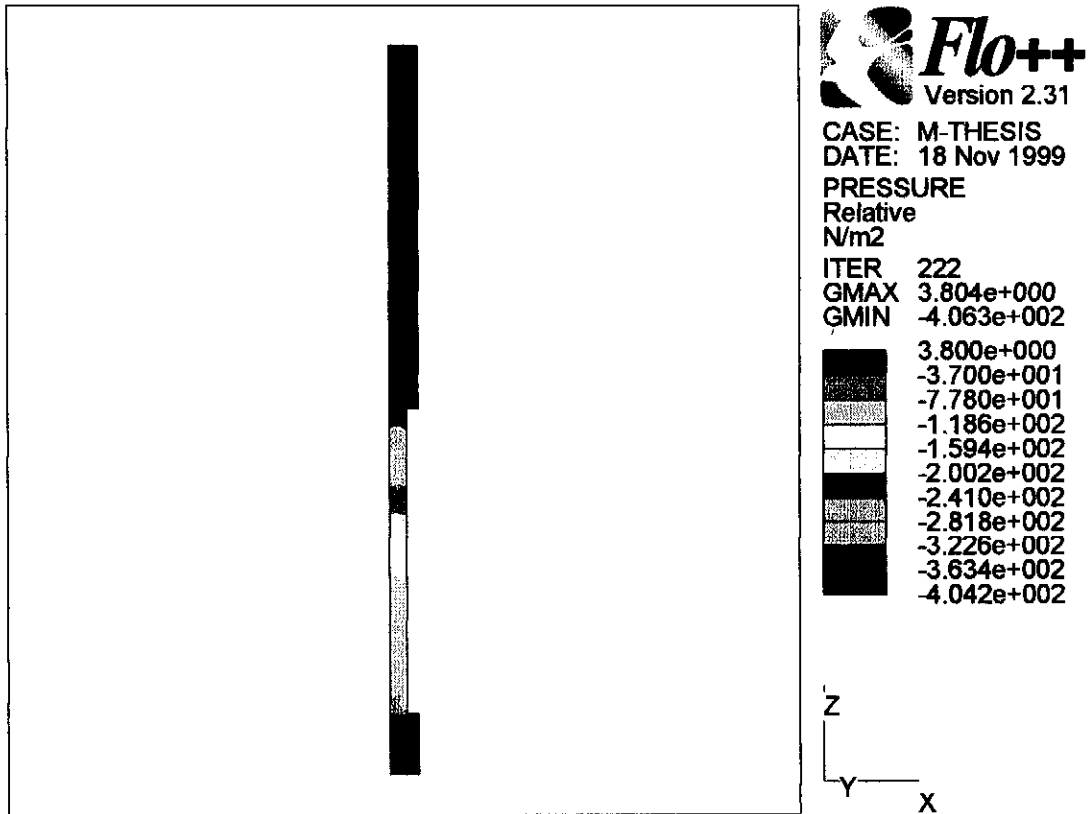


FIGURE G.21
Pressure Distribution in Contracting Nozzle ($L_{step} = 50$ mm)

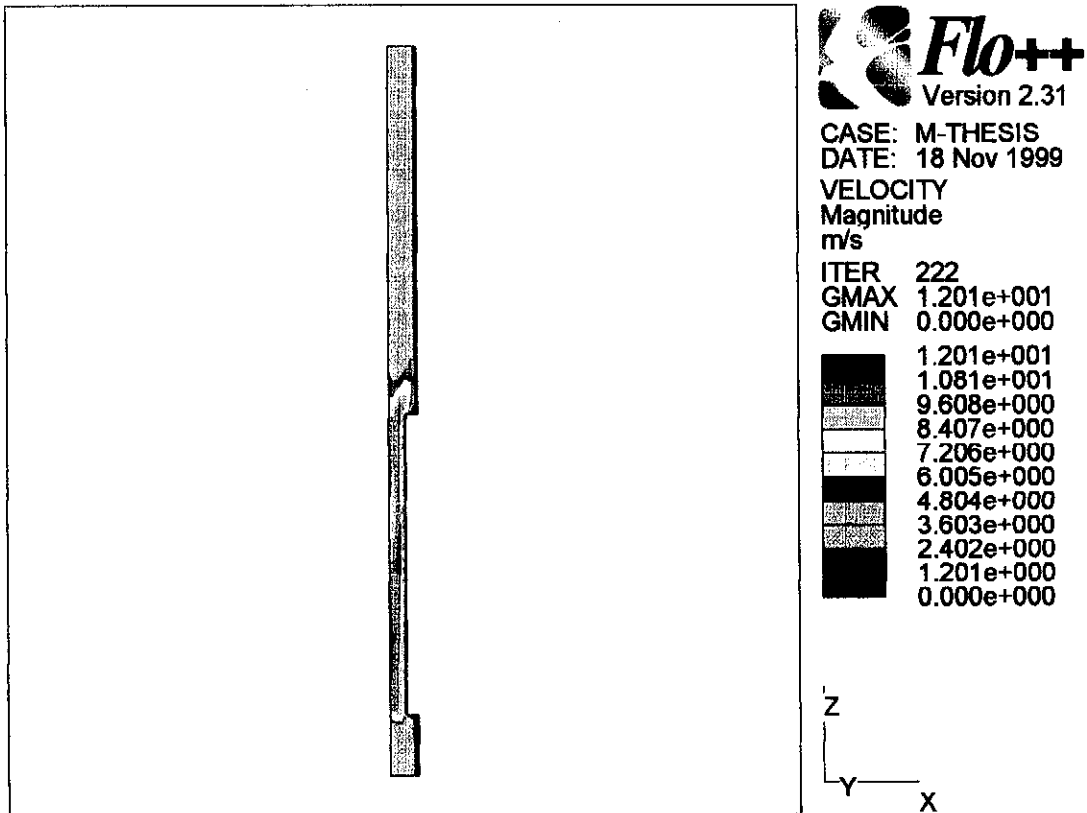


FIGURE G.22
Velocity Distribution in Contracting Nozzle ($L_{step} = 50$ mm)

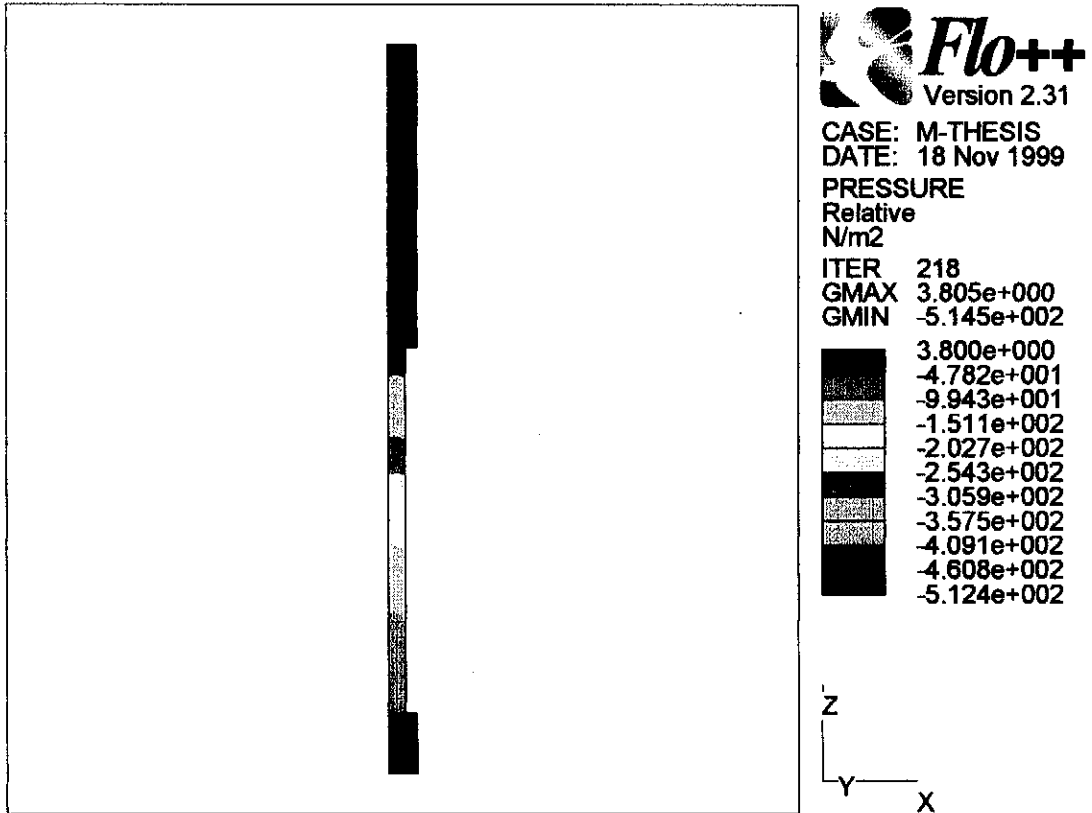


FIGURE G.23
Pressure Distribution in Contracting Nozzle ($L_{\text{step}} = 60 \text{ mm}$)

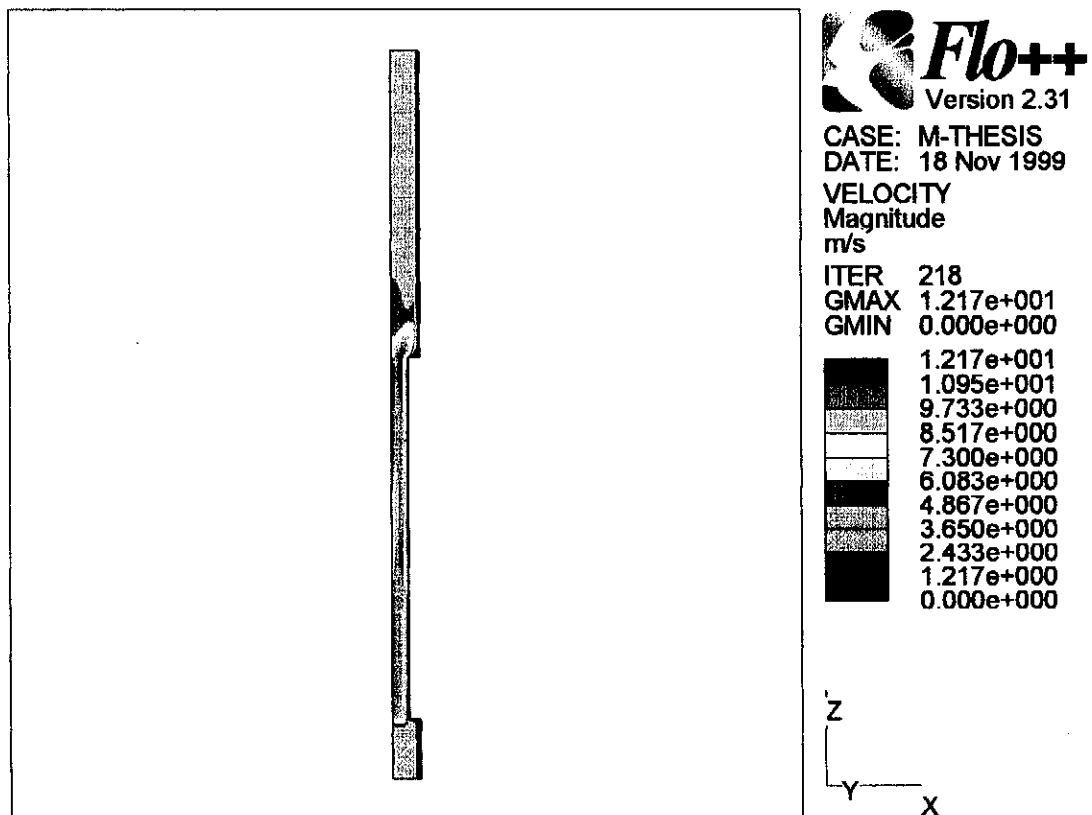


FIGURE G.24
Velocity Distribution in Contracting Nozzle ($L_{\text{step}} = 60 \text{ mm}$)

APPENDIX H

Turbo Pascal Pulse Generator

The Turbo Pascal program, which follows, was compiled to generate the different peak expiratory flow rate input envelopes for a certain impulse width from the customised Impulse envelopes

```

{$R+}
program PulsGen;

(=====Genetrating Pulse waveforms=====)
(=====June 1999=====)
Const
  FileLength = 40;
  maks = 1;(*1.571;*) {konstante om inset te normaliseer}
var
  SequenceNumber:INTEGER;
  i : integer;
  FileVar,InFile:text;
  RevMin,STEPSSEC: real;
  DECEQV:integer;
  FlowArray : Array[1..FileLength] Of real;
  data : real;
  STRI1: STRING[10];
  ofile: string[35];
  outfile:string[35];
  FlowCalFactor : integer;

Procedure OpenOutputFiles;
begin
  assign(filevar,outfile);
  rewrite(filevar);
  writeln(filevar,''+outfile);
  Writeln(FileVar,'PS');
  writeln(FileVar,'IN1A');
  writeln(FileVar,'IN2C');
  Writeln(FileVar,'LD3');
  Writeln(FileVar,'MC');
  Writeln(FileVar,'TR10');
  Writeln(FileVar,'H+');
  Writeln(FileVar,'Q1');
  close(filevar)
end;

Procedure ReadPulsFile;
begin
  {} ASSIGN(InFile,'a:\input2.prn');(*input.prn is die eerste wyer puls*)
  {$I-}Reset(InFile){$I+};
  For i:=1 to FileLength do
    BEGIN
      Read(InFile,data);
      FlowArray[i]:= data*FlowCalFactor/maks;
    END;
  Close(InFile);
end;

FUNCTION DIGIT(N:BYTE):CHAR;
BEGIN
  IF N<10
  THEN DIGIT:=CHR(ORD('0')+N)
  ELSE DIGIT:=CHR(ORD('A')+(N-10))
END;

Procedure ConvertToHex;
BEGIN
  assign(FileVar,outFile);

```

```

append(FileVar);
for i:=1 to FileLength do
  begin
    REVMIN:=(FLOWARRAY[i]*2.456);
    STEPSSEC:=(REVMIN*25000/60);
    DECEQV:=ROUND(STEPSSEC/54.93164);
    WRITELN(FILEVAR, 'RM', DIGIT(HI(DECEQV) DIV 16), DIGIT(HI(DECEQV) MOD 16)
    , (DIGIT(LO(DECEQV) DIV 16)), DIGIT(LO(DECEQV) MOD 16));
  {}      Writeln(FileVar, 'T0.008');
  end;
close(filevar);
END;

begin
  {}  Mkdir('c:\pulse2\t008');
  FlowCalFactor:=100;
  repeat
    writeln(flowcalfactor);
    str(FlowCalFactor, str1);
  {}  Ofile:='c:\pulse2\t008\puls'+str1;
    outfile:=ofile+'.prg';
    OpenOutputFiles;
    ReadPulsFile;
    ConvertToHex;
    assign(filevar, OutFile);
    append(filevar);
    writeln(FileVar, 'RM00000');
    writeln(FileVar, 'Q0');
    Writeln(FileVar, 'TR01');
    Writeln(FileVar, 'C');
    close(filevar);
    FlowCalFactor:=FlowCalfactor+5;
  until FlowCalFactor>500;
end.

```

Turbo Pascal Sampler

The Turbo Pascal program, which follows, was compiled to sample the pressure and flow rate, and subsequently determine the activation points for each input Impulse envelope tested for a specific whistle.

PROGRAM Puls2;

{Download a Pulse-sequence to the SX-8}

{05/06/1999}

USES dos, crt, async2, ASA_Drv, rtgsubs, graph, rtstdhdr, rtfft,
rtgcommo;

Const

FileLength = 93;
AantalToetse = 2;

Const

{AtoD constants start here}

BaseAdress = \$360;
PointerLength = 3000;
MaxSampleArray = 3000;
InitialSampleRate = 6000; {Hz}
ADChi = \$362; (* ADC hi bytes and Int line *)
DAC0 = \$364;
DAC1 = \$366;
PressureAtoDCalFactor = 0.004887;
BeginPosition = 2.8;

{Filter constants start here}

CutOffFreqF = 48/InitialSampleRate; {Hz}
FilterOrder = 246; {Digial Filter size. See QuinnCurtiss}
FilterWindow = 0; {Type of filter window See QuinnCurtiss}
CutOffFreqP = 800/InitialSampleRate; {Hz}

type

longArray=array[1..MaxSampleArray] of RealType;

VAR

err, cport : Integer;
HexArray : ARRAY[1..FileLength] OF STRING[14];
i,
LoopCounter : Integer;
FileVar : Text;
klaar, LoopQuit : boolean;
beginvloei,
eindVloei : integer;
Infile, stril, stri2,
Ifile : STRING[35];

{AtoD variables start here}

Dat : ADDData;
deltaT : Real;
Vector1 : pointer;
SampledArray : ARRAY[1..4, 0..PointerLength] OF Integer;
Head, Tail : integer;
adsample2,
adsample3 : Real;
OkToCapture : Boolean;
PressureFileData,
FlowFileData : ^longArray;
FileCounter : Integer;
EndOfExperiment : Boolean;
PressureData : rtvaluearraytype;

{Filtering variables start here}

FilterCoeff : ARRAY[0..FilterOrder] of REAL;
filteredFlowFileData : ^longArray;

{QC vertoon veranderlikes begin hier}

(*xAxis : array[1..MaxSampleArray] of realtype;*)

teller, MaxTeller, TenPercentTeller,

```

NinetyPercentTeller           : integer;
NinetyPercentFlow,TenPercentFlow,
MaximumFlow,DeltaFlow         : realtype;
MaxMessage,RisetimeMessage,
AantalLusseMessage           : String[10];
RiseTime                      : Real;
TenPercentFound,NinetyPercentFound : Boolean;
AantalLusse                   : Integer;
NinetyLusse,TenLusse         : Integer;
xMarker,Ymarker : array[1..3] of realType;
ofile: string[35];
outfile:string[35];
FileVarOut                    : Text;
ActFile,ActOutFile : string[35];
FileVarAct : text;
ActivationTeller : Integer;
ActivationPressure,ActivationFlow : realType;
Mean,SumMeanDiff,MaximumPressureStdev:real;
ActivationFound:Boolean;
ActivationPoint:real;

(=====)
{This is the ISR for each sample at samplerate}
Procedure GetInterruptSample;
interrupt;

begin
  inline ($FA);           ( Stop Intrr. )
  asm
    mov di,offset DAT
    mov cx,4
  @2:
    mov dx,BaseAddress
    in al,dx              {Read low byte}
    mov bl,al
    mov dx,BaseAddress+2
    in al,dx              {Read high byte}
    and al,0FH
    mov bh,al
    and al,08H
    jz @3
    sub bx,1000H
  @3:
    mov [di],bx          {Store channel A/D data}
    inc di
    inc di
    loop @2
  end;
  SampledArray[1,Head] := Dat[0];
  SampledArray[2,Head] := Dat[1];
  SampledArray[3,Head] := Dat[2];
  SampledArray[4,Head] := Dat[3];
  inc(Head,1);
  IF (Head>MaxSampleArray) then Head := 0;
  port [$20] := $20;      { Herstell 8259 }
  inline ($FB);
end;{GetInterruptSample}
(=====)

{Set up the AtoD board}

```



```

Procedure SetUpASABoard(InterruptAddress:Pointer; InterruptRate:integer);
{Load all interrupts and timers for ASA board}

```

```

Begin
  ASA_TimerControl(BaseAddress,$34);           {Mode 2}
  ASA_WriteTimerCounter(BaseAddress,0,round(250000/InterruptRate));
      {Initial value @250kHz clock = 4Mhz/16}
  {ASA timer setup as follows.....
    4MHz osc / 16 = CLKSEL2 (250kHz)
    JMPR P5 - Out0,3 to U10,5 !CONVST
              - CLKSEL2,6 to CLK0,1
  }
  getintvec(13, Vector1);           {Old pointer for IRQ5 }
  setintvec(13, InterruptAddress);   {IRQ5 --> ISR of GetInterruptSample}
end;{SetUpASABoard}

```

```

{=====}
{Starts the interrupt process ISR at IRQ5 }
Procedure Init_Interrupt;

```

```

begin
  port [$21] := port [$21] and $DF;   { Stel 8259 vir IRQ5 }
  port [$20] := $20;                 { Herstel 8259 }
  inline ($FB);                       { Steun ondr. }
end;{Init_Interrupt}

```

```

{=====}
{ Stops the interrupt process ISR at IRQ5 }
Procedure Stop_Interrupt;

```

```

begin
  port [$20] := $20;                 { Herstel 8259 }
  inline ($FA);                       { Stuit ondr. }
end;{top_Interrupt}

```

```

{=====}
{Collecting samples at the specified sampling rate}
Procedure ServiceTheSample;

```

```

begin
IF Head<>Tail then {Check cyclic buffer counters}
  begin
    adsample2 :=(SampledArray[2,tail])*PressureAtoDCalFactor;
    adsample3 :=(SampledArray[3,tail])*PressureAtoDCalFactor;
    If OkToCapture = True then
      begin
        PressureFileData^[FileCounter]:=adsample2;{Volt}
        FlowFileData^[FileCounter]:=adsample3;   {Volt}
        Inc(FileCounter);
      end;
    inc(Tail,1);
    IF (Tail>MaxSampleArray) then Tail:=0;
    IF (FileCounter>MaxSampleArray) then EndOfExperiment:=true;
    IF (FileCounter>MaxSampleArray) then FileCounter:=1;
  end;
end;{ServiceTheSample}

```

```

{=====}
{DtoA: Outputs the Analogue voltage }
Procedure SNA(K,S : integer); {K->kanaal nommer, S->getal}

```

```

begin
  {K=0 ->start}
  {K=1 ->stop}
  if S > 511 then S := 511;

```

```

( if S < -512 then S := -512;)
  if S < 0 then S := 0;
  S := (S + 512) shl 6;
  if K = 0 then begin
    port[DAC0+1] := hi(S);
    port[DAC0] := lo(S);
  end
  else begin
    port[DAC1+1] := hi(S);
    port[DAC1] := lo(S);
  end;
end; {SNA}
{=====}
Procedure FindTheStart;
var
  CurrentPosition : real;
  Som : real;
begin
  CurrentPosition:=0;
  Writeln('Bepaal die huidige posisie...');
  OkToCapture := True;
  EndOfExperiment:=False;
  tail:=head-1;
  FileCounter:=1;
  Som:=0;
  repeat
    ServiceTheSample;
  until EndOfExperiment;
  OkToCapture := False;
  FOR i:=1 to MaxSampleArray do
    begin
      Som:=Som+FlowFileData^[i];
    end;
  CurrentPosition:=Som/MaxSampleArray;
  Writeln('Die huidige posisie is ',CurrentPosition:3:1);
  If CurrentPosition > BeginPosition then
    begin
      Writeln('Beweeg vorentoe...');
      writelnCom(CPORT, 'PS',ERR);
      writelnCom(CPORT, 'IN1A',ERR);
      writelnCom(CPORT, 'IN2C',ERR);
      writelnCom(CPORT, 'LD3',ERR);
      writelnCom(CPORT, 'MC',ERR);
      writelnCom(CPORT, 'TR10',ERR);
      writelnCom(CPORT, 'H+',ERR);
      writelnCom(CPORT, 'Q1',ERR);
      writelnCom(CPORT, 'RM0100',ERR);
      writelnCom(CPORT, 'T20',ERR);
      writelnCom(CPORT, 'Q0',ERR);
      writelnCom(CPORT, 'TR01',ERR);
      writelnCom(CPORT, 'C',ERR);
    end;
  If CurrentPosition < BeginPosition then
    begin
      Writeln('Beweeg terug...');
      writelnCom(CPORT, 'PS',ERR);
      writelnCom(CPORT, 'IN1A',ERR);
      writelnCom(CPORT, 'IN2C',ERR);
      writelnCom(CPORT, 'LD3',ERR);
      writelnCom(CPORT, 'MC',ERR);
      writelnCom(CPORT, 'TR10',ERR);
    end;
end;

```

```

        writelnCom(CPORT, 'H-', ERR);
        writelnCom(CPORT, 'Q1', ERR);
        writelnCom(CPORT, 'RM0100', ERR);
        writelnCom(CPORT, 'T20', ERR);
        writelnCom(CPORT, 'Q0', ERR);
        writelnCom(CPORT, 'TR01', ERR);
        writelnCom(CPORT, 'C', ERR);
    end;
{Pulse the START switch}
    SNA(0,256);
    delay(100);
    SNA(0,0);
    OkToCapture := True;
    EndOfExperiment:=False;
    tail:=head-1;
    FileCounter:=1;
    repeat
        ServiceTheSample;
    until (adsample3>BeginPosition-0.1) and
           (adsample3<BeginPosition+0.1);
    OkToCapture := False;
{Pulse the STOP switch}
    SNA(1,256);
    delay(100);
    SNA(1,0);
{Maak die buffers skoon}
    FOR i:=1 to MaxSampleArray do PressureFileData^[i]:=0;
    FOR i:=1 to MaxSampleArray do FlowFileData^[i]:=0;
    FOR i:=1 to MaxSampleArray do FilteredFlowFileData^[i]:=0;
end;

{-----}
PROCEDURE ReadAtsFile;
BEGIN
    Writeln('Busy reading the file...');
    assign(filevar,infile);
    reset(filevar);
    FOR i:=1 TO FileLength do readLN(filevar,HEXARRAY[i]);
    close(filevar);
END;
{-----}
Procedure StelCommPoortOp;
    begin
        cport := 0; {0->comm1, 1->comm2}
        opencom(CPORT,9600,'N',1,8,err);
        SETHARDHANDSHAKE(CPORT,0);
    end;
{=====}
Procedure MoveThePistonBack;
begin
    writeln('Moving piston back to START');
    writelnCom(CPORT, 'PS', ERR);
    writelnCom(CPORT, 'IN1A', ERR);
    writelnCom(CPORT, 'IN2C', ERR);
    writelnCom(CPORT, 'LD3', ERR);
    writelnCom(CPORT, 'MC', ERR);
    writelnCom(CPORT, 'TR10', ERR);
    writelnCom(CPORT, 'H-', ERR);
    writelnCom(CPORT, 'Q1', ERR);
    writelnCom(CPORT, 'RM0100', ERR);
    writelnCom(CPORT, 'T20', ERR);

```

```

writelnCom(CPORT, 'Q0', ERR);
writelnCom(CPORT, 'TR01', ERR);
writelnCom(CPORT, 'C', ERR);
{Pulse the START switch}
  SNA(0,256);
  delay(100);
  SNA(0,0);
  OkToCapture := True;
  EndOfExperiment:=False;
  tail:=head-1;
  FileCounter:=1;
  repeat
    ServiceTheSample;
  until (adsample3>BeginPosition-0.1) and
        (adsample3<BeginPosition+0.1);
  OkToCapture := False;
{Pulse the STOP switch}
  SNA(1,256);
  delay(100);
  SNA(1,0);

{Maak die buffers skoon}
  FOR i:=1 to MaxSampleArray do PressureFileData^[i]:=0;
  FOR i:=1 to MaxSampleArray do FlowFileData^[i]:=0;
  FOR i:=1 to MaxSampleArray do FilteredFlowFileData^[i]:=0;
end;
{-----}

Procedure GetFilterData(CutOffFreq:real);

VAR
  filtcoef : realpntr;

begin
  getmem(Filtcoef, sizeof(realtype)*FilterOrder);
  RTFirFreqSample(Filtcoef, CutOffFreq, FilterOrder, 0, 0, FilterWindow);
  FOR i := 0 to FilterOrder-1 DO  FilterCoeff[i] := getpntreal(Filtcoef, i);
  freemem(Filtcoef, sizeof(realtype)*FilterOrder);
end;
{-----}
Procedure DoThePressureFiltering;      {All the filtering is done here}
VAR n,m : integer;
begin
{filter die druk}
  for n:=0 to MaxSampleArray do filteredFlowFileData^[n] := 0;
  For n:= (FilterOrder-1) to MaxSampleArray do
    begin
      for m:=0 to (FilterOrder-1) do
        begin

filteredFlowFileData^[n]:=filteredFlowFileData^[n]+(FilterCoeff[m]*PressureFileD
ata^[n-m]);
          {digital filter formulae}
        end;
      end;
          {end of filtering section}
    for n:=0 to MaxSampleArray do PressureFileData^[n]:=filteredFlowFileData^[n];
  end;
{-----}
Procedure DoTheFlowFiltering;      {All the filtering is done here}
VAR n,m : integer;
begin

```

```

(filter die vloei)
for n:=0 to MaxSampleArray do filteredFlowFileData^[n] := 0;
For n:= (FilterOrder-1) to MaxSampleArray do
  begin
    for m:=0 to (FilterOrder-1) do
      begin

filteredFlowFileData^[n]:=filteredFlowFileData^[n]+(FilterCoeff[m]*FlowFileData^
[n-m]); {digital filter formulae}
      end;
    end; {end of filtering section}
    for n:=0 to MaxSampleArray do FlowFileData^[n]:=filteredFlowFileData^[n];
end;

{-----}
PROCEDURE WriteFiles;

BEGIN
  str(LoopCounter,stri2);
  Ofile:='c:\mav\C8500'+stri2;
  OutFile:=Ofile+'.txt';
  assign(FileVarOut,OutFile);
  Writeln('Saving to ',Outfile);
  Rewrite(FileVarOut);
  Writeln(fileVarOut,'Pressure',',',',','Flow');
  FOR i:=1 to MaxSampleArray do
writeln(FileVarOut,PressureFileData^[i]:3:3,',',',',FlowFileData^[i]:3:3);

  Close(FileVarOut);
END;
{-----}
PROCEDURE OpenTheActivationFile;

BEGIN
  ActFile:='c:\mav\dummy';
  ActOutFile:=ActFile+'.txt';
  assign(FileVarAct,ActOutFile);
  Rewrite(FileVarAct);
  Writeln(FileVarAct,'Teller',',',',','Pressure',',',',','Flow',',',',','MaxFlow');
  Close(FileVarAct);
END;
{-----}

PROCEDURE WriteTheActivationFile;

BEGIN
  ActFile:='c:\mav\dummy';
  ActOutFile:=ActFile+'.txt';
  assign(FileVarAct,ActOutFile);
  Writeln('Saving to ',ActOutfile);
  Append(FileVarAct);

Writeln(FileVarAct,ActivationTeller,',',',',ActivationPressure:3:3,',',',',ActivationFlo
w:3:3
  ',',',',MaximumFlow:3:2);
  Close(FileVarAct);
END;
{-----}

Procedure DetermineTheActivationPoint;

```

```

begin

{CalculateTheStandardDeviation}
for teller:=1 to MaxSampleArray do filteredFlowFileData^[teller]:=0;
ActivationPressure:=0;
ActivationFlow:=0;
ActivationTeller:=0;
For teller:= 1 to (MaxSampleArray-5) do
begin
mean:=(PressureFileData^[teller]+
        PressureFileData^[teller+1]+
        PressureFileData^[teller+2]+
        PressureFileData^[teller+3]+
        PressureFileData^[teller+4])/5;
SumMeanDiff:=
(PressureFileData^[teller]-mean)*(PressureFileData^[teller]-mean)+
(PressureFileData^[teller+1]-mean)*(PressureFileData^[teller+1]-mean)+
(PressureFileData^[teller+2]-mean)*(PressureFileData^[teller+2]-mean)+
(PressureFileData^[teller+3]-mean)*(PressureFileData^[teller+3]-mean)+
(PressureFileData^[teller+4]-mean)*(PressureFileData^[teller+4]-mean);
filteredFlowFileData^[teller]:=sqrt((SumMeanDiff/5));
end;

{FindTheMaximumValue}
MaximumPressureStdev:=0;
MaxTeller:=0;
For teller := 1 to MaxSampleArray do
begin
if PressureFileData^[teller] >= MaximumPressureStdev
Then
Begin
MaximumPressureStdev:=PressureFileData^[teller];
MaxTeller:=teller;
end;
end;

{FindTheActivationPoint}
ActivationFound := false;
ActivationPoint:=0.05;
For teller:=MaxTeller DownTo 1 do
Begin
If FilteredFlowFileData^[teller] <= 0.05
then
If ActivationFound = false
Then
begin
ActivationTeller:=teller;
ActivationFound:=True;
end;
end;

ActivationPressure:=PressureFileData^[ActivationTeller];
ActivationFlow:=
(FlowFileData^[ActivationTeller+1]+
FlowFileData^[ActivationTeller+2]+
FlowFileData^[ActivationTeller+3]+
FlowFileData^[ActivationTeller+4]+
FlowFileData^[ActivationTeller+5]+
FlowFileData^[ActivationTeller-1]+
FlowFileData^[ActivationTeller-2]+
FlowFileData^[ActivationTeller-3]+

```

```

    FlowFileData^[ActivationTeller-4]+
    FlowFileData^[ActivationTeller-5])/10;
WriteTheActivationFile;
end;
(-----)
(*Procedure DisplayVolumeAndFlow;

begin
{Flow = rtstat[1]}
  rtsetwindowoptions(rtstat[1],rt_resize or rt_maximize or rt_hide or rt_iconize
  or rt_savewinimage or rt_3dborder or rt_3dinner);
  rtsetpercentwindow(rtstat[1], 0.01, 0.1, 0.99, 0.5);
  rtsetwin2plotratio(rtstat[1], 0.15,0.15,0.15,0.15);
  rtsetViewBackground(rtstat[1],7);
  rtscalePlotArea(rtstat[1],0,0,MaxSampleArray,700);
  rtsetxyintercepts(rtstat[1], 0.0, 0.0);
  setcolor(5);
  rtdrawyaxis(rtstat[1], 10, 0);
  rtlabelyaxis(rtstat[1],5, 0, 0);
  rtdrawxaxis(rtstat[1],100,0);
  rtlabelxaxis( rtstat[1],1, 0,0);
  For i:= 1 to MaxSampleArray do xAxis[i]:=i;{*deltaT;}
*)

(*  rtLinePlotData(rtstat[1],@xaxis,@FlowFileData,MaxSampleArray,0,0);
  xMarker[1]:=MaxTeller;yMarker[1]:=MaximumFlow;
  xMarker[2]:=TenPercentTeller;yMarker[2]:=TenPercentFlow;
  xMarker[3]:=NinetyPercentTeller;yMarker[3]:=NinetyPercentFlow;
  rtScatterPlotData(rtstat[1],@xMarker,@yMarker,3,4,5);
  setcolor(14);
  rttitlexaxis(rtstat[1],'Time (s)');
  rttitleyaxis(rtstat[1],'Flow');
{Volume = rtstat[2]}
  rtsetwindowoptions(rtstat[2],rt_resize or rt_maximize or rt_hide or rt_iconize
  or rt_savewinimage or rt_3dborder or rt_3dinner);
  rtsetpercentwindow(rtstat[2], 0.01, 0.6, 0.99, 0.99);
  rtsetwin2plotratio(rtstat[2], 0.15,0.15,0.15,0.15);
  rtsetViewBackground(rtstat[2],7);
  rtscalePlotArea(rtstat[2],0,0,MaxSampleArray,10);
  rtsetxyintercepts(rtstat[2], 0.0, 0.0);
  setcolor(5);
  rtdrawyaxis(rtstat[2], 1, 0);
  rtlabelyaxis(rtstat[2],1, 1, 0);
  rtdrawxaxis(rtstat[2],100,0);
  rtlabelxaxis( rtstat[2],1, 0,0);
  rtLinePlotData(rtstat[2],@xaxis,@PressureFileData,MaxSampleArray,red,0);
  setcolor(14);
  rttitlexaxis(rtstat[2],'Time (s)');
  rttitleyaxis(rtstat[2],'Volume');
  REPEAT
    rtprocesswindowoptions;
  UNTIL KEYPRESSED;
readln;
rtClearWindow(rtstat[1]);
rtClearWindow(rtstat[2]);
rtCloseGraphics(1);
end;
*)
(=====)
Procedure CalculateParameters;

```

```

begin
{Covert to volume: gebruik Pressure array hiervoor}
  For teller:=1 to MaxSampleArray do
    FilteredFlowFileData^[teller]:=abs((FlowFileData^[teller]-
FlowFileData^[1])*(1/0.10265)*(0.365/5));{liter}
{Convert to flow}
  FlowFileData^[1]:=0;
  For teller:=2 to MaxSampleArray do
    FlowFileData^[teller]:=(FilteredFlowFileData^[teller]-
FilteredFlowFileData^[teller-1])/deltaT*60;{liter/min}

GetFilterData(CutOffFreqF);
DoTheFlowFiltering;
GetFilterData(CutOffFreqP);
DoThePressureFiltering;
WriteFiles;
{FindTheMaximumValue}
MaximumFlow:=0;
MaxTeller:=0;
For teller := 1 to MaxSampleArray do
  begin
    if FlowFileData^[teller] >= MaximumFlow
      Then
        Begin
          MaximumFlow:=FlowFileData^[teller];
          MaxTeller:=teller;
        end;
    end;
{CalculateTheRiseTime}
NinetyPercentFlow:=(0.9*MaximumFlow);
TenPercentFlow:=(0.1*MaximumFlow);
TenPercentFound:=False;
DeltaFlow:=0.1;
AantalLusse:=0;
Repeat
  For teller:=MaxTeller DownTo 1 do
    Begin
      If (TenPercentFlow-deltaFlow<= FlowFileData^[teller])
and (FlowFileData^[teller]<TenPercentFlow+deltaFlow)
then
        If TenPercentFound = false
          Then
            begin
              TenPercentTeller:=teller;
              TenPercentFound:=True;
            end;
        end;
      DeltaFlow:=DeltaFlow+0.1;
      Inc(AantalLusse);
      Until (TenPercentFound);
      DeltaFlow:=0.1;
      TenLusse:=AantalLusse;
      AantalLusse:=0;
      NinetyPercentFound:=False;
    Repeat
      For teller:=MaxTeller DownTo 1 do
        begin
          If (NinetyPercentFlow-DeltaFlow <= FlowFileData^[teller])
and (FlowFileData^[teller]<NinetyPercentFlow+DeltaFlow)
then

```



```

        If NinetyPercentFound = False
            then
                begin
                    NinetyPercentTeller:=teller;
                    NinetyPercentFound:=True;
                end;
            end;
DeltaFlow:=DeltaFlow+0.1;
Inc(AantalLusse);
Until (NinetyPercentFound);
NinetyLusse:=AantalLusse;
RiseTime:=(NinetyPercentTeller-TenPercentTeller)*DeltaT;
{display data}
(*rtopenrtg(detect,0,defaultgraphdir,3,1);
DisplayVolumeAndFlow;*)
Writeln('TenPercentTeller : ',TenPercentTeller);
Writeln('NinetyPercentTeller : ',NinetyPercentTeller);
Writeln('Ninety Percent Flow : ',NinetyPercentFlow:3:2);
Writeln('TenPercentFlow : ',TenPercentFlow:3:2);

Writeln('Rise Time = ',RiseTime:3:2,' Max Flow = ',MaximumFlow:3:2,
' Ten lusse : ',TenLusse,' Ninety lusse : ',NinetyLusse);
{CalculateTheDwellTime}
DetermineTheActivationPoint;

end;
{=====}
PROCEDURE atsPulse;
Begin
    For LoopCounter:= 1 to AantalToetse do
        begin
            (* Write('Press <ENTER> to download ', infile);
            Readln;
            *)
            For i:=1 to FileLength do writelnCom(CPORT,hexarray[i],ERR);
            delay(1000);
{Sample the data}
            Writeln('Sampling.....');
            OkToCapture := True;
            EndOfExperiment:=False;
            tail:=head-1;
            FileCounter:=1;
{Pulse the START switch}
            SNA(0,256);
            delay(100);
            SNA(0,0);
            repeat
                ServiceTheSample;
            until EndOfExperiment;
            OkToCapture := False;
{Pulse the STOP switch}
            SNA(1,256);
            delay(100);
            SNA(1,0);
            delay(1000);
{Claculate the Parameters}
            CalculateParameters;
(*WriteFiles;*)
            MoveThePistonBack;

        end;
    end;
end;

```

```

end;

{=====Main Program=====}
BEGIN
OpenTheActivationFile;
new(PressureFileData);
new(FlowFileData);
new(FilteredFlowFileData);{Set up the AtoD card}
  ClrScr;
{Set up the AtoD card}
  deltaT:=1/InitialSampleRate; {stel vir die monster tempo}
  SetUpASAbord(@GetInterruptSample,InitialSampleRate); {Setup sample interval}
  Init_Interrupt;          {Init all vectors and Interr.CONTroller}
  ASA_ReadAtoD(BaseAdress,Dat);    {clears the ASA buffer}
{Make sure the START/STOP switches are off}
{0->start}
{1->stop}
  SNA(0,0);
  SNA(1,0);
{Clear the buffers}
  FOR i:=1 to MaxSampleArray do PressureFileData^[i]:=0;
  FOR i:=1 to MaxSampleArray do FlowFileData^[i]:=0;
  FOR i:=1 to MaxSampleArray do FilteredFlowFileData^[i]:=0;
  StelCommPoortOp;
  FindTheStart;
  Writeln('Tik beginvloei in > 100 l/min in inkremente van 5');
  Readln(BeginVloei);
  Writeln('Tik eindvloei in < 550 l/min in inkremente van 5');
  Readln(EindVloei);
  KLAAR:=FALSE;
  REPEAT
    str(BeginVloei, str1);
    IFile:='c:\pulse\t008\puls'+str1;
    InFile:=ifile+'.prg';
    writeln(Infile);
    ReadAtsFile;
    atsPulse;
    BeginVloei:=BeginVloei+5;
    If beginVloei >= EindVloei then klaar := true
  UNTIL KLAAR;
  closecom(cport);
  Stop_Interrupt;
Dispose(PressureFileData);
Dispose(FlowFileData);
Dispose(FilteredFlowFileData);
END.

```


Validation Of Data Acquisition


The preceding program was verified for accuracy with each test through a multiphase MathCad program.


Phase 1: Augmenting Program


An augmenting program was written to accumulate the data from the different tests in one global database to speed up the analysis and subsequent validation process.


```


:= 
C:\mav\data\T22201.txt


:= 
C:\mav\data\T22202.txt


:= 
C:\mav\data\T22203.txt


:= 
C:\mav\data\T22204.txt


:= 
C:\mav\data\T22205.txt


:= 
C:\mav\data\T22206.txt


b1 := augmen(f1, f2)
b2 := augmen(f3, f4)
b3 := augmen(f5, f6)
b4 := augmen(b1, b2)
b5 := augmen(b4, b3)
:= 
C:\mav\data\T22207.txt

:= 
C:\mav\data\T22208.txt

:= 
C:\mav\data\T22209.txt

:= 
C:\mav\data\T22210.txt

:= 
C:\mav\data\T22211.txt

:= 
C:\mav\data\T22212.txt

b6 := augmen(f7, f8)
b7 := augmen(f9, f10)
b8 := augmen(f11, f12)

```

```

b9 := augmen(b6, b7)
b10 := augmen(b8, b9)
b11 := augmen(b5, b10)

```



C:\Rawdata for T2220.txt

b11

Phase 2: Data Trimmer

Data was minimised through a trimmer program to reduce processing power required.

:=



C:\mav\8TH.txt

```

column := cols(data)
row := rows(data) - 1
maximum =
  c ← 1
  r ← 0
  while c < column
    b ← submatrix(data, 0, row, c, c)
    carryr ← max(b)
    r ← r + 1
    c ← c + 2
  carry
maxpos :=
  c ← 1
  t ← 0
  while c < column
    r ← 0
    while datar,c ≠ maximumr
      r ← r + 1
    carryt ← r
    c ← c + 2
    t ← t + 1
  carry

```

```

toptrimpos:= c←1
              t←0
              while c< column
                r←maxpos§
                while datar,c>0
                  r←r-1
                  carryt←r
                  c←c+2
                  t←t+1
                carry
bottomtrimpos:= c←1
                t←0
                while c< column
                  r←maxpos§
                  while datar,c>0
                    r←r+1
                    carryt←r
                    c←c+2
                    t←t+1
                  carry
toptrim:= max(toptrimpos)
bottomtrim:= min(bottomtrimpos)
processeddata := submatrix(data, toptrim, bottomtrim, 0, (column-1))


```

Phase 3: Dwell Time Calculations

The dwell time for each test had to be determined to ensure that the envelope generated complies with the requirements of the American Thoracic Society (ATS).

This was compiled in MathCad.

```

:= 
C:\mav\smoothed8TH.txt

column:= cols(data)
row := rows(data) - 1

```

```

maximum:= c←0
           r←0
           while c < colum
             b← submatrix(data, 0, row, c, c)
             carryr← max(b)
             r← r + 1
             c← c + 1
           carry
maxpos:= c←0
          t←0
          while c < colum
            r←0
            while datar,c ≠ maximumr
              r← r + 1
            carryt← r
            c← c + 1
            t← t + 1
          carry

```

value90:= round(.9·maximum)

```

value90posbottom:= c←0
                    t←0
                    while c < colum
                      r← maxpost
                      while datar,c > value90t
                        r← r + 1
                      carryt← r
                      c← c + 1
                      t← t + 1
                    carry

```

```

value90postop:= c←0
                 t←0
                 while c < colum
                   r← maxpost
                   while datar,c > value90t
                     r← r - 1
                   carryt← r
                   c← c + 1
                   t← t + 1
                 carry

```

value90upt:= $\frac{\text{value90posto}}{6000}$

$$\text{value90downt} := \frac{\text{value90posbotto}}{6000}$$

$\text{dwelltime} := (\text{value90downt} - \text{value90up}) \cdot 1000$
 $\text{Dwell} := \text{mean}(\text{dwelltime})$
 $\text{Dev} := \text{stdev}(\text{dwelltime})$
 $\text{Dev} = \blacksquare$
 $\text{Dwell} = \blacksquare$

Phase 4: Graphing of activation

The actual validation was executed through visual inspection of the appropriate pressure data and Turbo Pascal Determined activation point to ensure the correct location of the activation point. This visual inspection required graphing which was done in Mathcad.

$:=$ 
 C:\.\Rawdata for T2220.txt

$:=$ 
 C:\.\T22a220.txt

$\text{pos} := \text{submatrix}(\text{act}, 1, 12, 0, 0)$
 $\text{window} := 100$
 $\text{row} := \text{rows}(\text{pos})$

```

windowarray:= c←0
               p←0
               s←1
               k←0
               o←2
               u←3
               while c<row
                 r←(posc - window)
                 t←0
                 q←0
                 while r<(posc + window)
                   carryt,k←datar,p
                   carryt,s←r
                   carryt,o←q
                   carryt,u←posc
                   t←t+1
                   q←q +  $\frac{4}{(2 \cdot \text{window})}$ 
                   r←r+1
                 c←c+1
                 s←s+4
                 k←k+4
                 o←o+4
                 u←u+4
                 p←p+2
               carry

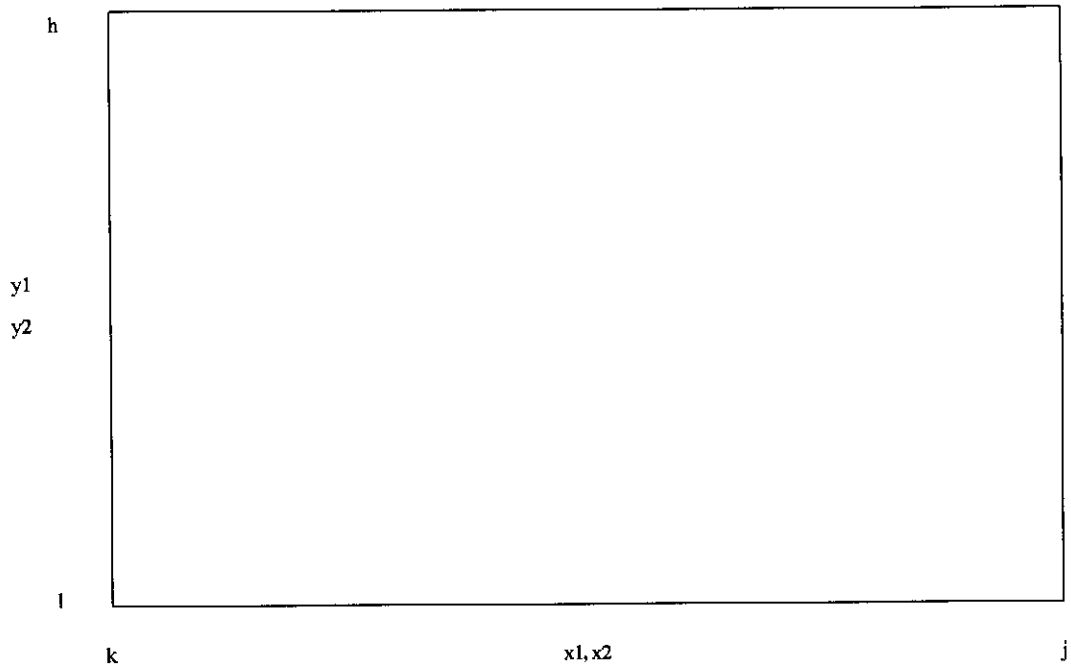
```

set := 0

```

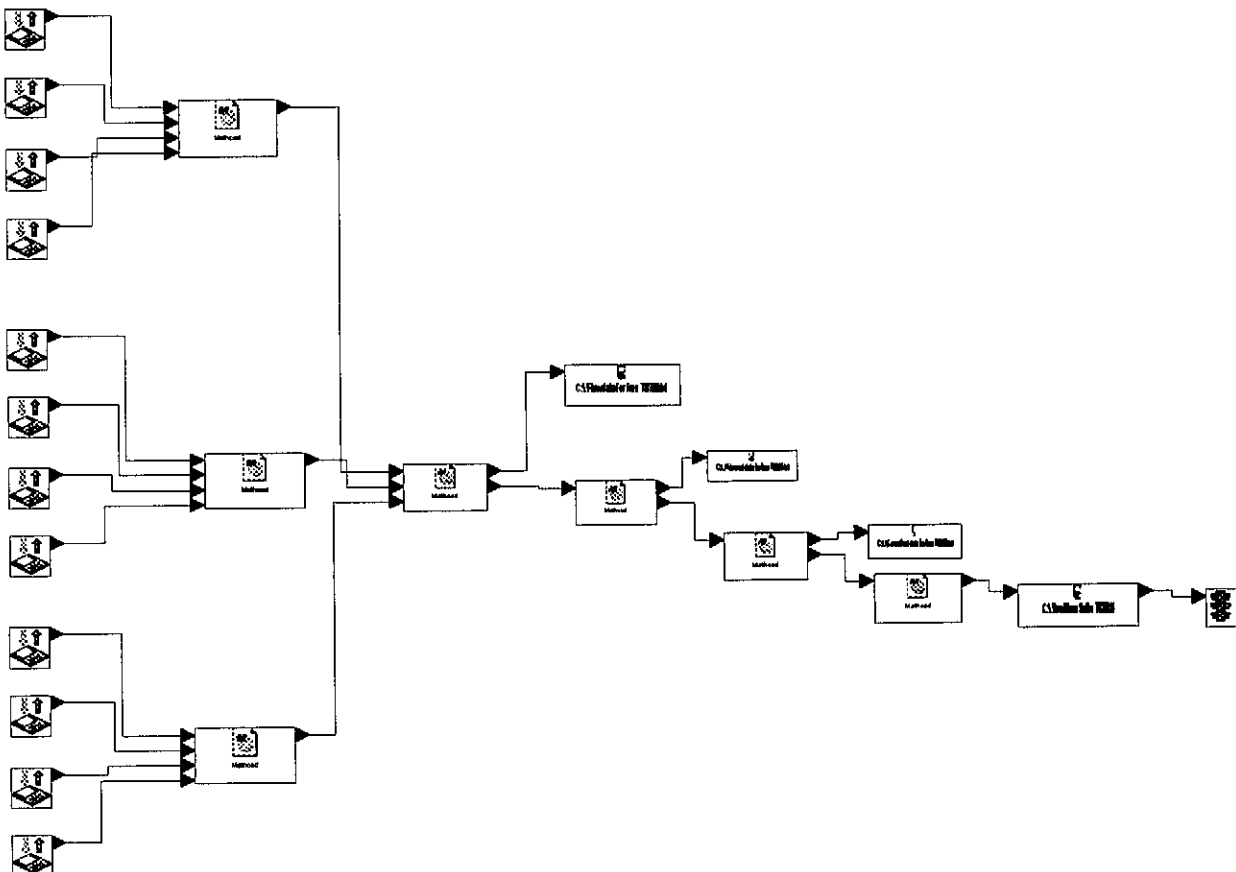
y1 := windowarray<set>
y2 := windowarray<set+2>
x1 := windowarray<set+1>
x2 := windowarray<set+3>
h := max(y2)
l := min(y1)
j := max(x1)
k := min(x1)

```

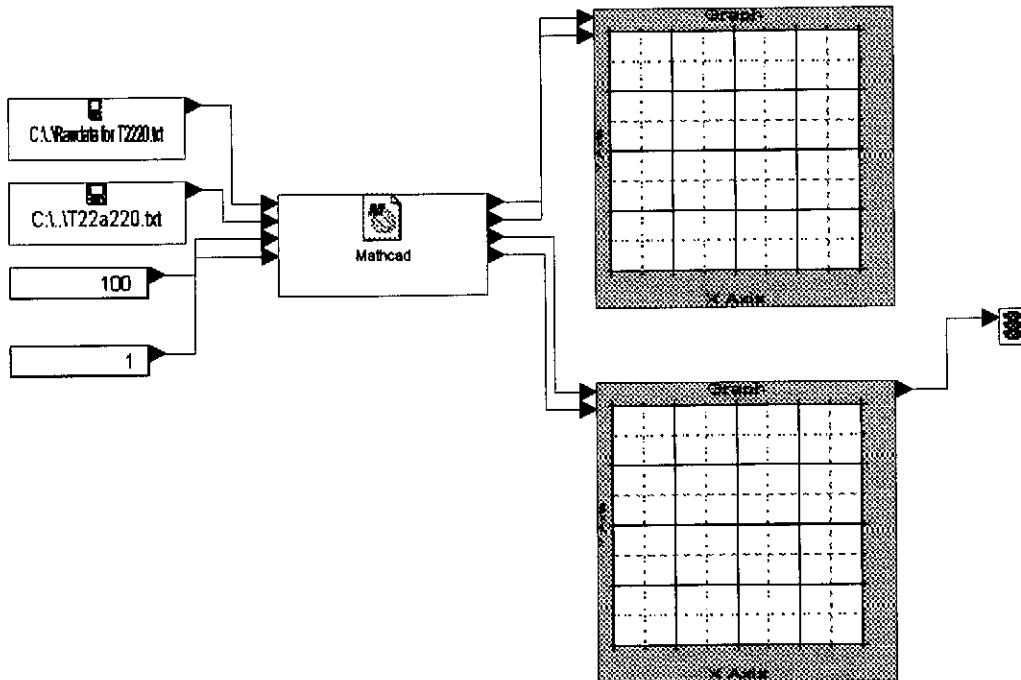



Mathconnex Integration

The four phases mentioned in the validation process were integrated in two Mathconnex electronic circuit board simulations to optimise the speed of the validation techniques. The first simulation was the data processing.



The second simulation executed the graphing phase.



Numerical Integration of Pressure and Flow rate data to point of activation

The final researched comprised of numerically integrating the pressure and flow rate curves acquired in each envelope test (3072), to the point of activation with respect to time. This was done in a Mathcad compiled program.

:= 
C:\Rawdata for T2150.txt


C:\T2a150.txt

act := submatrix(activationpoints 1, 12, 0, 0)
column := cols(rawdata)

```

newdataset:= c←0
              t←0
              while c < colum
                r←0
                while r < actt
                  carryr,t←rawdatar,c
                  r←r + 1
                t←t + 1
                c←c + 2
              carry
colum2:= cols(newdataset)
toptrimpos:= c←0
              while c < colum2
                r←(actc - 1)
                while newdatasetr,c > 0
                  r←r - 1
                carryc←r
                c←c + 1
              carry
toptrimvalue= max(toptrimpos)
intarray:= submatrix(newdataset, toptrimvalue, (rows(newdataset) - 1), 0, (colum2 - 1))
limit= rows(intarray) - 1
integration= c←0
              while c < colum2
                sum←submatrix(intarray, 1, (limit - 1), c, c)
                carryc← $\frac{(\text{intarray}_{0,c} + \text{intarray}_{\text{limit},c} + 2 \cdot \sum \text{sum})}{12000}$ 
                c←c + 1
              carry

```